Triarylboranes in azo and carbene chemistry

Theodore Anthony Gazis

A thesis submitted to Cardiff University in candidature for the degree of Doctor of Philosophy

December 2021

I. Acknowledgements

No work of this size is possible without the help and collaboration of a multitude of individuals. First and foremost, I would like to express my appreciation to my supervisors Professor Rebecca Melen and Professor Duncan Wass, for their direction and encouragement during the last three years. I also must thank all members of the Melen research group for assisting me. I would especially like to thank Dr Yashar Soltani for guiding me during my first few months in the group. Also, Dr Darren Wilcox, Dr Darren Ould, Dr Jamie Carden and Mashael Alharbi for their contributions to my work and papers. Thanks go to Dr Tanja Kaehler for proofreading this thesis. I am grateful to the catalysis CDT and the EPSRC for funding. I would also like to thank Dr Luke Kidwell and Dom Ward from the Easun group for the numerous upbeat and amusing moments they have provided.

Throughout my PhD, I have collaborated with several academics to whom I owe my gratitude. Firstly, thanks to Professor Thomas Wirth from Cardiff University and Professor Michael Hill from Bath University for their support and advice during project development and paper writing. Appreciation must be given to Maurice Metzler, Professor Dr Mathias Wagner and the Wagner group of Goethe University Frankfurt for allowing me to undertake an internship and making my stay so enjoyable. Dr Benson Kariuki and Professor Jeremy Rawson taught me the basics of single crystal X-ray diffraction and how to solve and refine structures. Professor Jeremy Rawson, in particular, was responsible for checking the majority of my crystal structural assignments and completing the Computational sections of Chapters 3 and 5.

A PhD is a tumultuous journey with numerous ups and downs. The following people have helped me through the lowest points. Firstly, I owe a debt of gratitude to my chemistry teacher, Mr Dhmhtrhs Babakas, for setting me on this journey and cultivating my love for chemistry. A heartfelt thanks to Annika Schulz for the past four years. My father pushed me to achieve my full potential and motivated me when I needed it the most. Lastly, I would like to thank my mother, who taught me to believe in myself at a young age and never give up. Without her, I would have never gotten to this point. I dedicate this thesis to her memory.

III. Aims

The overarching goal of this thesis is to explore the reactivity of several azo- containing compounds and iodonium ylides with fluorinated triarylboranes. An exhaustive study into reaction outcomes is envisaged by varying the fluorine substitution pattern on the triarylborane and hence, their Lewis acidity. To achieve this objective, state of the art analytical techniques such as multinuclear NMR spectroscopy, mass spectrometry, single crystal X-ray diffraction, and DFT calculations were utilised. Thus, valuable insights into the emerging and highly topical field of triarylborane azo and carbene activation would hopefully be achieved.

In Chapter 3, the goal is to expose hydrazones and hydrazides to fluorinated triarylboranes under various reaction conditions. As a result, an assortment of dative and covalent N–N–B systems, including adducts, chain and heterocyclic compounds, are hoped to be furnished. Subsequently their structural properties will be thoroughly investigated.

Chapter 4 aims to expand the reaction protocols developed in Chapter 3 to diaziridines. Firstly, the effect of triarylborane Lewis acidity and temperature will be explored to determine if divergent reactivity from Chapter 3 is observed. Secondly, Frustrated Lewis Pairs will be introduced to explore their potential in nitrogen activation and conversion.

The impetus behind Chapter 5 is the transfer of aryl halogenated groups to acyclic diazo and iodonium ylide carbene precursors. Through a rare 1,3-carboboration a library of boron dienolates are expected to be furnished. Subsequently, their hydrolysis will be attempted as well as substrate scope expansion to cyclic iodonium ylides.

III. Compounds synthesised in this thesis

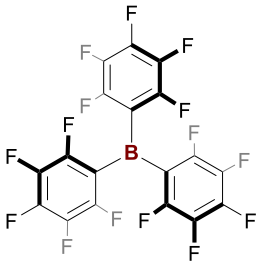

B$(C_6F_5)_3$

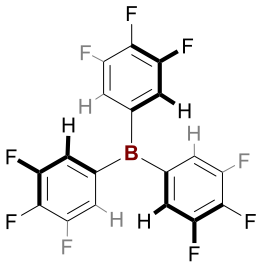

B$(3,4,5\text{-}F_3C_6H_2)_3$

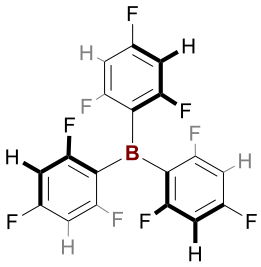

B$(2,4,6\text{-}F_3C_6H_2)_3$

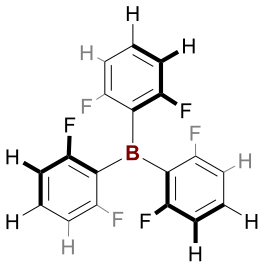

B$(2,6\text{-}F_2C_6H_3)_3$

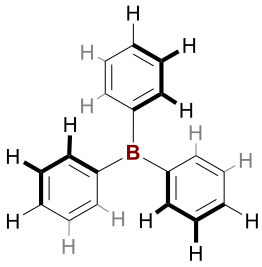

BPh_3

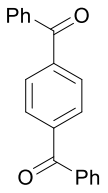

1

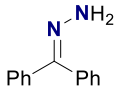

2a

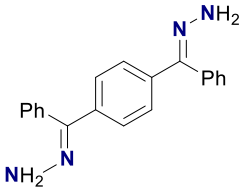

2b

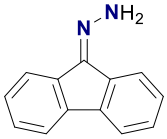

2c

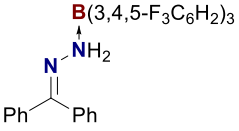

3a

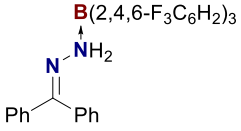

3b

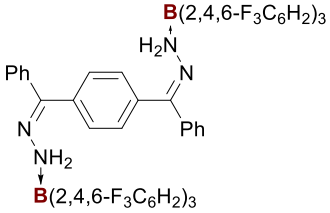

3c

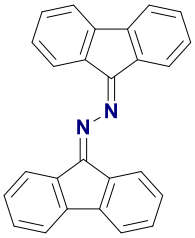

4

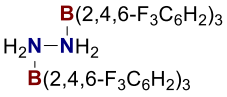

5

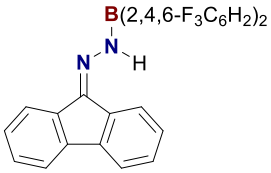

6

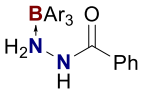

Ar = 2,4,6-$F_3C_6H_2$ **7a**

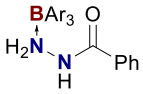

Ar = C_6F_5 **7b**

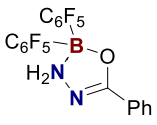

8

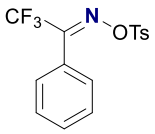

9

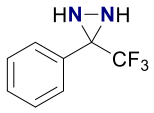

10a

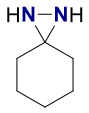

10b

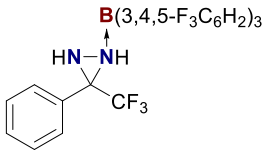

11

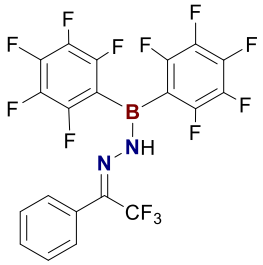

12

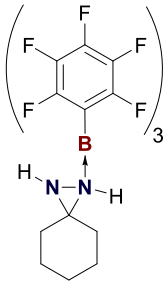

13a

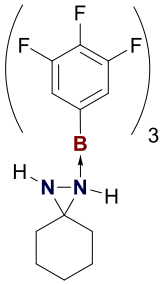

13b

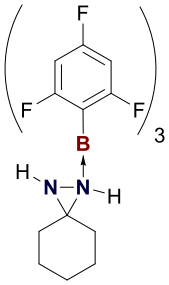

13c

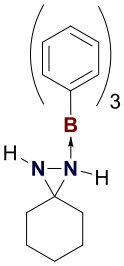

13d

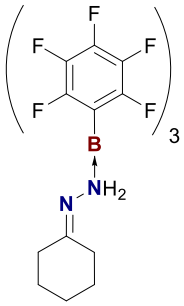

14a

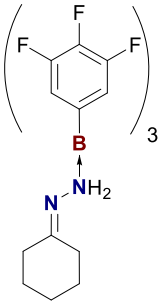

14b

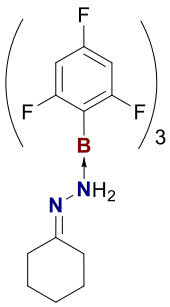

14c

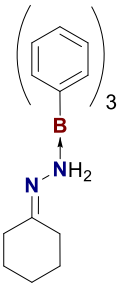

14d

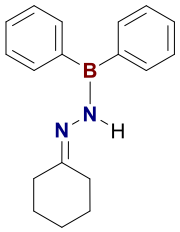

15

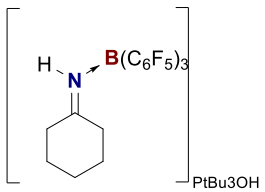

16

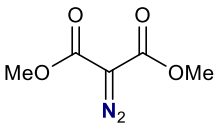

17

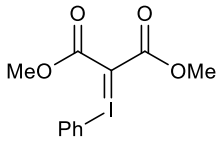

18a

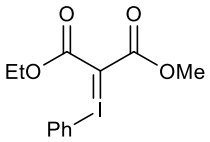

18b

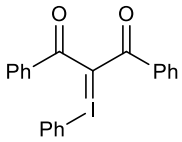

18c

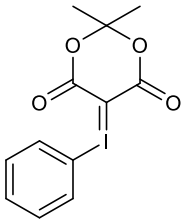

18d

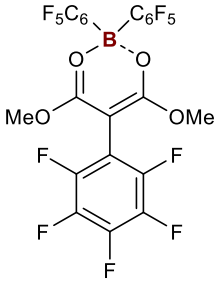

19a

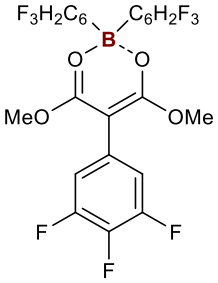

19b

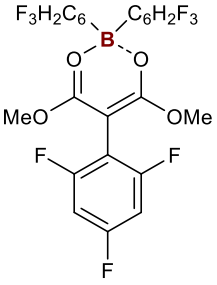

19c

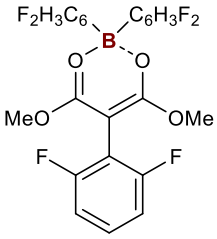

19d

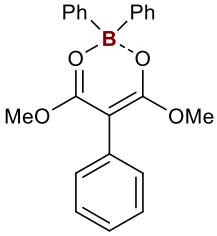

19e

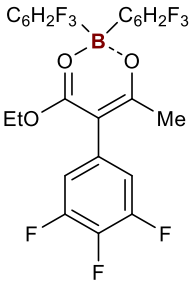

20a

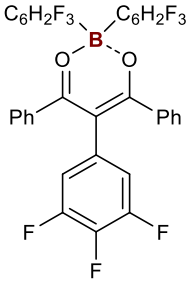

20b

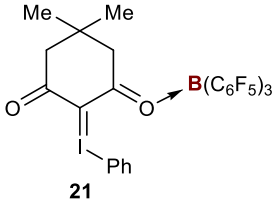

21

IV. Table of contents

V. Abstract

The research presented in this thesis can be broadly divided into two themes. The first one, presented in Chapters 3 and 4, concerns the activation of nitrogen-containing compounds facilitated by triarylboranes. Subsequently, triarylborane carboboration of carbene precursors is presented in Chapter 5.

Chapter 3 disclosed the difference in reactivity of various triarylboranes (BAr_3) towards hydrazones and hydrazides. Initially, adduct formation was observed, which led to aryl elimination for selected examples upon heating. Thus, novel covalent N–N–B systems were generated, including chain and heterocyclic compounds. The synthetic protocols developed in Chapter 3 were then implemented to activate diaziridines in Chapter 4. Stoichiometric reactions with electrophilic triarylboranes initially lead to adduct formation. These adducts readily rearranged upon gentle heating. As temperatures were further increased, organohydrazinoboranes could be isolated for certain derivatives. Frustrated Lewis Pairs were also employed for the deprotonation of certain diaziridines. Finally, Chapter 5 centred on synthesising a range of boron dienolates. Heating a diazo malonate and acyclic iodonium ylides with stoichiometric quantities of aryl boranes results in 1,3-carboboration products. Cyclic iodonium ylides proved resistant to this transformation. Attempts to hydrolyse the dienolates proved unsuccessful as they were stable under a range of acidic, basic and aqueous conditions.

Author's note on numbering: Selected compounds in Chapter 1: Introduction are labelled with an **I** followed by the appropriate number, *i.e.* **I10**. The triarylboranes presented in Chapter 2 are labelled in their shorthand notation, *i.e.,* $B(C_6F_5)_3$ for tris(pentafluorophenyl)borane. Finally, the compounds in Chapters 3–7 are labelled sequentially (**1–21**).

Chapter 1: Introduction

Chapter 1.1 The emerging role of boron in dinitrogen activation

The importance of dinitrogen (N_2) in supporting life on earth is beyond dispute. Besides making up approximately 78% of the atmosphere, it constitutes an essential elemental building block alongside hydrogen, carbon and oxygen. However, its exceptionally high bond energy of 941.6 kJ/mol necessitates sophisticated enzymes for its activation and utilisation.[1] These are known as nitrogenases and are responsible for fracturing and fixating dinitrogen into ammonia and related nitrogen-containing compounds. Thus, the nitrogen cycle, which provides nourishment for life on earth, is set in motion.[2]

From an industrial perspective, ammonia has a multitude of applications ranging from established (fertilisers, cleaners) to emerging ones (rocket fuel, stimulant).[3] Therefore, vast quantities are produced to satisfy these needs, with 178 million tons generated in 2018.[4] It is of little wonder that the eventual direct conversion of N_2 to NH_3 via the Haber Bosch process left an indelible mark on the 20th century from a socioeconomic perspective.[5]

This seminal process drew inspiration from nature. At the heart of nitrogenase enzymes lie metals, specifically iron, thanks to their ability to engage in σ-donation and π-back bonding with N_2. Thus, bond weakening of N_2 occurs, which facilitates its cleavage (Figure 1.1).[6,7,8] Similarly, the Haber-Bosch process relies on an iron catalyst to fixate dinitrogen and convert it to ammonia. The procedure continues to garner significant attention to this day, with an ever-expanding catalogue of publications devoted to its optimisation.[9]

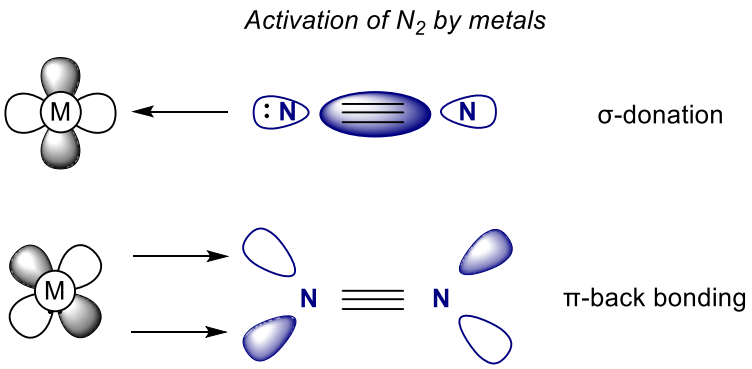

Figure 1.1: Bonding orbital interactions observed in metal N_2 activation.

Despite these concerted efforts, specific issues persist. It remains an energy-intensive process with approximately 3–5% of the global natural gas consumption devoted to generating the required elevated temperatures and high pressures.[10] In addition, there are serious concerns over wastewater treatment with specialist removal equipment required to prevent ammonia from entering the water stream.[11] When this is coupled with the 21st-century drive to 'greenify' chemistry, the quest for sustainable metal-free alternatives has ramped up.[12]

In this respect, focal studies have shown the potential of boron-containing compounds to act as dinitrogen co-activators with metals like Fe, Mo and W.[13,14] Initially, the metal systems coordinate to dinitrogen. Introduction of $B(C_6F_5)_3$ leads to further polarisation and weakening of the $M{=}N_2$ bond, thus promoting hydrogenation[13], silylation[14] and borylation[14] (Figure 1.2). The importance of $B(C_6F_5)_3$ in the Fe system cannot be overstated. In its absence, protonation of the metal occurred rather than N_2 activation.[13]

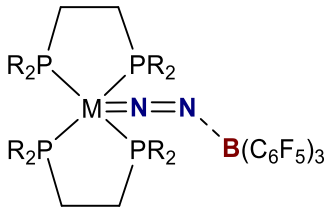

Figure 1.2: Co-activation of N_2 by metals and $B(C_6F_5)_3$.

A significant limitation main group elements face regarding nitrogen activation is their lack of suitable d-orbitals for π-back bonding. Boron follows this trend as it is notoriously electron deficient and its d-orbitals are innacesible. The Braunschweig group managed to address this issue by employing two cyclic (alkyl)(amino)carbene (CAAC) borylenes which activate dinitrogen between the two boron centres.[15] With an oxidation state of +1, these highly electronegative compounds can accept electron density from the nitrogen's full p-orbital, whilst π-back donating into the nitrogen's empty p-orbitals, thus leading to an isolable product (Figure 1.3a).

Following this seminal discovery, the same CAAC based borylene system was employed to catenate a four-membered nitrogen chain using dinitrogen and potassium graphite under reductive conditions (Figure 1.3b).[16]

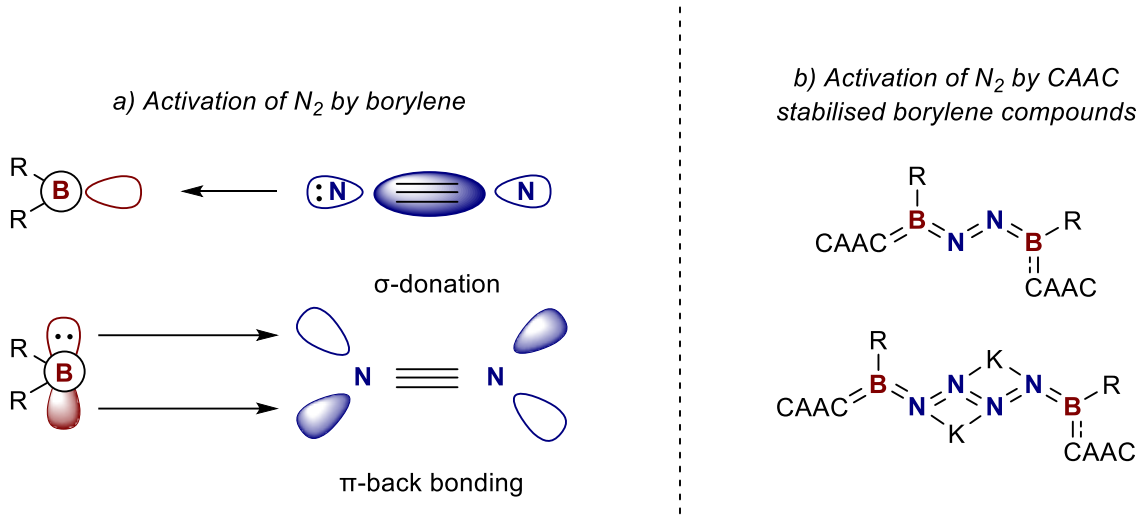

Figure 1.3: a) Orbital interactions between dinitrogen and borylene systems. b) N_2 activation using borylene systems.

These pivotal discoveries have triggered a wave of research on triarylborane activation of azo-containing compounds, encompassing diazos, azides, hydrazones, and diazenes. This section aims to serve as a comprehensive guide by documenting the current research in the field. It will thus set the scene and tone for the discoveries presented in the following chapters.

Chapter 1.2 Activation of diazo compounds by triarylboranes

1.2.1 Stoichiometric activation of diazo compounds

The diazo functionality ($R_2C=N_2$) represents an adjustable chemical handle with a breadth of synthetic applications.[17181920] However, its adoption on an industrial scale has been severely curtailed by its high reactivity and stability issues. Pressure build-up and high exothermicity arising from the release of dinitrogen gas are significant concerns.[20]

In an academic setting, it has captured the attention of transition metal chemists worldwide as an invaluable reagent in synthesis. This influx in interest is partly thanks to its versatility, allowing it to act as a carbene precursor or simply as a nucleophile. Typically, transition metals such as rhodium and copper are employed in its activation.[21,22] Investigations into its reactivity in a metal-free setting and, more specifically with triarylboranes, remain few and far between.

A standard method to stabilise diazo compounds is to delocalise electron density by placing carbonyl groups in the vicinity of the diazo functional group. The vast majority of stoichiometric triarylborane diazo activation in the literature focus on these stabilised derivatives. The one study on non-stabilised derivatives is presented below.

In a seminal paper, Stephan *et al*. demonstrated that even in the absence of an adjacent stabilising ester functionality, the release of N_2 could be accomplished. [23, 24] Stoichiometric combination of diphenyldiazomethane with $B(C_6F_5)_3$ at -30 °C indicated the formation of adduct **I1**. However, this $Ph_2CN=N–B(C_6F_5)_3$ adduct proved too thermally unstable to obtain conclusive, multinuclear NMR evidence.

However, low-temperature studies of **I1,** undertaken at -78 °C helped elucidate the underlying reactivity by crystallographic analysis (Figure 1.4). Of particular interest was the similarity of the N–N bond length [1.177(7) Å] to the ones reported previously for $M–N–N–B(C_6F_5)_3$ systems [M = Fe, Mo, W; N–N length = 1.186(3)–1.212(6) Å].[13, 14] Accordingly, it was proposed the Ph_2C: carbene part of the diphenyldiazomethane had taken the role of the transition metals of previous reports. In addition, this adduct potentially paves the way for a Frustrated Lewis Pair mediated N_2 activation.

Whilst heating adduct **I1**, *in-situ* NMR studies indicated irreversible N_2 release generating **I2**. Unfortunately, this product could not be isolated. In a related study,

the $Ph_2CN_2 \rightarrow BPh_3$ adduct (**I3**) could not be observed, presumably due to the reduced Lewis acidity of BPh_3 (Figure 1.4). [25]

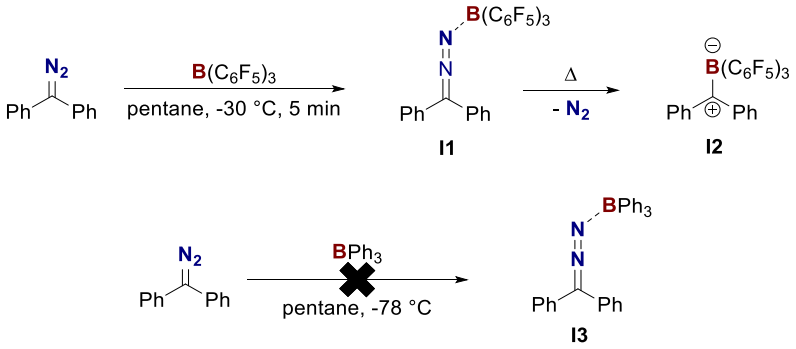

Figure 1.4: Reactions of diphenyldiazomethane with triarylboranes.

To further explore this reactivity, decamethylcobaltocene (Cp^*_2Co) was introduced to the ephemeral $Ph_2CN{=}N{-}B(C_6F_5)_3$ (**I1**) adduct at -35 °C.[25] This single electron donor proved capable of suppressing dinitrogen release (Figure 1.5 top). Instead, two divergent reaction pathways were reported.

Firstly, as Cp^*_2Co is a strong σ-donor, one of the Cp* rings abstracted a hydrogen atom, resulting in hydrazinoborane salt **I4**. Concurrently, $B(C_6F_5)_3$ replaced a hydrogen atom in one of the Cp* methyl groups leading to zwitterion **I5**.

No reactivity was previously detected between diphenyldiazomethane and BPh_3 at -78 °C.[25] A stoichiometric amount of decamethylchromocene (Cp^*_2Cr) was sufficient to promote this reaction at -35 °C (Figure 1.5 bottom). Thus, intermediate adduct **I6** was furnished and characterised. It was subsequently rapidly converted to two discrete products. Either hydrazinoborane adduct **I7**, stabilised by the chromocene cation or heterocycle **I8** formed by intramolecular cyclisation of the diazo compound (Figure 1.5). Hence, by utilising the appropriate reducing transition metal species, the authors confirmed the existence of ephemeral adducts that generally would not be observed.

Computational studies confirmed that both reactions proceeded through an initial single electron transfer from the metal species to the unstable diazomethane-borane adduct. The ensuing anions willingly participate in hydrogen transfer from C–H bonds to give anionic species **I4–I5** and **I7–I8**. These species were more stable than the ephemeral neutral adducts (**I1** and **I3**) previously investigated (Figure 1.4).[23]

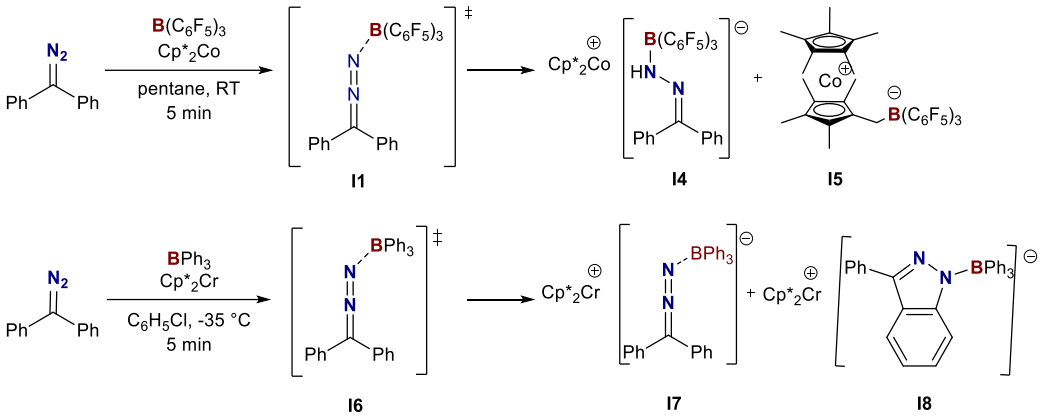

Figure 1.5: Reactivity of diphenyldiazomethane and triarylboranes in the presence of Cp^*_2Co and Cp^*_2Cr.

In the same study, the reactivity of 9-diazofluorenone was examined with both $B(C_6F_5)_3$ and BPh_3.[25] Firstly, in the presence of $B(C_6F_5)_3$, a 1,1-carboboration occurred to furnish **I9** via N_2 release (Figure 1.6 top).

On the other hand, BPh_3 required introducing an equimolar amount of Cp^*_2Cr to react with the fluorenone species. As a result, three inseparable products were obtained (Figure 1.6 bottom).

Hydrogen abstraction yielded product **I10**, and its zwitterionic counterpart **I11**, whereas an intermolecular cyclisation yielded **I12**. Computational studies highlighted that all three products were derived from a common precursor, a short-lived radical. Its formation was facilitated by electron transfer from the chromium to the borane-diazo adduct.[25]

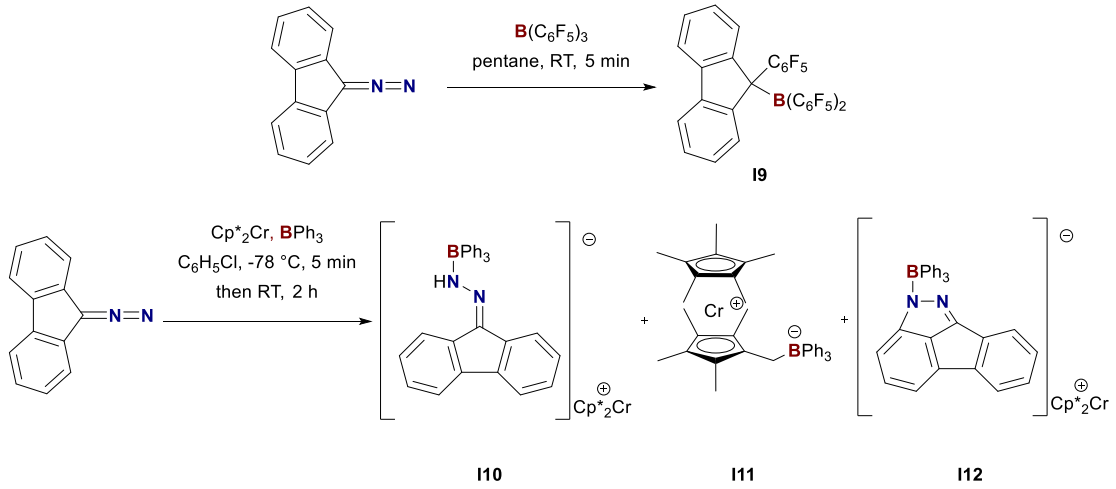

Figure 1.6: Triarylborane facilitated activation of 9-diazofluorenone.

The Stephan group also reported on the reactivity of ethyl diazoacetates with phosphines and $B(C_6F_5)_3$ (Figure 1.7).[26] Investigations began by adding the appropriate phosphine (PR_3, R = Ph, Cy, ^{t}Bu), resulting in adducts **I13**. When $B(C_6F_5)_3$ was introduced to these adducts, they proved resilient towards the expected carboboration reaction. Instead, standard Lewis acid-base behaviour was observed between $B(C_6F_5)_3$ and the carbonyl atom of the ethyl diazoacetates, resulting in **I14**. Upon exposure to water or phenol, Brønsted-Lowry adducts **I15** and **I16** were formed, respectively, by the release of $B(C_6F_5)_3$.[26]

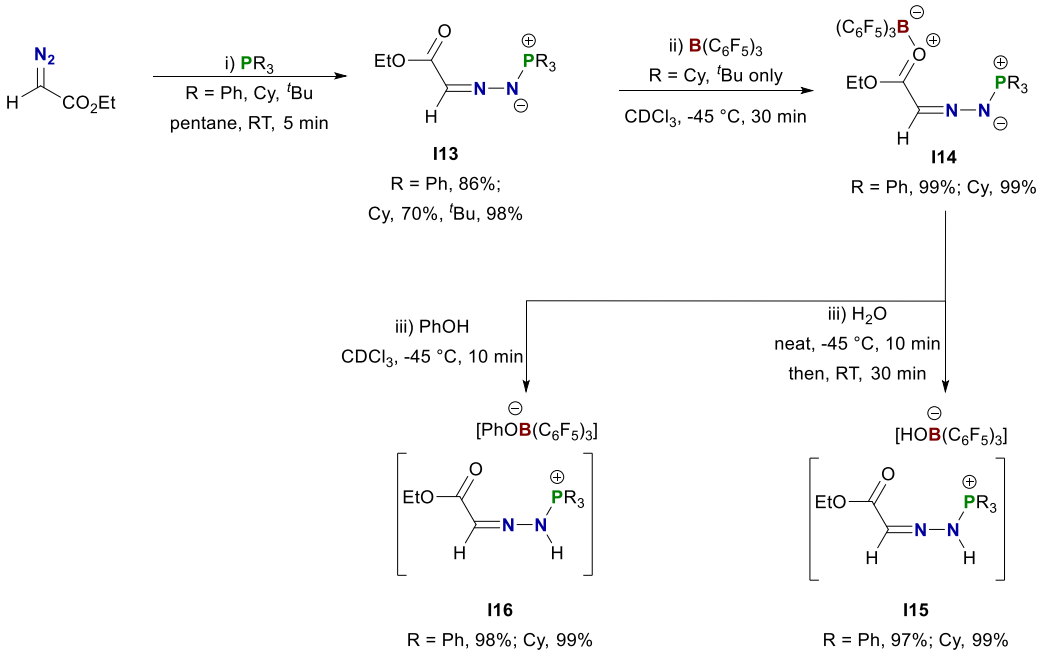

Figure 1.7: Activation of diazomethanes by phosphines and triarylboranes.

In addition, Stephan has reported the insertion of diazoacetates into the B–C bonds of triarylboranes as well as boronic acids and esters.[27] When reacting $B(C_6F_5)_3$ with ethyl α-diazomethylacetate, the product obtained depends on the ratio of borane to diazoacetate used. Thus, either boron enolate **I17** (2:1 of diazoacetate: borane) or boron dienolate **I18** (1:1 of diazoacetate: borane) could be isolated. Product **I18** was obtained in a 4:1 *E/Z* ratio. The less Lewis acidic BPh_3 also afforded the expected boron dienolate **I19** when using a stoichiometric amount of the diazoacetate. This dienolate was attained as a racemic mixture.

Mechanistically, the reactions were postulated to proceed via initial dinitrogen release promoted by a 1,1-carboboration. A subsequent rearrangement afforded the observed products. The Lewis acid-base character of the $B(C_6F_5)_3$ containing

products was affirmed by reaction with pyridine. Thus, adducts **I20** and **I21** were afforded.[27]

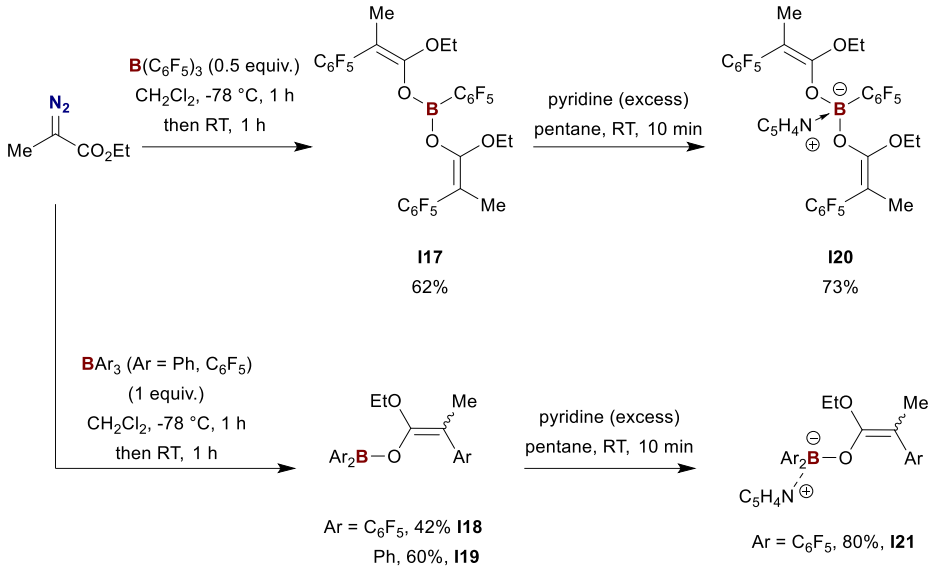

Figure 1.8: Stoichiometric insertion of diazoacetates into the B–C bonds of $B(C_6F_5)_3$ and BPh_3.

The facile release of N_2 upon exposure to $B(C_6F_5)_3$ facilitated explosive growth in the field. Consequently, attempts were made to explore other triarylboranes as diazo activators. The Melen and Wirth group applied them to the synthesis of pharmaceutically valuable 3,3-disubstituted benzofuranones (Figure 1.9).[28]

To begin with, loss of N_2 and aryl group transfer from the appropriate triarylborane to the α-diazoacetates was achieved, as previously demonstrated by Stephan *et al*.[27] The resultant boron enolates **I22** were formed in high to excellent yields (Figure 1.9a).

A causal link was established between the Lewis acidity of the triarylborane as measured by the Gutmann-Beckett method [29, 30] and the number of aryl rings transferred to the diazo compound. Thus, the more Lewis acidic boranes $B(C_6F_5)_3$ and $B(3,4,5\text{-}C_6F_3H_2)_3$ could be used in a substoichiometric ratio (1:3 borane: diazoacetate), as all three aryl rings were incorporated into the enolate products **22**. On the other hand, only one aryl ring was transferred from BPh_3, whereas $B(4\text{-}FH_4C_6)_3$ and $B(2,6\text{-}F_3H_2C_6)_3$ transferred two aryl rings.

A simple basic workup of the boron enolates proved sufficient to afford the α-functionalised carbonyl compounds **I23** with $B(OH)_3$ as a by-product. Of all products synthesised, a late-stage precursor to antidepressant diclofensine was notable (Figure 1.9b).

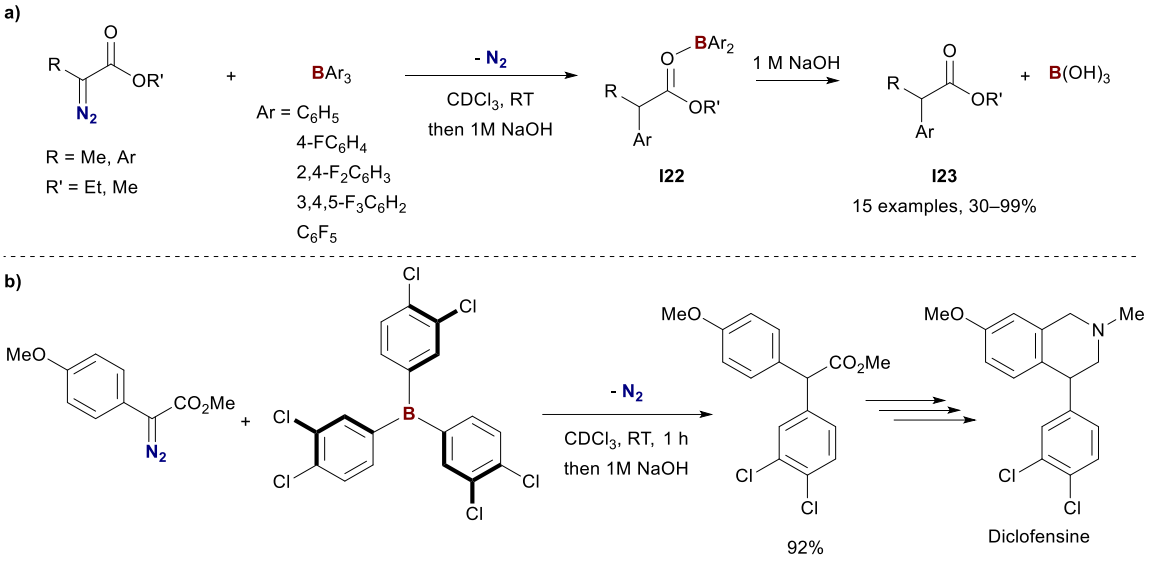

Figure **1.9:** a) Borane-mediated aryl transfer reactions with diazo compounds. b) Synthesis of a diclofensine precursor.

During this study, divergent reactivity was observed when 2-benzyloxy substituted diazo compounds were reacted with either $B(C_6F_5)_3$ or $B(3,4,5\text{-}C_6F_3H_2)_3$. A tandem rearrangement-lactonisation lead to 3,3 disubstituted benzofuran-2-(*3H*)-ones **I24** (Figure 1.10). [28]

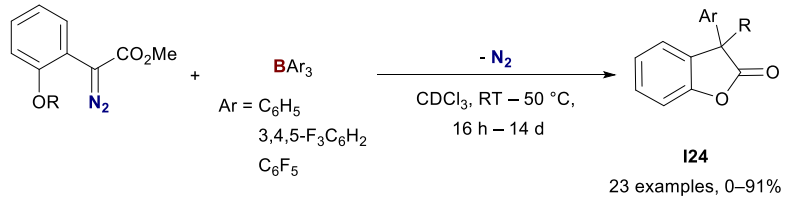

Figure 1.10: Tandem rearrangement/lactonisation of triarylboranes with α-diazoacetates.

In-situ NMR spectroscopy provided valuable mechanistic insights (Figure 1.11). Initially, the reaction proceeded by forming the expected boron enolate intermediate **I22**. This intermediate was formed via a 1,2-aryl transfer from the triarylborane to the diazoacetates coupled with dinitrogen release. In the absence of base, the unstable intermediates **I22** underwent an intramolecular rearrangement (**I22a**), giving rise to intermediate **I22b**. These precursors readily converted to 3,3 disubstituted benzofuran-2-(*3H*)-ones by lactonisation. Side product formation was a common occurrence, with **I25** and **I26** being the most common ones observed.

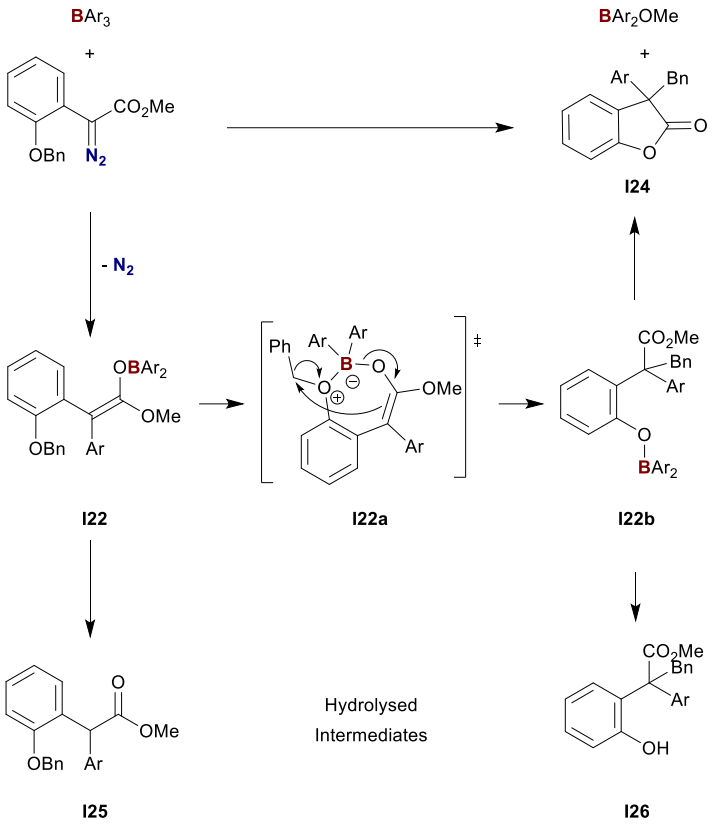

Figure 1.11: Mechanism for the synthesis of 3,3-disubstituted benzofuranones.

The reactions above were tolerant to various carbocation stabilising groups on the phenolic oxygen atom, including benzylic, allylic and cinnamic functionalities. Nitrogen and sulphur functional groups were also not affected, proving high chemoselectivity for these reactions.[28]

Multicomponent carboboration reactions between triarylboranes and diazos have also been reported. Using Hooz's work on aldol formation between trialkylboranes, aldehydes and diazacarbonyls[31] as a template, Miranda developed a triphenylborane or trialkylborane based Hooz reaction/oxidation sequence.[32] By mixing α-diazocarbonyl compounds, aromatic aldehydes and either triphenylborane or trialkylboranes, C–C bond formation could occur. As a result, 1,3-diketones, as well as β-ketoesters **I28**, were generated (Figure 1.12).

This two-step process first involved the loss of dinitrogen from the diazocarbonyl compound facilitated by the borane. Thus, a boron enolate was furnished. Afterwards, the addition of an appropriate aldehyde led to aldols **I27**. Finally, a simple oxidation using Pyridinium ChloroChromate (PCC) resulted in the desired products.

Where triphenylborane is concerned, one 1,3-diketone and two β-ketoesters were furnished in 40–65% yield. Albeit beyond the purview of this Chapter, 11 aldols were collectively obtained when using various trialkylboranes.

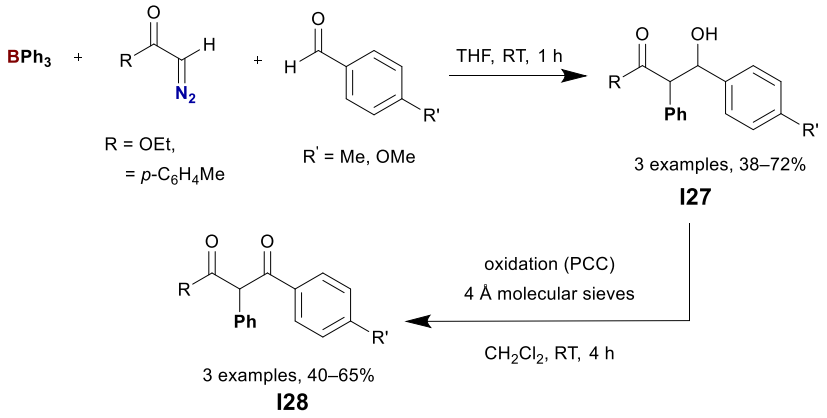

Figure 1.12: Multicomponent carboborations involving BPh_3.

Similarly, by mixing a diazo compound with a carbonate imine and either BPh_3, $B(4\text{-}C_6FH_4)_3$ or $B(4\text{-}C_6CH_3OH_4)_3$, a catalyst-free Mannich reaction was accomplished in a concerted fashion (Figure 1.13).[33] The resultant β-amino carbonyl compounds **I29** were furnished in a highly diastereoselective manner (>20:1) without a catalyst. Modification of the triarylborane aryl substituents or the diazo substituents had no measurable effect on yields. By utilising six different carbonate imines with α-diazoacetophenone and BPh_3, a brief substrate scope was conducted, demonstrating the broad applicability of this methodology. Yields of 81–86% and a consistently high diastereoselective ratio (>20:1) were achieved. From all the products formed, **I30** was of note as itresulted from a (-)phenylmenthol chiral diazo ester.

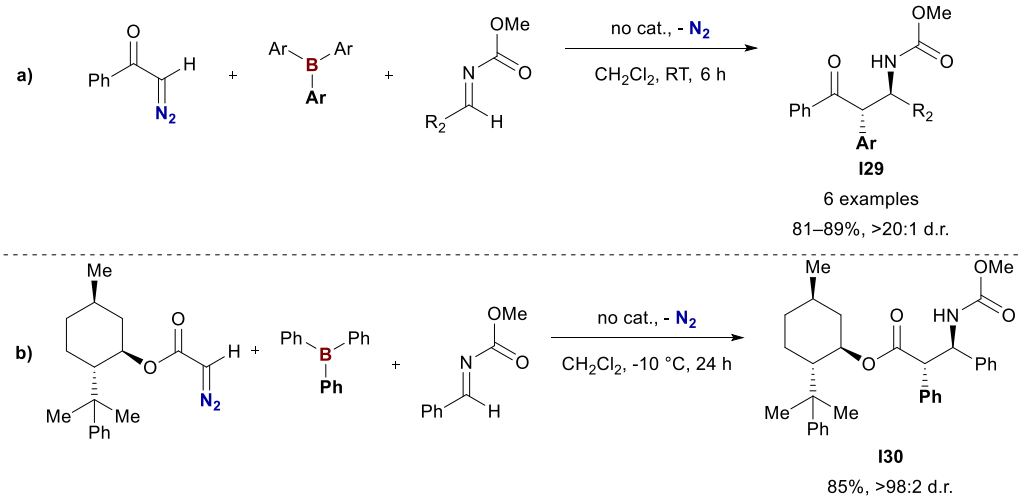

Figure 1.13: a) A Mannich triarylborane reaction leading to diastereoselective β-amino carbonyls. b) Synthesis of a (-)phenylmenthol chiral diazo ester.

1.2.2 Catalytic activation of diazo compounds

The aforementioned studies are all stoichiometric in nature and generally result in the direct reaction of the diazo compound with the triarylborane. However, careful regulation of reaction conditions can prevent hydrazinoboranes, adducts or similar products from forming. Consequently, the triarylborane is forced to behave as a catalyst. As a side note, the catalytic studies presented below have almost exclusively been performed using the archetypal triarylborane $B(C_6F_5)_3$.

With this in mind, the functionalisation of allyl alcohols with diazoesters was recently reported by the group of Prabhu (Figure 1.14).[34] The C–C bond scission and formation reaction proceeded smoothly despite being performed at room temperature, under high dilution and low catalyst loading.

A comprehensive substrate scope investigation was conducted, demonstrating the high applicability of this transformation. A wide tolerance of steric and electronic effects (electron-donating and -withdrawing) was observed. This was true for both the diazo and alcohol substrates. In total, 27 olefins (**I31**) were furnished in poor to good yields.

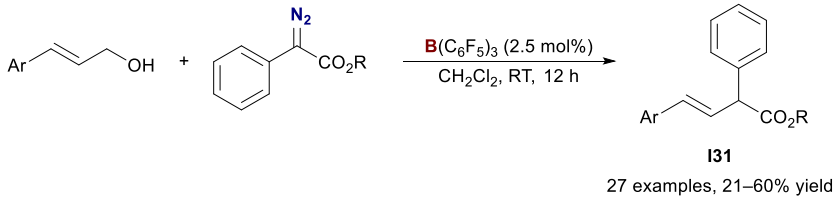

Figure 1.14: Generation of olefins **31**.

Mechanistically, experimental probes were employed to gain insights into reaction intermediates (Figure 1.15). The first step involves activating the diazoester by the borane (**I31a**). Next, N_2 release facilitated by $B(C_6F_5)_3$ leads to a carbene (**I31b**) which is prone to electrophilic attack by the β-sp^2 carbon of the allylic alcohol. The neighbouring oxygen atom stabilises the resultant benzylic cation (**I31c**). Two subsequent rearrangements lead to **I31d** and oxetane system **I31e**. A final rearrangement followed, which yielded the desired product (**I30**).

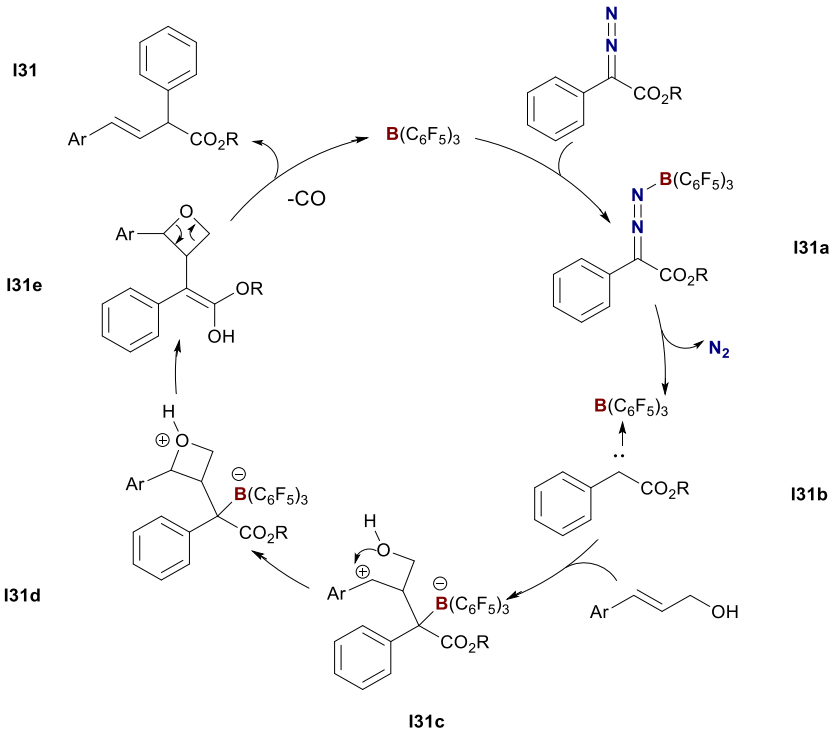

Figure 1.15: Mechanism of $B(C_6F_5)_3$ catalysed C–C bond scission and formation between allyl alcohols and diazo compounds.

Prabhu *et al*. further expanded the applicability of this methodology to a $B(C_6F_5)_3$ mediated catalytic transfer of a carbonate functionality from dicarbonates to diazo acceptors (Figure 1.16).[35] This resulted in 14 examples of carbonates **I32** in yields of 26–96%. An active methine group could be positioned next to the carbonate functionality by employing suitable dicarbonates. Consequently, late-stage modification in natural product synthesis is now feasible.

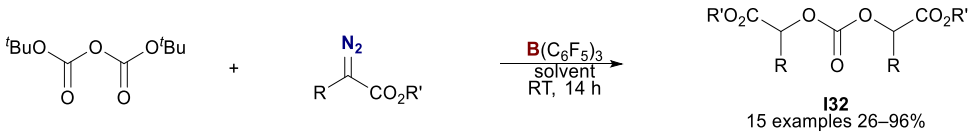

Figure 1.16: Reaction scheme for the synthesis of carbonates **32**.

The suggested mechanism was analogous to the one proposed earlier (Figure 1.15) but distinct from conventional organic carbonate reaction protocols (Figure 1.17). The coordination of $B(C_6F_5)_3$ (**I32a**) resulted in the release of dinitrogen hence promoting the formation of **I32b**. This carbene was stabilised by $B(C_6F_5)_3$. However, this stabilisation was insufficient to prevent nucleophilic attack from the dicarbonate to form oxonium ylide **I32c**. A rearrangement led to intermediate **I32d** via loss of $B(C_6F_5)_3$ and the removal of a carbonate functionality. Another equivalent of diazo-

generated intermediate **I32b** reacted with **I32d** to form a second oxonium ylide (**I32e**). Finally, carbonate elimination regenerated the borane catalyst and formed **I32**.

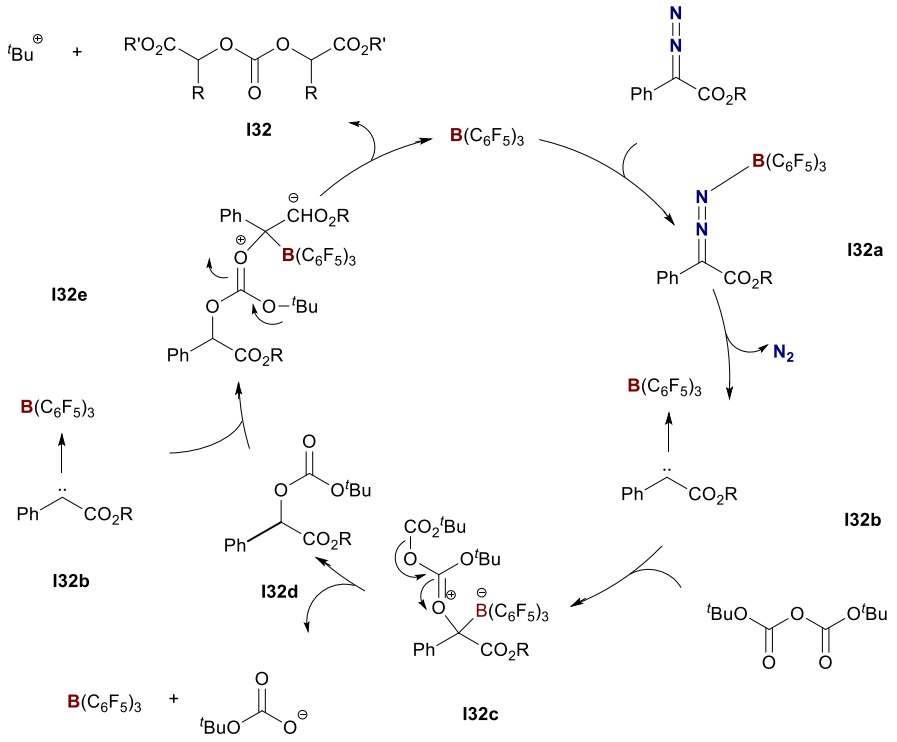

Figure 1.17: Carbonate functionality transfer from dicarbonates to diazo compounds using $B(C_6F_5)_3$ as a catalyst.

As noted above, the high Lewis acidity of triarylboranes allows them, in some instances, to assume the role of metals and replace them as catalysts. Amongst other factors, the presence of highly electronegative fluorine atoms on the aryl rings allows $B(C_6F_5)_3$ to transcend mere mimicry of metal systems and facilitate markedly divergent reactivity from transition metal catalysts.

A good example is the selective ortho-functionalisation of phenols,[36] a problematic substrate due to its numerous reactive sites. When considering the reactivity of phenols with diazos, insertions into the O–H bond when using transition metal catalysts are well documented (Figure 1.18a).[37] Examples of para functionalisation of unprotected phenols facilitated by phosphite-gold catalysts also exist (Figure 1.18b).[38]

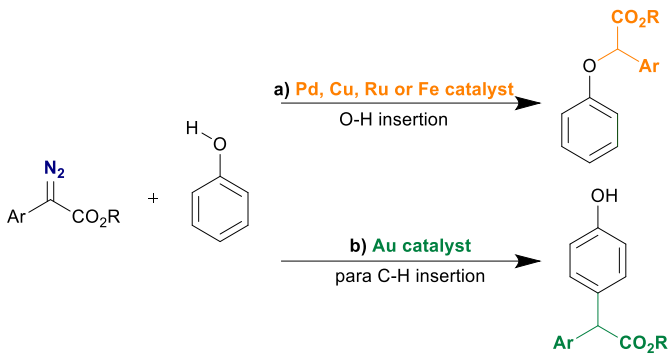

Figure 1.18: The different reaction pathways promoted by transition metals in the functionalisation of phenols with diazos.

In contrast, $B(C_6F_5)_3$ promotes a highly stereo- and chemoselective ortho functionalisation of phenols (Figure 1.19).[36] In total, 55 ortho-diaryl acetates examples (**I33**) were furnished in moderate to good yields of 50–83%.

From a mechanistic perspective, the expected nitrogen activation occurs between the diazoester and the central boron atom. Subsequently, one of the fluorine atoms of $B(C_6F_5)_3$ acts as a directing group by engaging in hydrogen bonding with the phenol hydroxide group. This weak interaction furnishes intermediate **I33a** and is sufficient to overcome the greater steric hindrance the ortho position possesses over the para position.

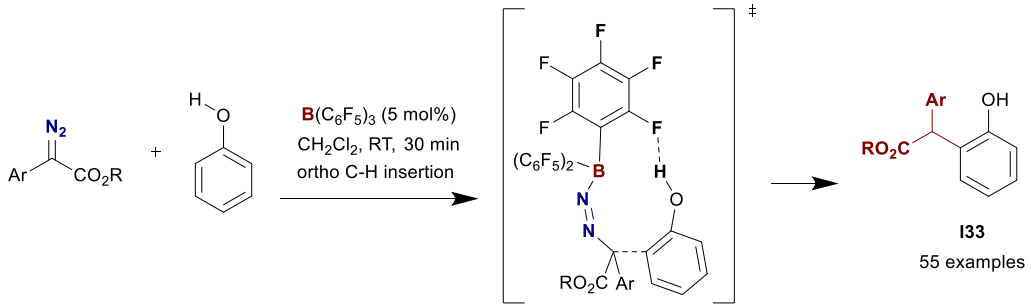

Figure 1.19: $B(C_6F_5)_3$ catalysed ortho C–H insertion of phenols representing critical catalytic intermediate I**33a**.

Triarylboranes are notorious for their water sensitivity, a major limitation for their application as catalysts; complexation of water results in a BAr_3-OH_2 adduct, whereupon the boron's empty p orbital is fully engaged in bonding with the oxygen atom. Consequently, a strong Brønsted-Lowry acid is furnished with an acidity comparable to HCl (8.4 in MeCN).[39]

In addition, this adduct is highly susceptible to B–C bond protonolysis leading to irreversible catalyst poisoning.[40] This is particularly true for $B(C_6F_5)_3$ due to its distinctly high Lewis acidity, which imparts a high degree of oxophilicity to the electrophilic boron.

This effect can be ameliorated either by substituting fluorine for bromine or chlorine atoms on the aryl rings or carefully fine-tuning reaction conditions.[40] As a result, $B(C_6F_5)_3$ promoted transformations performed in water or aerobic conditions are both rare and noteworthy.

One example, whereupon $B(C_6F_5)_3$-OH_2 is utilised as a Brønsted-Lowry acid, involves the conversion of α-aryl α-diazoesters to alcohols **I34** (Figure 1.20). This reaction displayed a broad substrate scope (24 examples) and short reaction times (as little as 30 minutes).[41]

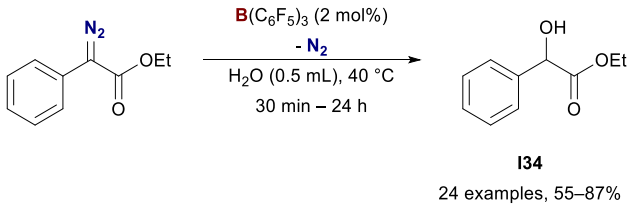

Figure 1.20: $B(C_6F_5)_3{\cdot}OH_2$ catalysed conversion of α-aryl α-diazoesters into alcohols.

Two potential mechanisms were examined (Figure 1.21). The first one suggested $B(C_6F_5)_3{\cdot}OH_2$ acted as a bifunctional catalyst activating the α-diazoester through the complexed water group. Concomitantly, it engages in hydrogen bonding with water via a fluorine atom on one of its fluoroaryl rings.

The second mechanism outlined a stepwise transformation, whereupon the diazoester is protonated by $B(C_6F_5)_3{\cdot}OH_2$ and subsequently nucleophilically attacked by the water solvent. Adding credence to the bifunctional catalyst postulate was the lack of reactivity with HCl and HOTf, classic Brønsted-Lowry acid catalysts incapable of hydrogen bonding. However, conclusive proof of the HO–H···F interaction could not be attained.

The mild conditions required make $B(C_6F_5)_3{\cdot}OH_2$ an attractive alternative to the established metal catalysts typically employed for this transformation.

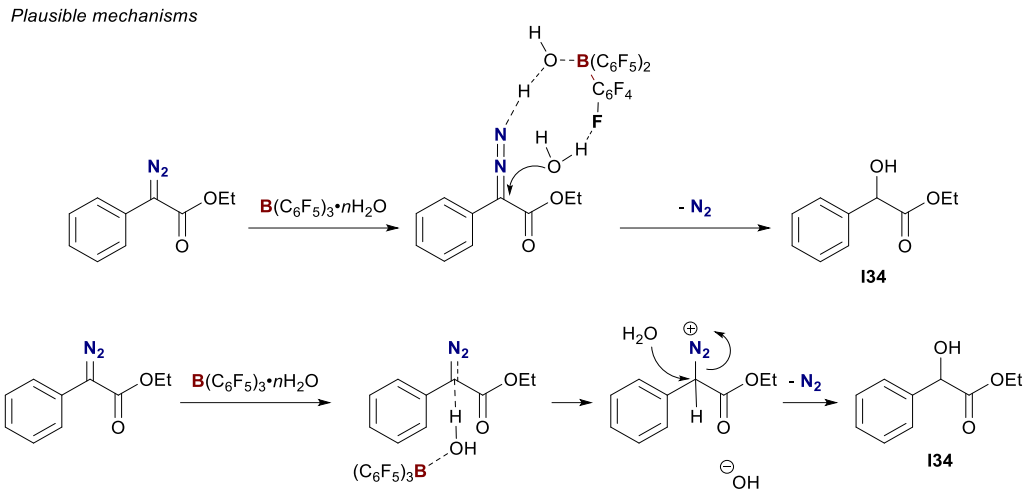

Figure 1.21: The two proposed mechanisms for the generation of alcohols **I34**.

The Tang group recently expanded catalytic diazoester functionalisation to include azide insertion promoted by $B(C_6F_5)_3$ (Figure 1.22).[42] Once again, the reaction demonstrated high functional group tolerance, with catechols, thiophenes, and numerous electron-withdrawing functionalities remaining unchanged. In total, 23 azides (**I35**) were furnished from the parent diazoesters. These were converted to valuable 1,2,3-triazoles **I36** in 50–66% yield by employing click chemistry.

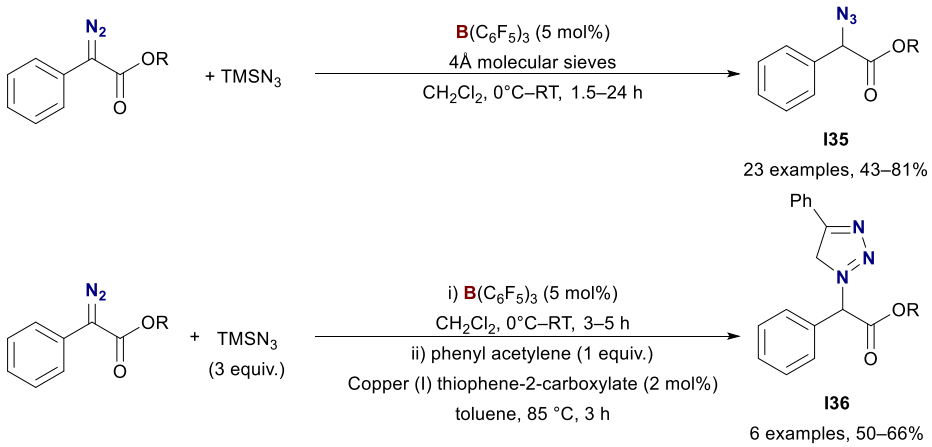

Figure 1.22: Azide insertion into diazo compounds and subsequent click reaction into triazoles.

Experimental probes revealed that this reaction followed the established pattern of diazo activation by $B(C_6F_5)_3$ as the initial step (Figure 1.23). Subsequently, nucleophilic attack by trimethylsilyl azide ($TMSN_3$) yielded intermediate **I35a**. This rapidly converted to a silyl enol ether species (**I35b**), detected by *in-situ* NMR spectroscopy. Finally, the desired azide was isolated after hydrolysis and purification by silica gel chromatography.

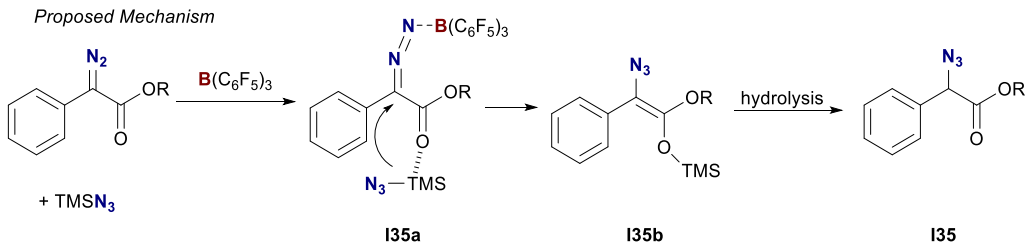

Figure 1.23: Mechanism for the synthesis of azides **I35**.

The Melen group has also recently contributed to catalytic diazoester activation by functionalising a range of heterocycles and aromatics (Figure 1.24).[43] A quick catalyst screening of $B(C_6F_5)_3$, $B(3,4,5\text{-}C_6F_3H_2)_3$ and $B(2,4,6\text{-}C_6F_3H_2)_3$ revealed $B(C_6F_5)_3$ was optimal to catalytically insert diazoesters into the C–H bonds of pyrroles and indoles (Figure 1.24a).

These reactions proceeded in a regioselective manner, as confirmed by computational calculations. Specifically, indoles would preferentially form C3 activated products **I37**.

On the other hand, pyrroles were preferentially activated at the C2 position, giving rise to **I38**. In total, 27 products were garnered in good to excellent yields (65–90%). In the case of furans, $B(2,4,6\text{-}C_6F_3H_2)_3$ was found to promote their ring-opening with nine examples of **I39** at 61–80% yield (Figure 1.24b).

Finally, the substrate scope was expanded to include $B(C_6F_5)_3$ catalysed cyclopropanation of olefins **I40** (9 examples, 70–83%), indenes **I41** (6 examples, 70–76%) and benzofuran analogues **I42** (4 examples, 78–92%) (Figure 1.24c).

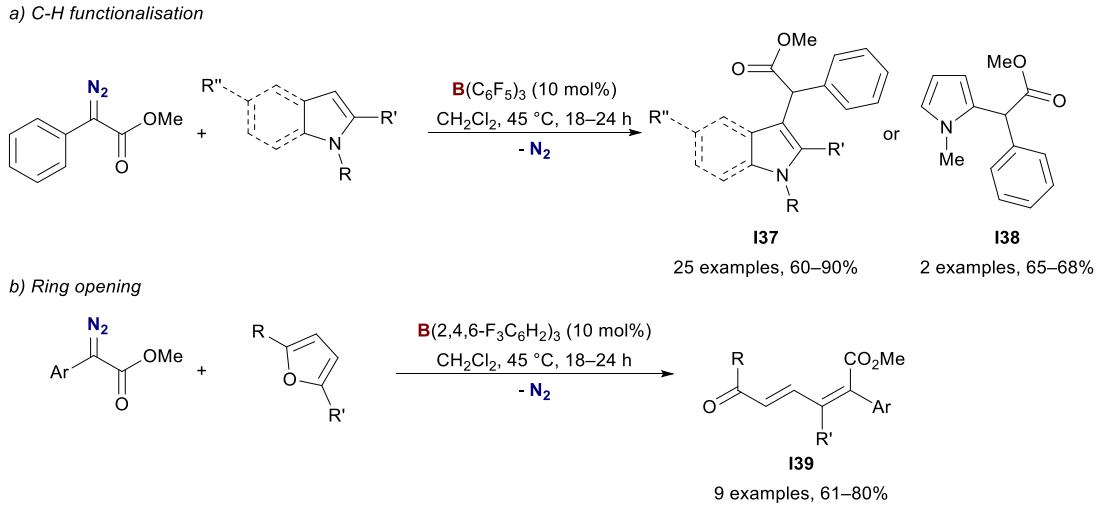

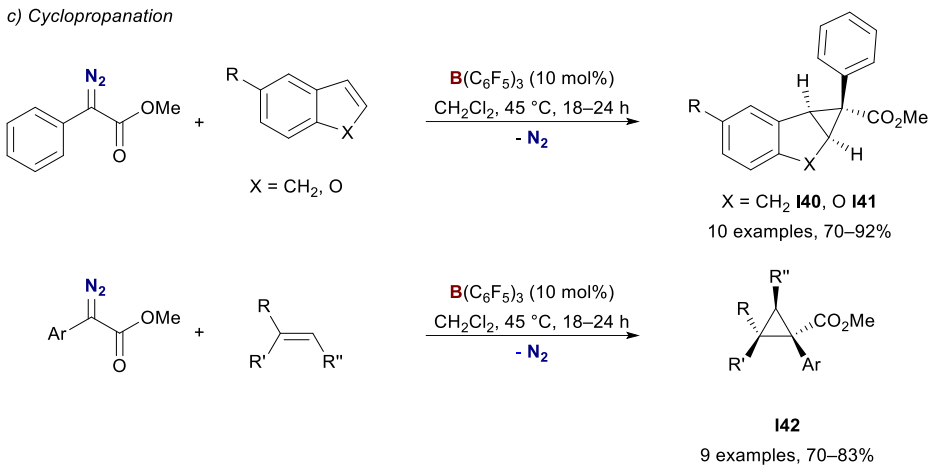

Figure 1.24: Triarylboranes employed as catalysts towards the functionalisation of aromatic compounds and heterocycles with diazoesters.

Furthermore, in an attempt to access medicinally relevant heterocycles, the Melen group has developed a procedure to generate dienes **I43** and olefins **I44**.[44] By performing mild propargylic and benzylic alkenylation reactions mediated by $B(C_6F_5)_3$, 31 products were furnished in 36–87% from diazo compounds and aryl esters (Figure 1.25).

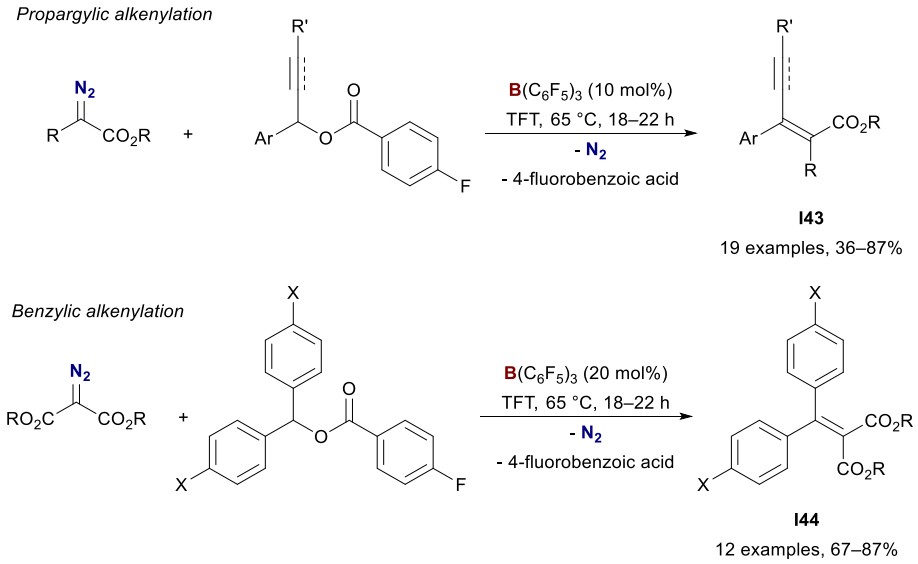

Figure 1.25: Formation of dienes **I43** and olefins **I44** by $B(C_6F_5)_3$.

Contrary to literature precedence, computational calculations revealed that the triarylborane catalyst activated the aryl ester instead of the expected diazo compound (Figure 1.26). This generated intermediate **a**, which readily rearranges due to its low energy. Concomitantly, the release of an electrophilic carbenium ion was observed, resulting in **b**. This carbenium ion is attacked by the diazo compound furnishing

intermediate **c**. Finally, an E2 type elimination is instigated by the release of $B(C_6F_5)_3$, thus forming the C–C bonded product **I43** or **I44**, in addition to by-products 4-fluorobenzoic acid and dinitrogen.

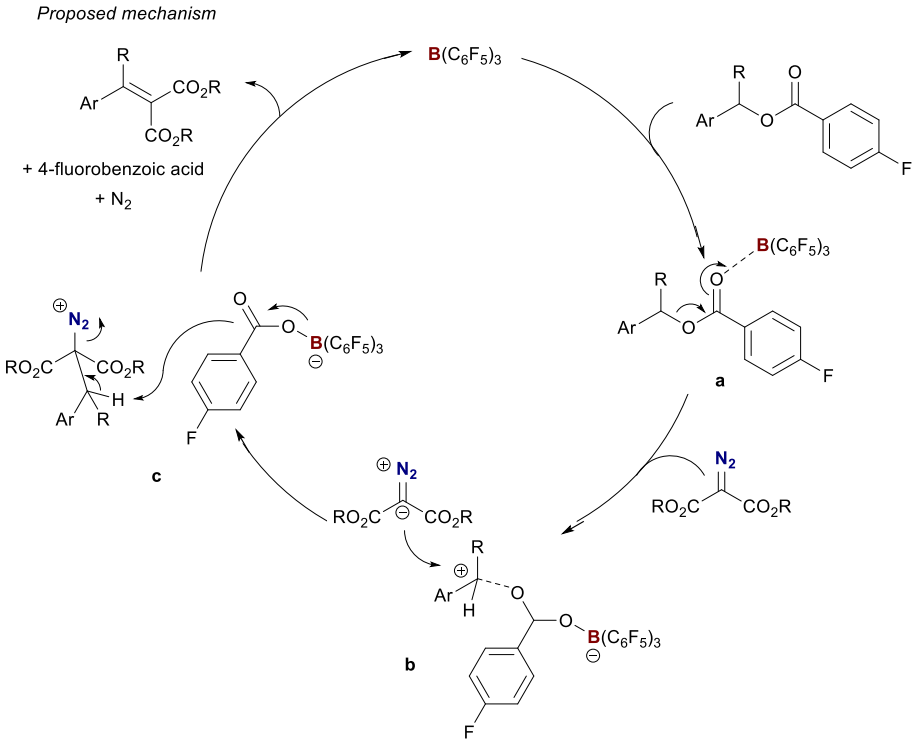

Figure 1.26: Mechanism of alkenylation reactions of aryl esters with diazo compounds facilitated by $B(C_6F_5)_3$.

In an independent study, the Wilkerson-Hill group also made brief forays into $B(C_6F_5)_3$ catalysed cyclopropanation of styrenes with diazo compounds (Figure 1.27).[45] Herein, 26 cyclopropanate olefins **I45** were furnished in good to excellent yields. The broad applicability of this methodology was demonstrated by using a variety of styrene and diazo derivatives.

Experimental probes were utilised to elucidate the reaction mechanism. To begin with, the borane catalyst activated the diazo compound, forming an adduct (**I45a**). Next, dinitrogen release generated borane-stabilised carbocation **I45b**. The addition of an appropriate styrene led to intermediate **I45c**. Finally, a concerted cycloaddition facilitated by the liberation of the catalyst yielded the desired cyclopropanate olefins **I45** (Figure 1.19).

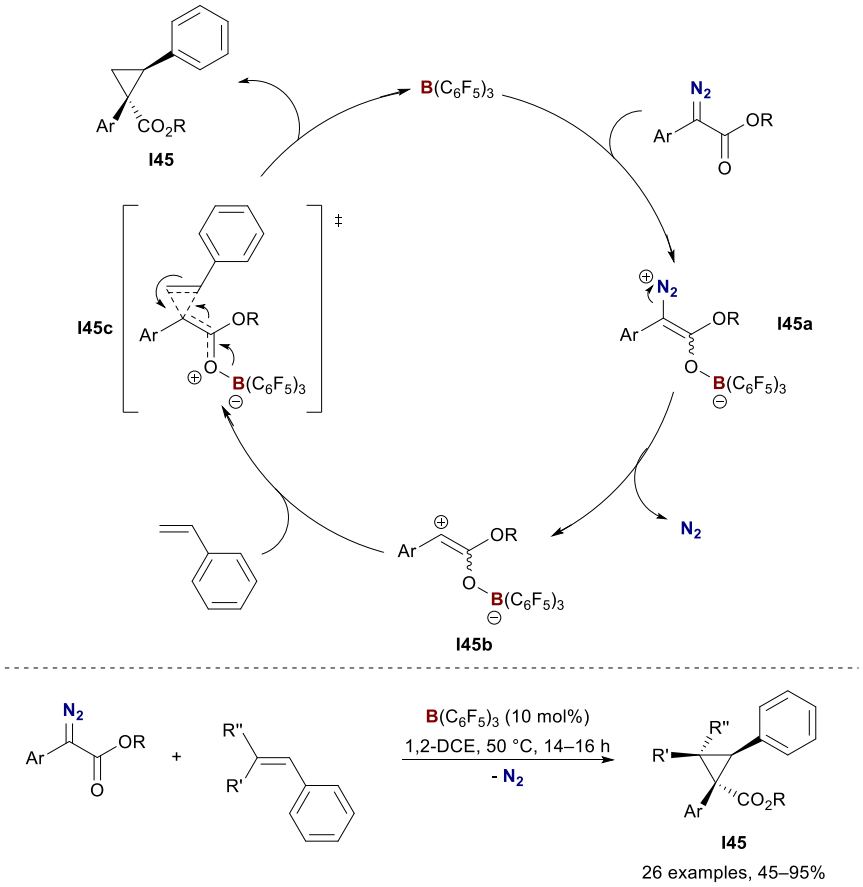

Figure 1.27: $B(C_6F_5)_3$ catalysed cyclopropanation of styrenes.

Chapter 1.3: Diazo analogues

Leading on from the success of diazo activation, numerous structural analogues have been activated using triarylboranes. Hydrazones constitute one such class of compounds. Whilst probing the reactivity of diphenyldiazomethane with $B(C_6F_5)_3$ (see Figure 1.4), the Stephan group also examined the reaction of diphenylhydrazone with this borane (Figure 1.28).[23, 24] Formation of adduct **I46** was observed upon adding a stoichiometric amount of $B(C_6F_5)_3$ to the hydrazone at room temperature. This compound featured a bond between the boron atom and the terminal nitrogen. Subsequent heating to 110 °C for 20 hours resulted in a 1,1-carboboration yielding **I47** (26% yield) via loss of pentafluorobenzene. (Figure 1.28a). These results served as the impetus behind Chapter 3 of this thesis.[46] Salt **I48** was also formed by deprotonation from the $B(C_6F_5)_3/P^tBu_3$ Frustrated Lewis Pair (FLP) (Figure 1.28b).

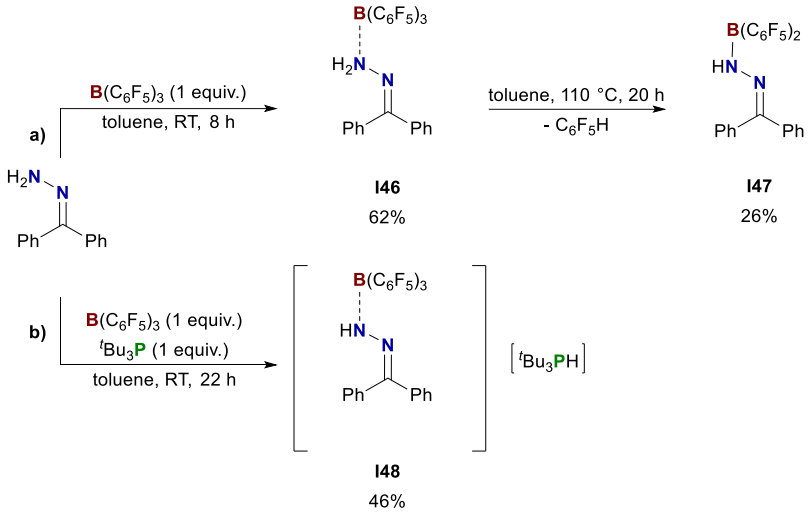

Figure 1.28: a) 1,1-carboboration of $B(C_6F_5)_3$ with diphenylhydrazone b) FLP induced deprotonation of diphenylhydrazone.

$B(C_6F_5)_3$ can also catalytically induce hydrogenative cyclisation of N-tosyl hydrazones with anilines yielding 3,4,5-triaryl-1,2,4-triazoles **I49** in an oxidant free fashion (Figure 1.29).[47] The optimal reaction conditions were established as 80 °C in benzene with a 5% catalyst loading. Thus, both symmetrical and unsymmetrical products are furnished in good to excellent yields (57–87%).

Notably, other Lewis acids were found to be inactive as catalysts. These included weaker Lewis acid and less sterically hindered BPh_3, stronger Lewis acid $BF_3{\cdot}Et_2O$ as well as traditional metal catalysts such as $Sc(OTf)_3$, $FeCl_3$ and $ZnCl_2$. Interestingly, the reaction proceeded in a chemoselective manner, with carbomethoxy- and cyano-functional groups remaining unchanged.

A mechanism was proposed based on a joint experimental and computational approach. Initially, tosylhydrazone activation by $B(C_6F_5)_3$ occurs, forming intermediate **I49a**. This intermediate undergoes a series of nucleophilic attacks, first by the aniline (**I49b**) and then by another equivalent of N-tosylhydrazone (**I49c**). Subsequently, a second equivalent of aniline induces cyclisation, forming **I49d**. The final step involves the dehydrogenation of **I49d** by an aniline·$B(C_6F_5)_3$ FLP furnishing **I49**. The hydrogenated FLP (**I49e**) released dihydrogen (**I49f**) and subsequently disassociated. Worthy of note is the dual role of $B(C_6F_5)_3$ as both a hydrazone activator to nucleophilic attack and as an FLP for the dehydrogenation step.

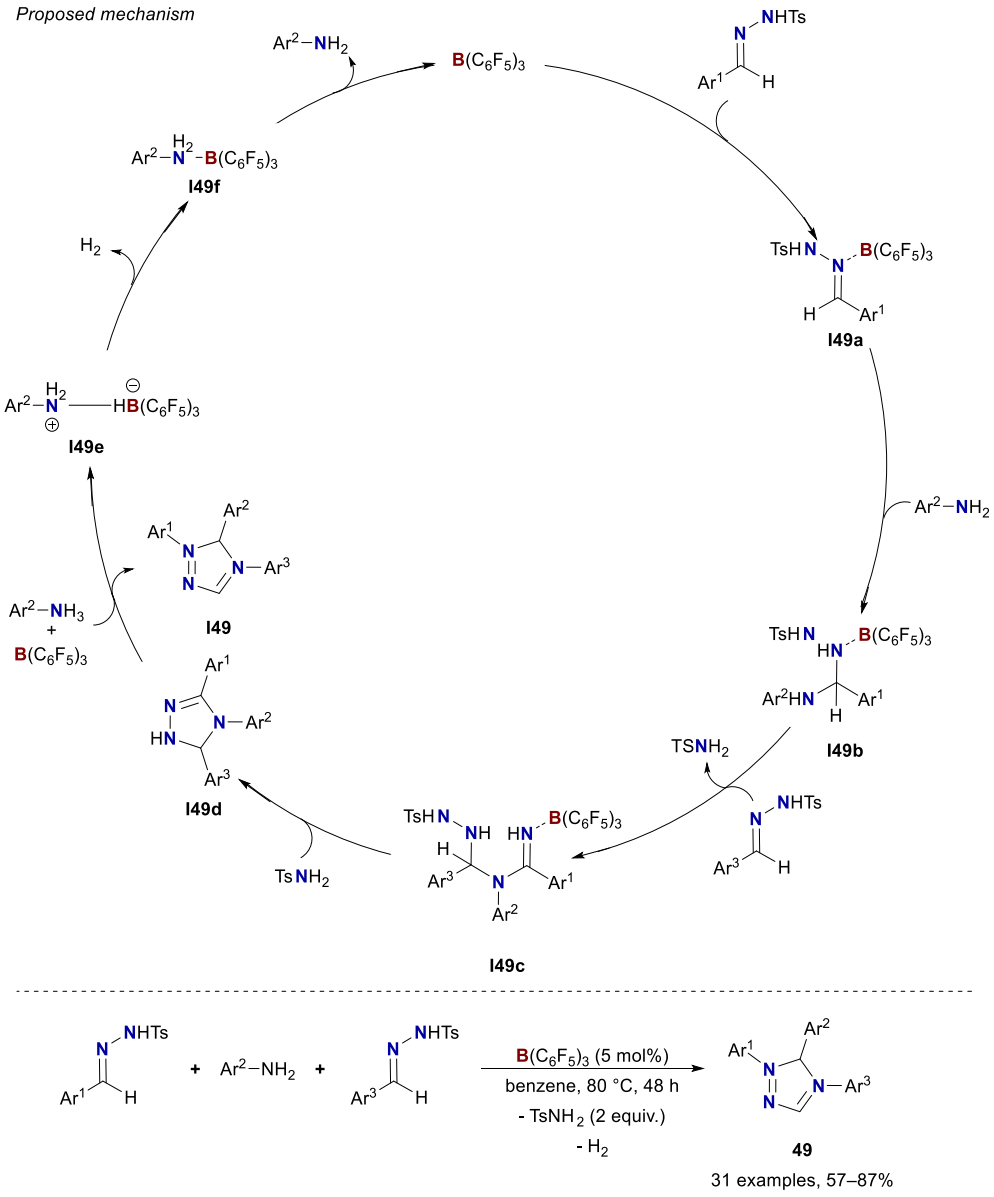

Figure 1.29: Mechanistic insights into the preparation of 3,4,5-triaryl-1,2,4-triazoles **I49**.

Recently the Schulz group has helped extend the frontiers of triarylboron driven nitrogen activation by stabilising labile moieties such as the highly toxic and explosive hydrazoic acid (HN_3) (Figure 1.30).[48] HN_3 was prepared *in-situ* and condensed onto a solution of $B(C_6F_5)_3$ in xylene, leading to adduct **I50** at -40 °C. The adduct willingly released dinitrogen at temperatures higher than -20 °C with the concomitant migration of a fluoroaryl group from $B(C_6F_5)_3$ to nitrogen yielding aminoborane **I51**. Hydrolysis of this species resulted in free amine **I52** and $B(OH)_3$.

This methodology could be adapted to substituted organic azides N_3–R [R = Ph, TMS, 3,5-$(CF_3)_2C_6H_3$].[48] Fine-tuning of the reaction conditions was required for each azide to account for their differing volatilities. The resultant adducts **I50** were characterised *in-situ* but not isolated. Nonetheless, the equivalent aminoboranes **I51** were isolated in good yields, and the subsequent hydrolysis provided a facile path to -C_6F_5 substituted secondary amines **I52** (Figure 1.30).

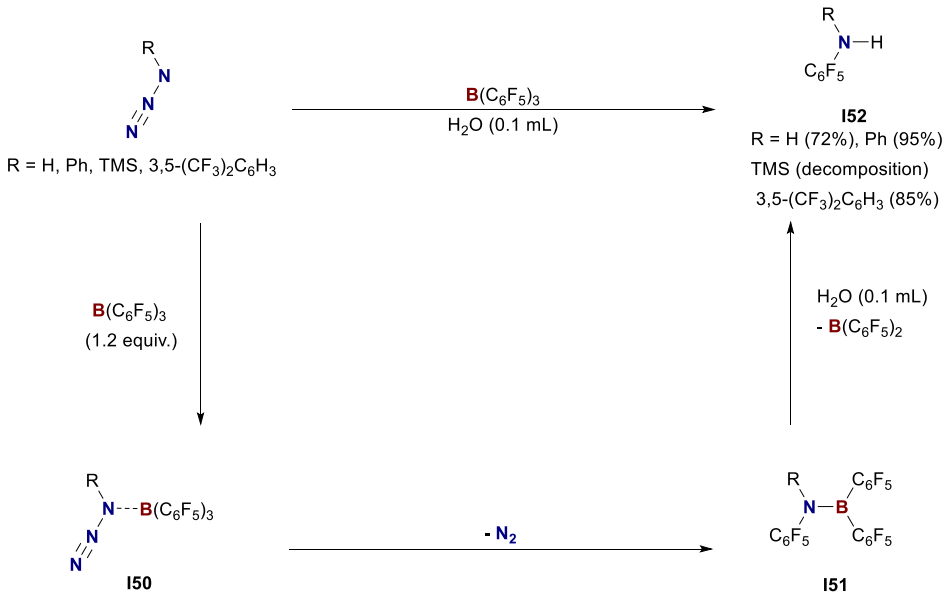

Figure 1.30: Synthesis of aryl functionalised amines from ephemeral azides.

Expanding upon this theme, the Schulz group has also coaxed ephemeral diazenes into forming adducts with $B(C_6F_5)_3$ (Figure 1.31).[49] Specific reaction conditions needed to be applied for each diazene species. For example, trans-*N,N'*-bisphenyl diazene required exposure to UV irradiation to undergo photoisomerisation to the thermodynamically favoured *cis* derivative prior to forming adduct **I53** with $B(C_6F_5)_3$.

The authors also examined *N*-phenyl diazenes with trimethylsilyl (TMS) functional groups attached.[49] The observed reactivity was dependent upon the number of TMS groups present. Consequently, an equimolar solution of *trans-N,N'*-

bis(trimethylsilyl)diazene and $B(C_6F_5)_3$ at -80 °C formed adduct **I54** after a *cis-trans* isomerisation of the starting diazene. On the other hand, *N*-phenyl-*N'*-trimethylsilyl diazene furnished **I55** via an alternate reaction pathway. $B(C_6F_5)_3$ initially induced a 1,2-TMS shift at -80 °C yielding iso-diazene adduct **I55**.

As adducts **I54** and **I55** were gradually warmed, carboboration reactions readily gave hydrazinoborane **I56**. As a side note, adduct **I55** was suggested to undergo isomerisation to an iso-diazene species prior to carboboration. However, this species could not be isolated.

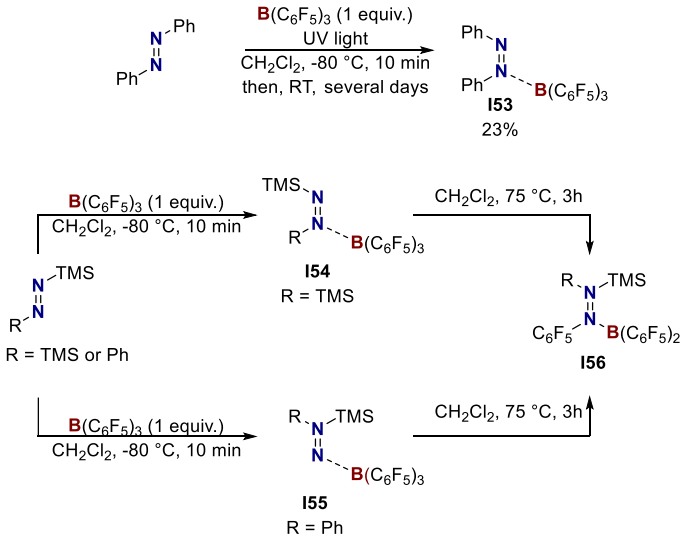

Figure 1.31: Highly transient azide and diazene species trapped and functionalised by $B(C_6F_5)_3$.

Finally, albeit outside the scope of this thesis, the Higuchi group reported the synthesis of an azide substituted triarylborane.[50] In addition, the trapping of several other short-lived nitrogen compounds using $B(C_6F_5)_3$ has been reported. These include thionylimides (H–NSO)[51] and a dimer of hydrogen cyanide.[52] However, these studies were limited in scope, and subsequent reactivity was not examined.

Chapter 1.4 Conclusions

In this Chapter, a brief foray into activating azo-containing compounds by triarylboranes has been conducted. By achieving the facile release of N_2, triarylboranes have claimed their rightful place amongst traditional transition metal azo-activators and fuelled exponential growth in the field of metal-free nitrogen activation. Thus, a plethora of stoichiometric reactions have been performed with both stabilised and non-stabilised diazo compounds. Early success has also been achieved in triarylborane catalytic activation of diazo compounds, primarily utilising the archetypal triarylborane $B(C_6F_5)_3$. These early inroads have set the stage for triarylborane activation of various diazo analogues, including hydrazones, diazenes and azides. With such a tantalising scope of potential reactivity, this thesis is devoted to pushing the frontiers of triarylborane azo activation.

Chapter 1.5 References

1 S. Khan, A. Kalemos and E. Miliordos, *J. Phys. Chem. C*, 2019, **123**, 21548.

2 L. Stein and M. Klotz, *Curr. Biol.*, 2016, **26**, R94.

3 P. Kempton, *Nature*, 1922, **110**, 805.

4 U.S. Geological Survey, Mineral commodity summaries, 2020.

5 A. Travis, Determinants in the Evolution of the European Chemical Industry, 1900–1939, *Springer*,1998, 3.

6 B. MacKay and M. Fryzuk, *Chem. Rev.*, 2004, **104**, 385.

7 N. Hazari, *Chem. Soc. Rev.*, 2010, **39**, 4044.

8 M. Fryzuk, *Chem. Commun.*, 2013, **49**, 4866.

9 I. Cheema, *Model-based analysis and optimisation of Haber-Bosch process designs for power-to-ammonia*, Cuvillier, 2019.

10 B. Smith, *Science*, 2002, **297**, 1654.

11 Y. Liu, H. Ngo, W. Guo, L. Peng, D. Wang and B. Ni, *Environment International*, 2019, **123**, 10.

12 K. Sanderson, *Nature*, 2011, **469**, 18.

13 J. Geri, J. Shanahan and N. Szymczak, *J. Am. Chem. Soc.,* 2017, **139**, 5952.

14 A. Simonneau, R. Turrel, L. Vendier and M. Etienne, *Angew. Chem. Int. Ed.*, 2017, **56**, 12268.

15 M. Légaré, G. Bélanger-Chabot, R. Dewhurst, E. Welz, I. Krummenacher, B. Engels and H. Braunschweig, *Science*, 2018, **359**, 896.

16 M. Légaré, M. Rang, G. Bélanger-Chabot, J. Schweizer, I. Krummenacher, R. Bertermann, M. Arrowsmith, M. Holthausen and H. Braunschweig, *Science*, 2019, **363**, 1329.

17 T. Ye and M. McKervey, *Chem. Rev.*, 1994, **94**, 1091.

18 G. Maas, *Chem. Soc. Rev.*, 2004, **33**, 183.

19 Y. Zhang and J. Wang, *Eur. J. Org. Chem.*, 2011, **2011**, 1015.

20 S. Müller and T. Wirth, *ChemSusChem*, 2014, **8**, 245.

21 A. Padwa, *Chem. Soc. Rev.*, 2009, **38**, 3072.

22 B. Castano, E. Gallo, D. Cole-Hamilton, V. Dal Santo, R. Psaro and A. Caselli, *Green Chem.*, 2014, **16**, 3202.

23 C. Tang, Q. Liang, A. Jupp, T. Johnstone, R. Neu, D. Song, S. Grimme and D. Stephan, *Angew. Chem. Int. Ed.*, 2017, **56**, 16588.

24 R. Melen, *Angew. Chem. Int. Ed.*, 2017, **57**, 880.

25 L. Cao, J. Zhou, Z. Qu and D. Stephan, *Angew. Chem. Int. Ed.*, 2019, **58**, 18487.

26 C. Schneider, J. LaFortune, R. Melen and D. Stephan, *Dalton Trans.*, 2018, **47**, 12742.

27 R. Neu, C. Jiang and D. Stephan, *Dalton Trans.*, 2013, **42**, 726.

28 M. Santi, D. Ould, J. Wenz, Y. Soltani, R. Melen and T. Wirth, *Angew. Chem. Int. Ed.*, 2019, **58**, 7861.

29 U. Mayer, V. Gutmann and W. Gerger, *Monatsh. Chem.*, 1975, **106**, 1235.

30 M. Beckett, G. Strickland, J. Holland and K. Sukumar Varma, *Polymer*, 1996, **37**, 4629.

31 J. Hooz and S. Linke, *J. Am. Chem. Soc.,* 1968, **90**, 5936.

32 M. Sanchez-Carmona, D. Contreras-Cruz and L. Miranda, *Org. Biomol. Chem.*, 2011, **9**, 6506.

33 Y. Luan, J. Yu, X. Zhang, S. Schaus and G. Wang, *J. Org. Chem.*, 2014, **79**, 4694.

34 S. Rao, R. Kapanaiah and K. Prabhu, *Adv. Synth. Catal.*, 2019, **361**, 1301.

35 S. Rao, P. Ashwathappa and K. Prabhu, *Asian J. Org. Chem.*, 2019, **8**, 320.

36 Z. Yu, Y. Li, J. Shi, B. Ma, L. Liu and J. Zhang, *Angew. Chem. Int. Ed.*, 2016, **55**, 14807.

37 D. Gillingham and N. Fei, *Chem. Soc. Rev.*, 2013, **42**, 4918.

38 Z. Yu, B. Ma, M. Chen, H. Wu, L. Liu and J. Zhang, *J. Am. Chem. Soc.*, 2014, **136**, 6904.

39 C. Bergquist, B. Bridgewater, C. Harlan, J. Norton, R. Friesner and G. Parkin, *J. Am. Chem. Soc.,* 2000, **122**, 10581.

40 M. Ingleson and V. Fasano, *Synthesis*, 2018, **50**, 1783.

41 H. San, S. Wang, M. Jiang and X. Tang, *Org. Lett.*, 2018, **20**, 4672.

42 H. San, C. Wang, H. Zeng, S. Fu, M. Jiang and X. Tang, *J. Org. Chem.*, 2019, **84**, 4478.

43 A. Dasgupta, R. Babaahmadi, B. Slater, B. Yates, A. Ariafard and R. Melen, *Chem.*, 2020, **6**, 2364.

44 A. Dasgupta, K. Stefkova, R. Babaahmadi, L. Gierlichs, A. Ariafard and R. Melen, *Angew. Chem. Int. Ed.*, 2020, **59**, 15492.

45 J. Mancinelli and S. Wilkerson-Hill, *ACS Cat.*, 2020, **10**, 11171.

46 T. Gazis, A. Dasgupta, M. Hill, J. Rawson, T. Wirth and R. Melen, *Dalton Trans.*, 2019, **48**, 12391.

47 M. Guru, S. De, S. Dutta, D. Koley and B. Maji, *Chem. Sci.*, 2019, **10**, 7964.

48 F. Reiß, A. Schulz and A. Villinger, *Chem. Eur. J.*, 2014, **20**, 11800.

49 K. Bläsing, J. Bresien, R. Labbow, D. Michalik, A. Schulz, M. Thomas and A. Villinger, *Angew. Chem. Int. Ed.*, 2019, **58**, 6540.

50 J. Yoshino, S. Konishi, R. Kanno, N. Hayashi and H. Higuchi, *Eur. J. Org. Chem.*, 2019, **2019**, 6117.

51 R. Labbow, D. Michalik, F. Reiß, A. Schulz and A. Villinger, *Angew. Chem. Int. Ed.*, 2016, **55**, 7680.

52 K. Bläsing, J. Bresien, R. Labbow, A. Schulz and A. Villinger, *Angew. Chem. Int. Ed.*, 2018, **57**, 9170.

A HERCULEAN TASK

How BAr_3 are Taking the Weight of Nitrogen Activation off Metals

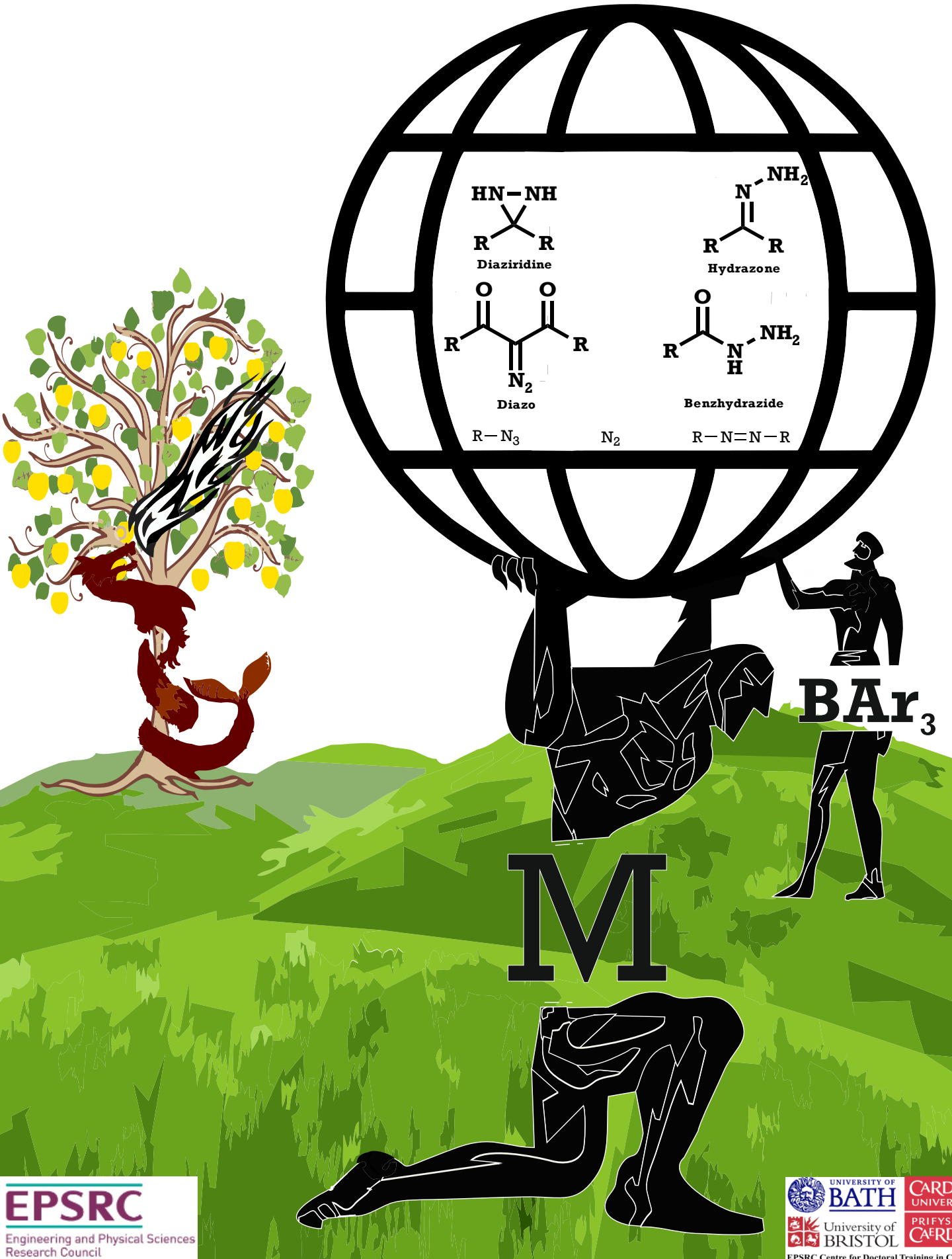

EPSRC
Engineering and Physical Sciences Research Council

UNIVERSITY OF BATH
University of BRISTOL
EPSRC Centre for Doctoral Training in C

Chapter 2: Triarylboranes

Chapter 2.1 Introduction

A detailed study into triarylborane mediated azo activation first necessitates synthesising and characterising a select few triarylborane examples (Figure 2.1). To begin with, this section introduces the primary preparation methods for the triarylboranes utilised during this thesis.

Then, with a detailed synthetic picture at hand, a brief introduction to the theory behind the core NMR nuclei utilised in this thesis (^{1}H, ^{19}F and ^{11}B) is given. Subsequently, the characteristic NMR resonances for these triarylboranes are disclosed and discussed.

Finally, as stated in the Aims section above, this thesis seeks insights into the role of triarylborane Lewis acidity on reaction outcomes. Consequently, at the end of this Chapter, the theory behind this fundamental property, the different techniques to measure it and a Lewis acidity ranking order for the triarylboranes used throughout this thesis will be presented.

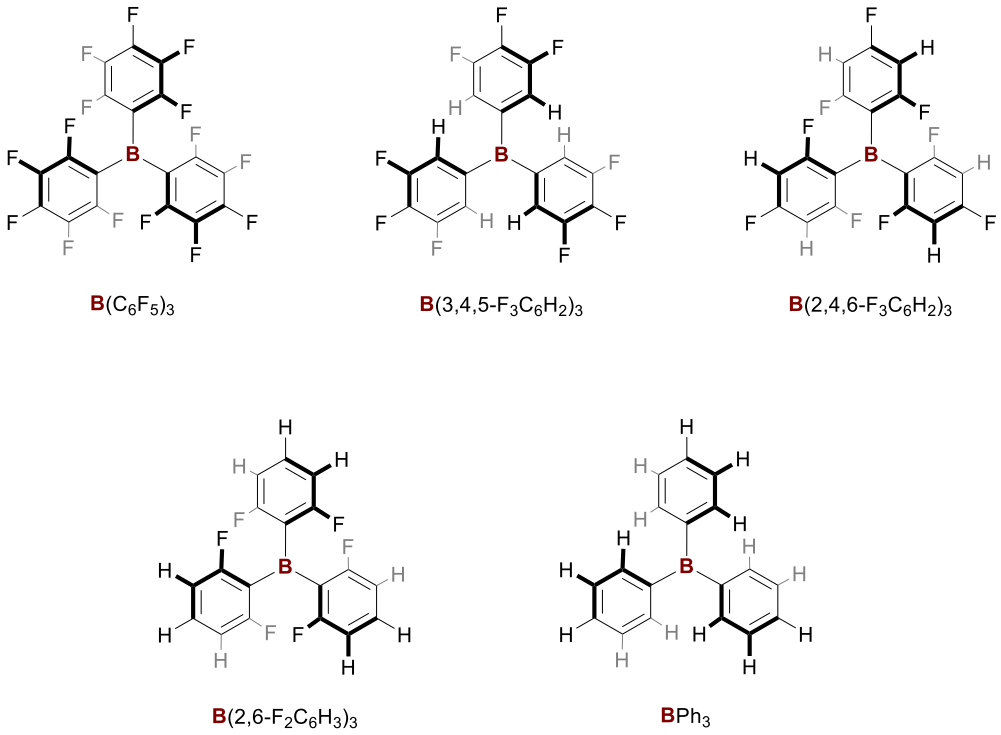

Figure 2.1: Summary of the triarylboranes used throughout this thesis.

Chapter 2.2 Synthetic strategies towards triarylboranes

The synthesis of all triarylboranes presented in this thesis relies on the same basic synthetic principle. Namely, the appropriate commercially available fluorinated bromoaryl is combined with $BF_3{\cdot}Et_2O$ in a 3:1 ratio under rigorous exclusion of water. Albeit minor adjustments are required for certain derivatives, the triarylboranes are generated using either the lithiation or the Grignard method. Experimental details are presented below.

2.1.1 The lithiation method

The generation of $B(3,4,5\text{-}F_3C_6H_2)_3$ via the lithiation method exemplifies this methodology (Figure 2.2)[1]. To a solution of 5-Br-1,2,3-$F_3C_6H_2$ (1 equiv.) in Et_2O, a 1.47M ^{n}BuLi in hexane solution (1 equiv.) was added dropwise at -78 °C. The resultant yellow solution was stirred until it converted to a white suspension (roughly 90 minutes), carefully maintaining the temperature below -50 °C. Subsequently, 0.33 equivalents of $BF_3{\cdot}OEt_2$ were added slowly. The mixture was allowed to warm to room temperature and stirred for five to twelve hours. Upon isolating the crude solid residue by removing the solvent *in vacuo*, it was subjected to a two-fold sublimation using a variable temperature Kugelrohr glass oven. Thus, $B(3,4,5\text{-}F_3C_6H_2)_3$ was isolated as a white crystalline solid in yields ranging from 12–25%.

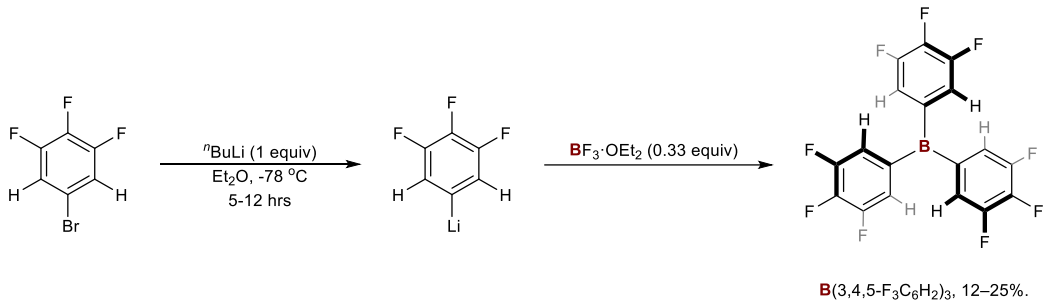

Figure 2.2: Synthesis of $B(3,4,5\text{-}F_3C_6H_2)_3$ utilising the lithiation method.

This procedure has several distinct advantages over its Grignard counterpart. The reaction is faster to set up, workup and purify, thus allowing for pure product isolation within a day. In addition, there are fewer by-products generated, thus easing purification and isolation. However, caution must be exercised when employing this procedure with bromofluoroaryls possessing ortho- fluorine substituents to the bromine functionality. In these cases, the ephemeral lithiated fluoroaryl intermediate is susceptible to ortho-halogen lithium elimination to generate a benzyne species (Figure 2.3). The explosive and unpredictable character of benzyne intermediates is

an unnecessary risk that must not be ignored. Even at the very low temperatures employed for this synthesis, there have been reports of explosions. [2]

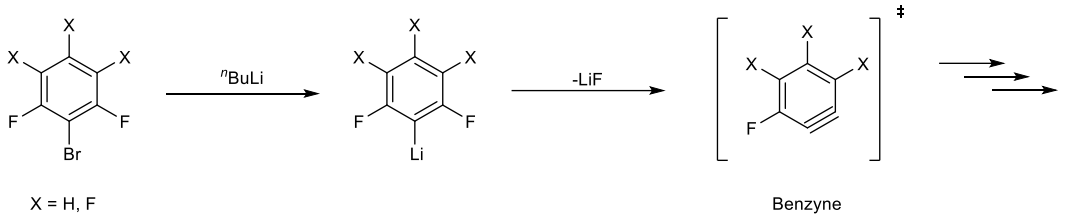

Figure 2.3: A potentially explosive aryne intermediate is generated by ortho-halogen lithium elimination.

2.1.2 The Grignard method

A safer procedure for ortho-bromofluoroaryl derivatives is the Grignard reaction (Figure 2.4). Two variations were utilised in this thesis.

For $B(C_6F_5)_3$, *in-situ* generation of the Grignard reagent is recommended. For the purposes of this thesis, the preparation first reported by Lancaster was applied.[3] Initially, C_6F_5Br is added dropwise to magnesium turnings suspended in diethyl ether whilst preventing reflux from occurring. After stirring the black mixture for 30 minutes at room temperature, it was transferred via filter cannula to a solution of $BF_3{\cdot}OEt_2$ in toluene. Subsequently, diethyl ether is removed *in vacuo*. Removing all ethereal solvent is crucial to ensure the appropriate temperature is reached in the next step and prevent the formation of the inseparable side product $(Et_2O)B(C_6F_5)_2F$.[3] Upon allowing the mixture to stir at 100 °C overnight, all volatiles are removed *in vacuo*. The resultant brown cake was subjected to a two-fold sublimation using either a standard glass sublimator or a variable temperature Kugelrohr glass oven. Finally, the desired product is collected as a white microcrystalline solid with yields in the range of 63–88%.

The two remaining boranes can be formed via an expedited Grignard transfer process.[4] Using $B(2,4,6\text{-}F_3C_6H_2)_3$ as an example, 2-Br-1,3,5-$F_3C_6H_2$ (1 equiv.) is suspended in freshly distilled tetrahydrofuran (100 mL) and cooled to -20 °C. An excess of 2M ^{i}PrMgCl in tetrahydrofuran is added dropwise. After stirring the solution at 0 °C for one hour, $BF_3{\cdot}Et_2O$ (0,.33 equiv.) was added at -50 °C. Gradual warming for one hour was followed by stirring at room temperature for an additional hour. Solvent removal *in vacuo* afforded a pale white cake. The derivative was obtained as a white powder in 72–83% yields upon a twofold sublimation. $B(2,6\text{-}C_6F_2H_3)_3$ was furnished as a white microcrystalline solid in 53–66% yield.

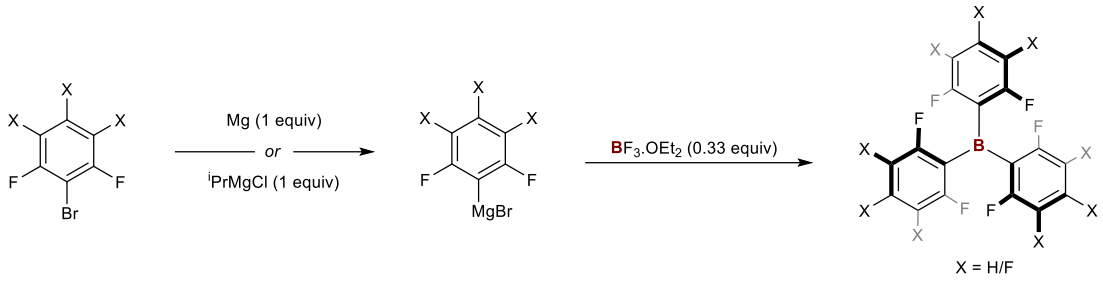

Figure 2.4: The synthesis of $B(C_6F_5)_3$, $B(2,4,6\text{-}F_3C_6H_2)_3$ and $B(2,6\text{-}C_6F_2H_3)_3$.

Chapter 2.3 NMR analysis of triarylboranes

2.3.1 NMR theory

For all triarylboranes and most products, multinuclear NMR analyses proved essential to confirm their formation. Albeit final structural assignment rested with single crystal X-ray diffraction, especially when the reaction outcome was uncertain, NMR spectroscopy was the first analytical technique employed following product preparation. In this thesis, NMR spectroscopy heavily relied on three nuclei: ^{1}H, ^{11}B and ^{19}F.

The theory behind ^{1}H NMR spectroscopy has been extensively covered elsewhere and is well understood.[5] Although broadly similar, the behaviour of the ^{1}H nuclei under a magnetic field shows several critical differences compared to heavier counterparts. The most noteworthy is the difference in measuring the chemical shift environments. For all nuclei under a magnetic field, all wave functions in the ground and excited states must be considered when calculating the chemical shift.

However, for a ^{1}H NMR spectrum, the signal positions are almost exclusively influenced by the value of the diamagnetic shielding constant (σd), a tensor sensitive to the electron-withdrawing or donating properties of adjacent substituents. For heavier nuclei, including ^{11}B and ^{19}F, the paramagnetic shielding tensor (σρ) needs to be considered as well when calculating signal location. σp is responsible for calculating the total circulation of electrons in the ground state and higher energy states caused by the NMR machine's magnetic field. Thus, signal location is not only influenced by the electron-withdrawing and donating properties of neighbouring substituents but also by the coordination geometry, the electron density surrounding the core nuclei and the degree of π-bonding.[6]

With this distinction in mind, a closer look at the key properties of boron NMR spectroscopy is warranted.[6] Boron is an NMR active, quadrupolar nuclei possessing nuclear spins (*I*) greater than 1/2 for both naturally occurring boron isotopes, ^{10}B (*I* = 3) and ^{11}B (*I* = 3/2). Due to this quadrupolar moment, line broadening is inevitable, with the fine structure of signals often being obscured. As a result, signals often appear as broad singlets.

Out of the two isotopes, ^{11}B is the nuclide of choice for NMR spectroscopy, thanks to several factors. These include its lower magnetic spin, higher natural abundance of 80% (*cf.* 20% for ^{10}B), higher gyromagnetic ratio (γ) of 13.7 MHz/T, its lower quadrupolar moment and better resolution.

^{11}B also exhibits relatively high receptivity (970 times higher than ^{13}C). In addition, unlike the narrow spectral width of ^{1}H NMR spectra (δ = 14–0 ppm), $^{11}B\{^{1}H\}$ NMR spectra display a broad chemical shift range from δ = +250 to -250 ppm.

Under ideal circumstances and while avoiding sample saturation, the peak area of the chemical shifts is equivalent to the number of boron atoms present. However, in the context of this thesis, $^{11}B\{^{1}H\}$ NMR spectroscopy was used in a more quantitative fashion to accrue three pieces of information for both the starting triarylboranes and their products:

a) To verify complete consumption of the starting material had occurred and determine whether a single boron-containing product had been obtained upon product purification.

b) To calculate the reaction timescale as revealed by the disappearance of the chemical resonance corresponding to the parent triarylborane.

c) To differentiate between tri- and tetracoordinate boron species. On electronegativity grounds, both classes of compounds are expected at low resonances (δ = 10 to 0 ppm). However, for trivalent species, the π-bonding aptitude of the ligands is sufficient to push chemical shifts to higher resonance values. This is an effect observed and exploited throughout this thesis. For example, the characteristic resonance of tricoordinate $B(C_6F_5)_3$ appears at δ = 58.6 ppm. However, tetracoordinate $B(C_6F_5)_3$ adducts, such as those in Figure 2.5, appear at a significantly more upfield position (close to δ = 0 ppm).

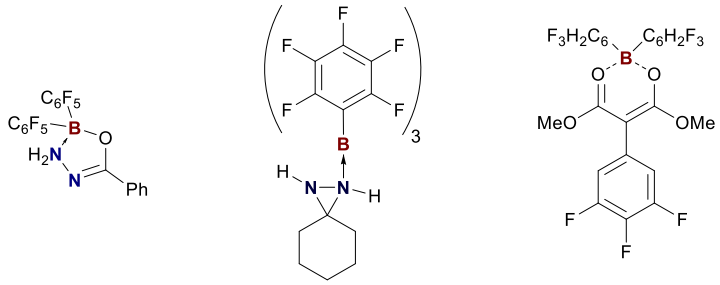

8
-4.3 ppm

13a
-6.43 ppm

19b
7.48 ppm

Figure 2.5: Illustrative tetracoordinate boron species and their $^{11}B\{^{1}H\}$ NMR resonances.

Given the above statements, it is evident that $^{11}B\{^{1}H\}$ NMR spectroscopy is insufficient to confirm a given structural assignment. NMR studies on additional magnetically active nuclei in the same molecule are necessary. The presence of fluorine atoms on the aryl rings of the triarylboranes allows for ^{19}F NMR spectra to act as a useful chemical probe. This fact was fully exploited throughout Chapter 5.

The ^{19}F nuclei bears many similarities to ^{1}H. It is monoisotopic in nature, possesses a nuclear spin of I = 1/2 and a large gyromagnetic ratio (40.08 MHz/T). This results in very high receptivity relative to other NMR active nuclei (0.83 relative to ^{1}H). Finally, reliable integration values can be obtained thanks to the high relaxation times this nucleus possesses. When this is coupled with the vast range of possible chemical shifts, overlapping signals are a rare occurrence. [7]

2.3.2 Characteristic NMR values of triarylboranes

Where $^{11}B\{^{1}H\}$ NMR spectroscopy is concerned, all triarylborane signals appeared as broad singlets in the δ = 55–70 ppm range. This relatively high downfield position ensured no overlap with the tetracoordinate products generated in the following chapters. This feature, in turn, allowed for easy distinction between starting material and product.

The lack of hydrogen nuclei in $B(C_6F_5)_3$ rendered ^{1}H NMR spectroscopy of little use to confirm product formation. For the remainder of the triarylboranes, a very distinct resonance at the 6–8 ppm range corresponded to the aryl protons of the triarylborane. Using $B(2,4,6\text{-}F_3C_6H_2)_3$ as an example, the ^{1}H NMR spectrum displays a broad doublet of doublets at δ = 6.64 ppm with a coupling constant value of $^{3}J_{FH}$ = 14 Hz.

A clear downfield chemical shift was visible for all triarylboranes in the ^{19}F NMR spectra compared to the bromofluoroaryl precursor resonances. This is a result of the boron nuclei reducing electron density. Thus, the fluorine atoms are deshielded, and their resonances are pushed downfield. Accordingly, for $B(2,4,6\text{-}F_3C_6H_2)_3$, two resonances were present at δ = -95.74 and -100.30 ppm with an integration ratio of 2:1. The NMR spectra of $B(2,4,6\text{-}F_3C_6H_2)_3$ are presented below for reference.

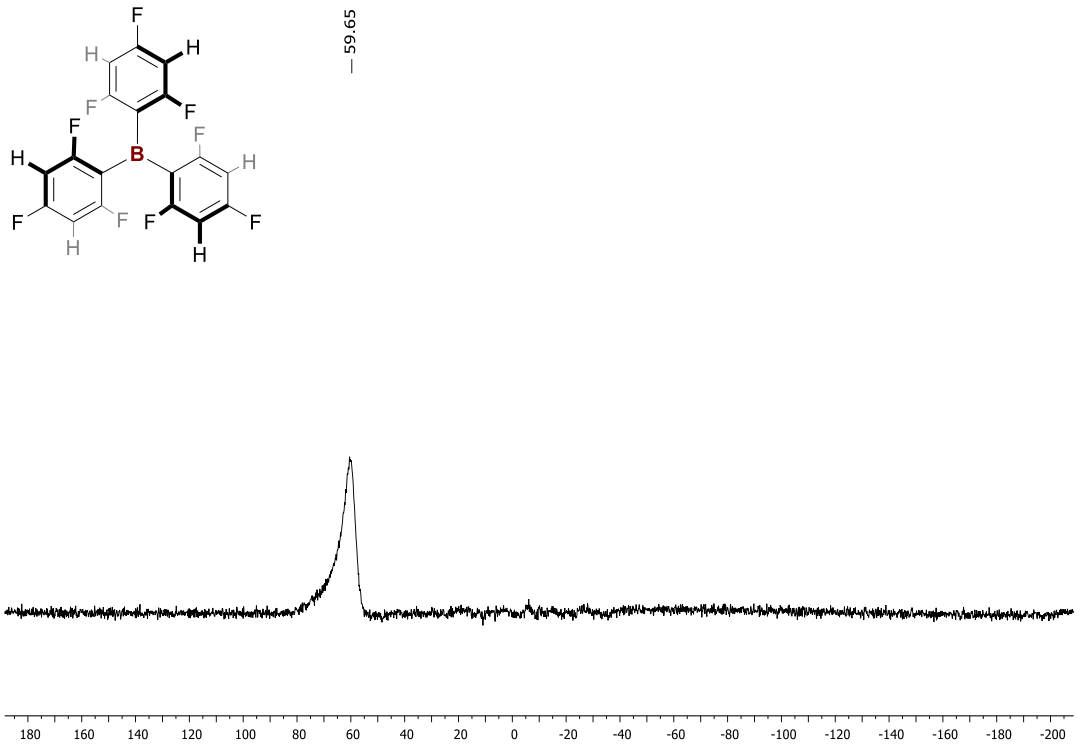

Figure 2.6: $^{11}B\{^{1}H\}$ NMR (160 MHz, $CDCl_3$, 298 K) spectrum of $B(2,4,6\text{-}F_3C_6H_2)_3$.

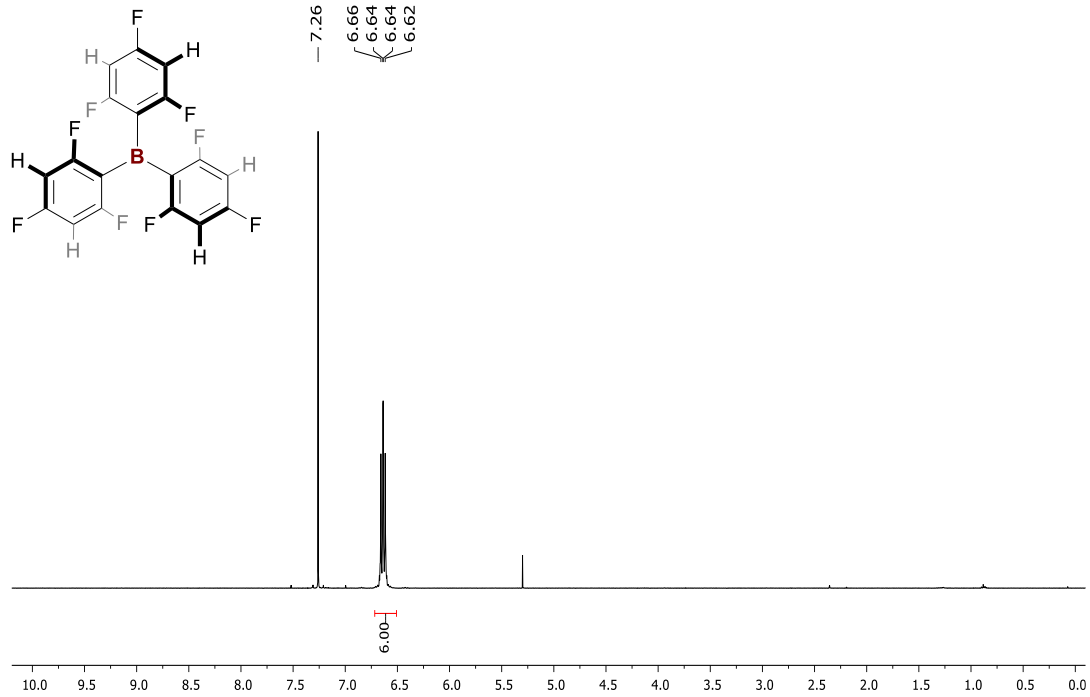

Figure 2.7: ^{1}H NMR (500 MHz, $CDCl_3$, 298 K) spectrum of $B(2,4,6\text{-}F_3C_6H_2)_3$.

Figure 2.8: ^{19}F NMR (471 MHz, $CDCl_3$, 298 K) spectrum of $B(2,4,6\text{-}F_3C_6H_2)_3$.

Chapter 2.4 Triarylborane Lewis acidities

Commercially available $B(C_6F_5)_3$ is widely recognised as the archetypal triarylborane and often the first port of call when using triarylboranes in azo activation. Unfortunately, its high Lewis acidity presents some drawbacks, such as coordination to sterically uncongested, electron-donating functionalities. These include ketones, amines and (thio)ethers amongst others and inevitably leads to catalyst poisoning.[8] However, by reducing the number of fluorine atoms on the aryl rings, boranes exhibiting reduced Lewis acidity can be generated. This reduction in Lewis acidity offers greater functional group tolerance on a case-by-case basis.

As an overarching aim of this thesis is to explore the effect of triarylborane Lewis acidity on reactivity, reaction rates, product yields and other factors, a brief primer on calculating this fundamental property would be pertinent.

The list of acidity measuring techniques is large and ever-expanding. However, the different acidity metrics can broadly be placed in three categories: effective, global and intrinsic metrics.[9]

Effective metrics are indirect methodologies relying on the effect a Lewis acid has on the spectroscopic properties of a probe molecule. The Childs and Gutmann-Beckett (GB) techniques make up this category.[10, 11, 12] In the Childs method, coordination of the Lewis acid to crotonaldehyde (probe molecule) results in a resonance shift of the H^3 proton visible in the ^1H NMR spectrum. The relative acidity can be determined by comparing this signal shift to the shift BBr_3 generates (set to 1.0) (Figure 2.9a). The GB method relies on the formation of a Lewis acid-base complex between triethylphosphine oxide (Et_3PO) and the borane. Boranes coordinate to the Lewis basic oxygen in Et_3PO, thus resulting in deshielding of the neighbouring phosphorus atom. This coordination directly translates to a shift in resonance in the ^{31}P NMR spectrum. This shift is fed into an equation to calculate the acceptor number (AN) for that borane (Figure 2.9b).

Global metrics utilise computational methods to gain insights into the whole procedure of adduct formation. The two most widely used examples of this method are the Hydride Ion Affinity (HIA) and the Fluoride Ion Affinity (FIA) method.[13, 14] The advantage of these methodologies is that they allow the determination of thermodynamic outputs such as intramolecular coordination in the initial Lewis acid

(Eintra), deformation energies and preorganisation (Eprep) in addition to the immediate interaction energy (Einter).

HIA relies on calculating the isodesmic reaction between superhydride and the borane in question (Figure 2.9c). In contrast, FIA calculates the change in enthalpy upon the complexation of a fluoride anion (generated from a fluorophosgene precursor) to a free gaseous Lewis acid (Figure 2.9d).

The final category comprises intrinsic metrics, which allow for examination of the electronic structure of the free Lewis acid. They utilise a combination of quantum-theoretical numbers and spectroscopy. The most important example of this category is the Global Electrophilicity Index (GEI).[15] This technique relies on the tendency of a molecule to take up electrons, thus eliminating the need for a Lewis base.

It is clear that the variations in measuring techniques will affect the Lewis acidity metrics for each triarylborane. However, these discrepancies are minor, with most metrics showing good agreement.

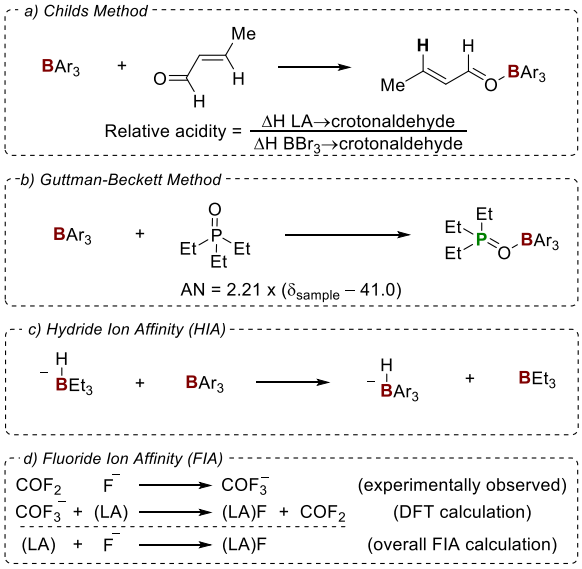

Figure 2.9: Established techniques to determine the Lewis acidity of boranes.

With the above information at hand, the Lewis acidity of the triarylboranes in this thesis can be calculated. A quick literature review reveals the Gutmann-Beckett values for all triarylboranes. By setting the Lewis acidity of $B(C_6F_5)_3$ as 1, comparisons can be drawn.

Five boranes are furnished by removing two fluorine substituents from each of the perfluorinated rings; however, only two of them are relevant for this thesis: B(3,4,5-$F_3C_6H_2)_3$[16] and B(2,4,6-$F_3C_6H_2)_3$.[17] The Lewis acidity of B(3,4,5-$F_3C_6H_2)_3$ was found to closely correspond to that of $B(C_6F_5)_3$ with a relative Lewis acidity of 103%, whereas B(2,4,6-$F_3C_6H_2)_3$ was 70% as Lewis acidic. [17]

Further reduction of fluorine substituents to two per aryl ring leads to B(2,6-$F_2C_6H_3)_3$. This borane also exhibits a reduced Lewis acidity with respect to $B(C_6F_5)_3$ (56%).[17] Finally, BPh_3 has a Lewis acidity of 59% in comparison to $B(C_6F_5)_3$.[18]

Chapter 2.5 Conclusions

This Chapter revealed the library of triarylboranes utilised throughout this thesis, focusing on their synthesis, NMR analysis, and Lewis acidity. Synthesis relied on three reaction protocols. Firstly, the lithiation method afforded $B(3,4,5\text{-}F_3C_6H_2)_3$ in a clean and facile manner. Where this procedure was deemed too hazardous to employ, the Grignard reaction was applied instead. Thus, $B(C_6F_5)_3$ was furnished using *in-situ* generated C_6F_5MgBr as a substrate. On the other hand, a more straightforward Grignard transfer process successfully yielded the derivatives $B(2,4,6\text{-}F_3C_6H_2)_3$ and $B(2,6\text{-}C_6F_2H_3)_3$.

Regarding characterisation, a brief theoretical overview of the properties of the three primary NMR nuclei used in this thesis, namely ^{11}B, ^{1}H and ^{19}F, was presented. Subsequently, typical resonance, multiplicities and integrations for each triarylborane were analysed and summarised in Section 2.3.2.

Finally, various Lewis acidity measurements applicable to triarylboranes were introduced and categorised as either effective, global or intrinsic. The triarylboranes encountered herein were placed on a Lewis acidity scale (see Table 2.1).

With these starting materials prepared and their main properties analysed, studies into azo activation with triarylboranes could begin in earnest. Table 2.1 contains all triarylboranes used in this thesis with their most important synthetic and analytical characteristics.

Table 2.1: Summary of key properties of the triarylboranes used in this thesis.

	$^{11}B\{^{1}H\}$ NMR resonance	^{19}F NMR resonances	^{1}H NMR resonances	Rel. Lewis acidity
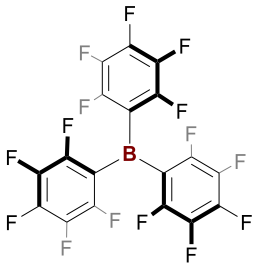	58.6 ppm	-27.87 ppm -42.68 ppm -59.99 ppm	N/A	100%
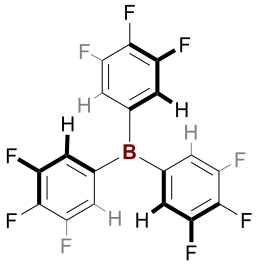	65.9 ppm	-33.18 ppm -52.38 ppm	7.20–7.13 ppm	103%
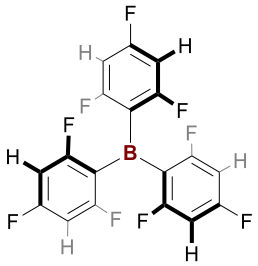	59.6 ppm	-95.74 ppm -100.30 ppm	6.64 ppm	70%
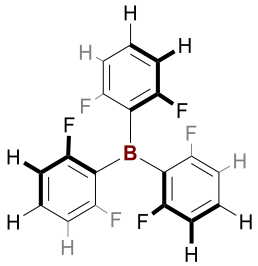	63.2ppm	-100.46	7.42–7.35 ppm	56%
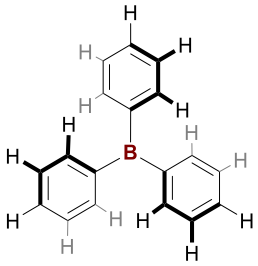	60.3 ppm	N/A	-6.2 ppm	59%

Chapter 2.6 References

1 M. Santi, D. Ould, J. Wenz, Y. Soltani, R. Melen and T. Wirth, *Angew. Chem. Int. Ed.*, 2019, **58**, 7861.

2 E. Delany, S. Kaur, S. Cummings, K. Basse, D. Wilson and J. Dutton, *Chem. Eur. J.*, 2019, **25**, 5298.

3 S. Lancaster, *ChemSpider SyntheticPage*s, 2003.

4 T. Gazis, A. Dasgupta, M. Hill, J. Rawson, T. Wirth and R. Melen, *Dalton Trans.*, 2019, **48**, 12391.

5 K. Wong, *J. Chem. Educ.*, 2014, **91**, 1103.

6 H. Nöth.and B. Wrackmeyer, *Nuclear Magnetic Resonance Spectroscopy of Boron Compounds*, Spinger Berlin, 1978.

7 T. Claridge, *High-Resolution NMR Techniques in Organic Chemistry (Third Edition)*, Routledge, 2016.

8 M. Ingleson and V. Fasano, *Synthesis*, 2018, **50**, 1783.

9 L. Greb, *Chem. Eur. J.*, 2018, **24**, 17881.

10 U. Mayer, V. Gutmann; W. Gerger, *Monatsh. Chem.*, 1975, *106*1235.

11 M. Beckett, G. Strickland, J. Holland, K. Varma, *Polymer*, 1996, **37**, 4629

12 R. Childs, D. Mulholland, A. Nixon, *Can. J. Chem.*, 1982, ***60***, 801.

13 K. Christe, D. Dixon, D. McLemore, W. Wilson, J. Sheehy and J. Boatz, *J. Fluor. Chem.*, 2000, **101**, 151.

14 M. Mock, R. Potter, D. Camaioni, J. Li, W. Dougherty, W. Kassel, B. Twamley and D. DuBois, *J. Am. Chem. Soc.*, 2009, **131**, 14454.

15 A. Jupp, T. Johnstone and D. Stephan, *Dalton Trans.*, 2018, **47**, 7029.

16 Y. Soltani, S. Adams, J. Börger, L. Wilkins, P. Newman, S. Pope and R. Melen, *Dalton Trans.*, 2018, **47**, 12656.

17 J. Nicasio, S. Steinberg, B. Inés and M. Alcarazo, *Chem. Eur. J.*, 2013, **19**, 11016.

18 A. Saida, A. Chardon, A. Osi, N. Tumanov, J. Wouters, A. Adjieufack, B. Champagne and G. Berionni, *Angew. Chem. Int. Ed.*, 2019, **58**, 16889.

Chapter 3 Activation of hydrazides and hydrazones with Lewis acidic boranes

Chapter 3.1 Introduction

Chapter 1 demonstrated the prowess of triarylboranes as azo activators in stoichiometric and catalytic reactions using a multitude of diazo compounds and analogues.[1] Of particular importance was the work of the Stephan group on the liberation of N_2 from Ph_2CN_2 (*cf.* Figure 1.4). Furthermore, when using Ph_2CNNH_2 as a substrate, adduct formation and aryl elimination occurred (*cf.* Figure 1.20).[2] Both reactions were facilitated by $B(C_6F_5)_3$, the typical triarylborane employed in azo activation.

The use of different triarylboranes in this area has been limited, as illustrated in the introduction. The Melen group has had a keen interest in exploring the effect triarylborane Lewis acidity has on reaction rates and yields, amongst other factors. On a few occasions, divergent reactivity has been observed depending on the triarylborane species utilised.[3]

In this regard, this Chapter focuses on exposing triarylboranes, including but not limited to $B(C_6F_5)_3$, to a variety of hydrazones and hydrazides (Figure 3.1).[4] It was envisaged that these might provide alternative reactivity and reaction rates depending upon the Lewis acidity of the triarylborane as previously observed with diazo compounds.[3]

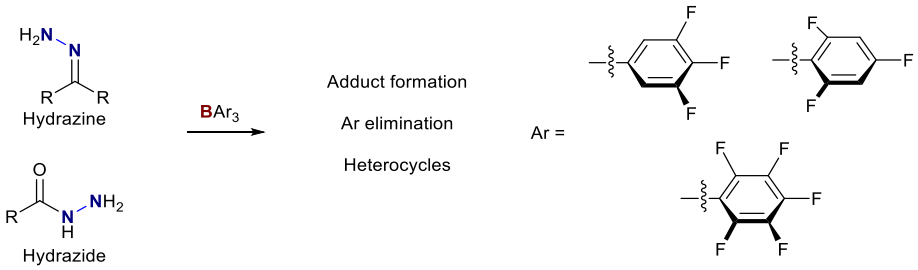

Figure 3.1: Summary of results obtained in this Chapter.

Chapter 3.2: Synthesis and NMR analysis of precursor 1 and hydrazones 3a–3c

Synthesis of bis-hydrazone **2c** first required the generation of the appropriate starting ketone (**1**).[5] In this regard, a suspension of terrephthaloyl chloride in dry benzene was added portion-wise to a slight excess of $AlCl_3$ in benzene, and the reaction mixture was brought to reflux for two hours. The title compound was isolated as a white powder in 63% yield upon performing an aqueous workup. Proof of successful synthesis was sought through ^1H NMR spectroscopy. Good agreement with literature reported values was achieved,[5] with the observed aromatic signals at δ = 7.89 ppm (singlet), 7.85–7.84 ppm (multiplet) and 7.65–7.62 ppm (singlet) collectively integrating to fourteen protons, as expected.

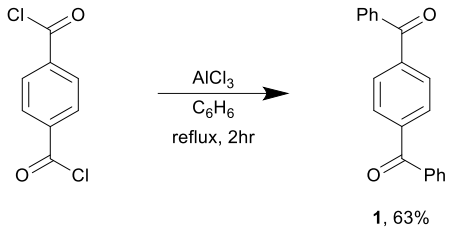

Figure 3.2: Synthesis of ketone precursor **1**.

Benzhydrazide (**2d**) was available commercially. The synthesis of the remaining three non-commercial hydrazones used in this study (**2a–2c**) was conducted similarly to that described by Fu *et al.* (Figure 3.3).[6] The appropriate ketone was added to a stirred solution of excess hydrazine monohydrate in ethanol. Catalytic amounts of acetic acid were introduced dropwise, and the reaction mixture was heated at reflux for twelve hours. The resultant solid was washed with water followed by pentane to afford the desired product upon drying *in vacuo*.

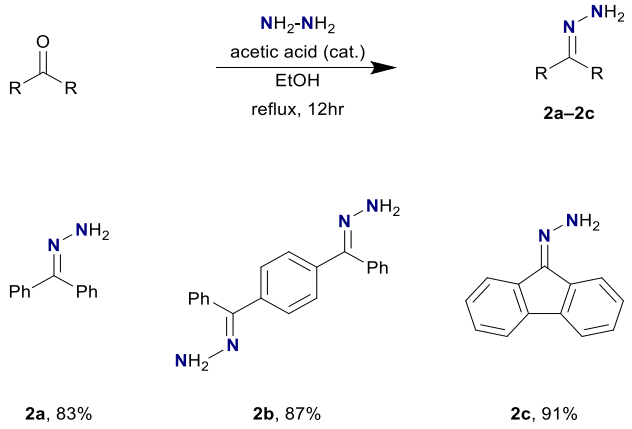

Figure 3.3: Generation of starting materials **2a–2c**.

The formation of the desired starting materials was once more confirmed by ^{1}H NMR spectroscopy, where the appearance of a new singlet signal with an integration of two was visible.[6, 7] This corresponded to the amide –NH_2 moiety. Using **2a** as an example, the expected multiplets at δ = 7.33–7.30 ppm (2H), 7.26–7.23 ppm (3H) and 7.09–7.04 ppm (5H) of the two phenyl rings were present alongside a new singlet at δ = 5.21 ppm with an integration of two belonging to the –NH_2 functional group.

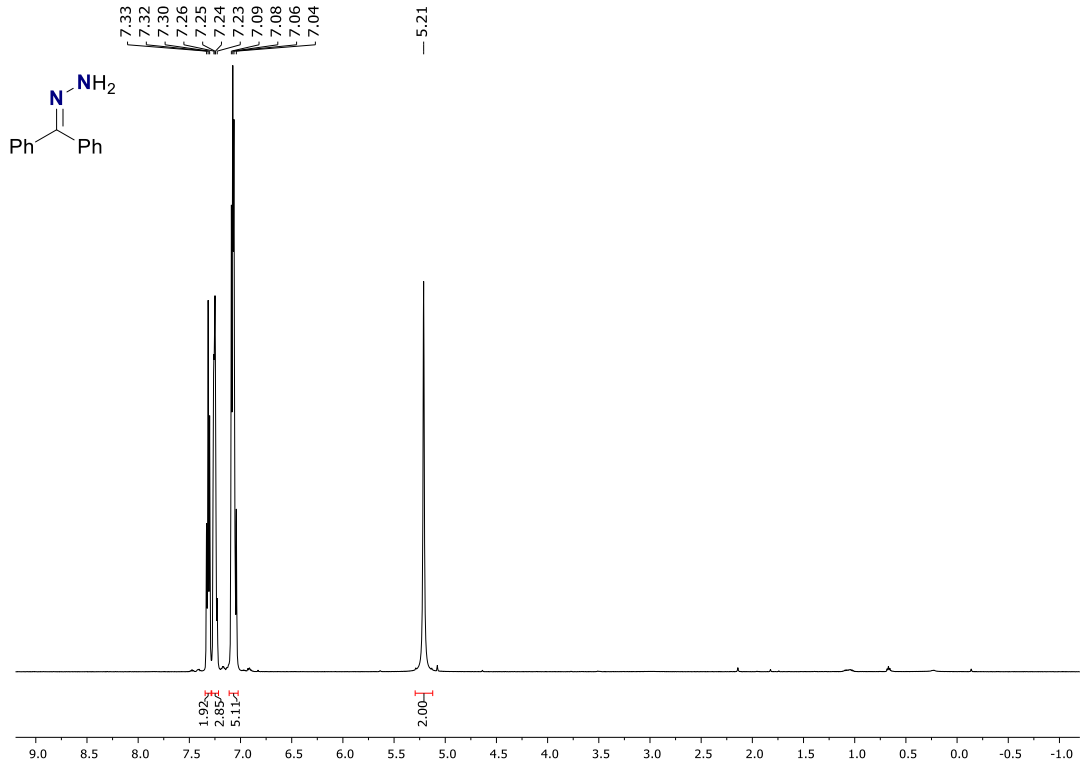

Figure 3.4: ^{1}H NMR (400 MHz, $CDCl_3$, 295 K) spectrum of diphenyl hydrazone **2a**.

Chapter 3.3 Synthesis and characterisation of products 3a–8.

*3.3.1 Synthesis and NMR analysis of hydrazone adducts **3a**–**3c***

The procedure first developed by Stephan *et al.* was followed for all adducts generated in this study.[2] Using the synthesis of adduct **3a** as an example, one equivalent of diphenylmethylenehydrazone (**2a**) and one equivalent of B(2,4,6-$F_3C_6H_2)_3$ were stirred in toluene for ten hours at room temperature. Then, the solvents were removed *in vacuo,* and the desired product was obtained via recrystallisation using the layering method (CH_2Cl_2/pentane). Products were obtained as colourless crystals with yields of 61% (**3a**), 65% (**3b**) and 56% (**3c**).

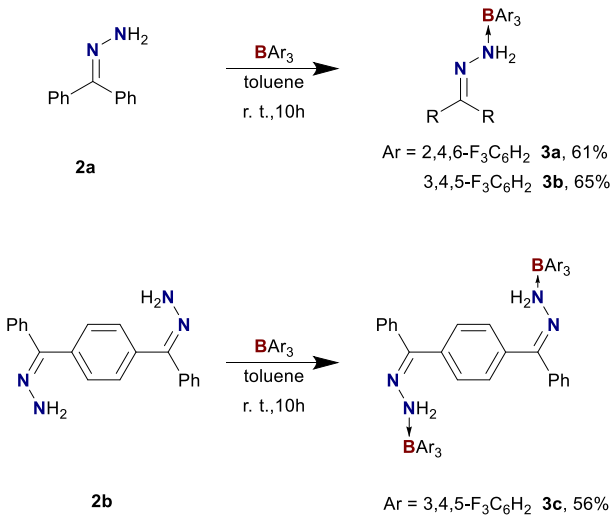

Figure 3.5: Reaction plan of hydrazone **2a** and **2b** with Lewis acidic boranes.

Herein, multinuclear NMR spectroscopy helped ascertain the nature of the products. Of particular importance was $^{11}B\{^1H\}$ NMR spectroscopy. A significant upfield signal shift to the +15 to -15 ppm area in the $^{11}B\{^1H\}$ spectrum has long been attributed to the complexation of a ligand or base to a tricoordinate borane species.[8]

Products **3a** and **3b** follow this pattern with $^{11}B\{^1H\}$ NMR spectroscopy showing a significant resonance shift to δ = -6.1 ppm and -2.6 ppm, respectively (*cf.* 59.6 ppm for B(2,4,6-$F_3C_6H_2)_3$ and 65.9 ppm for B(3,4,5-$F_3C_6H_2)_3$. Complete consumption of the starting triarylborane was also evident, with no trace of it detectable in the spectrum.

^{19}F NMR spectroscopy did not provide much analytical insight as the number and integration ratios of the adduct signals remained essentially unchanged to those of the parent triarylboranes. However, a chemical resonance shift was evident with

signals now located at δ = -99.92 and -112.79 ppm for **3a** and δ = -135.66 and -163.24 ppm for **3b**.

The most distinguishing feature of the ^{1}H NMR spectra was the emergence of signals centred at 6.47 ppm (**3a**) and 6.62–6.59 ppm (**3b**) corresponding to the aryl proton resonances of the triarylboranes. In addition, the –NH_2 signal shifted considerably downfield from a singlet at δ = 5.21 ppm to two overlapping singlets at δ = 6.93 ppm for **3a** and to a multiplet at δ = 6.62–6.59 ppm for **3b**.

Finally, the spectrum displayed the expected diphenylhydrazone aromatic signals that collectively integrated to ten for both **3a** and **3b**. Collectively, these phenyl signals had moved slightly downfield but retained their integration ratios and multiplicities. Thus, the NMR data obtained for adducts **3a–3b** is consistent with the complexation of the hydrazone to the triarylborane resulting in a tetracoordinate boron species. The ^{11}B{^{1}H}, ^{19}F and ^{1}H NMR spectra of **3a** are presented below.

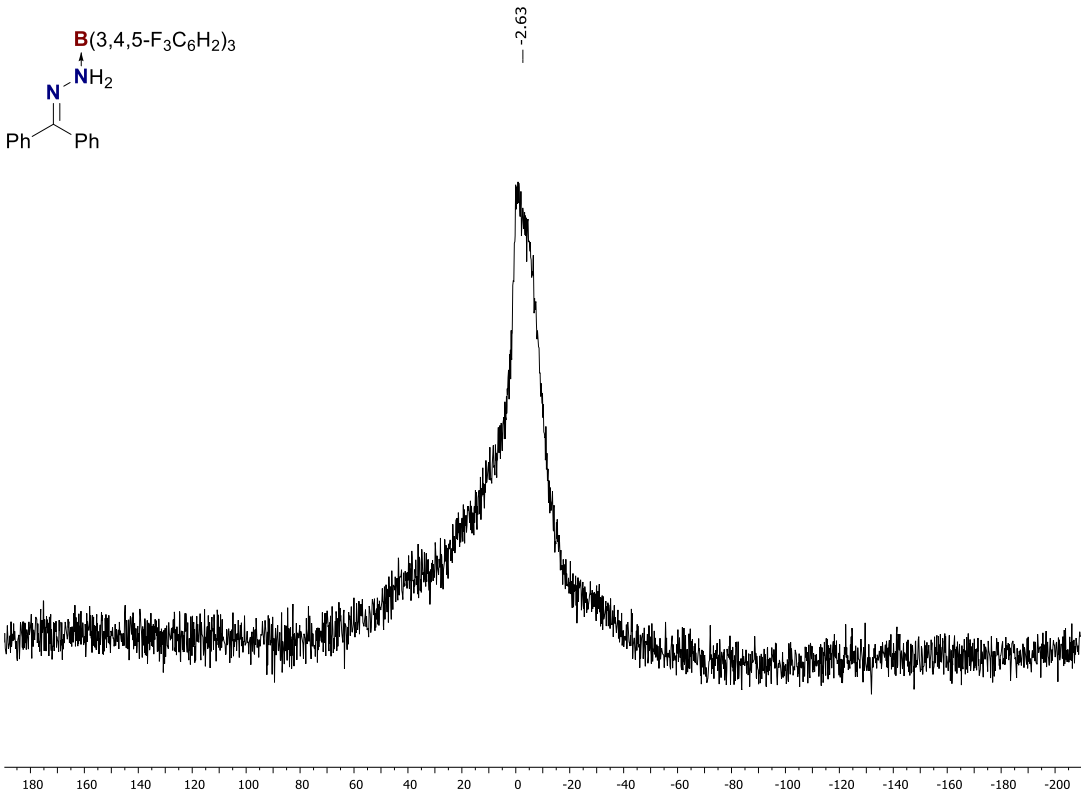

Figure 3.6: ^{11}B{^{1}H} NMR (160 MHz, $CDCl_3$, 298 K) spectrum of **3a**.

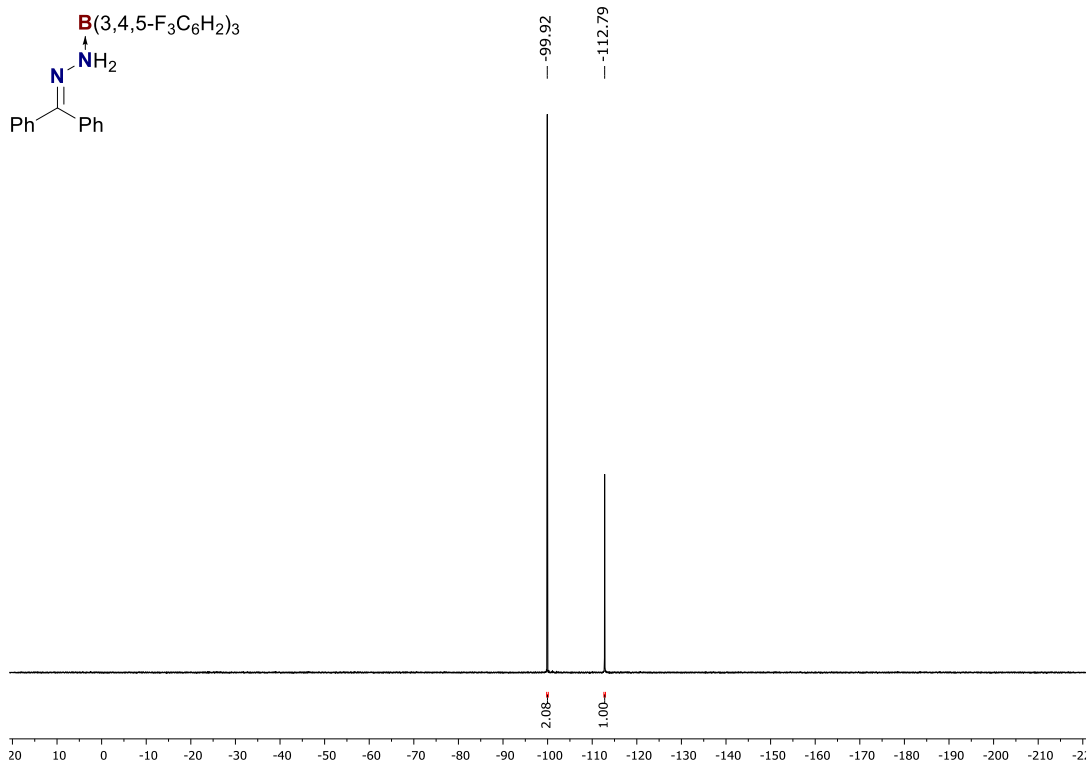

Figure 3.7: ^{19}F NMR (471 MHz, $CDCl_3$, 298 K) spectrum of **3a**.

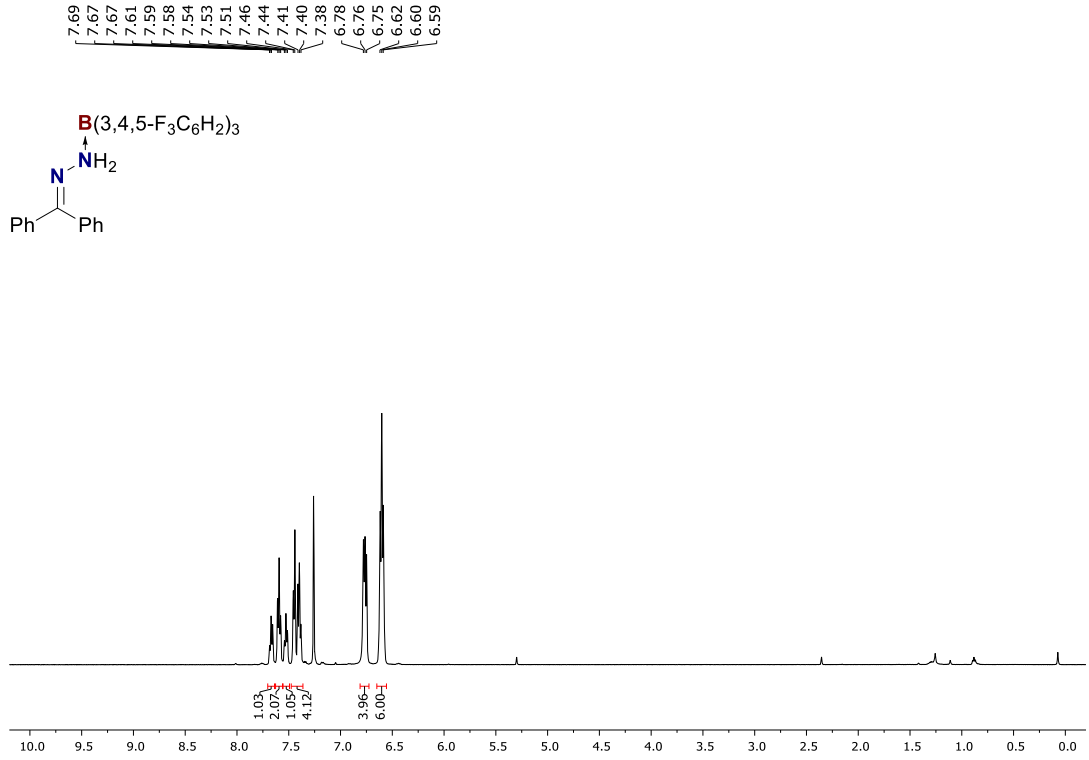

Figure 3.8: ^{1}H NMR (500 MHz, $CDCl_3$, 298 K) spectrum of **3a**.

A similar NMR analytical pattern to **3a** was also observed for **3c**. The $^{11}B\{^{1}H\}$ NMR spectrum displays a singlet resonance at δ = -6.2 ppm, the region commonly

associated with tetracoordinate boron centres. The ^{19}F spectrum closely resembled **3a** with two singlets at δ = -99.9 and -112.54 ppm with an integration ratio of 2:1 (eighteen F in total). Finally, the ^{1}H NMR spectrum is consistent with adduct formation, displaying the triarylborane proton signals as a multiplet at δ = 6.46–6.42 ppm. The two $–NH_2$ signals converged into a singlet at the significantly more downfield position of δ = 6.86 ppm. All aromatic signals were accounted for with a collective integration of fourteen.

*3.3.2 Solid-state structural analysis of **3a–3c***

Multinuclear NMR spectroscopy constitutes the workhorse of this thesis providing valuable chemical, electronic and structural information for the compounds generated. Single crystal X-ray diffraction complements NMR spectroscopy by providing more detailed information on bond lengths, angles and geometry, amongst other properties. Its importance for structure elucidation and analysis throughout this doctorate cannot be overstated. In some instances, it provided the first glimpse into potential reactivity (see Section 3.3.4 and Chapter 5).

For products **3a–3c**, crystals suitable for single crystal X-ray diffraction were grown by layering pentane upon a saturated solution of CH_2Cl_2. **3a** was found to crystallise in the triclinic *P*-1 space group with one molecule in the asymmetric unit cell (Z'), rising to two in the unit cell (Z). On the other hand, the space group of **3b** was monoclinic ($P2_1/n$), with one molecule in the asymmetric cell growing to four molecules in the unit cell.

The solid-state structures of **3a–3b** strongly resembled each other. Corroborating the $^{11}B\{^{1}H\}$ NMR findings, structure refinement revealed the boron centre to be tetracoordinate and tethered to the terminal nitrogen atom of the hydrazone. The complexation of the triarylborane is responsible for N–N bond lengths of 1.437(9) Å for **3a** and 1.443(4) Å for **3b**. The B–N bond lengths of adducts **3a** [1.647(10) Å] and **3b** [1.652(5) Å] are slightly longer to literature reported $Ph_2C{=}NNH_2{\rightarrow}B(C_6F_5)_3$ [*cf.* 1.610(4) Å].[2] Finally, the C=N bond lengths [1.284(4)–1.294(8) Å] largely correlate to typical C=N bond values.[9]

Where **3c** is concerned, its space group was determined as *P*-1. As the product possessed a symmetry element, the asymmetric unit cell consisted of half a molecule, increasing to four molecules in the unit cell. The bond metrics for **3c** were comparable to those of **3b** with B–N, N–N and C=N bond lengths of 1.647(4) Å, 1.437(4) Å and 1.294(4) Å, respectively.

Table 3.1: Space groups and selected bond metrics of literature reported $Ph_2C{=}NNH_2{\rightarrow}B(C_6F_5)_3$ [2] and adducts **3a–3c**.

	$Ph_2C{=}NNH_2{\rightarrow}B(C_6F_5)_3$	**3a**	**3b**	**3c**
Space group	*I*2/*c*	*P*-1	*P*2$_1$/*n*	*P*-1
Selected bond				
B–N	1.610(4) Å	1.647(10) Å	1.652(5) Å	1.647(4) Å
N–N	1.453(3) Å	1.437(9) Å	1.443(4) Å	1.437(4) Å
C=N	1.287(3) Å	1.294(8) Å	1.284(4) Å	1.294(4) Å

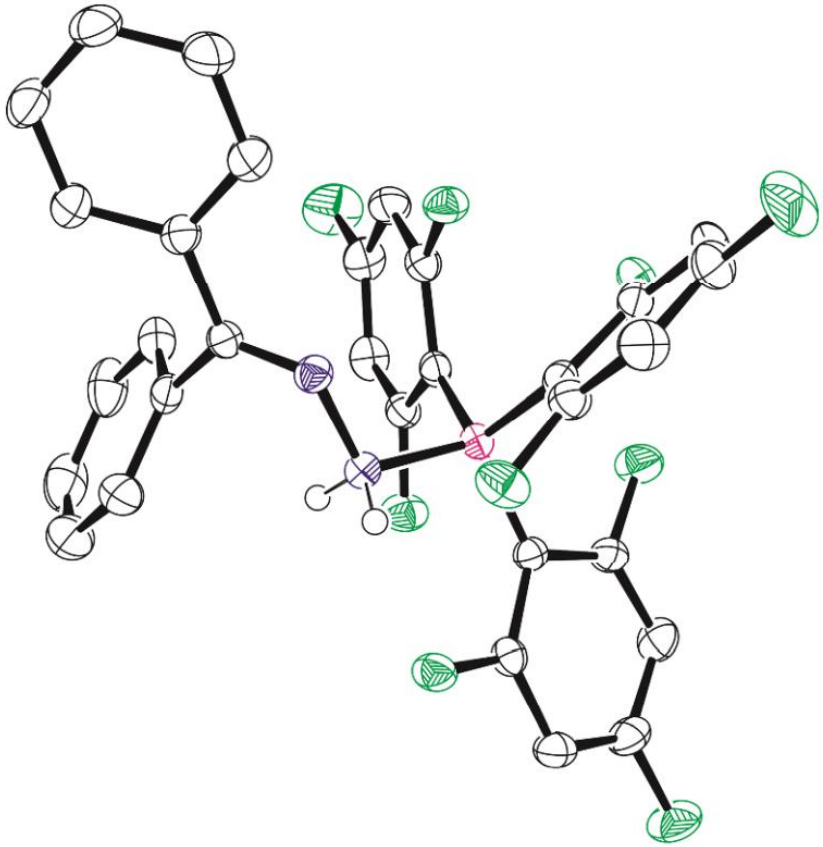

Figure 3.9: Solid-state structure of adduct **3a**. Thermal ellipsoids are drawn at 50% probability. H-atoms, except for those on nitrogen, were omitted for clarity.

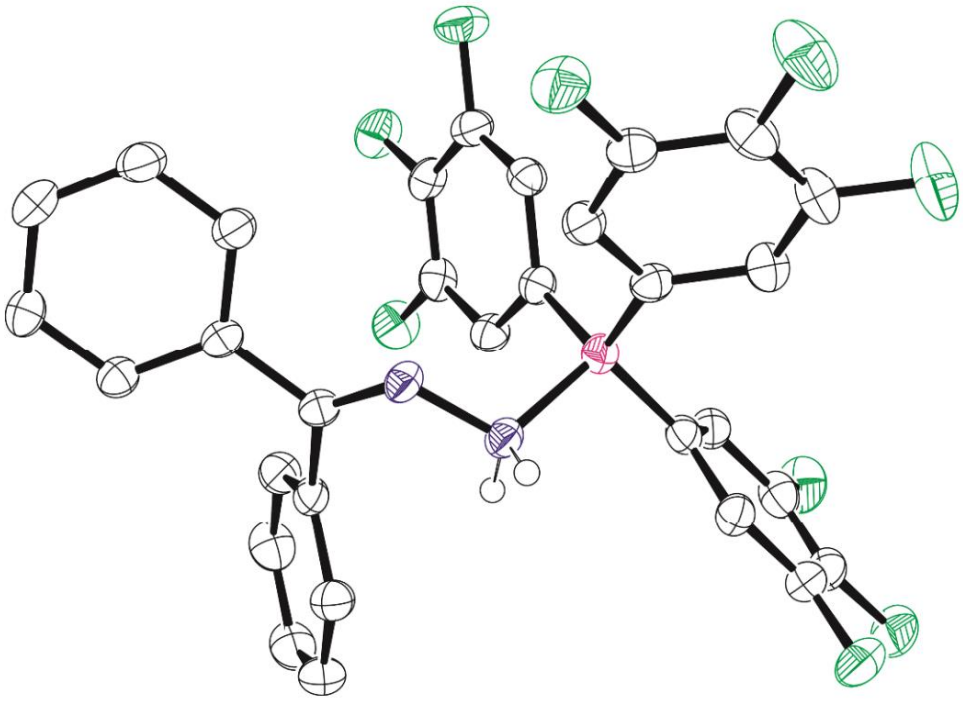

Figure 3.10: Solid-state structure of adduct **3b**. Thermal ellipsoids are drawn at 50% probability. H-atoms, except for those on nitrogen, were omitted for clarity.

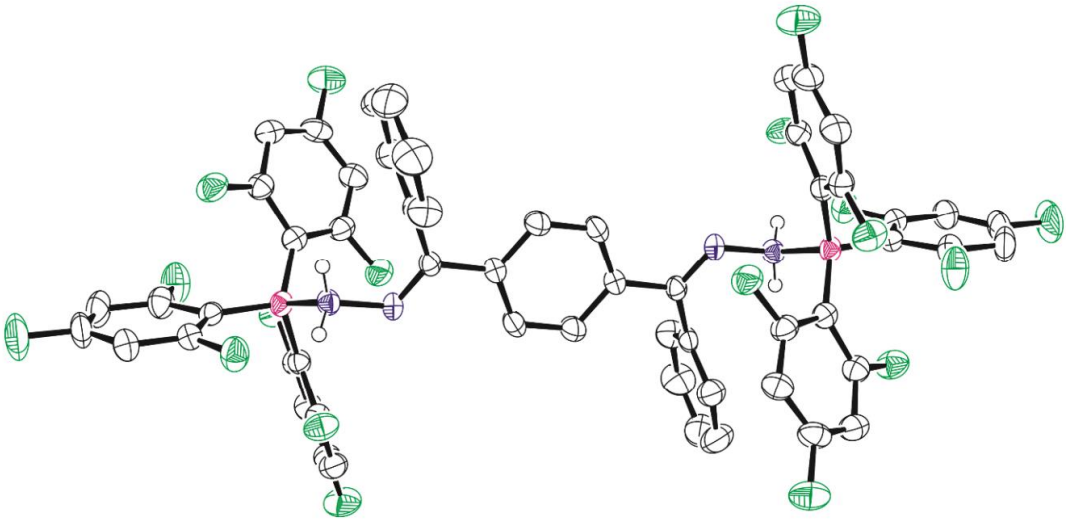

Figure 3.11: Solid-state structure of adduct **3c**. Thermal ellipsoids are drawn at 50% probability. H-atoms, except for those on nitrogen, were omitted for clarity.

*3.3.3 Attempted synthesis and initial NMR analysis of products **4**, **5** and **6**.*

The procedure initially employed for the reaction of (9H-fluoren-9-ylidene)hydrazone (**2c**) with B(2,4,6-$F_3C_6H_2)_3$ bore many similarities with those for hydrazone adducts **3a**–**3c**. First, equimolar amounts of **2c** and the triarylborane were stirred in toluene for ten hours. Then, the solvent was removed *in vacuo,* and the resultant solid was crystallised by layering CH_2Cl_2 with pentane. As a result, the batch of crystals was obtained at a high yield (76%) and appeared homogeneous to the naked eye.

However, the $^{11}B\{^1H\}$ NMR spectrum revealed the presence of at least two boron species (peaks at δ = -4.2 ppm and -5.7 ppm). The absence of a peak at δ = 59.65 ppm served as proof of complete consumption of the starting triarylborane. The ^{19}F, ^1H and $^{13}C\{^1H\}$ NMR spectra could not shed any further light on the reactivity as the spectra were particularly complex. This suggested the presence of a mixture of products. Nevertheless, no traces of unreacted starting material **2c** in the ^1H NMR spectrum were evident as the characteristic amide peak at δ = 6.3 ppm was no longer present.

Single crystal X-ray diffraction revealed the generation of product set **4–5** and product **6** (Figure 3.12).

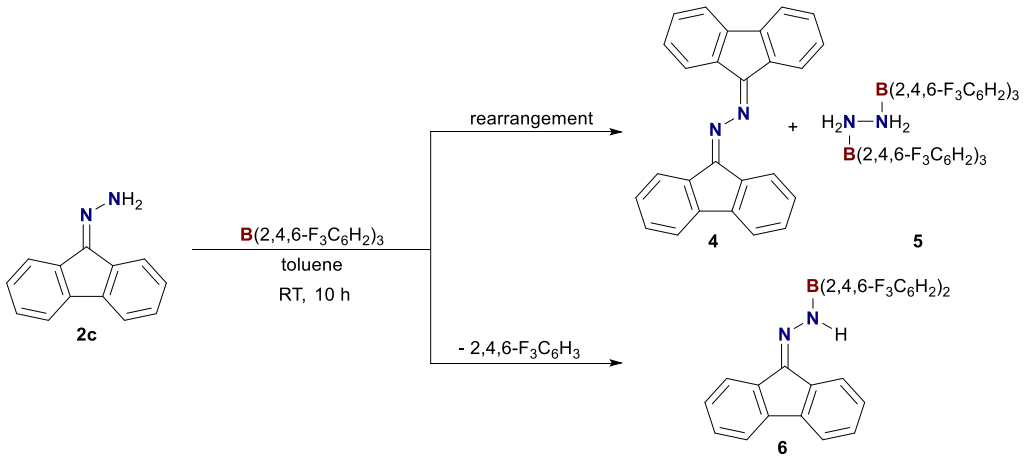

Figure 3.12: Reaction profile of **2c** with B(2,4,6-$F_3C_6H_2)_3$.

*3.3.4 Solid-state structural analysis of **4**, **5** and **6**.*

Although NMR analysis provided some rudimentary insight into potential reaction outcomes, it stopped short of conclusively identifying the products. Upon examining the crystal batch under a microscope, three distinct types could be discerned: long yellow needles (**4**), transparent blocks (**5**) and red rods (**6**). Each type was

subjected to single crystal X-ray diffraction, allowing their identity to be unambiguously established.

The solid-state structure of **4** has previously been described in detail by the group of Ismail.[10] In the interest of completion, the space group and characteristic bond lengths of this compound have been summarised in Table 3.2.

Table 3.2: Space groups and selected bond metrics of product **4**.

	4
Space group	
	P-1
Selected bond	
B–N	N/A
N–N	1.437(9) Å
C=N	1.294(8) Å

In contrast, the cell parameters of products **5** and **6** did not provide a positive match in the Cambridge Crystallographic Data Centre (CCDC) database, the principal repository of single crystal X-ray data. The solid-state structures were not previously described in the literature, so they were subjected to X-ray analysis.

In the case of **5**, the product was found to crystallise in the monoclinic *I*2/*a* space group with half a molecule in the asymmetric unit cell, increasing to four in the unit cell. The structure possesses an inversion centre around the core N–N bond. Structurally, **5** was reminiscent of the simplified hydrazine bisborane $N_2H_4(BH_3)_2$ with one tetracoordinate boron centre tethered to each nitrogen atom.[11]

The N–N bond distance of **5** [1.461(2) Å] is significantly shorter than that of $N_2H_4(BH_3)_2$ (1.609 Å)[11] but falls within the range of hydrazine bisboranes previously reported by Szymczak [1.475(3) Å] and Gabbai (1.688 Å).[12, 13] A similar trend is true for the B–N bond [1.673(20) Å], with it being slightly longer than for $N_2H_4(BH_3)_2$ (1.603 Å) but closely resembling other chelating bisborane complexes [1.688(2)–1.698(2) Å].[11, 12, 13]

Table 3.3: Space group and selected bond metrics of $N_2H_4(BH_3)_2$, the Szymczak and Gabbai chelating bisboranes and product **5**.[11-13]

	$N_2H_4(BH_3)_2$	Szymczak	Gabbai	5
Space group				
	*P*2$_1$/*n*	*P*-1	*C*2/*c*	*I*2/*a*
Selected bond				
N–N	1.609 Å	1.475(3) Å	1.469(2) Å	1.461(2) Å
B–N	1.461(2) Å	1.697(2) Å	1.688(2) Å	1.673(2) Å
		1.698(2) Å		

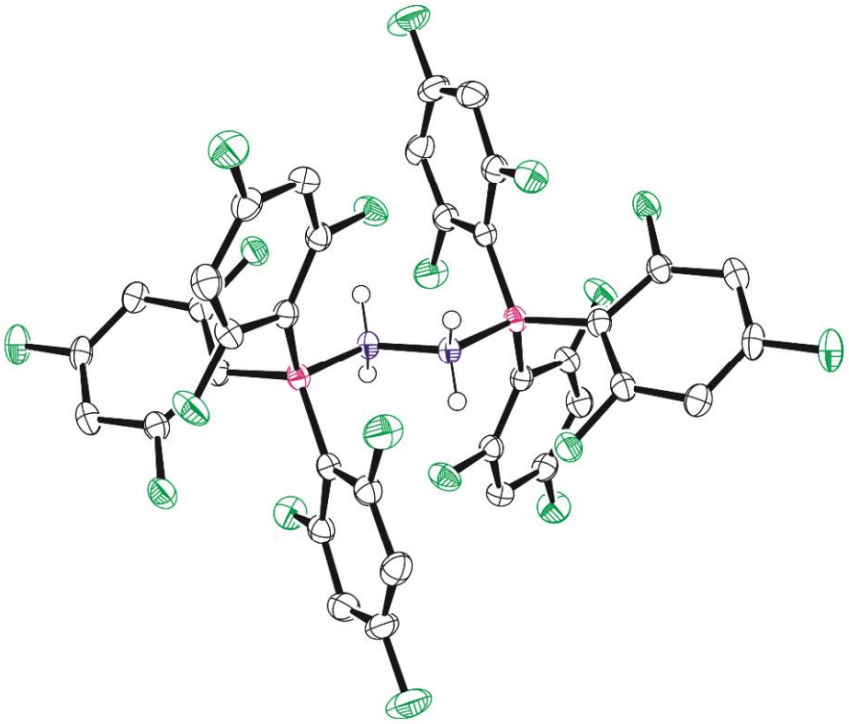

Figure 3.13: Solid-state structure of product **5**. Thermal ellipsoids are drawn at 50% probability. H-atoms, except for those on nitrogen, were omitted for clarity.

From structure solution and refinement, **6** crystallised in the monoclinic *P*2$_1$/*c* space group with one molecule in the asymmetric unit cell, increasing to four in the unit cell. The solid-state structure revealed a tricoordinate boron centre, with two N–B–C bond angles of 117.76(13)° and 119.71(13)° and a C–B–C bond angle of 122.49(13)°. As the observed bond angles approach 120°, the boron atom has a slightly distorted trigonal planar geometry and is sp^2 centred.

In addition, the B–N bond distance of 1.397(2) Å is significantly shorter than for adducts **3a** and **3c** (*cf.*1.647(4) Å for both). The N–N and C=N bond distances are 1.379(17) Å and 1.288(19) Å, respectively. Finally, all the CNNB atoms lie in the same plane. When the previous observations are taken in conjunction, they allude to strong N–B π-back bonding generating a CNNB diene core and forcing the product to adopt a *trans* conformation.

Table 3.4: Space groups and selected bond metrics of product **6**.

	6
Space group	$P2_1/c$
Selected bond	
B–N	1.397(2) Å
N–N	1.379(17) Å
C=N	1.288(19) Å
Selected Angle	
N –B–C	117.76(13) °
N –B–C	119.71(13) °
C –B–C	122.49(13) °

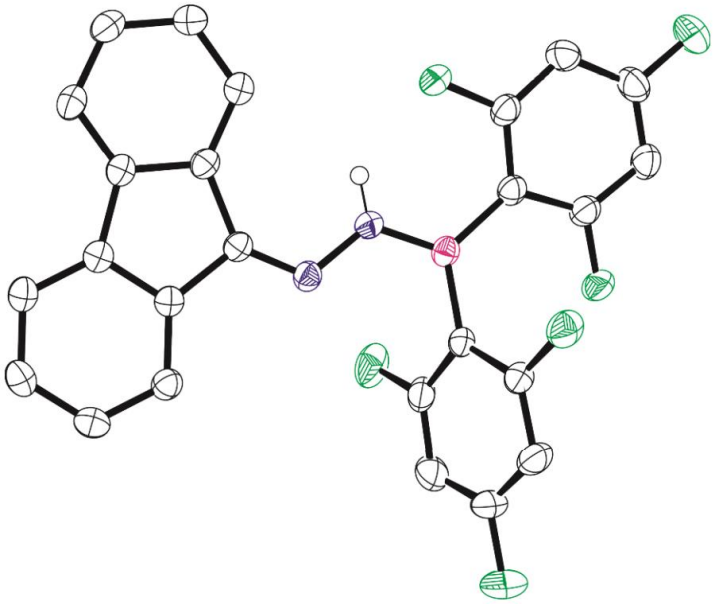

Figure 3.14: Solid-state structure of product **6**. Thermal ellipsoids are drawn at 50% probability. H-atoms, except for those on nitrogen, were omitted for clarity.

*3.3.5 Independent synthesis, analysis and characterisation of products **4–5** and **6**.*

As crystallisation proved unable to separate product sets **4**–**5** and **6**, attempts were made to influence the reaction outcome by altering the conditions. Out of the various reaction variables, including pressure, type of solvent used and stoichiometric ratios, temperature is the simplest to modify and monitor. Indeed, upon decreasing the temperature to 0 °C, compound **6** was selectively obtained after crystallisation (layering, CH_2Cl_2/pentane) in 46% yield (Figure 3.15). This result was contrary to expectations, as previously, aryl elimination in reactions with triarylboranes and hydrazones were only observed upon protracted heating (110 °C for twenty hours).[2]

On the other end of the spectrum, increasing the temperature from room temperature to 50 °C predominantly afforded products **4** and **5**, albeit minute traces of **6** were always present. Any further temperature increases beyond 50 °C led to decomposition.

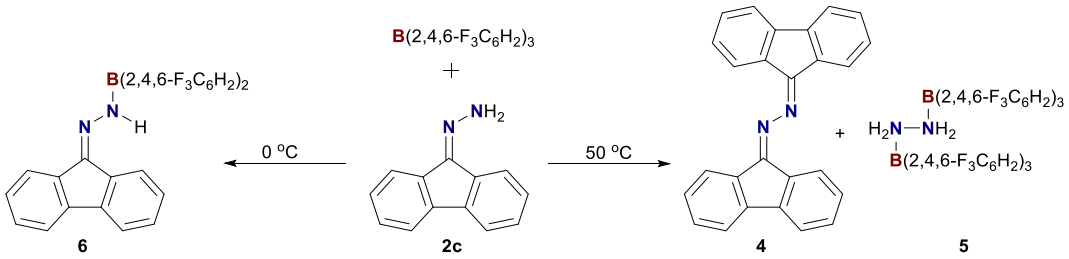

Figure 3.15: Temperature controlled synthesis of products **4–6**.

From a mechanistic perspective, both product sets proceed from a common starting point. This is more than likely adduct formation between fluorenone **2c** and the triarylborane. Although this adduct could not be isolated despite repeated attempts, its formation is strongly supported by the literature (see Introduction) and the experimental observations from adducts **3a–3c**. Adding further credence to this hypothesis, low temperature *in-situ* $^{11}B\{^1H\}$ NMR studies in toluene verified the formation of a single species with a characteristically broad peak at δ = -2.1 ppm. This species rapidly converted to either product set **4–5** or **6** as the temperature was gradually increased.

A hydrazone metathesis reaction is most likely responsible for furnishing azine **4** and borane hydrazone adduct **5**, whereas an Ar^FH elimination generates **6** similar to the literature reported $Ph_2C{=}NNH{-}B(C_6F_5)_2$.

Out of the three products generated, product set **4–5** is of particular interest. Product **4** belongs to the family of N–N linked diimines. These are industrially relevant compounds with applications as chromophores in optoelectronic devices.[14] This product has previously been synthesised from the decomposition of diazos with $Pt(C_2H_4)(PPh_3)_2$ acting as a catalyst.[15] Other synthetic methods to generate a diazine from hydrazones generally necessitate harsh reaction conditions and protracted timescales such as reflux in ethanolic hydrogen chloride for several hours.[16]

Hydrazone adduct **5** is also furnished in this reaction pathway. Coordinated hydrazones analogous to **5** have long been postulated as intermediates in nitrogen fixation cycles. Additionally, analogous hydrazine bisborane $N_2H_4(BH_3)_2$, generated by mixing sodium borohydride with hydrazine sulfate, has been examined as a hydrogen storage material containing 16.9 wt% hydrogen. [1212, 17, 18]

Given the growing interest in this class of compounds, attempts were made to synthesise **5** independently, starting from hydrazine monohydrate. Indeed, combining $B(2,4,6\text{-}F_3C_6H_2)_3$ and hydrazine monohydrate ($N_2H_4{\cdot}H_2O$) in a 2:1 ratio with 0.4 Å pre-activated molecular sieves resulted in the desired product in 45% yield, as evidenced by multinuclear NMR spectroscopy.

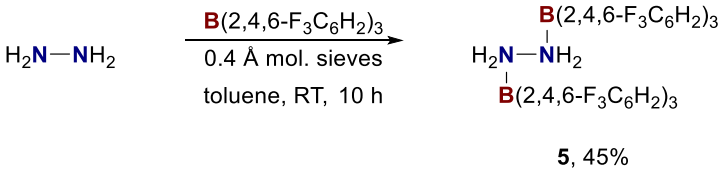

Figure 3.16: Independent synthesis of **5** using hydrazine monohydrate, molecular sieves and $B(2,4,6\text{-}F_3C_6H_2)_3$.

Having established a dependable method for synthesising and separating products **4–5** and **6**, attention turned to characterising them. Confirmation of separation was first established by $^{11}B\{^1H\}$ NMR spectroscopy, whereupon the peak at δ = -5.7 ppm could now be reliably assigned to **5** and the peak at δ = -4.2 ppm to **6**.

^{19}F NMR spectroscopy could be utilised to characterise products **5** and **6**. For **5**, the expected two signals moved slightly downfield to δ = -99.91 (4F, meta) and -112.45 ppm (2F, ortho). However, the integration ratio remained unchanged at 2:1. The collective integration was set as nine, denoting three aryl rings on the borane. This assignment would be in accordance with the crystallographic data. Product **6** also exhibited two singlet resonances at δ = -99.90 (4F, meta) and -112.54 (2F,

ortho) ppm. These values are significantly more downfield than the starting triarylborane B(2,4,6-$F_3C_6H_2)_3$ (δ = -95.74 and -100.3 ppm). Once more, the integration ratio was 2:1, collectively integrating to six.

Given the lack of fluorine and boron heteronuclei, the characterisation of **4** relied heavily on ^{1}H NMR spectroscopy. There are four aromatic signals instead of the five seen in starting hydrazone **3c**, and the signals are all slightly downshifted to δ = 7.67–7.64, 7.55–7.50, 7.44–7.31 and 7.25–7.21 ppm. More important is the disappearance of the amine singlet at δ = 6.3 ppm in the product. There is also no triarylborane signal that usually appears within the δ = 6.0 to 8.0 ppm range. When taken in conjunction, these observations support the formation of **4** and are in accordance with literature reported values. Product confirmation was also obtained using High Resolution Mass Spectrometry (HRMS) using the positive ElectroSpray method (ES^+) with the $[M+H]^+$ $[C_{26}H_{18}N_2]^+$ for **4** at 357.1392 (theoretical: 357.1396).

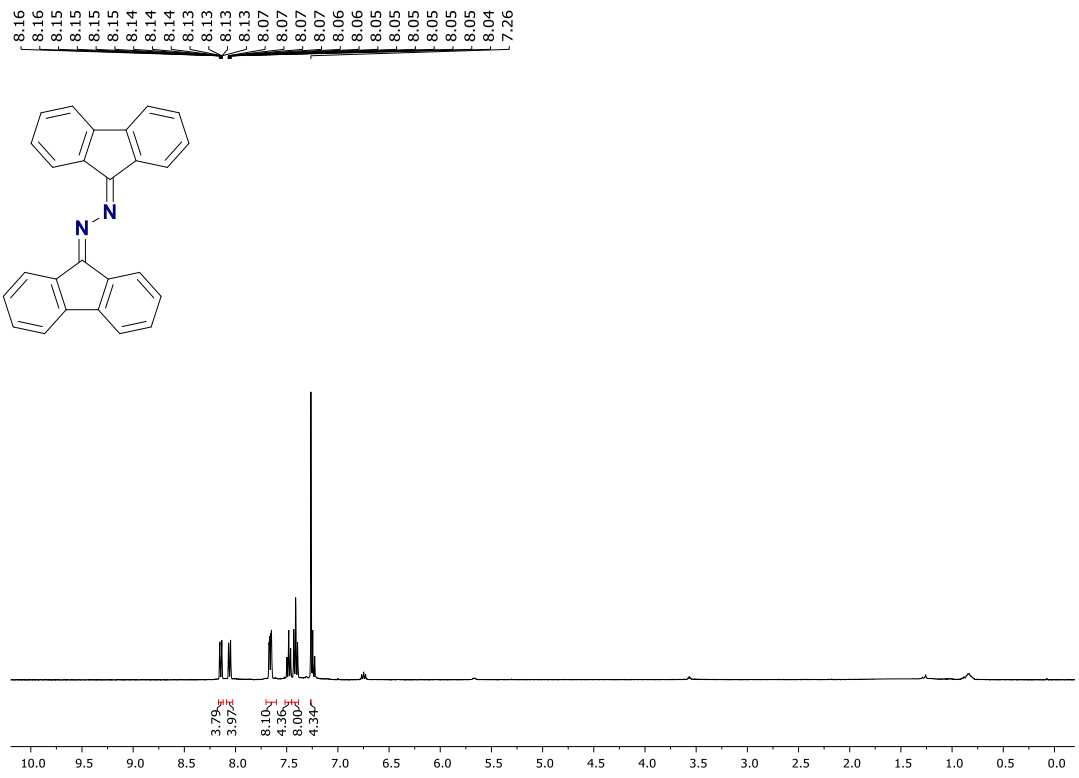

Figure 3.17: ^{1}H NMR (500 MHz, $CDCl_3$, 298 K) spectrum of **4**.

The ^{1}H NMR spectrum of **5** consisted of two broad singlets overlapping at δ = 6.85 ppm attributed to the two $–NH_2$ signals. In addition, the B(2,4,6-$F_3C_6H_2)_3$ signals appeared at δ = 6.43 ppm as a broad triplet. Finally, the CH_2Cl_2 solvent signal was visible at δ = 5.23 ppm.

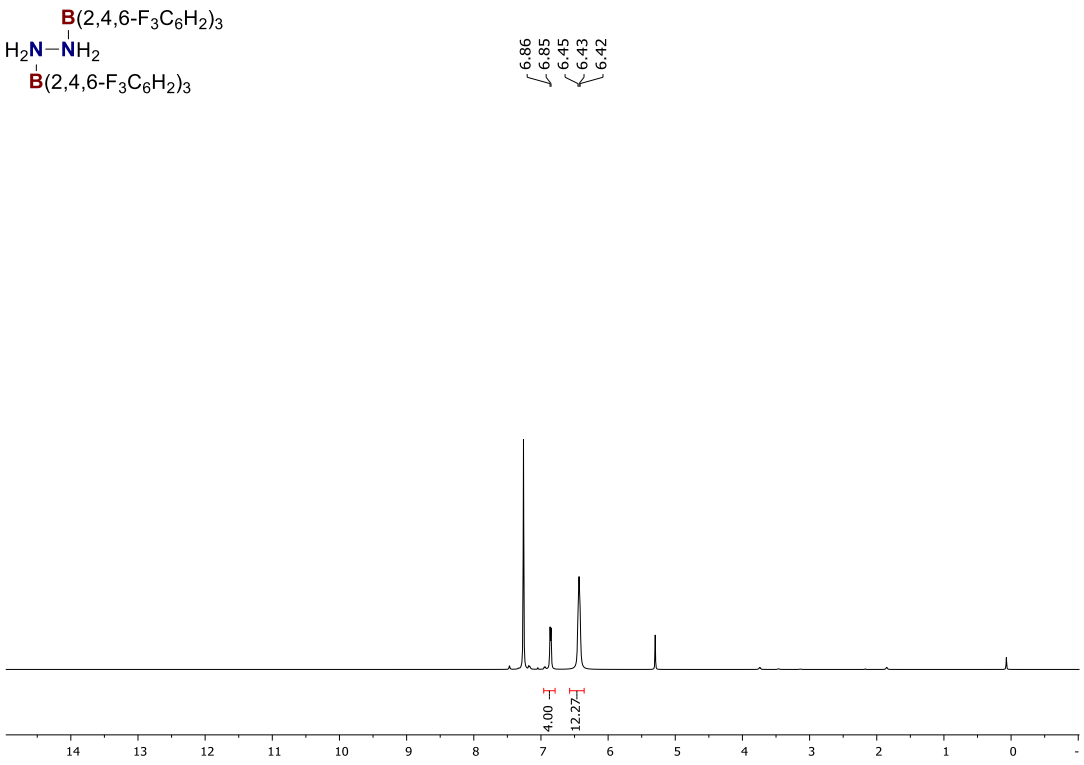

Figure 3.18: ^{1}H NMR (500 MHz, $CDCl_3$, 298 K) spectrum of **5**.

For **6**, the amide signal was now centred at δ = 8.07 ppm with an integration of one. Such a distinctive downfield chemical resonance shift is commonly associated with N=NH–B tricoordinate species, such as literature reported Ph_2C=NNH–$B(C_6F_5)_2$ (δ = 8.77 ppm). This fact, coupled with the emergence of the triarylborane triplet signal at δ = 6.48 ppm with an integration of four, stood as a strong testament to the aryl elimination having occurred.

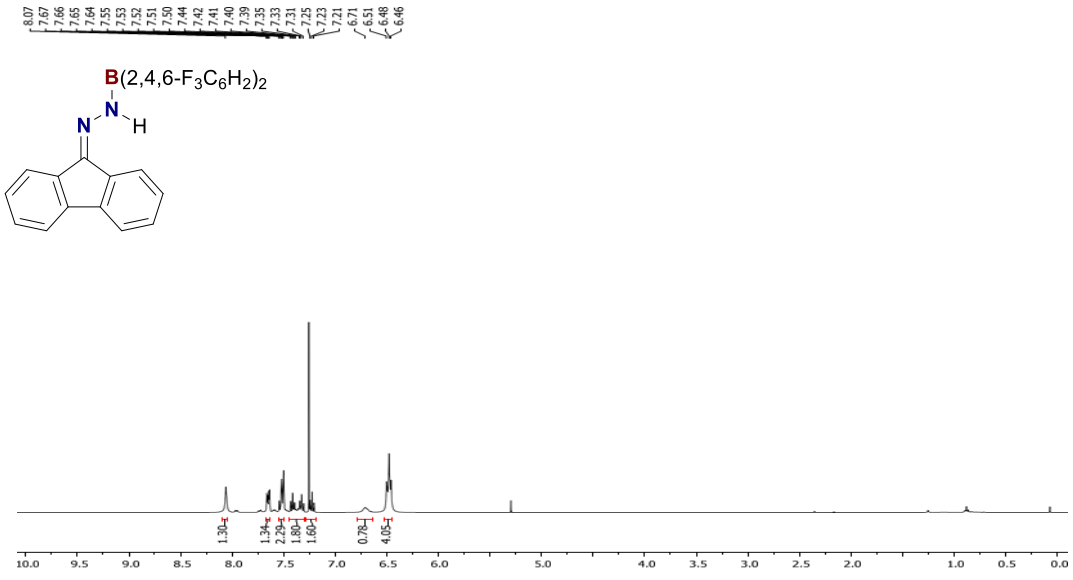

Figure 3.19: ^{1}H NMR (500 MHz, $CDCl_3$, 298 K) spectrum of **6**.

*3.3.6 Synthesis and NMR analysis of benzhydrazide derivatives **7a**–**7b** and **8**.*

To commercially available benzhydrazide (**2d**), the triarylboranes $B(C_6F_5)_3$ and $B(2,4,6\text{-}F_3C_6H_2)_3$ were added to examine the effect of an oxygen atom adjacent to the hydrazone functional group (Figure 3.20). To begin with, the synthesis of benzhydrazide adducts **7a** and **7b** was performed as previously described for **3a–3c**. Namely, an equimolar toluene solution of the appropriate triarylborane and **2d** was stirred for ten hours at room temperature. Subsequently, all volatiles were removed *in vacuo*. Recrystallisation by slow evaporation of the solvent (CH_2Cl_2) afforded the desired products with yields of 56% (**7a**) and 71% (**7b**) (Figure 3.20).

Heating of adduct **7a** led to its rapid decomposition to a complex mixture of products as revealed by multinuclear NMR spectroscopy. On the other hand, CON_2B heterocycle **8** was generated via *in-situ* heating of adduct **7b** to 110 °C for twelve hours. Herein, aryl elimination from the triarylborane had occurred with the oxygen atom forming a dative connection to the borane. Upon removing all volatiles and crystallisation by layering (CH_2Cl_2/pentane), **8** was afforded in 82% yield (Figure 3.20). Noteworthy was the size and appearance of the single crystal furnished, which was of a deep pink hue and weighed approximately 97 mg.

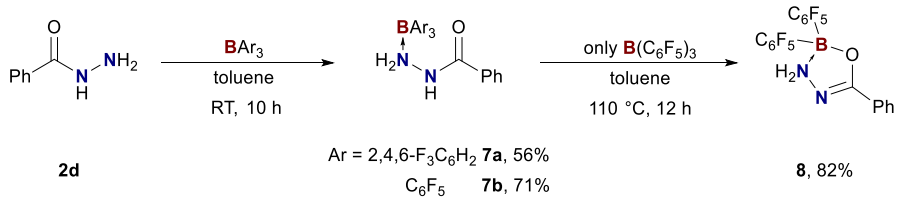

Figure 3.20: Reaction of hydrazide **2d** with $B(C_6F_5)_3$ and $B(2,4,6\text{-}F_3C_6H_2)_3$.

Inspection of the $^{11}B\{^1H\}$ NMR spectra revealed a single broad chemical shift at δ = -6.1 ppm for **7a** and δ = -6.2 ppm for **7b**. These values are typical for tetracoordinate boron compounds of this type. For reference, the $^{11}B\{^1H\}$ NMR chemical shift of adduct **3b** is δ = -2.6 ppm.

For **7a**, the ^{19}F NMR spectrum showed the expected two chemical signals at δ = -105.32 (ortho fluorines) and -110.68 ppm (meta fluorines) with an integration ratio of 2:1 (9 fluorines in total). Likewise, the ^{19}F NMR spectrum of **7b** is composed of the three expected signals at positions δ = -135.6 (ortho fluorines), -153.98 (para fluorines) and -161.64 ppm (meta fluorines) with an integration ratio of 2:2:1 (collectively 15 fluorines).

Finally, the ^{1}H NMR spectrum of adducts **7a** and **7b** showed little change in the phenyl region from starting material **2d**. In contrast, the signal corresponding to the amide functionality had significantly shifted downfield from δ = 4.56 ppm to δ = 7.46–7.42 (**7a**) and 7.97 ppm (**7b**) in account of the increased electron density imparted by the triarylborane to the benzhydrazide.

Adduct **7a** also displayed an additional triplet resonance at δ = 6.53 ppm with an integration of six, corresponding to the two aromatic protons on each of the fluorophenyl rings. For reference, the relevant spectra of **7b** are presented below.

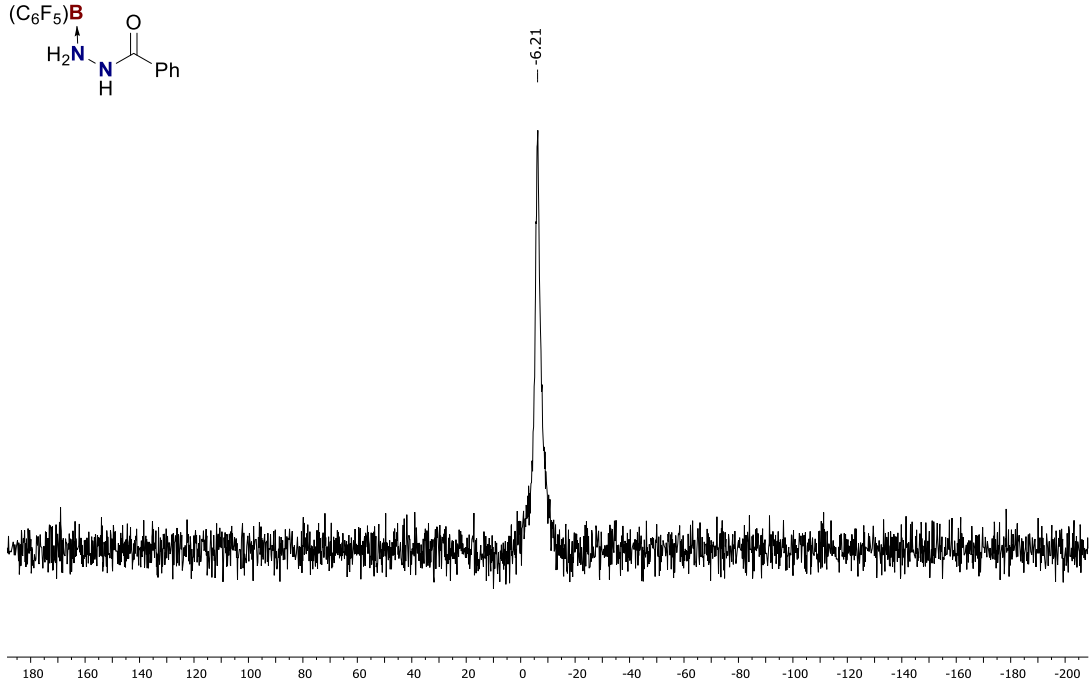

Figure 3.21: ^{11}B{^{1}H} NMR (128 MHz, $CDCl_3$, 298 K) spectrum of **7b**.

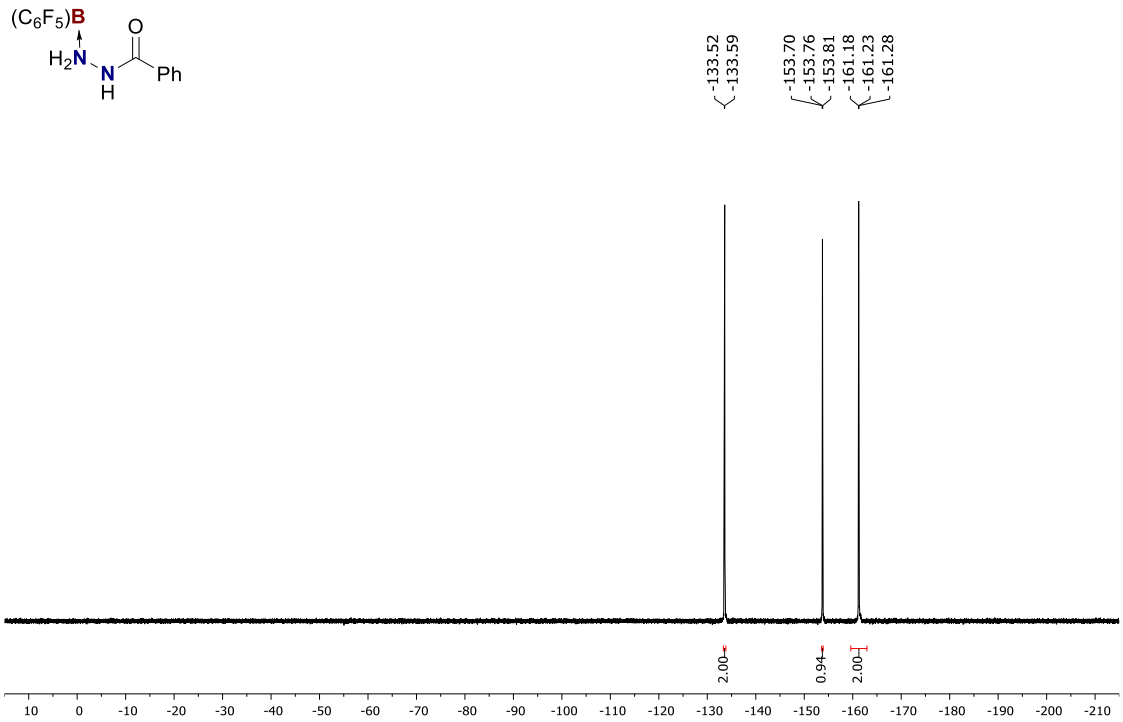

Figure 3.22: ^{19}F NMR (376 MHz, $CDCl_3$, 298 K) spectrum of **7b**.

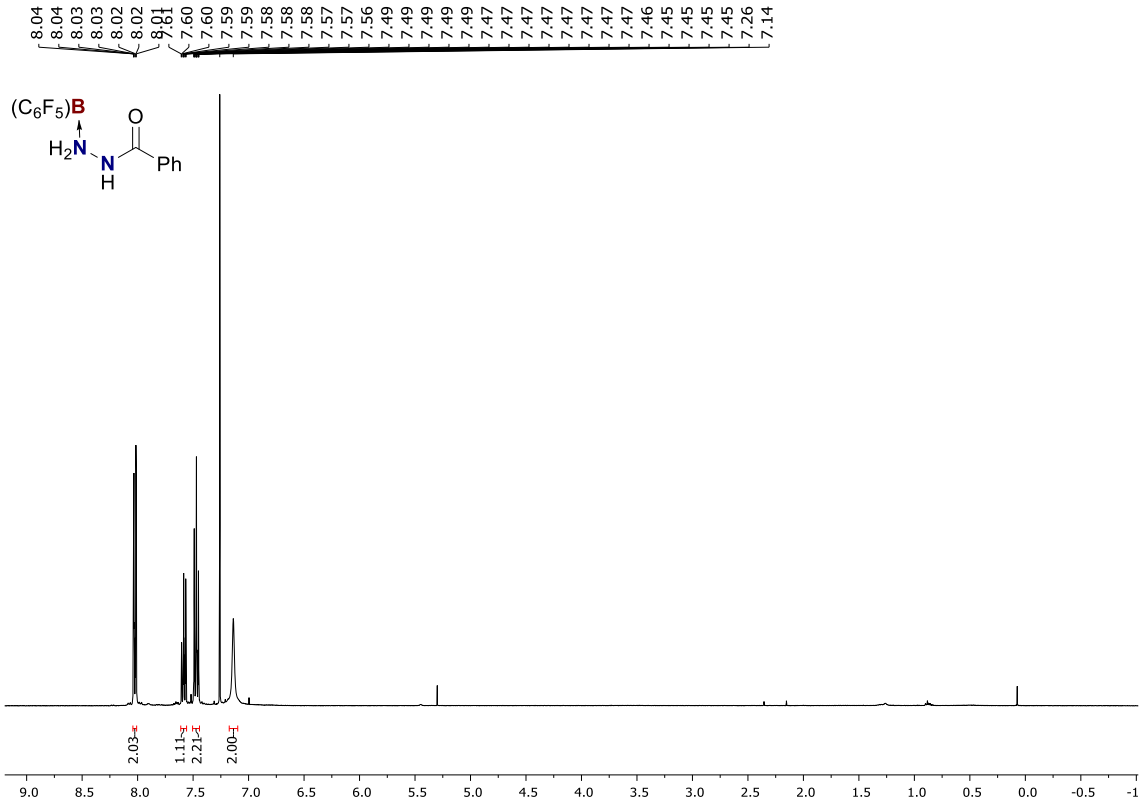

Figure 3.23: ^{1}H NMR (500 MHz, $CDCl_3$, 298 K) spectrum of **7b**.

Multinuclear NMR analysis was also used for the characterisation of heterocycle **8**. The $^{11}B\{^{1}H\}$ NMR spectrum was composed of a singlet at δ = -4.3 ppm, which is slightly downfield compared to **7b** (*cf.* δ = -6.2 ppm) but still suggestive of a tetracoordinate boron species. On a similar note, the ^{19}F NMR spectrum bears many similarities to **7b**. There are three resonances at δ = -135.6, -153.98 and -161.64 ppm with an integration ratio of 2:2:1 (collectively ten fluorines).

The ^{1}H NMR spectrum is distinctly different from adduct **7b** with the expected three aromatic signals shifted slightly downfield to positions δ = 8.04–8.01, 7.61–7.56 and 7.49–7.45 ppm. More importantly, the signal corresponding to the amide functionality was still present and shifted from δ = 7.97 ppm in adduct **7b** to a broad singlet located at δ = 7.14 ppm. Finally, the signal corresponding to the –NH functional group was missing resulting in a collective integration of seven for all proton signals. This observation bears witness to the aryl elimination having occurred. The $^{11}B\{^{1}H\}$, ^{19}F, and ^{1}H NMR spectra of **8** are presented below.

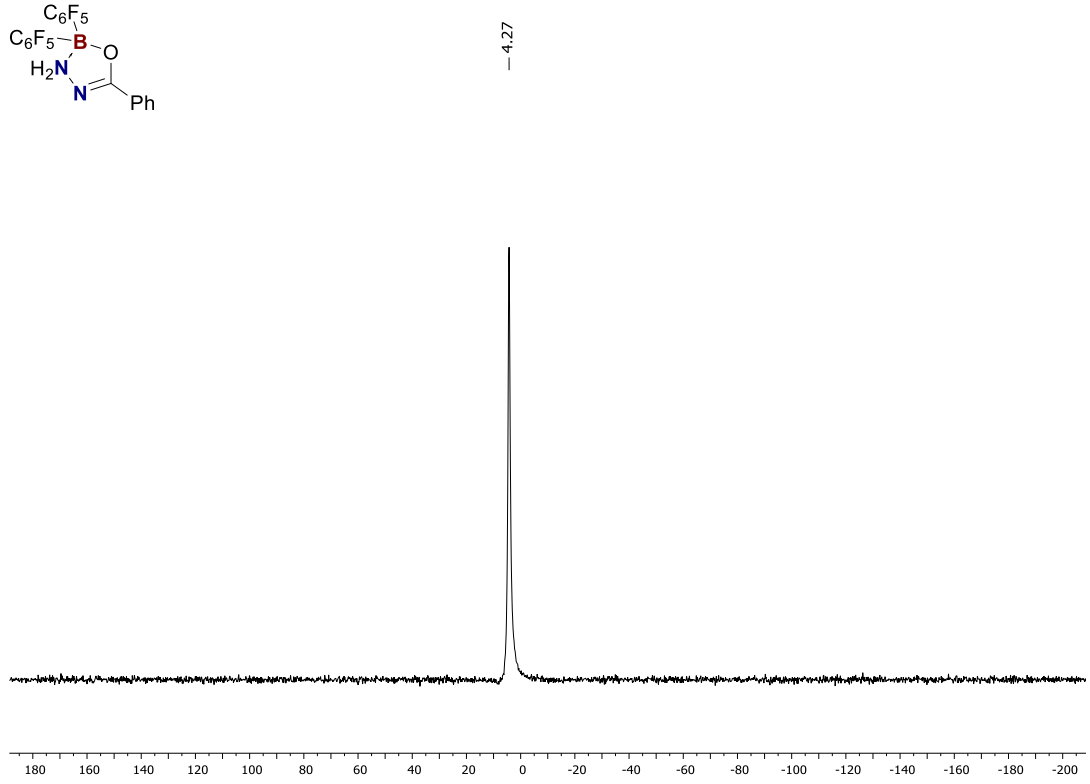

Figure 3.24: $^{11}B\{^{1}H\}$ NMR (128 MHz, $CDCl_3$, 298 K) spectrum of **8**.

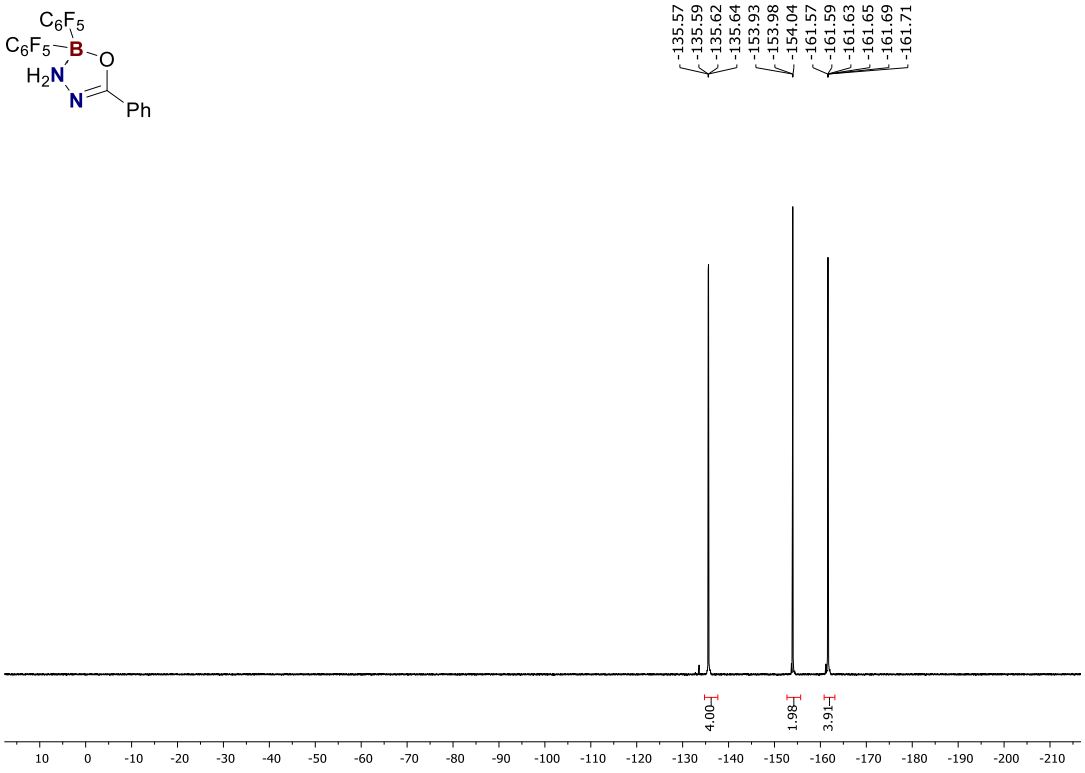

Figure 3.25: ^{19}F NMR (376 MHz, $CDCl_3$, 298 K) spectrum of **8**.

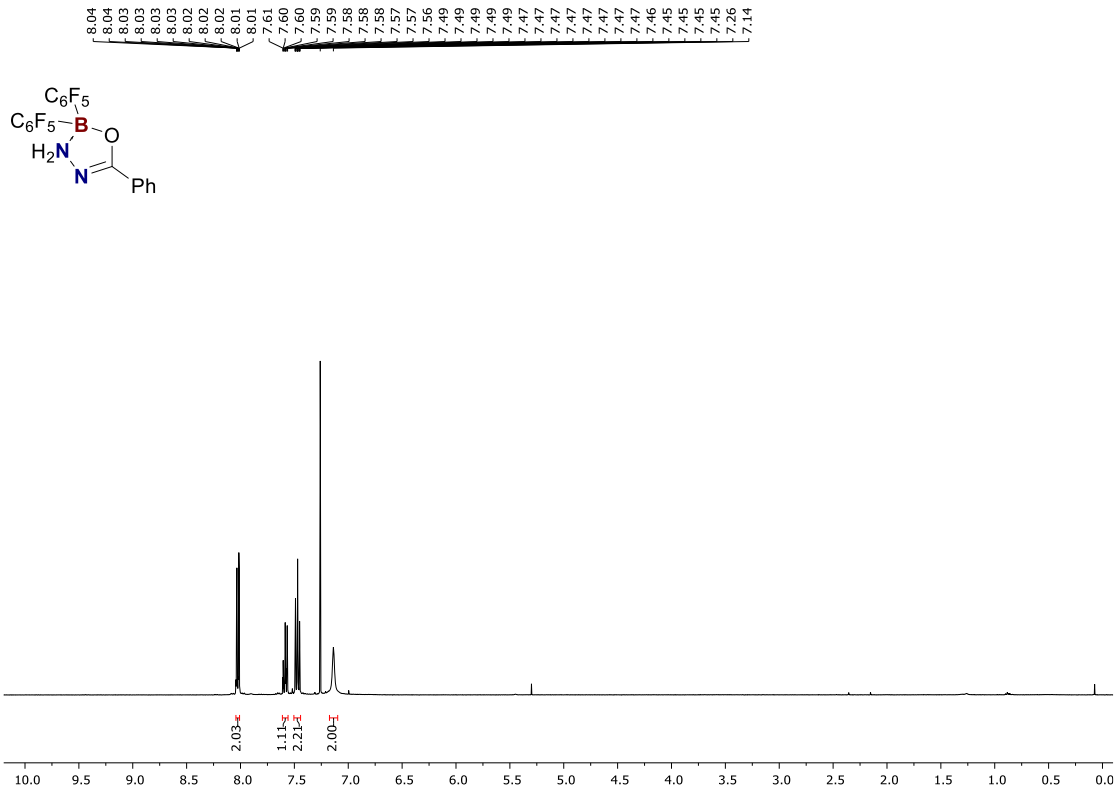

Figure 3.26: ^{1}H NMR (400 MHz, $CDCl_3$, 298 K) spectrum of **8**.

*3.3.7 Computational analysis of the elimination to form **8**.*

Professor Jeremy Rawson from Windsor University conducted Density Functional Theory (DFT) studies to gain a mechanistic understanding of the aryl elimination from **7b**. In particular, clarification was sought on whether the reaction proceeded through a 1,4- or 1,5-elimination.

Due to computational expense, a slightly altered computational model was used, whereupon BPh_3 replaced $B(C_6F_5)_3$ and the phenyl group of **7b** was changed to a methyl group (**7b'**, Figure 3.27). Initially, this structure was minimised using an initial force field model, followed by a complete DFT geometry optimisation. All calculations implemented the B3LYP functional and 6-31G(d,p) basis set within Jaguar[19] using an a posteriori D3-correction for dispersion.[20]

The two potential reaction pathways considered were elimination from either the amine NH_2 group (a 1,4-elimination) or from the amide N–H group (a 1,5-elimination). These reactions would yield **P_{14}** and **P_{15}**, respectively (Figure 3.27).

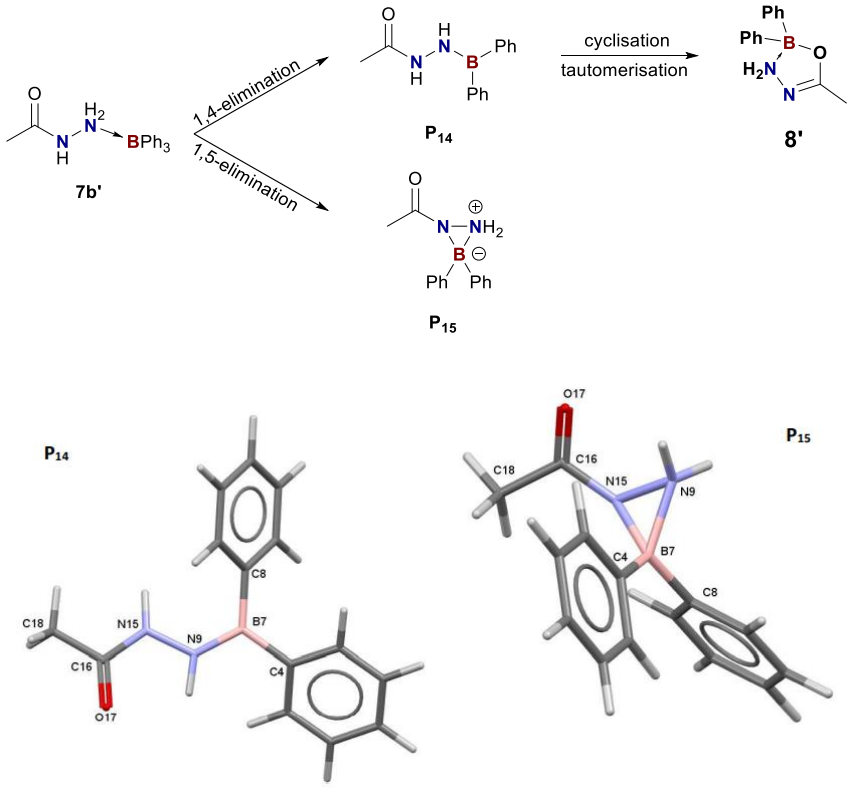

Figure 3.27: a) The two potential reaction pathways to heterocycle **8**. b) Structures for elimination products **P_{14}** and **P_{15}** (the sum of angles for an idealised trigonal planar geometry was set as 360° and for a tetrahedral geometry = 656.82°).

For both potential pathways, upon restricting the intramolecular N–H···C–B distances range between 2.40 Å and 1.09 Å, geometry optimisations were conducted using the [B3LYP-D3/6-31G(d,p)] basis set. At each step, the geometry was allowed to relax in the C···H bond-forming process. As a result, the dispersion term was revealed to have no significant influence on the reaction profiles. The calculated energy dependence for 1,4- and 1,5-elimination (excluding the D3 correction) are plotted in Figure 3.28.

The 1,5-elimination demonstrates a more facile initial shortening of the N–H···C–B distance as it is less strained, *i.e.*, implementing the amide N–H group but converging to a strained three-membered BN_2 ring (**P** $_{15}$). This process has been calculated as near energy-neutral (Figure 3.28). Albeit the 1,4-elimination demonstrates higher activation energy, a more energetically favourable intermediate (**P** $_{14}$) is attained. This product possesses a core structural centre (OCNNB) which approaches planarity. This rigid conformation is thanks to extensive π-conjugation throughout the structure and can be formally considered a five centre, $6e^-$ system (Figure 3.27). It is thus safe to assume the 1,4-elimination constitutes the thermodynamic, whereas the 1,5-elimination is the kinetic process.

The flexibility acyclic **P$_{14}$** exhibits, should favour intramolecular C=O→B coordination (at the expense of some loss in π-stabilisation) and cyclisation. This is quickly followed by tautomerisation to form the cyclic product (tautomerisation prior to ring closure appears less likely as it will break the π-conjugation in the system).

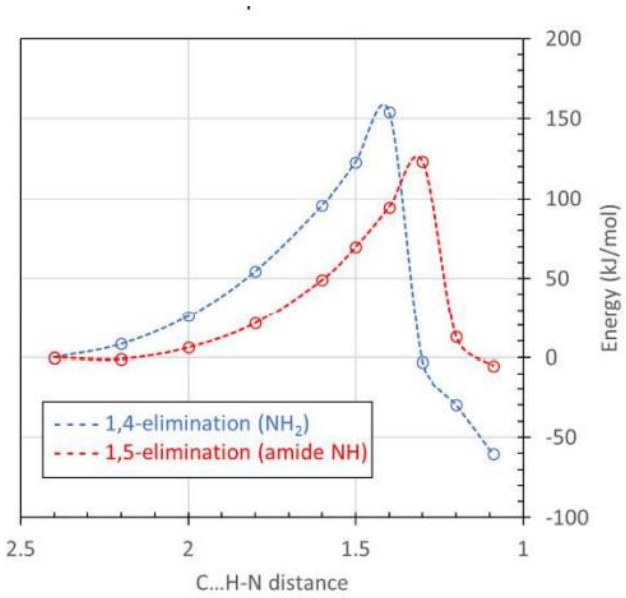

Figure 3.28: The potential energy surface of **8**'.

*3.3.8 Solid-state structures of **7a**–**7b** and **8**.*

The crystals of adducts **7a**–**7b** and heterocycle **8** were once more covered in paratone oil, removed from the glovebox and placed inside the crystallographic apparatus under a cryostream (100 K).

The first samples to be subjected to single crystal X-ray diffraction were the two adducts. For **7a**, the space group was determined as *C*2/*c*, with one and eight molecules in the asymmetric and unit cell, respectively. Meanwhile, **7b** was monoclinic in nature with $P2_1/c$ as the space group, one molecule in the asymmetric unit and four in the unit cell.

The solid-state structures of these adducts were in accordance with the NMR observations in Section 3.3.6. A four-coordinate boron centre was apparent, displaying a dative connection to the terminal nitrogen of the hydrazine functionality.

The N–N bond values of 1.429(3) Å (**7a**) and 1.426(2) Å (**7b**) were perceptibly shorter than for adducts **3a**–**3c** [1.437(3)–1.437(9) Å]. The B–N bond distances of **7a–7b** (1.635(3) Å and 1.643(2) Å respectively) and the C–N bond values of 1.363(3) Å (**7a**) and 1.360(2) Å (**7b**) are typical for bonds of this type.[9]

Table 3.3: Space groups and selected bond metrics of adducts **7a–7b**.

	7a	**7b**
Space group		
	*C*2/*c*	$P2_1/c$
Selected bond		
B–N	1.635(3) Å	1.643(2) Å
N–N	1.429(3) Å	1.426(2) Å
C–N	1.363(3) Å	1.360(2) Å

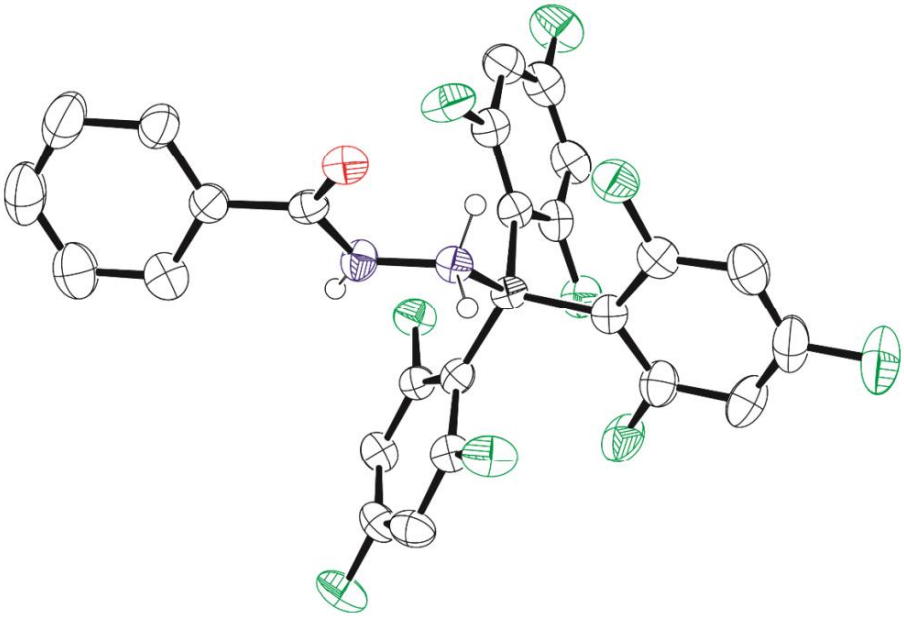

Figure 3.29: Solid-state structure of adduct **7a**. Thermal ellipsoids are drawn at 50% probability. H-atoms, except for those on nitrogen, were omitted for clarity.

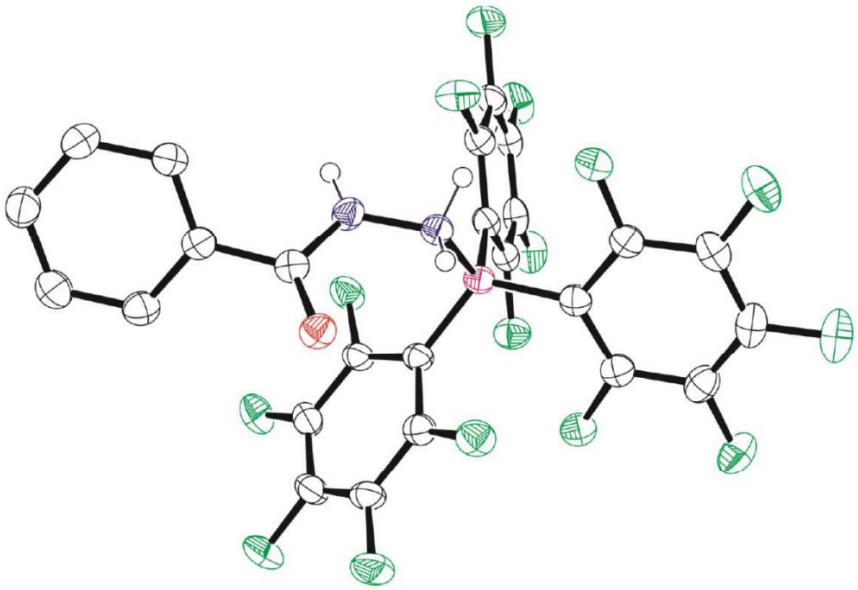

Figure 3.30: Solid-state structure of adduct **7b**. Thermal ellipsoids are drawn at 50% probability. H-atoms, except for those on nitrogen, were omitted for clarity.

With the structure solution at hand and having refinement completed to a satisfactory degree, **8** was found to crystallise in the triclinic *P*-1 space group with two molecules in the asymmetric cell, rising to four in the unit cell.

As seen in adducts **7a** and **7b**, the boron centre was tetracoordinate. In this instance, however, the boron heteronuclei had relinquished one of the aryl rings and formed a covalent bond to the oxygen and terminal nitrogen atoms of the benzhydrazide (**2d**). The corresponding intramolecular CON_2B chelate created by these interactions is planar with a root mean square deviation (r.m.s.d.) of 0.010 and 0.023. The B–O bond length was 1.483(2) Å and 1.487(2) Å. Unsurprisingly, the B–N bond length of 1.621(2) and 1.608(3) Å is marginally shorter than for adducts **7a** [1.635(3) Å] and **7b** [1.643(2) Å]. Of note is the similar length of the N–N bond [1.468(2) and 1.464(3) Å] to the N–N bond of adduct **7b** [1.426(2) Å].

Table 3.4: Space groups and selected bond metrics of heterocycle **8**.

	8
Space group	
	P-1
Selected bond	
B–N	1.608(3)–1.621(2) Å
N–N	1.468(2)–1.464(3) Å
C=N	1.290(2)–1.278(2) Å
B–O	1.483(2)–1.488(2) Å

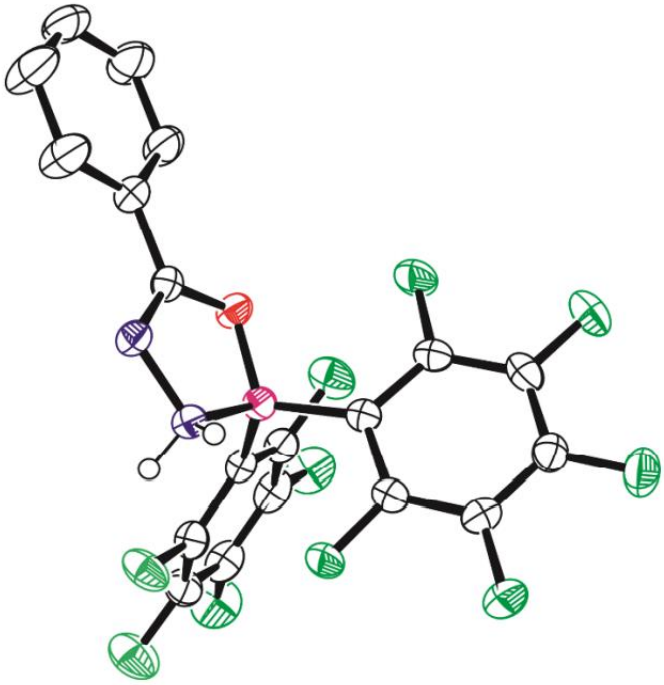

Figure 3.31: Solid-state structure of heterocycle **8**. Thermal ellipsoids are drawn at 50% probability. H-atoms, except for those on nitrogen, were omitted for clarity.

Chapter 3.4 Conclusions

This chapter presented the reactivity of a range of triarylboranes with hydrazones **2a–2c** and hydrazide **2d**. Initially, triarylboranes B(2,4,6-$F_3C_6H_2)_3$ and B(3,4,5-$F_3C_6H_2)_3$ were stoichiometrically added to **2a**, leading to adducts **3a** and **3b**. On the other hand, adding a 2:1 excess of B(2,4,6-$F_3C_6H_2)_3$ to **2b** resulted in adduct **3c**.

A mixture of products was obtained when utilising the same procedure with **2c** and triarylborane B(2,4,6-$F_3C_6H_2)_3$. These were identified as azine **4**, borane adduct **5**, and aryl elimination product **6**. Temperature variation could preferentially generate either product set **4–5** or product **6**. Given the potential industrial applications of **5**, its independent synthesis was achieved using B(2,4,6-$F_3C_6H_2)_3$ and hydrazine monohydrate with molecular sieves present.

Finally, the reaction of commercially available benzhydrazide **2d** with triarylboranes B(2,4,6-$F_3C_6H_2)_3$ and B($C_6F_5)_3$ at room temperature resulted in adducts **7a** and **7b**, respectively. *In-situ* heating of **7b** resulted in the generation of CON_2B heterocycle **8**.

Mechanistic insights were sought into the transformation of adduct **7a** to heterocycle **8** through DFT calculations. Preliminary studies using the B3LYP-D3/6-31G(d,p) basis set were conducted on the $MeCONHNH_2 \rightarrow BPh_3$ model compound. Firstly, the 1,5-elimination reaction pathway (from the –NH proton) was examined, revealing a near energetically neutral kinetic process. The formation of a three-membered BN_2 heterocycle intermediate preceded rearrangement to **8**. On the other hand, the 1,4-elimination of C_6H_6 was determined as the preferred thermodynamic process forming acyclic $MeCON(H)N(H)BPh_2$ as an intermediate. Cyclisation and tautomerisation of this intermediate led to **8**.

Analysis of the solid-state structures of adducts **3a**–**3c**, **5**, **7a** and **7b** showed a considerable weakening of the N–N bond. The B–N and N–N bond metrics obtained were broadly similar with literature reported $Ph_2C{=}NNH_2{\rightarrow}B(C_6F_5)_3$ adduct.[2] Remarkably, the bond metrics of **3a** and **3c** were almost identical. As the acidity of the triarylborane was increased, a slight but noticeable shortening of the B–N bond was observed. Finally, as the boron centre in **7b** switched from a tetracoordinate to a tricoordinate configuration in **8**, the enhanced electronic donation resulted in a significantly longer N–N and shorter B–N bond.

A summary of the products synthesised, and their fundamental analytical properties are presented in Figure 3.32 and Table 3.5 below.

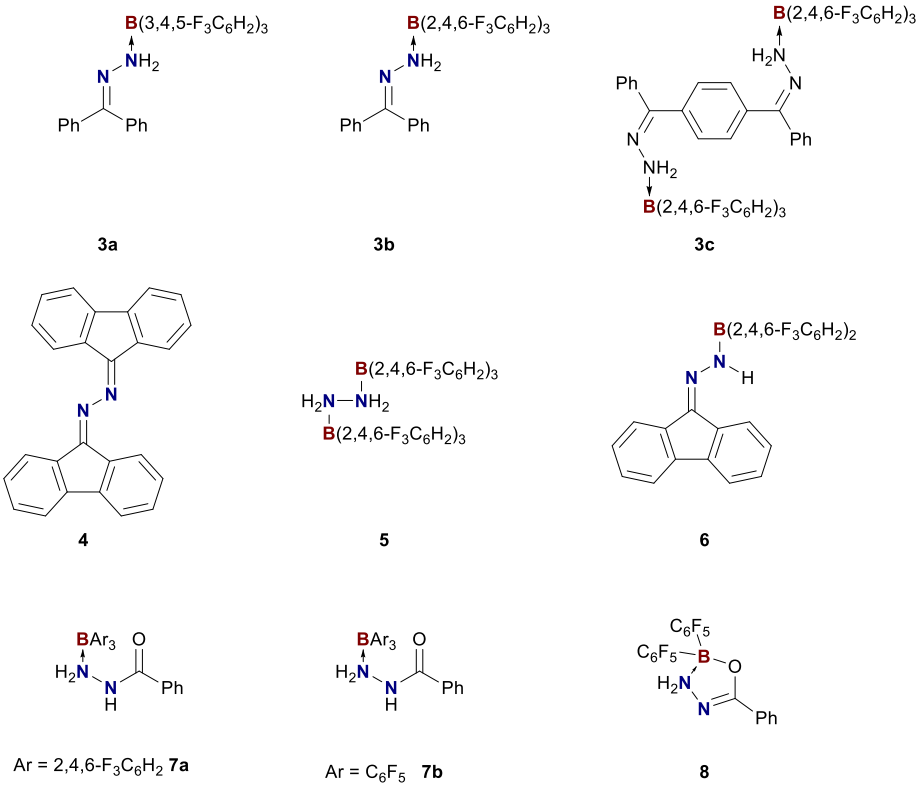

Figure 3.32: Summary of compounds synthesised in Chapter 3.

Table 3.5: Summary of key characteristics of products synthesised in Chapter 3.

	3a	**3b**	**3c**
$^{11}B\{^{1}H\}$ NMR chemical shift	-2.6 ppm	-6.1 ppm	-6.2 ppm
Space group	*P*-1	$P2_1/n$	*P*-1
Selected bond			
B–N	1.647(10) Å	1.652(5) Å	1.647(4) Å
N–N	1.437(9) Å	1.443(4) Å	1.437(4) Å
C=N	1.294(8) Å	1.284(4) Å	1.294(4) Å
	4	**5**	**6**
$^{11}B\{^{1}H\}$ NMR chemical shift	N/A	-4.2 ppm	-6.3 ppm
Space group	*P*-1	I_2/a	$P2_1/c$
Selected bond			
B–N	N/A	1.673(2) Å	1.397(2) Å
N–N	1.437(9) Å	1.461(2) Å	1.379(17) Å
C=N	1.294(8) Å	N/A	1.288(18) Å
	7a	**7b**	**8**
$^{11}B\{^{1}H\}$ NMR chemical shift	-6.1 ppm	-6.2 ppm	-4.3 ppm
Space group	*C*2/c	$P2_1/c$	*P*-1
Selected bond			
B–N	1.635(3) Å	1.643(2) Å	1.608(3) Å 1.621(2) Å
N–N	1.429(3) Å	1.426(2) Å	1.468(2) Å 1.464(3) Å
C=N	1.363(3) Å	1.360(2) Å	1.290(2) Å 1.278(2) Å
B–O	N/A	N/A	1.483(2) Å 1.488(2) Å

Chapter 3.5 References

1 T. A. Gazis, J. Carden, M. Alharbi and R. L. Melen, *Triarylboranes in the Activation of Azo Containing Compounds*, EIBC, 2021.

2 C. Tang, Q. Liang, A. Jupp, T. Johnstone, R. Neu, D. Song, S. Grimme and D. Stephan, *Angew. Chem. Int. Ed.*, 2017, **56**, 16588.

3 M. Santi, D. Ould, J. Wenz, Y. Soltani, R. Melen and T. Wirth, *Angew. Chem. Int. Ed.*, 2019, **58**, 7861.

4 T. Gazis, A. Dasgupta, M. Hill, J. Rawson, T. Wirth and R. Melen, *Dalton Trans.*, 2019, **48**, 12391.

5 R. Murray and A. Trozzolo, *J. Org. Chem.*, 1961, **26**, 3109.

6 J. Li, Q. Lefebvre, H. Yang, Y. Zhao and H. Fu, *Chem. Commun.*, 2017, **53**, 10299.

7 M. Bartucci, P. Wierzbicki, C. Gwengo, S. Shajan, S. Hussain and J. Ciszek, *Tetrahedron Lett.*, 2010, **51**, 6839.

8 M. Légaré, G. Bélanger-Chabot, R. Dewhurst, E. Welz, I. Krummenacher, B. Engels and H. Braunschweig, *Science*, 2018, **359**, 896. Also see: C. Hering-Junghans, *Angew. Chem., Int. Ed*., 2018, **57**, 6738; M. Légaré, M. Rang, G. Bélanger-Chabot, J. Schweizer, I. Krummenacher, R. Bertermann, M. Arrowsmith, M. Holthausen and H. Braunschweig, *Science*, 2019, **363**, 1329.

9 F. Allen, D. Watson, L. Brammer, A. Orpen and R. Taylor, *Int. Tables Crystallogr.*, 2006, **9.5(C)**, 790.

10 J. Lasri, N. Eltayeb and A. Ismail, *J. Mol. Struct.*, 2016, **1121**, 35.

11 S. Mebs, S. Grabowsky, D. Förster, R. Kickbusch, M. Hartl, L. Daemen, W. Morgenroth, P. Luger, B. Paulus and D. Lentz, *J. Phys. Chem.*, 2010, **114**, 10185.

12 J. Kiernicki, M. Zeller and N. Szymczak, *J. Am. Chem. Soc.*, 2017, **139**, 18194

13 C. Chen and F. Gabbaï, *Chem. Sci.*, 2018, **9**, 6210.

14 J. Safari and S. Gandomi-Ravandia, *RSC Adv.*, 2014, **4**, 46224 .

15 R. Bertani, M. Biasiolo, K. Darini, R. Michelin, M. Mozzon, F. Visentin and L. Zanotto, *J. Organomet. Chem.*, 2002, **642**, 32.

16 M. Trudell, N. Fukada and J. Cook, *J. Org. Chem.*, 1987, **52**, 4293.

17 Y. Yu, W. Brennessel and P. Holland, *Organometallics*, 2007, **26**, 3217; Y. Lee, N. Mankad and J. Peters, *Nat. Chem.*, 2010, **2**, 558; C. Saouma, C. Lu and J. Peters, *Inorg. Chem.*, 2012, **51**, 10043; K. Umehara, S. Kuwata and T. Ikariya, *J. Am. Chem. Soc.*, 2013, **135**, 6754; Y. Li, Y. Li, B. Wang, Y. Luo, D. Yang, P. Tong, J. Zhao, L. Luo, Y. Zhou, S. Chen, F. Cheng and J. Qu, *Nat. Chem.*, 2013, **5**, 320.

18 T. Hügle, M. Kühnel and D. Lentz, *J. Am. Chem. Soc.*, 2009, **131**, 7444

19 Jaguar, v9.8, Schrodinger, Inc., New York, NY, 2017; A. Bochevarov, E. Harder, T. Hughes, J. Greenwood, D. Braden, D. Philipp, D. Rinaldo, M. Halls, J. Zhang, R. Friesner, Int. *J. Quantum Chem.*, 2013, **113**, 2110.

20 S. Grimme, J. Antony, S. Ehrlich and H. Krieg, *J. Chem. Phys.*, 2010, **132**, 154104.

Chapter 4: Reactivity of diaziridines with triarylboranes and FLPs.

Chapter 4.1 Introduction

The previous chapter explored in detail the reactivity of hydrazones and hydrazides with a variety of triarylboranes. Covalent N–N–B systems were generated following adduct formation, including chain and heterocyclic compounds.[1] Intriguingly, several of the adducts (**3a–3c** and **7a** specifically) proved reluctant to undergo the expected aryl elimination. Instead, inseparable mixtures formed at elevated temperatures with repeated crystallisations unable to isolate a single product. Even the literature reported product $Ph_2C{=}NNH{-}B(C_6F_5)_2$ was furnished in only 26% yield.[2] These results served as the impetus to search for alternative azo based starting materials that might be more amenable to aryl elimination.

Diaziridines are three-membered nitrogen heterocycles that have found widespread use in the materials and pharmaceutical industry. Furthermore, they constitute a facile substrate in synthetic chemistry with transformations ranging from additions to ring expansions and oxidations.[3] Of note is their susceptibility to acids. They rapidly undergo hydrolysis reverting to the parent ketone and liberating a hydrazine derivative. Hence, water exclusion must be ensured to suppress this degradation.[4]

Crucially, diaziridines represent heterocyclic structural analogues of hydrazones. It was postulated that the additional ring strain observed in these compounds could allow the aryl elimination to occur in a concerted fashion and at a lower temperature. When separation of the desired products proved challenging once more, Frustrated Lewis Pairs were used as potential activating agents.

This chapter exposes diaziridines (**10a** and **10b**) to triarylboranes and Frustrated Lewis Pairs (FLPs) to further expand the frontiers of metal-free azo activation (Figure 4.1).

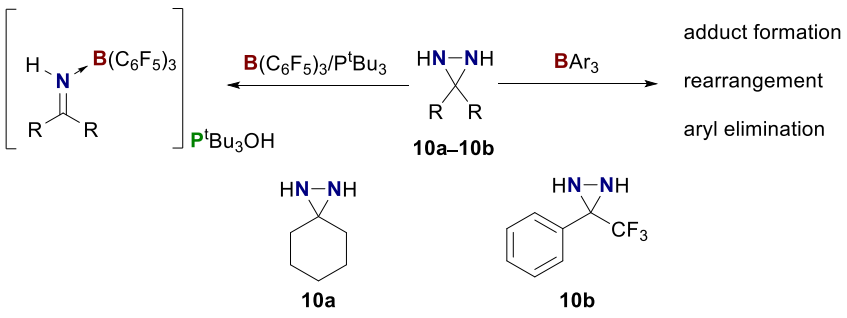

Figure 4.1: Summary of work presented in Chapter 4.

Chapter 4.2 Synthesis and NMR analysis of precursor 9 and diaziridines 10a–10b.

Due, in part, to the high ring strain and inherent stability issues of diaziridines, their synthesis was considerably more taxing than that for their hydrazone counterparts. Although simplified syntheses of a range of diaziridines have recently been reported, these results could not be replicated despite repeated attempts.[5] This may be due to a range of factors, including lack of proper equipment, reagent contamination or human error. Ultimately, these newer, expedited, general preparations were abandoned in favour of older, established syntheses tailored to each of the individual diaziridines

Whilst scouring the literature for suitable diaziridines, one example stood out. 3-phenyl-3-(trifluoromethyl)diaziridine (**10a**) constitutes a vital precursor to 3-phenyl-3-(trifluoromethyl) diazirine, the small photolabel of choice in the arsenal of biomolecular chemists.[6] Given this significance and the presence of a CF_3 group, which could act as a reactivity probe in ^{19}F NMR spectra, **10a** was an obvious synthetic target.

The procedure followed was first reported by Hashimoto *et al.* and relied upon using phenyl tosylate **9** as a starting material.[7] As this precursor was not commercially available, it was synthesised from the parent ketone (Figure 4.2). The synthesis began by dissolving 2,2,2-trifluoro-1-phenylethanone in pyridine and dropwise adding a slight excess of hydroxylamine hydrochloride. After stirring the mixture at 70 °C for one hour, the pyridine was removed, and an acidic workup followed. The resultant crude residue was dissolved in acetone at 0 °C, and an excess of triethylamine and *p*-toluene sulfonyl chloride were added. The reaction mixture was stirred at room temperature for one hour. After evaporating all volatiles, an aqueous workup and drying under vacuum, the desired product was furnished as an off-white solid at 67% overall yield.

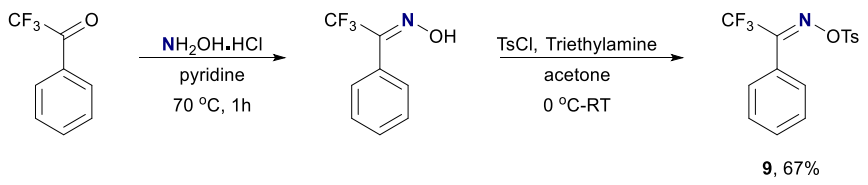

Figure 4.2: Preparation of tosylate precursor **9**.

The spectral data showed good agreement with the literature reported values (Figure 4.3).[7] The ^{1}H NMR spectrum displayed two multiplets in the aromatic region at δ = 7.91–7.88 ppm and 7.53–7.88 ppm, collectively integrating to the expected nine protons. In addition, a doublet at δ = 2.47 ppm with an integration of three corresponded to the methyl group. Intriguingly, the ^{19}F NMR spectrum showed two signals at δ = -61.49 and -66.78 ppm with an integration ratio of 2:1, which was in accordance with literature precedence.

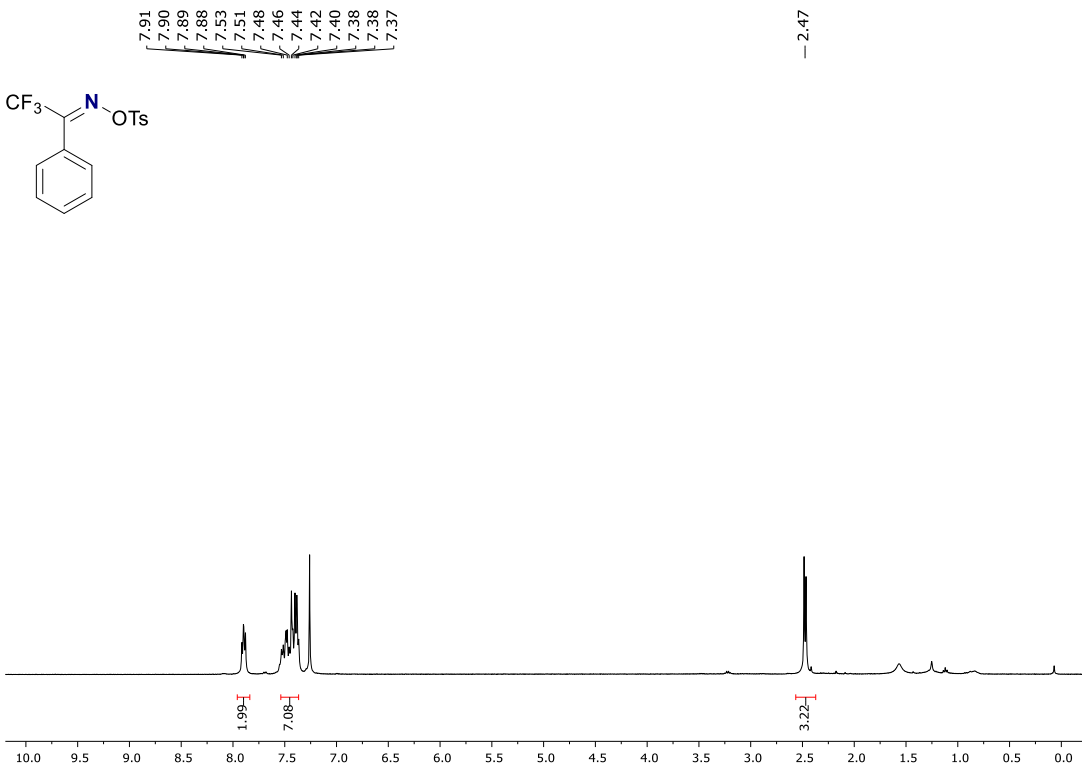

Figure 4.3: ^{1}H NMR (400 MHz, $CDCl_3$, 298 K) spectrum of **9**.

The formation of **10a** proceeded by following the synthetic protocol devised by Richards *et al.* (Figure 4.4).[8] Firstly, tosylate precursor **9** was dissolved in diethyl ether at -78 °C. Upon adding approximately 5 mL of freshly distilled liquid ammonia, the mixture was stirred in a sealed vessel for sixteen hours at room temperature. Upon reaction completion, unsealing the reaction vessel at room temperature resulted in evaporation of the liquid ammonia. The crystallised by-product, *p*-toluene sulfonyl amine, was removed by suction filtration. Subsequent water washes and drying *in vacuo* at 0 °C led to the crystallisation of **10a** as a white solid in 83% yield. Of note was the instability of this compound. Degradation was observed within 3–4 days regardless of storage conditions (-5 °C or -18 °C, inert atmosphere). The title compound was thus freshly prepared whenever required.

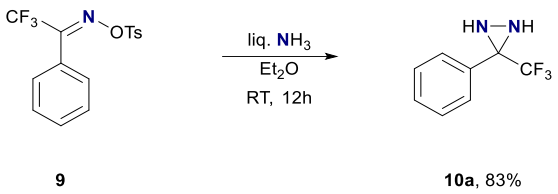

9 **10a**, 83%

Figure 4.4: Synthesis of diaziridine **10a** from precursor **9**.

Product identification was achieved once more using ^{1}H and ^{19}F NMR spectroscopy. The ^{1}H NMR spectrum showed the emergence of two broad singlets at δ = 2.81 and 2.25 ppm, with an integration of one, which can be attributed to the two –NH protons. As the compound is highly symmetrical with a C_2 axis of symmetry, there are only two multiplet aromatic signals at δ = 7.64–7.61 and 7.47–7.41 ppm. All tosylate proton signals were no longer present (Figure 4.5). Unlike **9**, the ^{19}F NMR spectrum showed a singlet centred at δ = -68.31 ppm corresponding to the $–CF_3$ group.

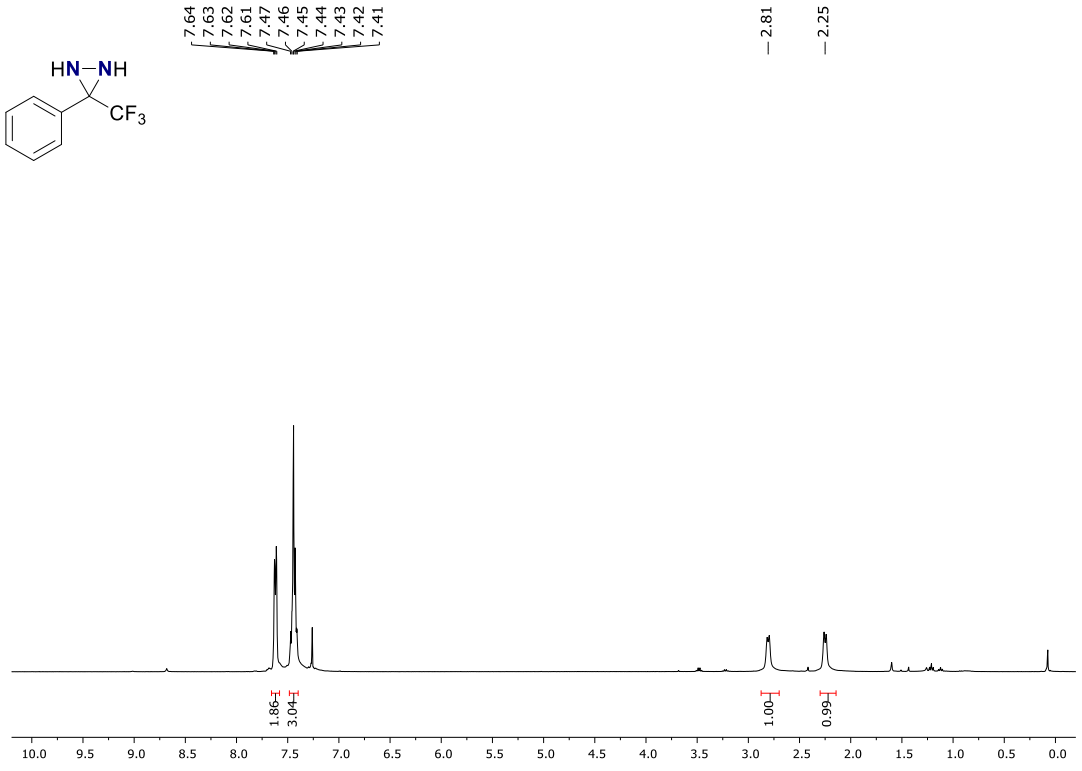

Figure 4.5: ^{1}H NMR (400 MHz, $CDCl_3$, 295 K) spectrum of diaziridine **10a**.

For the second target diaziridine, a structural analogue of hydrazine **3a** was envisaged to facilitate comparisons with the results of Chapter 3. However, as it is not chemically possible to have a diaziridine moiety directly attached to a phenyl group, a hexyl group was used instead as the six-membered ring.

According to a literature known procedure first formulated by Glass *et al.,* this diaziridine could be directly synthesised from cyclohexanone.[9] This protocol avoided the need for low temperatures and liquid ammonia. However, a crucial reagent for this preparation was hydroxylamine-O-sulfonic acid (Figure 4.6). Albeit commercially available, considerably higher yields of **10b** were obtained (19% contrasted to 42%) if it was freshly prepared. Its synthesis was achieved using hydroxylamine sulfate and chlorosulfonic acid, as first reported by Millard *et al.*[10] The resultant reagent was used without characterisation and stored at a -18 °C freezer in a tightly sealed container for no longer than three weeks.

Figure 4.6: Preparation of hydroxylamine-O-sulfonic acid.

The synthesis of **10b** began by dissolving cyclohexanone in approximately 40 mL of aqueous ammonia and cooling the resultant solution to 0 °C (Figure 4.7).[9] Next, an equimolar amount of hydroxylamine-O-sulfonic acid was added portion-wise. The mixture was stirred for another hour at 0 °C and left overnight at -18 °C. Subsequently, the precipitated crystalline cake was filtered and washed successively with ether and toluene. A final hot recrystallisation from toluene, ether washings and further drying allowed for the isolation of product **10b** as a microcrystalline white solid in 42% yield. Due to the potential for degradation, the product was immediately stored under inert cold (-30 °C) conditions.

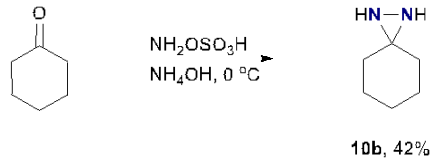

Figure 4.7: Preparation of **10b** using cyclohexanone.

The spectroscopic data showed good agreement with literature reported values.[9] The ^{1}H NMR spectrum displayed a distinctly broad multiplet at δ = 1.68–1.50 ppm (Figure 4.8). As ^{1}H NMR spectroscopy did not conclusively verify the identity of **10b**, ^{13}C{^{1}H} NMR spectroscopy was also used to corroborate the ^{1}H NMR findings. There were five singlets observable at δ = 57.6 (NCN), 36.2 (CH), 25.1 (CH) and 25.0 (CH) ppm. The ^{1}H and ^{13}C{^{1}H} NMR spectra are displayed below.

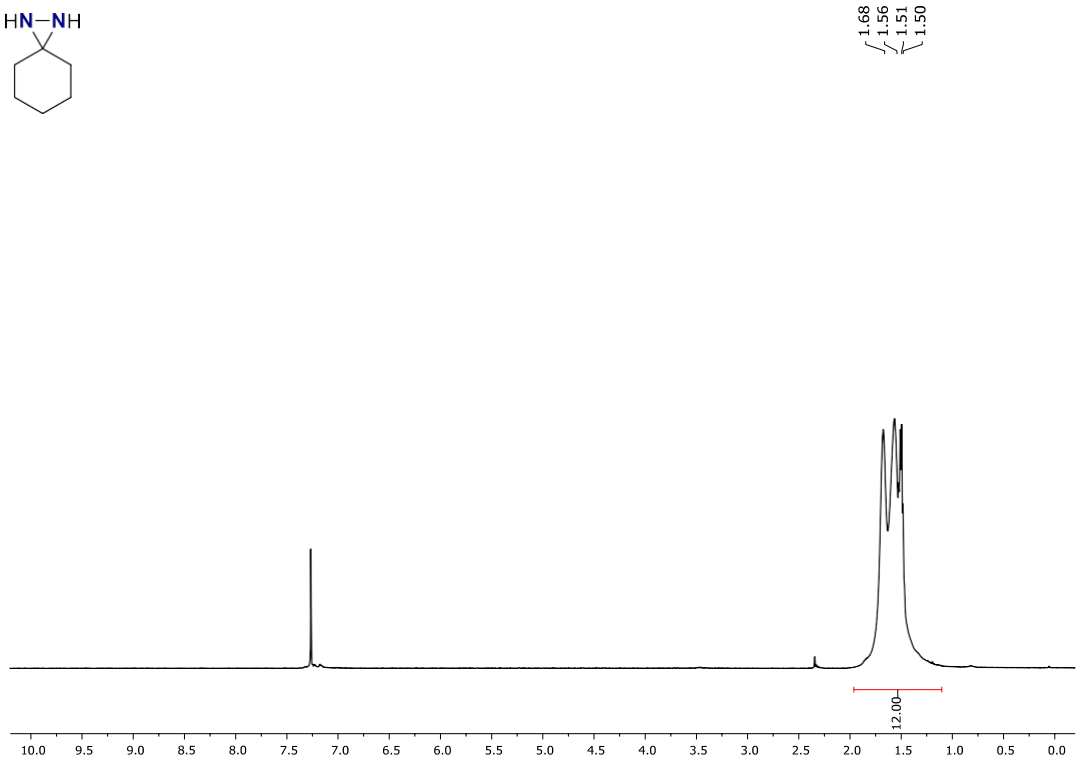

Figure 4.8: ^{1}H NMR (400 MHz, $CDCl_3$, 295 K) spectrum of diaziridine **10b**.

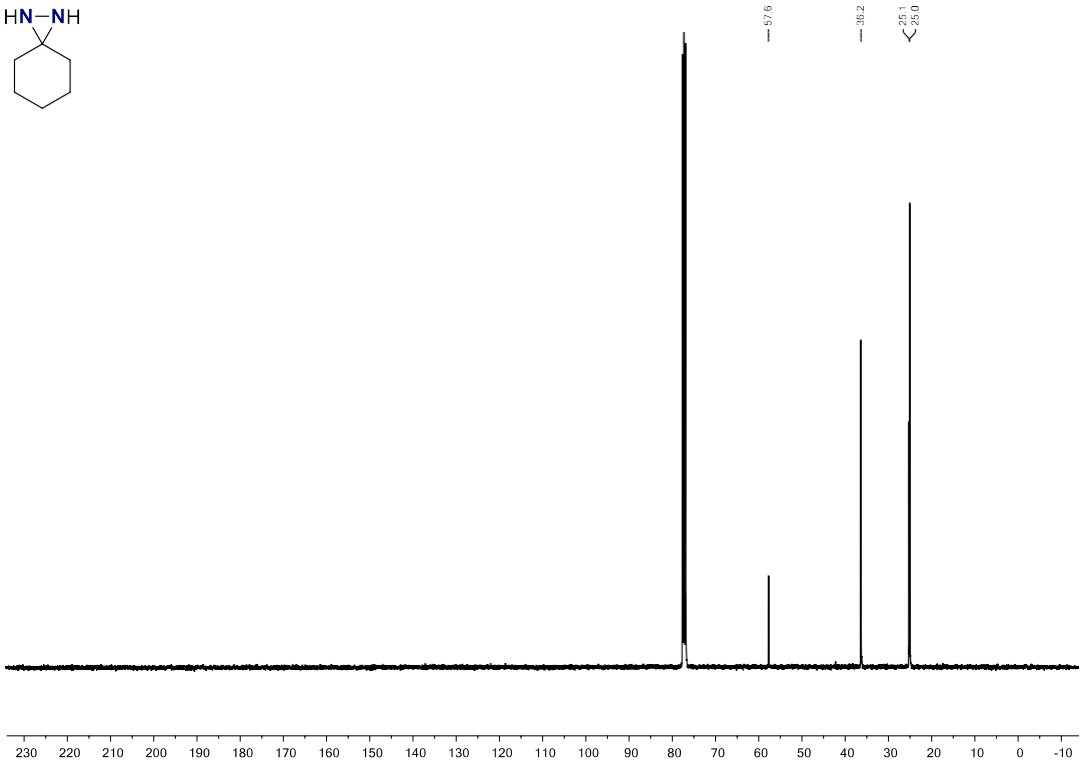

Figure 4.9: $^{13}C\{^{1}H\}$ NMR (101 MHz, $CDCl_3$, 298 K) spectrum of **10b**.

Chapter 4.3: Synthesis and characterisation of products 11–15.

*4.3.1 Synthesis and attempted isolation of adduct **11** and product **12***

In an analogous fashion to the method utilised for the synthesis of **3a–3c** in Chapter 3, adduct formation was attempted by mixing an equimolar toluene solution of **10a** with either $B(3,4,5\text{-}F_3C_6H_2)_3$ or $B(C_6F_5)_3$ at room temperature (Figure 4.10). The *in-situ* $^{11}B\{^1H\}$ and ^{19}F NMR spectra of both crude mixtures were plagued with impurities and markedly complex. However, a few single crystals were obtained for the reaction of $B(3,4,5\text{-}F_3C_6H_2)_3$ with **10a** that could be analysed by X-ray diffraction, demonstrating the formation of **11**.

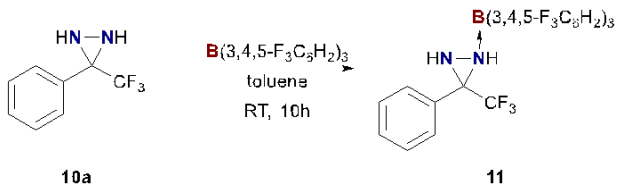

Figure 4.10: Synthesis of adduct **11**.

Despite the disappointing results obtained above, stoichiometric toluene solutions of **10a** with either $B(C_6F_5)_3$ or $B(3,4,5\text{-}F_3C_6H_2)_3$ were heated to 100 °C for ten hours. Subsequently, the crude residues were subjected to crystallisation. In spite of repeated attempts using various crystallisation techniques and solvents, separation of a single species was not achieved, as evidenced by complex multinuclear NMR spectra. However, crystals were furnished by slow evaporation of the solvent.

From these two samples, the crystals from the reaction of **10a** with $B(3,4,5\text{-}F_3C_6H_2)_3$ were highly twinned and of inferior quality. Therefore, the crystallographic data attained could not be solved and refined to a satisfactory degree. On the other hand, the reaction of **10a** with $B(C_6F_5)_3$ yielded suitable crystals for single crystal X-ray diffraction, thus revealing the structure of **12** (Figure 4.11).

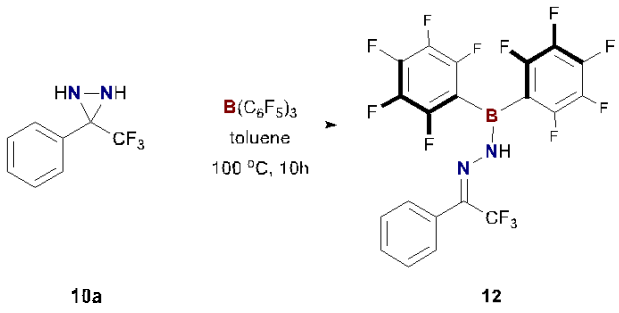

Figure 4.11: Synthesis of product **12**.

The inability to cleanly isolate the elimination product is reminiscent of the results in Chapter 3 and the meagre yield (26%) of literature known $Ph_2C{=}NNH{-}B(C_6F_5)_2$.[2]

*4.3.2 Solid-state structural analysis of **11** and **12***

As the nature of **11** and **12** could not be effectively ascertained using multinuclear NMR spectroscopy, single crystal X-ray diffraction was employed. Crystals suitable for single crystal X-ray diffraction for both products were obtained by slow evaporation of toluene over one week.

The data sets collected were subjected to structure solution and refinement, revealing the space group of **11** as *Fdd2*. One molecule was present in the asymmetric unit cell, growing to sixteen molecules in the unit cell. The solid-state structure disclosed that the diaziridine ring had remained intact with the boron centre coordinating to one of the –NH groups. This result is surprising given the tendency of diaziridines to undergo ring cleavage in the presence of much weaker acids than $B(3,4,5\text{-}F_3C_6H_2)_3$.[4]

The single N–N bond length of 1.502(3) Å and the non-coordinated C–N bond length of 1.453(3) Å appear unaffected with bond lengths typical for their respective types.[11] On the other hand, a slight bond elongation [1.464(3) Å] was apparent for the C–N(Boron) bond coordinated to $B(3,4,5\text{-}F_3C_6H_2)_3$ suggesting a slight weakening of this bond. The B–N bond length of 1.663(3) Å is within the same region as adducts **3a**–**3c** [*cf.* 1.646(5)–1.696(4) Å].

Table 4.1: Space groups and selected bond metrics of product **11**.

	11
Space group	*Fdd*2
Selected bond	
N–N	1.502(3) Å
C–N	1.453(3) Å
C–N(Boron)	1.464(3) Å
B–N	1.663(3) Å

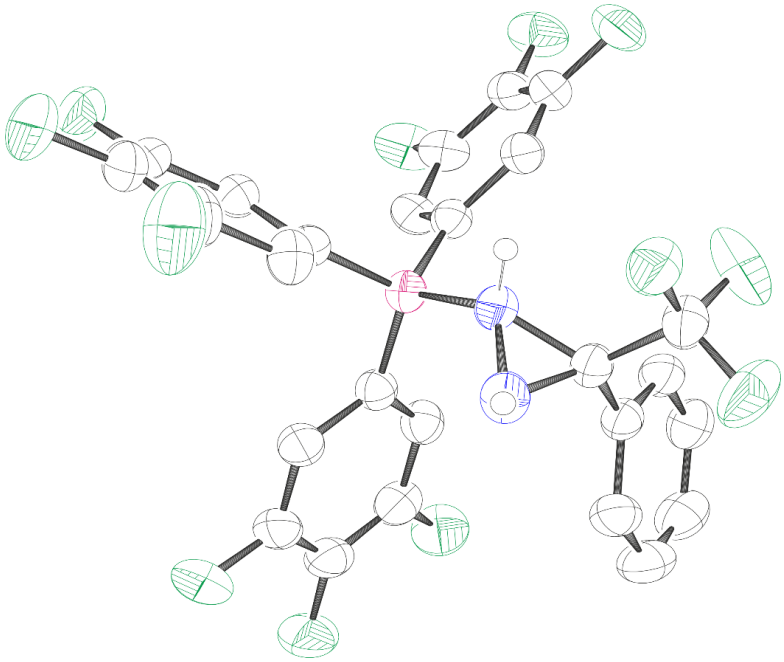

Figure 4.12: Solid-state structure of adduct **11**. Thermal ellipsoids are drawn at 50% probability. H-atoms, except for those on nitrogen, were omitted for clarity.

Product **12** crystallised in the $P2_1/c$ space group, with one molecule in the asymmetric cell rising to four in the unit cell. The solid-state structure revealed diaziridine ring cleavage had occurred across one of the C–N bonds, with concomitant aryl elimination from the triarylborane.

The boron centre exhibited a pseudo trigonal planar geometry around it with a C–B–C angle of 122.24(3)° and two C–B–N angles of 119.75(2)° and 117.85(2)°. The N–N [1.374(3) Å], B–N [1.396(2) Å], and C=N [1.278(4) Å] bond lengths follow closely those of **6** in Chapter 3 [*cf.* 1.397(2) Å, 1.379(17) Å and 1.288(19) Å]. This data is a strong indicator of significant π bonding character, with restricted rotation around the B–N bond. Consequently, the molecule is forced to adopt a *trans* diene structure, as previously observed in **6** (*cf*. Chapter 3).

Table 4.2: Space groups and selected bond metrics of products **6** and **12**.

	6	**12**
Space group		
	P-1	$P2_1/c$
Selected bond		

B–N	1.397(2) Å	1.396(4) Å
N–N	1.379(17) Å	1.374(3) Å
C=N	1.288(19) Å	1.278(4) Å
Selected Angle		
N –B–C	117.76(13)°	117.85(2) °
N–B–C	119.71(13)°	119.75(2) °
C –B–C	122.49(13)°	122.24(3) °

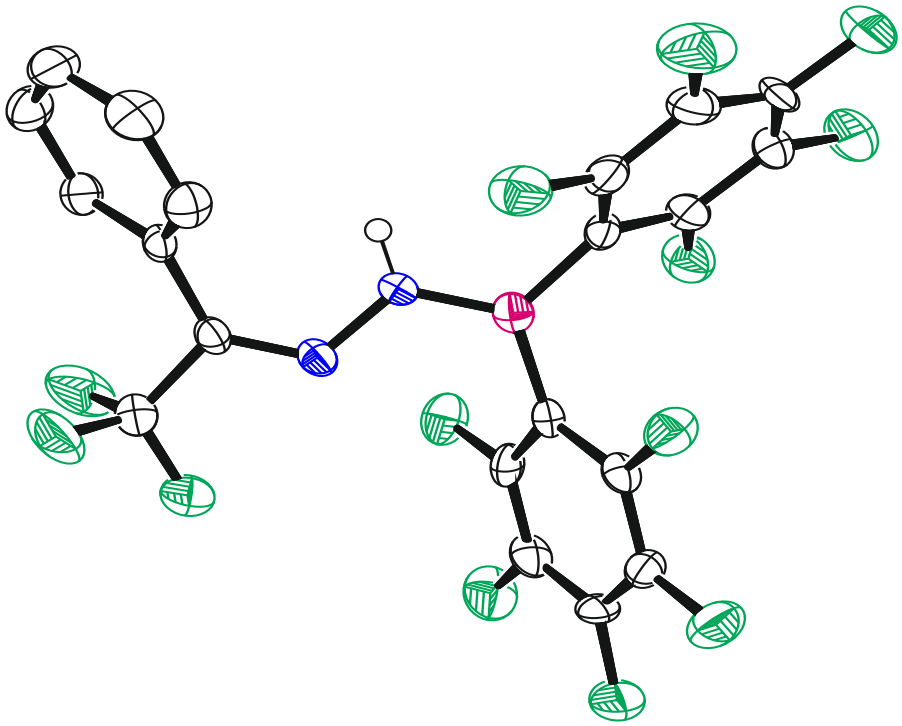

Figure 4.13: Solid-state structure of product **12**. Thermal ellipsoids are drawn at 50% probability. H-atoms, except for those on nitrogen, were omitted for clarity.

*4.3.3 Synthesis of adduct **13a***

The solid-state structures of **11** and **12** provided valuable insights into the prospective reactivity of diaziridines with triarylboranes. **12** was especially promising, as it revealed aryl elimination is possible with this class of compounds, much like their non-cyclic hydrazone counterparts.

However, given the instability of **10a** alongside the difficulties in purifying products **11** and **12**, alternative diaziridine **10b** was employed for subsequent transformations.

Upon combining **10b** with $B(C_6F_5)_3$ in deuterated chloroform at room temperature (Figure 4.14), a broad singlet emerged at δ = -6.4 ppm in the $^{11}B\{^1H\}$ NMR spectrum. No traces of unreacted triarylborane were discernible. This observation is consistent with N→B adduct formation rather than the desired aryl elimination.

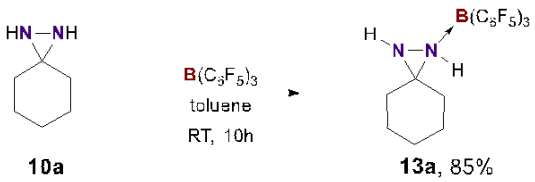

Figure 4.14: Reaction of diaziridine **10a** with $B(C_6F_5)_3$.

The ^{19}F NMR spectrum provided little analytical insight as the multiplicities and integration ratio remained fundamentally unchanged from the starting triarylborane. However, a slight downfield shift was observed for all signals, with the signals now located at δ = -132.80, -155.08 and -162.49 ppm, again suggesting adduct formation.

In the ^1H NMR spectrum, a –NH proton shift from δ = 1.4 ppm to δ = 5.3 ppm was observed. In addition, the non-coordinated –NH proton emerged as a broad singlet at δ = 2.90 ppm. Finally, the hexyl signals appeared as a series of singlets, doublets and multiplets at the alkyl region (δ = 2.34–1.01 ppm). Their integral was ten.

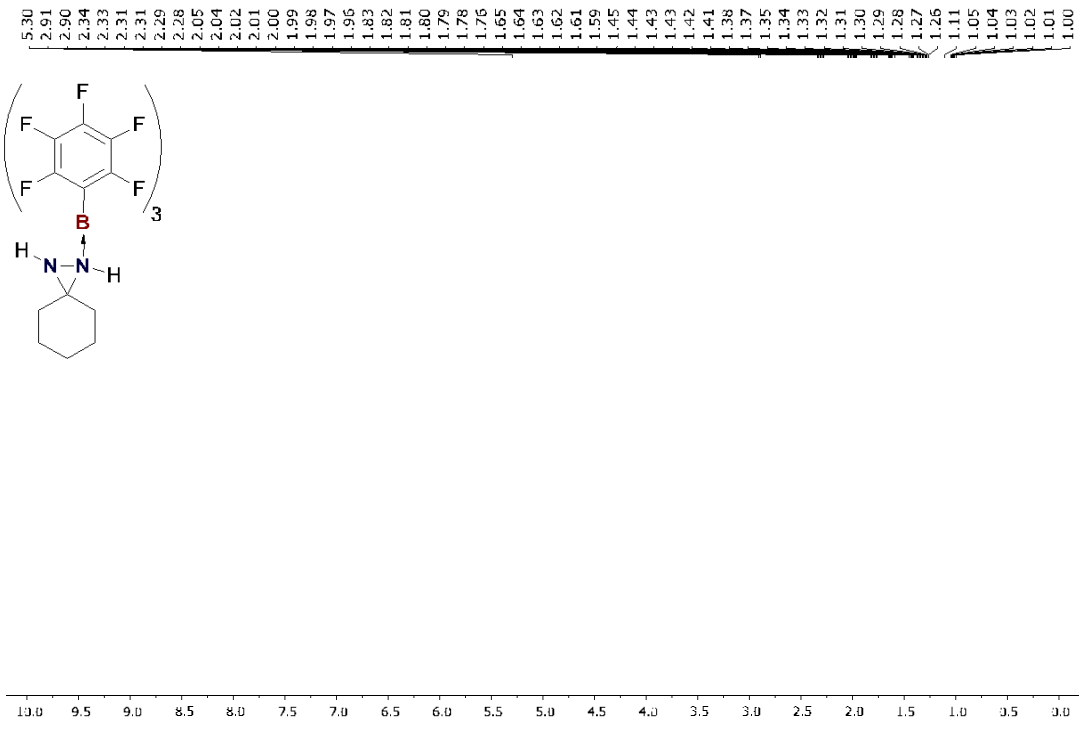

Figure 4.15: ^1H NMR (500 MHz, $CDCl_3$, 298 K) spectrum of **13a**.

Intriguingly, over two hours, new signals began to appear in the ^1H NMR spectrum, suggesting some form of degradation or further reaction. The crude residue was

placed in a vial within the -30 °C freezer inside the glovebox to impede this process. Gratifyingly, this action was sufficient to stop degradation and generate single crystals suitable for X-ray diffraction within the space of one day.

*4.3.4 Solid-state structure analysis of **13a***

The colourless crystal plates, which promptly formed upon storing a toluene solution of **13a** at -30 °C, proved amenable to X-ray analysis. After structure solution and refinement, **13a** was shown to crystallise in the $P2_1/n$ space group with one molecule in the asymmetric and four in the unit cell.

The solid-state structure had a similar geometry and metrics to **11**, with the diaziridine ring remaining intact. The formation of a dative bond between one of the nitrogens and the boron centre was evident. The hexyl ring has adopted a chair conformation whilst the diaziridine ring maintained its rigid planarity, as seen in adduct **11**.

Thus, the boron heteroatom is four-coordinate with a B–N bond length of 1.636(2) Å, slightly shorter than **11** [*cf.* 1.663(3) Å]. The boron coordinated C–N(Boron) bond measured 1.456(3) Å (*cf.* 1.464 Å for **11**). All other bond metrics, including the N–N [1.504(2) Å] and C–N bond [1.484(2) Å], were analogous to those of **11** (*cf.* Section 4.3.2 and Table 4.3).

Table 4.3: Space group and selected bond metrics of adducts **11** and **13a**.

	11	**13a**
Space group	*Fdd*2	$P2_1/n$
Selected bond		
B–N	1.663(3) Å	1.636(2) Å
N–N	1.502(3) Å	1.504(2) Å
C–N	1.453(3) Å	1.456(3) Å
C–N(Boron)	1.464(3) Å	1.484(2) Å

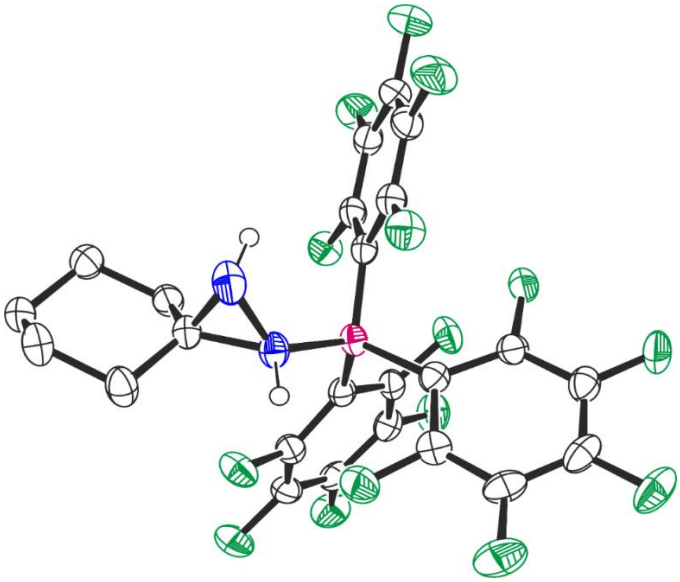

Figure 4.16: Solid-state structure of adduct **13a**. Thermal ellipsoids are drawn at 50% probability. H-atoms, except for those on nitrogen, were omitted for clarity.

*4.3.5 Synthesis and NMR analysis of **13b–13d**.*

The interesting results obtained above raised the question of how diaziridine **10b** would behave in the presence of a stoichiometric ratio of other triarylboranes. Thus, the substrate scope was expanded to include $B(3,4,5\text{-}F_3C_6H_2)_3$, $B(2,4,6\text{-}F_3C_6H_2)_3$, and BPh_3. Hence, a broad spectrum of Lewis acidities was covered, allowing the examination of its effect on the reaction (Figure 4.17). As with $B(C_6F_5)_3$, all triarylboranes afforded the expected adducts **13b–13d**. These adducts proved to be more stable than **13a**, allowing for storage at room temperature under inert conditions with no noticeable degradation even after two weeks.

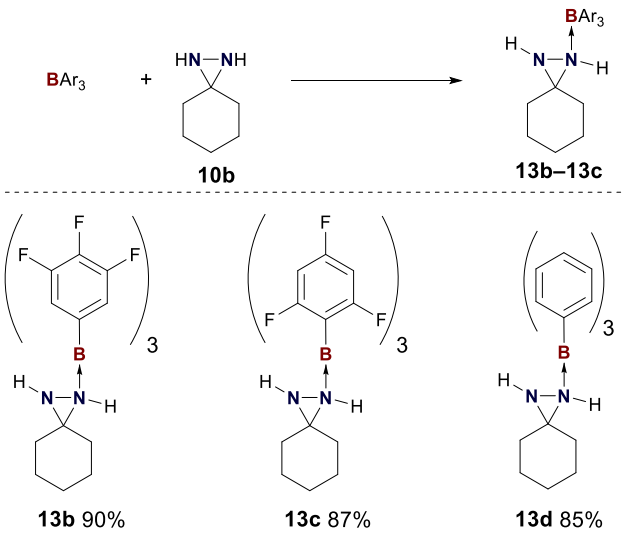

Figure 4.17: Generation of adducts **13b–13d**.

The analytically pure samples of **13b–13d** possessed a broad resonance in the $^{11}B\{^{1}H\}$ NMR spectrum between δ = -6.3 and 2.33 ppm, denoting a tetracoordinate boron centre.

The ^{19}F NMR spectra of all adducts showed a downfield shift from the parent triarylborane. Using **13b** as an example, the signals were located at δ = -139.52 and -153.16 ppm. However, the integration ratio, multiplicity and coupling constants remained unchanged from the parent triarylborane as seen previously with adduct **13a**.

Whilst examining the ^{1}H NMR spectrum of all adducts, the alkyl region (*cf.* δ = 1.0–1.4 ppm) was considerably crowded with various multiplets, broad singlets and doublets because of the hexyl moiety. Despite this fact, the sum of all integrals in this region matched those expected for a hexyl group (ten) and did not obscure any other proton signals.

These observations are exemplified by the ^{1}H NMR spectrum of **13b**. Herein the hexyl signals are located between δ = 1.10–2.27 ppm integrating collectively to ten protons. The two –NH signals were no longer equivalent with one located at δ = 5.49 ppm (likely the $B(3,4,5\text{-}F_3C_6H_2)_3$ coordinated one) and the other at δ = 2.86 ppm. Finally, the expected triplet arising from the triarylborane proton signals were located at δ = 6.54–6.49 ppm with an integration of six.

*4.3.6 Synthesis and NMR characterisation of rearrangement products **14a–14d**.*

Upon leaving a solution of **13a** to stand at room temperature, a new singlet resonance emerged in the ^{1}H NMR spectrum at δ = 7.15 ppm. Furthermore, the broad singlet resonance at the $^{11}B\{^{1}H\}$ NMR spectrum now appeared at δ = -7.2 ppm rather than δ = -6.43 ppm. However, the most noticeable difference was observed in the ^{13}C NMR spectrum with a significant shift in the –CN signal from δ = 70.4 to 176.7 ppm, indicating the formation of a new product, **14a** (Figure 4.18). Surprisingly the HRMS data obtained was identical to **13a**, suggesting structural rearrangement was occurring.

The transformation was complete within four days but could be expedited by warming the reaction mixture for one hour at 40 °C. Recrystallisation using CH_2Cl_2/pentane unambiguously verified the rearrangement to **14a**, obtained in 85% yield.

As adducts **13b–13d** were stable at room temperature for up to two weeks, more forcing conditions were required to affect the rearrangement to **14b**–**14d** (Figure

4.18). At this point, the Lewis acidity of the triarylborane began to affect the rearrangement process. Thus, the adduct of stronger Lewis acid $B(3,4,5\text{-}F_3C_6H_2)_3$ willingly underwent rearrangement to **14b** at 40 °C with a yield of 62% after recrystallisation. However, traces of impurities were still present despite repeated purification attempts. Conversely, more forcing conditions (heating to 70 °C) were needed with adducts **13c**–**13d** to form rearrangement products **14c**–**14d** in 67% and 82% yields, respectively, after recrystallisation. Most importantly, the multinuclear NMR spectra of these products were devoid of impurities.

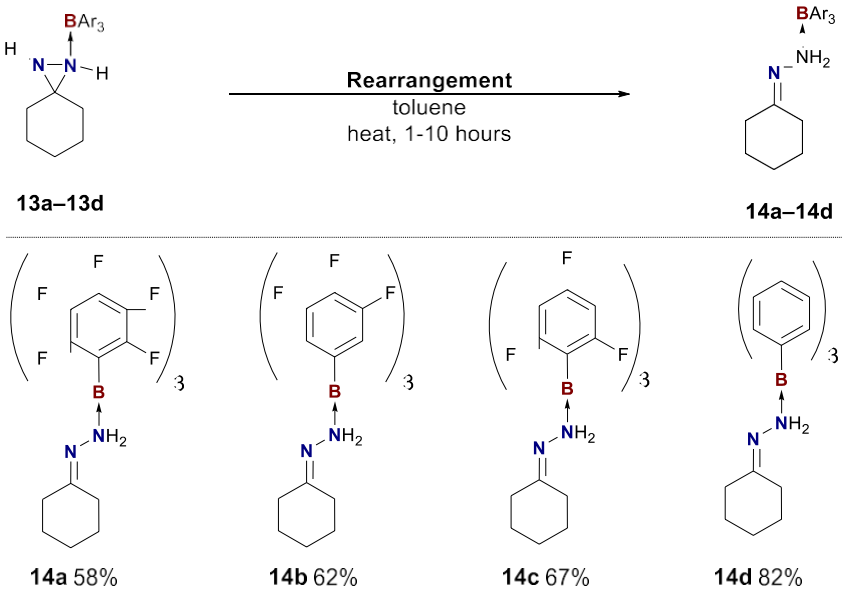

Figure 4.18: Synthesis of rearrangement products **14a–14b**.

Two deductions can be made regarding the Lewis acidity of the triarylboranes and product formation. On the one hand, the higher temperatures required to affect the transformation when the Lewis acidity decreases signifies a causal link between Lewis acidity and ease of formation of rearrangement products **14**.

On the other hand, the presence of impurities in the rearrangement products of higher Lewis acidity triarylboranes stands as a testament to the vulnerability of diaziridine rings to acids and high temperatures, even in the absence of water.[3] Thus, impurity formation becomes increasingly likely as Lewis acidity increases.

Like **14a**, $^{11}B\{^1H\}$ NMR spectroscopy was first used to verify the formation of rearrangement products **14**. Again, a broad singlet was observed between δ = -1.02 and -6.2 ppm, as seen previously in adducts **3a–3c**.

The ^{19}F NMR spectra of **14b–14c** were nondescript and retained many of the characteristics of adducts **13b–13c**. For reference, the chemical resonances for **14c** were located at δ = -98.10 and -111.72 ppm.

Using the ^{1}H NMR spectrum of **14c** as an example, the two singlets of the diaziridine –NH protons merged into a $–NH_2$ group and moved significantly downfield to δ = 7.33 ppm. The triarylborane signal remained became a multiplet at δ = 6.52–6.48 ppm with the hexyl multiplets still in the alkyl region and collectively integrating to ten.

*4.3.7 Solid-state structural analysis of **14a**.*

To unequivocally identify the exact nature of product **14a**, the crude residue was allowed to stand at room temperature in a 1:1 mixture of CH_2Cl_2/pentane under inert conditions. The resultant crystals were subjected to X-ray diffraction analysis revealing the structure of rearranged adduct **14a**. In this example, the adduct crystallised in the $P2_1/c$ space group with one molecule in the asymmetric unit cell, rising to four in the unit cell.

An N–N ring cleavage of the diaziridine ring had occurred, followed by a concurrent 1,2-hydride migration to generate a hydrazone functionality. The central boron adopted a tetrahedral geometry by attaching to the terminal $–NH_2$ group, thus ratifying the NMR interpretations. Throughout this process, the hexyl ring had maintained its chair conformation.

The B–N [1.618(6) Å], N–N [1.439(6) Å] and C=N [1.233(6) Å] bond distances closely resembled the metric parameters previously reported for $R=NNH_2 \rightarrow BAr_3$ adducts **3a–3c**.

Table 3.4: Space groups and selected bond metrics of rearrangement product **14a**.

	14a
Space group	
	$P2_1/c$
Selected bond	
B–N	1.618(6) Å
N–N	1.439(6) Å
C=N	1.233(6) Å

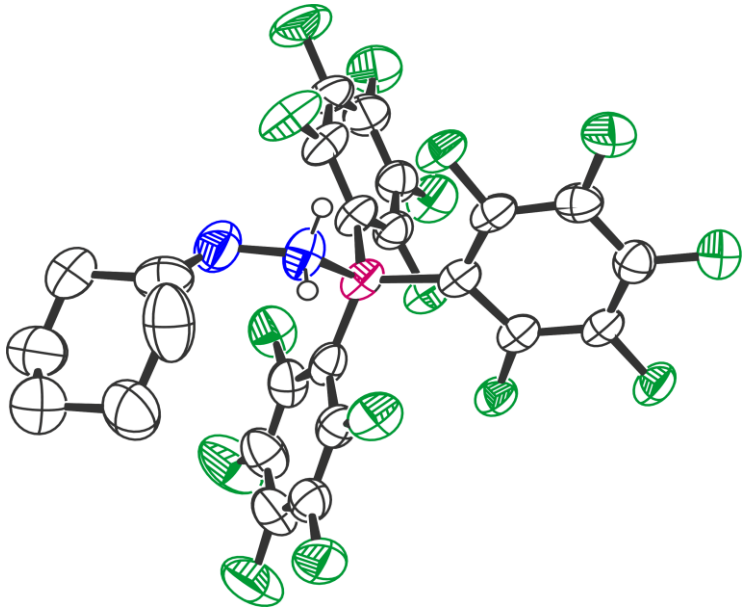

Figure 4.18: Solid-state structure of product **14a**. Thermal ellipsoids are drawn at 50% probability. H-atoms, except for those on nitrogen, were omitted for clarity.

*4.3.8 Synthesis and NMR analysis of **15**.*

As demonstrated earlier with **12**, adducts of the type RNHNH→BAr_3 can, albeit grudgingly, form organohydrazinoboranes upon heating via aryl elimination. Regrettably, most of the rearrangement adducts (**14a–14c**) did not perform the aryl elimination reaction cleanly. Instead, complex mixtures were attained, as revealed by their ^{1}H NMR spectrum.

A notable exception was hydrazone adduct **14d**, which readily underwent aryl elimination upon heating a toluene suspension of it to 90 °C for ten hours. Recrystallisation from a saturated solution of CH_2Cl_2 furnished **15d** in a yield of 74%. **15d** could also be formed directly by heating diaziridine **10b** and BPh_3 to 90 ˚C for ten hours in 61% yield.

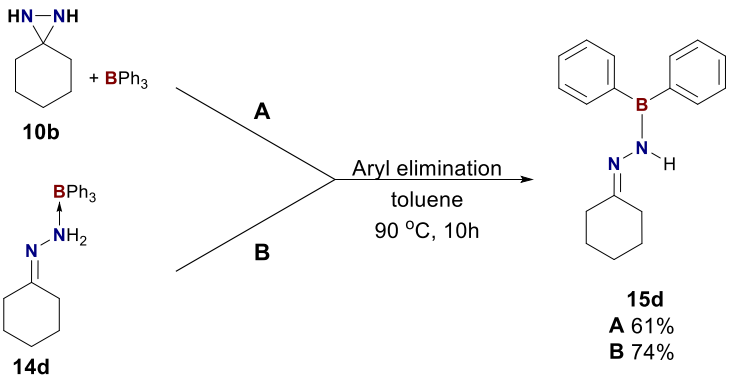

Figure 4.19: Formation of aryl elimination product **15d**.

The above observations can once more be justified by considering the Lewis acidity of the parent triarylboranes. The susceptibility of diaziridines to acids is well documented, often resulting in hydrolysis to the parent ketone. Even when experiments are conducted under rigorous exclusion of water, ring-opening and rearrangement can take place, leading to open-chain isomers.[3] Given this inherent weakness of diaziridines, side reactions can be prevented by lowering the Lewis acidity down the triarylborane series [$B(3,4,5\text{-}F_3C_6H_2)_3$ → BPh_3]. Accordingly, the desired hydrazinoboranes can be furnished in an analytically pure fashion.

From an analytic perspective, a distinct shift in the $^{11}B\{^1H\}$ NMR spectrum from δ = 1.0 ppm (**14d**) to 40.1 ppm was observed. This observation was attributed to the borane reverting to a tricoordinate species by eliminating C_6H_6 and yielding compound **15d**.

The ^1H NMR spectrum verified this observation. A doublet at δ = 7.92 ppm corresponding to the –NH functionality was visible integrating to one. Adjacent to it, a very broad multiplet resonance at δ = 7.54–7.29 ppm could be attributed to the two remaining aryl rings with a collective integration of ten. The alkyl region displayed two multiplets at δ = 2.42–2.33 and 1.80–1.53 ppm with integrations of four and six respectively, corresponding to the hexyl moiety. The NMR spectral data are depicted below.

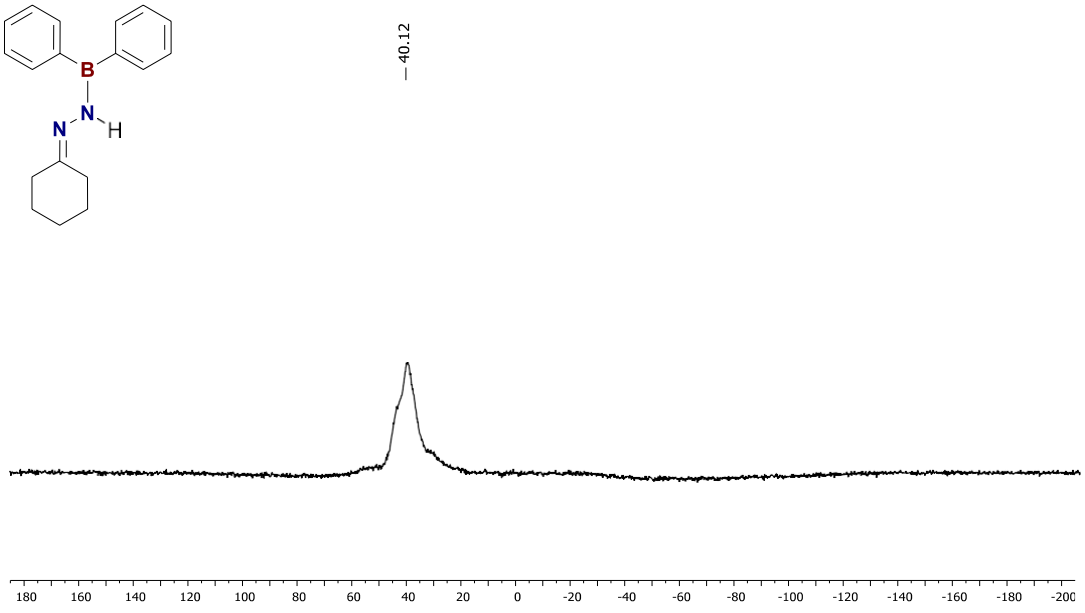

Figure 4.20: $^{11}B\{^1H\}$ NMR (160 MHz, $CDCl_3$, 298 K) spectrum of **15**.

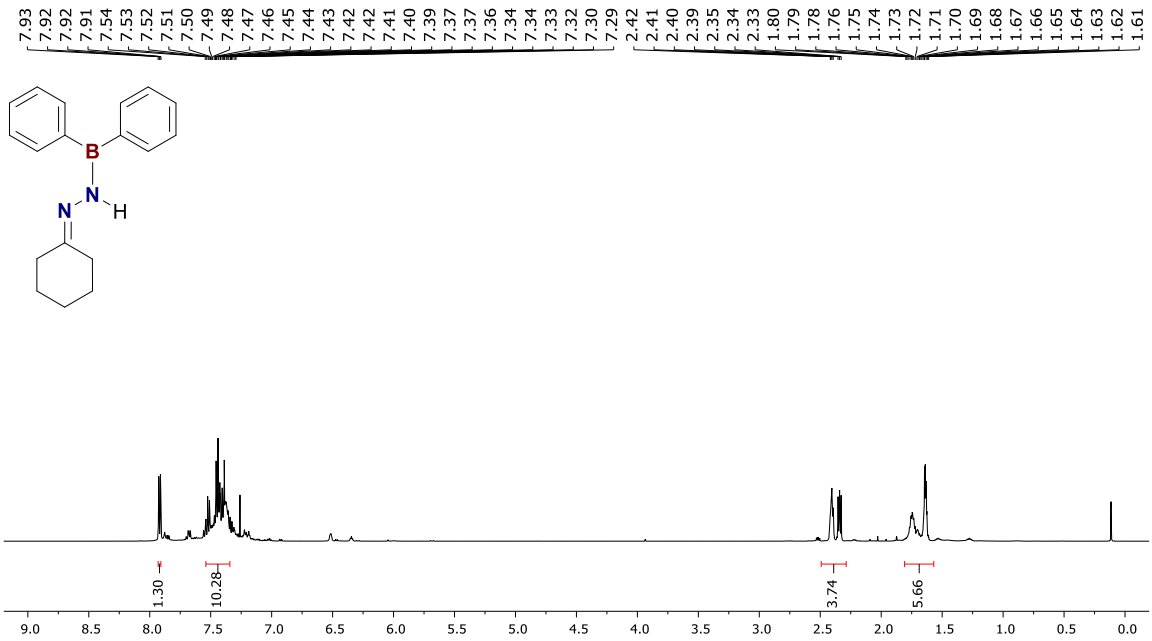

Figure 4.21: ^{1}H NMR (500 MHz, $CDCl_3$, 298 K) spectrum of **15**.

Chapter 4.4: Synthesis and characterisation of 16

*4.4.1 Attempted synthesis and isolation of **16***

The results obtained thus far have helped elucidate the behaviour of highly strained azo-based systems when exposed to Lewis acidic triarylboranes. The –NH moiety's reluctance to impart a hydrogen atom even at elevated temperatures led us to investigate alternative methods of deprotonation. These took the form of Frustrated Lewis Pairs (FLPs).

There exists some literature precedence for azo activation by FLPs, as outlined in Chapter 1. Of particular significance to this thesis was the reaction of diphenylhydrazone with archetypal FLP $B(C_6F_5)_3/P^tBu_3$ (Figure 4.22).[2] In this instance, deprotonation instigated by the phosphorus resulted in a cationic species. Complexation of $B(C_6F_5)_3$ stabilised the resultant anion resulting in the formation of salt $[^tBu_3PH][Ph_2CN_2HB(C_6F_5)_3]$. Experiments were conducted to examine if a similar reactivity would be observed with diaziridines.

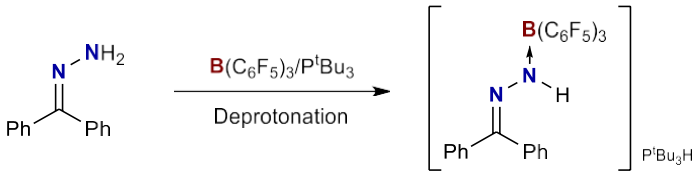

Figure 4.22: Literature reported reaction of diphenylhydrazone with FLPs.

To begin with, a stoichiometric amount of $B(C_6F_5)_3$ and P^tBu_3 were dissolved in deuterated benzene (Figure 4.23). The solution promptly took on a yellow tint, the signature colour of several triarylborane/phosphorus based FLPs. Encouragingly, when an equimolar amount of **10b** was added to the yellow FLP solution, it quickly became transparent. The colour change could potentially denote that the Lewis pair components have ceased to interact with each other, *i.e.,* the 'frustration' has been resolved. The ^{31}P and $^{11}B\{^1H\}$ NMR spectra corroborated this observation, as near-complete consumption of the starting Lewis acid and base was evident.

After storing the sample under inert conditions at -30 °C for two days, a few single crystals of **16** were obtained. Regrettably, these were coated with an oily precipitate that could not be removed despite repeated washes in various solvents. This impurity was responsible for multinuclear NMR spectra that were considerably complex. In addition, water contamination was verified by the crystal data obtained. Unfortunately, there was insufficient lab time to rectify this issue. Nonetheless, the crystals were solved and fully refined.

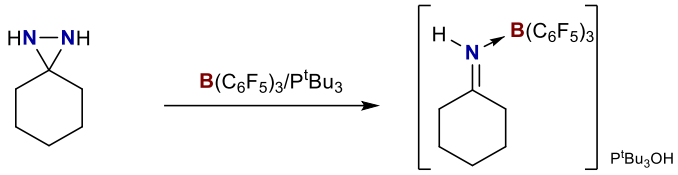

Figure 4.23: Formation of salt **16**.

*4.4.2 Solid-state structural analysis of **16**.*

Simply placing a C_6D_6 solution of **16** inside the glovebox freezer was sufficient to yield colourless single crystals. Following data acquisition, solution and refinement, the solid-state structure of **16** was revealed to have co-crystallised with benzene solvent molecules. Thankfully no specialist refinement techniques were needed as solvent disorder was not observed.

The space group of **16** was the monoclinic *P*1 with two molecules in the unit cell. Contrary to expectations, the solid-state disclosed deprotonation had not occurred. Instead, the FLP had instigated diaziridine ring cleavage with the concomitant detachment of an entire –NH group from the diaziridine. Unfortunately, water contamination resulted in a [P^tBu_3–OH] anion obscuring the underlying reactivity. Stabilising this moiety was a boron-based cation forming a dative bond with the remnant of the diaziridine [$C_6H_6NHB(C_6F_5)_3$]. The B–N and C=N bond lengths were 1.285(2) Å and 1.595(3) Å, respectively.

Table 4.5: Space group and selected bond metrics of **16**.

	16
Space group	
	P-1
Selected bond	
B–N	1.595(3) Å
C=N	1.285(3) Å
P –OH	1.573(3) Å

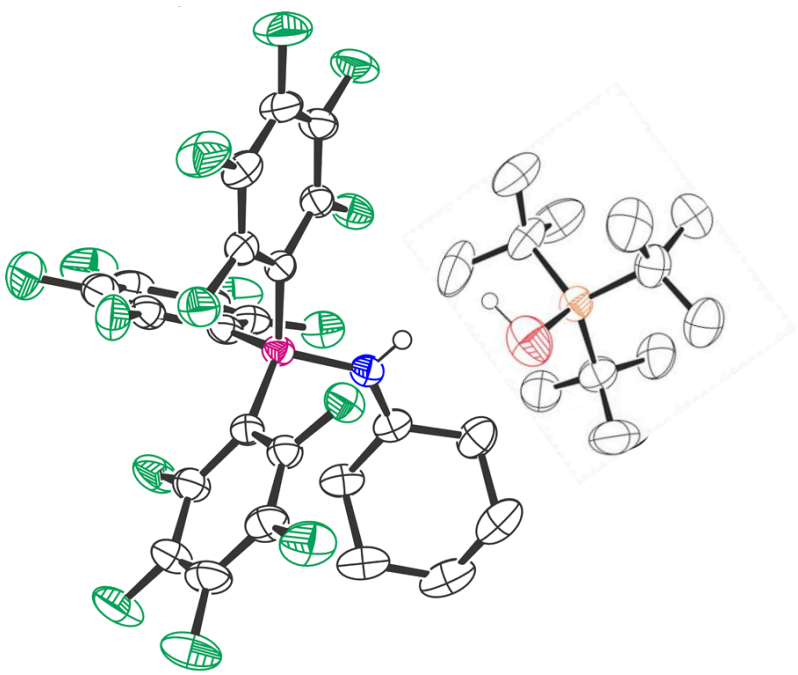

Figure 4.24: Solid-state structure of **16**. Thermal ellipsoids are drawn at 50% probability. H-atoms, except for those on nitrogen, were omitted for clarity.

Chapter 4.5 Conclusions

In this chapter, a comprehensive study into the reactivity of diaziridines ($PhN_2H_2CF_3$) (**10a**) and ($C_6H_{10}N_2H_2$) (**10b**) with triarylboranes of varying Lewis acidities has been conducted. Initially, stoichiometric reactions at room temperature led to adduct formation (**11**, **13a–13d**). The stability of these adducts differed, with **13a** requiring refrigeration. In contrast, adducts **13b–13d** were stable for at least two weeks at room temperature. Gentle heating (up to 70 °C) facilitated rearrangement to hydrazone adducts **14a–14d**, whose structures were reminiscent of **3a–3c**. As temperatures were further increased, the formation of organohydrazinoboranes could be observed for select examples. In the case of **12** crystals suitable for X-ray analysis were gathered, whereas **15** could be characterised by using both multinuclear NMR spectroscopy and HRMS.

As the desired deprotonation could not be induced solely by Lewis acidic triarylboranes, diaziridine **10b** was exposed to the $B(C_6F_5)_3/P^tBu_3$ FLP to effect this transformation. Albeit cleavage of the diaziridine ring had occurred followed by abstraction of an –NH group, water contamination interfered with product assignment. Due to time constraints, the reaction was not repeated.

The solid-state structures of adducts **11** and **13a** were examined, revealing that the diaziridine ring had, surprisingly, remained intact and planar. The boron centre adopted a tetrahedral geometry through attachment to one of the equivalent nitrogen rings. Most of the diaziridine metric parameters remained unchanged except the C–N bond complexed to the triarylborane, which was slightly elongated. Where the rearrangement products are concerned, crystals of **14a** were amenable to X-ray analysis. The bond metrics bore many similarities to those in Chapter 3 (**3a–3c**, **6a**). Similarly, the metrics of aryl elimination product **12** resembled those of heterocycle **8**. Finally, the solid-state structure of **16** verified the water contamination observed in the NMR spectra.

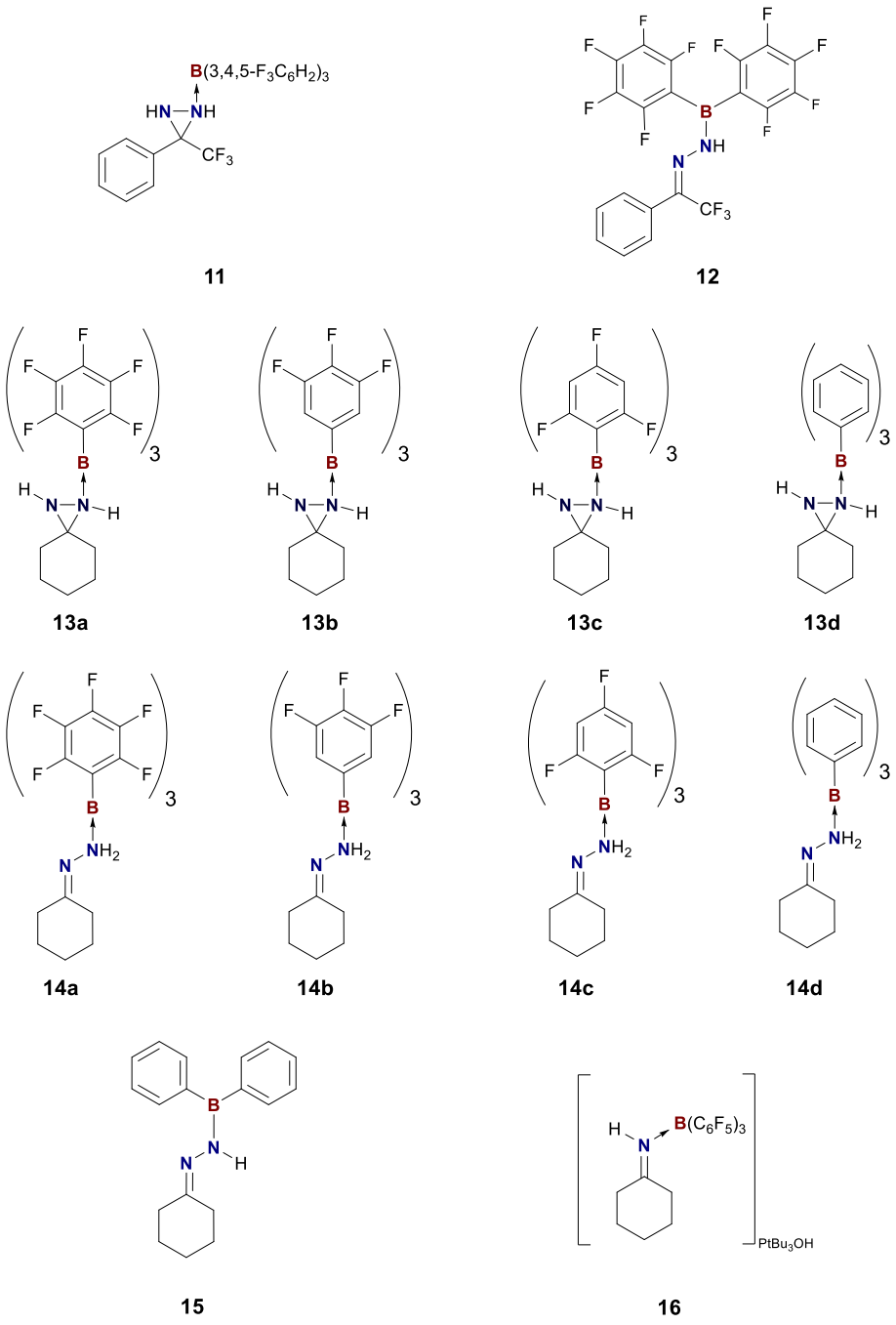

Figure 4.25: Summary of compounds synthesised in Chapter 4.

Table 4.6: Properties of diaziridine derived compounds **11**, **12**, **13a**, **14a**, and **16**.

	11	**13a**
$^{11}B\{^{1}H\}$ NMR chemical shift	N/A	-6.4 ppm
Space group	*Fdd*2	$P2_1/n$
Selected bond		
B–N	1.663(3) Å	1.636(3) Å
N–N	1.502(3) Å	1.502(3) Å
C–N	1.453(3) Å	1.453(3) Å
C–N(Boron)	1.464(3) Å	1.464(3) Å
	12	**14a**
$^{11}B\{^{1}H\}$ NMR chemical shift	N/A	-7.2 ppm
Space group	$P2_1/c$	$P2_1/c$
Selected bond		
B–N	1.396(4) Å	1.618(6) Å
N–N	1.374(3) Å	1.439(6) Å
C=N	1.278(4) Å	1.233(6) Å
	16	
$^{11}B\{^{1}H\}$ NMR chemical shift	N/A	
Space group	*P*-1	
Selected bond		
B–N	1.595(3) Å	
C=N	1.285(3) Å	
P–OH	1.573(3) Å	

Chapter 4.5 References

1 T. Gazis, A. Dasgupta, M. Hill, J. Rawson, T. Wirth and R. Melen, *Dalton Trans.*, 2019, **48**, 12391.

2 C. Tang, Q. Liang, A. Jupp, T. Johnstone, R. Neu, D. Song, S. Grimme and D. Stephan, *Angew. Chem. Int. Ed.*, 2017, **56**, 16588.

3 R. Kostyanovsky, R. Murugan, M. Sutharchanadevi, *Diaziridines and Diazirines*, Pergamon, England, 1996, 347.

4 Z. Tachrim, L. Wang, Y. Murai, M. Hashimoto, Molecules, 2021, **26**, 4496.

5 L. Wang, Z. Tachrim, N. Kurokawa, F. Ohashi, Y. Sakihama, Y. Hashidoko and M. Hashimoto, *Molecules*, 2017, **22**, 1389.

6 A. Kumar, J. Tipton and R. Manetsch, *Chem. Commun.***,** 2016, **52**, 2729.

7 L. Wang, Y. Murai, T. Yoshida, A. Ishida, K. Masuda, Y. Sakihama, Y. Hashidoko, Y. Hatanaka and M. Hashimoto, *Org. Lett.*, 2015, **17**, 616.

8 J. Brunner,S. Serin and F. Richards, *J. Biol. Chem.*, 1980, **255(8)**, 3313.

9 E. Schmitz, R. Ohme, E. Corey and R. Glass, *Org. Synth.*, 1965, **45**, 83.

10 W. Rathke, A. Millard, A. Brossi and J. Minamikawa, *Org. Synth.*,1978, **58**, 32.

11 F. Allen, D. Watson, L. Brammer, A. Orpen and R. Taylor, *Int. Tables Crystallogr.*, 2006, **9.5(C)**, 790.

Conclusions

Like Hercules bending the great Cretan Bull to his will, BAr_3 are able to tame and control highly volatile nitrogen compounds.

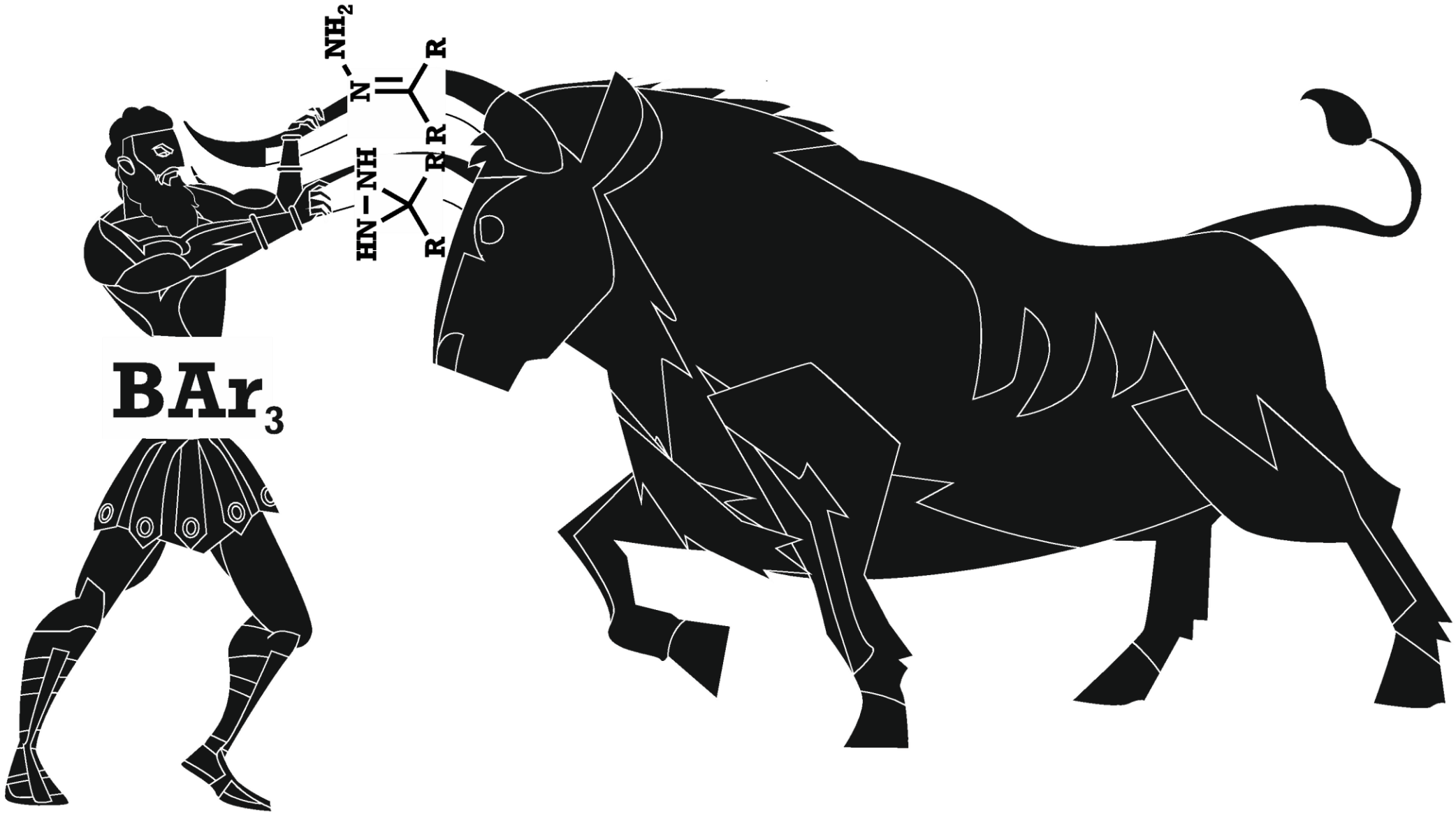

Chapter 5: 1,3-carboboration of carbene precursors

Chapter 5.1 Introduction

There is one notable class of nitrogen-based compounds whose activation has not been explored in this thesis: diazo compounds. As laid out in the introduction, $B(C_6F_5)_3$ represents a versatile catalyst promoting diazo activation and facilitating further reactivity with a range of substrates. Stoichiometric reactions have also been examined, although these were somewhat limited in scope, as of 2019 and relied heavily on aryldiazos and diazoesters.[1] Of relevance to this chapter was the transfer of halogenated aryl groups to diazoester species achieved by the Melen and Wirth groups and thoroughly described in the Introduction (page 8 and Figure 5.1).[2]

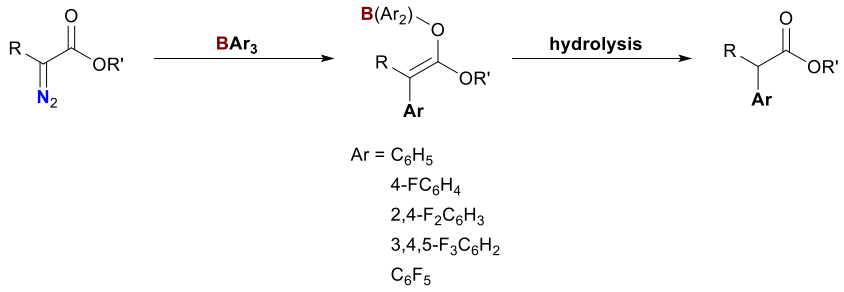

Figure 5.1: Aryl transfer of triarylboranes to diazo compounds.

Given the analogous nature between diazoesters and diazo malonates, it was envisaged that a similar aryl transfer was feasible. Thus, organic compounds with an aryl functionality embedded into the framework would hopefully be furnished upon hydrolysis (Figure 5.2).

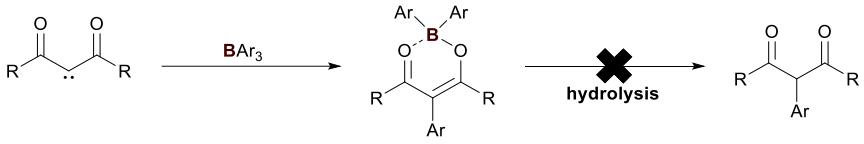

Figure 5.2: General reaction scheme leading to aryl dienolates.

This chapter describes the reaction of dimethyl diazo malonate (**17**) with archetypal triarylborane $B(C_6F_5)_3$ and crystallographic analysis of the results. Then, it presents:

a) the substrate expansion to iodonium ylides, and a library of triarylboranes which display a broad spectrum of Lewis acidities

b) attempts to hydrolyse the boron dienolates products

c) the reaction of triarylboranes with a dimedone based rigid iodonium ylide.

Chapter 5.2: Synthesis and NMR analysis of starting materials 17 and 18a–18d.

*5.2.1 Synthesis and NMR analysis of diazo malonate **17***

The synthetic method first published by Tullis and Helquist *et al.* was utilised in this instance.[3] To begin with, a slight excess of triethylamine was added to a suspension of 4-acetamidobenzenesulfonyl azide in acetonitrile. Subsequently, a stoichiometric amount of dimethyl malonate was added portion-wise at 0 °C for 10 minutes. The resultant solution was stirred for seventeen hours at room temperature. Filtration, trituration and successive washes with 1:1 diethyl ether and petroleum ether proved sufficient to remove the sulfonamide by-product. A final concentration process and filtration yielded **17** as a yellow-red oil in 65% yield. Verification of successful synthesis was sought by NMR spectroscopy. Analysis of the ^{1}H NMR spectrum revealed a singlet at δ = 3.79 ppm corresponding to the six methyl protons, which matched the literature reported values.[4]

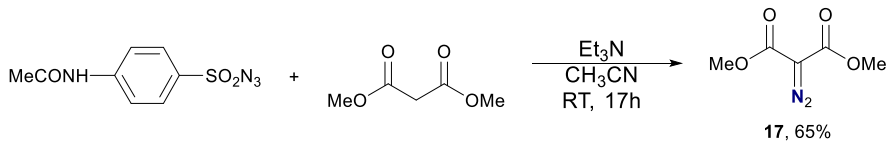

Figure 5.3: Synthesis of dimethyl diazo malonate **17**.

*5.2.2 Synthesis and NMR analysis of iodonium ylides **18a–18d**.*

Upon the course of this study, the substrate scope was expanded to include alternative carbene precursors. These took the form of λ^{3} iodonium ylides, a class of hypervalent iodine reagents that have widespread use in heterocycle generation and cyclopropanation of alkenes.[5] Boranes have previously been utilised in activating iodonium ylides, primarily $BF_3{\cdot}OEt_2$.[6] However, triarylborane mediated activation/reactivity studies are limited to a few select examples.[7]

Iodonium ylides are notorious for their relatively low thermal stability, being particularly susceptible to iodophenyl release upon degradation. Even the relatively stable β-dicarbonyl species in this chapter demand low temperatures during their generation and storage.[8] An established methodology for their synthesis was formulated by the group of Charette and has been briefly summarised herein.[9] A large excess (5 equiv.) of KOH is dissolved in acetonitrile. To this mixture, the appropriate diester is added. Upon stirring the resultant heterogeneous mixture for 5 minutes at 0 °C, iodobenzene diacetate (1.1 equiv.) is added in one portion.

The mixture is subsequently stirred at 0 °C for a further two hours. Finally, an aqueous workup is performed, followed by successive washes with water and ethanol and drying *in vacuo*. By following this procedure, iodonium ylides **18a** and **18b** were furnished as off-white solids in 65% and 16% yield, respectively.

The synthesis of **18c** was performed using a slightly altered procedure first reported by Liang *et al*.[10] It largely resembled the protocol for **18a–18b** but required an even larger KOH excess (20 equiv.) and used methanol as the reaction solvent (see Chapter 6 for a detailed experimental procedure). Thus, **18c** was furnished as a yellow powder in 21% yield.

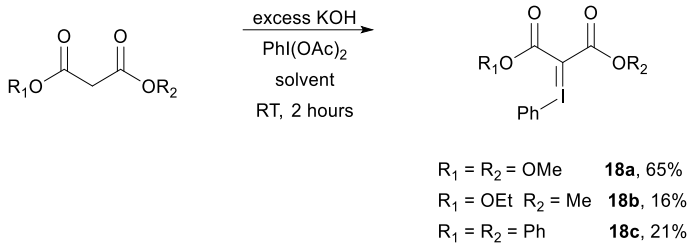

Figure 5.4: Generation of iodonium ylides **18a–18c**.

The final iodonium ylide to be employed as a substrate in this study was a cyclic analogue of **18a**, namely 5,5-dimethyl-2-(phenyliodaneylidene)cyclohexane-1,3-dione (**18d**) whose synthesis was achieved by following a preparation from Ermert *et al.*[11] To begin with, dimedone and a significant excess of KOH (10 equiv.) were added in one portion to a suspension of iodobenzene diacetate in CH_2Cl_2 at 10–15 °C. The resultant mixture was stirred for 50 minutes until complete consumption of the starting materials was confirmed by Thin-Layer Chromatography (TLC) analysis. Upon removing the solid by-products, the solvent was evaporated at room temperature. Precipitation at -20 °C for one hour using CH_2Cl_2 and hexane afforded the desired iodonium ylide. The title compound was isolated as a white fibrous solid (53%). Albeit this derivative required low temperatures for its synthesis, it could be stored at room temperature.

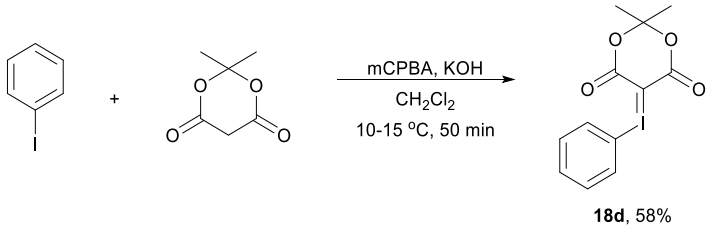

Figure 5.5: Synthesis of **18d**.

In the case of **18a** and **18b**, the products partially decomposed during NMR sample preparation. This degradation is common with iodonium ylides, arising from their low thermal stability. Despite this, the ^{1}H NMR spectrum acquired for **18a** was comparable to literature reported ones.[9] It displayed a singlet at δ = 3.74 ppm with an integration of six, which was attributed to the methyl protons. In addition, the aromatic region contained the expected three multiplet signals at δ = 7.75–7.72, 7.55–7.51, 7.43–7.38 with a collective integration of five corresponding to the iodophenyl group.

Compound **18c** was novel. Nonetheless, the ^{1}H NMR spectrum signals closely matched expected values with a triplet at δ = 1.22 ppm corresponding to the ethyl ester protons. A quartet at δ = 4.13 ppm and a broad singlet at δ = 2.59 ppm corresponded to the two methyl functionalities. Finally, the expected three iodophenyl signals were located at δ = 7.78–7.77, 7.54–7.51 and 7.40–7.37 ppm.

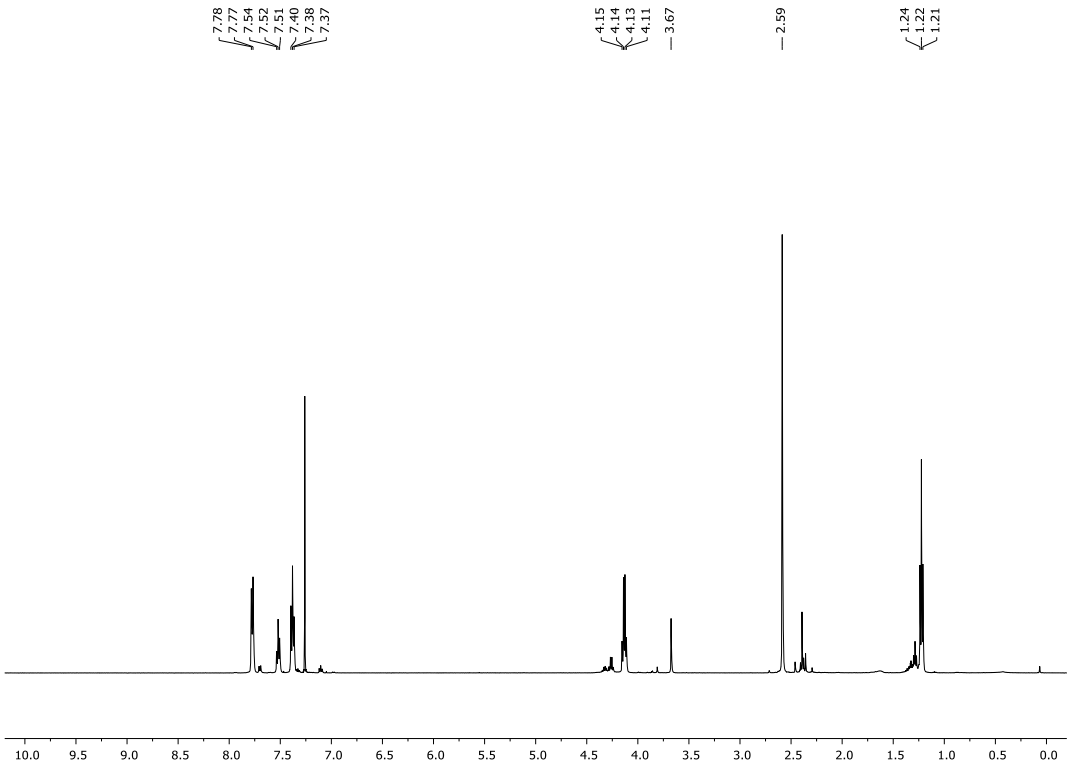

Figure 5.6: ^{1}H NMR (400 MHz, $CDCl_3$, 298 K) spectrum of **18b**.

The ^{1}H NMR spectrum of **18c** did not display any product decomposition but had a markedly more complex spectrum due to the phenyl rings. Six aromatic multiplets were located at positions δ = 8.03–8.00, 7.57–7.52, 7.43–7.38, 7.24–7.22, 7.05–7.01 and 6.93–6.91 ppm collectively integrating to fifteen.

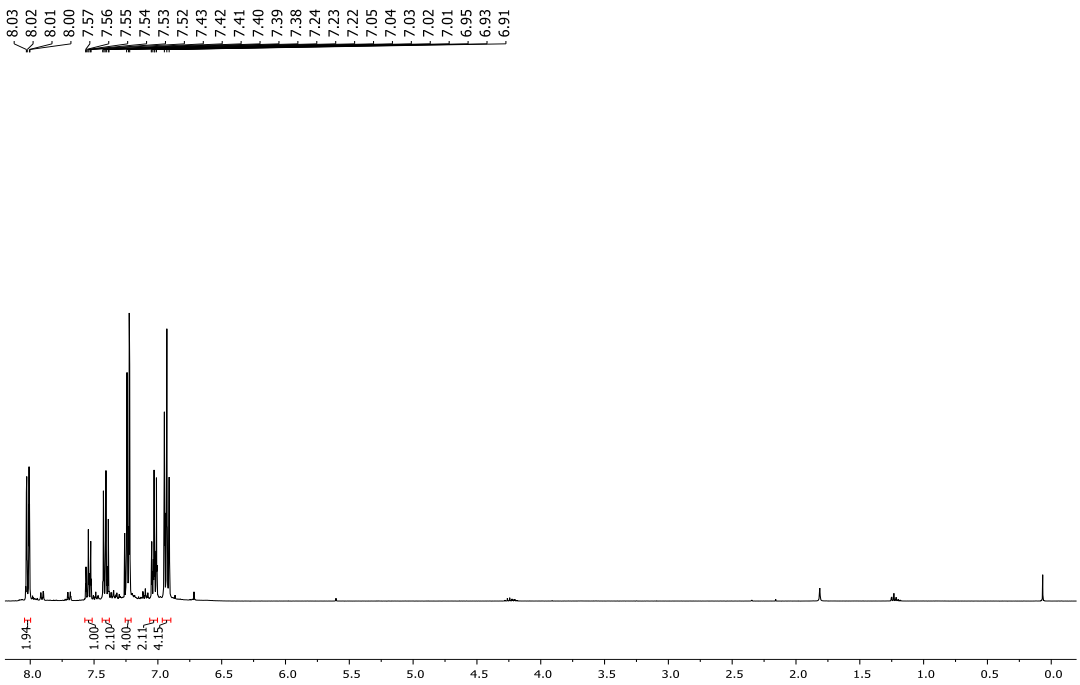

Figure 5.7: ^{1}H NMR (400 MHz, $CDCl_3$, 298 K) spectrum of **18c**.

The ^{1}H NMR data of **18d** was in accordance with literature reported values with the resonance for all six methyl protons located as a singlet at δ = 1.05 ppm.[11] Moving slightly downfield, the four dimedone signals formed as a singlet at δ = 2.5 ppm with a collective integration of four. Finally, the three iodophenyl signals appeared as a series of multiplets at δ = 7.37–7.35, 7.50–7.53 and 7.82–7.83 ppm.

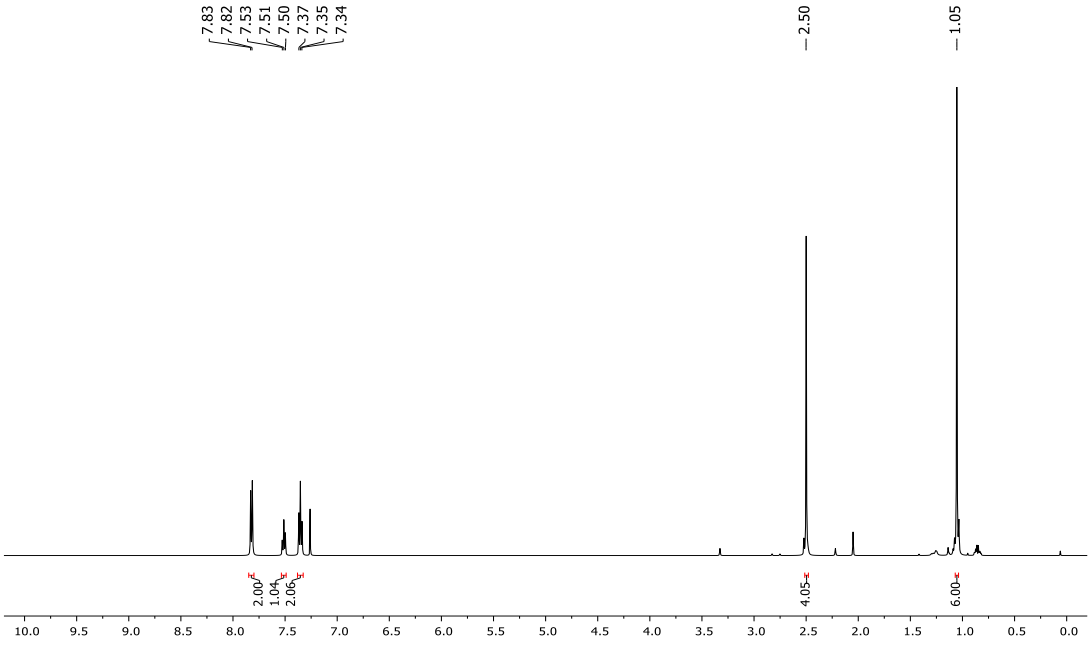

Figure 5.8: ^{1}H NMR (500 MHz, $CDCl_3$, 298 K) spectrum of **18d**.

Chapter 5.3: Synthesis and NMR analysis of 19a–19d and 20a–20b.

*5.3.1 Synthesis and NMR analysis of boron dienolate **19a***

Following the reaction protocol previously applied for the aryl transfer to diazoesters,[2] diazo malonate **17** was dissolved in CH_2Cl_2 under inert conditions. An equimolar amount of $B(C_6F_5)_3$ was added, followed by refluxing the solution for ten hours. Upon removing all volatiles *in vacuo* and recrystallisation by layering (CH_2Cl_2/pentane), colourless crystal plates suitable for single crystal X-ray diffraction were obtained. Despite successive washes with pentane, all crystals were contaminated with impurities, as revealed by multinuclear NMR spectroscopy. Nonetheless, valuable structural and reactivity insights were gained by analysing product **19a** via single crystal X-ray diffraction.

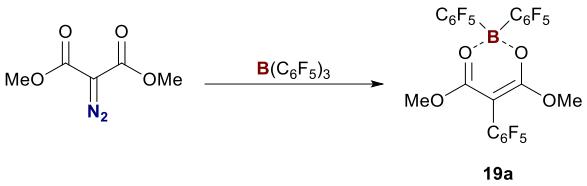

Figure 5.9: Synthesis of boron dienolate **19a**.

*5.3.2 Solid-state structural analysis of **19a***

Compound **19a** crystallised in the *P*2$_1$/*n* space group with one molecule comprising the asymmetric unit; this increased to four in the unit cell. The solid-state structure of **19** confirmed dinitrogen release had occurred, resulting in the equivalent carbene. This was coupled with a 1,3-aryl transfer from the triarylborane to the malonate functionality.

The boron centre had adopted a tetrahedral geometry by coordinating to the two oxygen atoms of the diazo malonate. Thus, a C_2O_2B ring had been generated that was non-planar. Instead, it took on an envelope-type geometry.

The boron heteroatom hung out of the plane, thus forming a non-planar central core with a root mean square deviation value of 0.137. The O–B–O bond angle of 107.5(4)° indicates the boron heteroatom is slightly distorted from a tetrahedral geometry. The B–O bond lengths [1.523(3) Å] and [1.525(3) Å] were found to be slightly longer than typically observed (1.468 Å in BO_4)[12], with the C–O bond lengths also being slightly elongated [1.287(3) Å and 1.288(3) Å] compared to typical values. These values are approximately intermediate between a single and double C–O bond character.[12]

Taken in conjunction, these observations are a strong indication of the resonance character of the core C_2O_2B six-membered ring. Adding credence to this postulate, the C–C bond lengths are once more in between single and double bond character [1.389(3) Å and 1.396(3) Å]. These geometric and bond metrics are largely similar to related diketone structures previously reported by the group of Chujo.[13]

Table 5.1: Space groups and selected bond metrics of boron dienolate **19a**.

	19a
Space group	$P2_1/n$
Selected bond	
B–O	1.523(3) Å
	1.525(3) Å
C–O	1.287(3) Å
	1.288(3) Å
C–C	1.389(3) Å
	1.396(3) Å
Selected Angle	
O–B–O	107.5(4) °

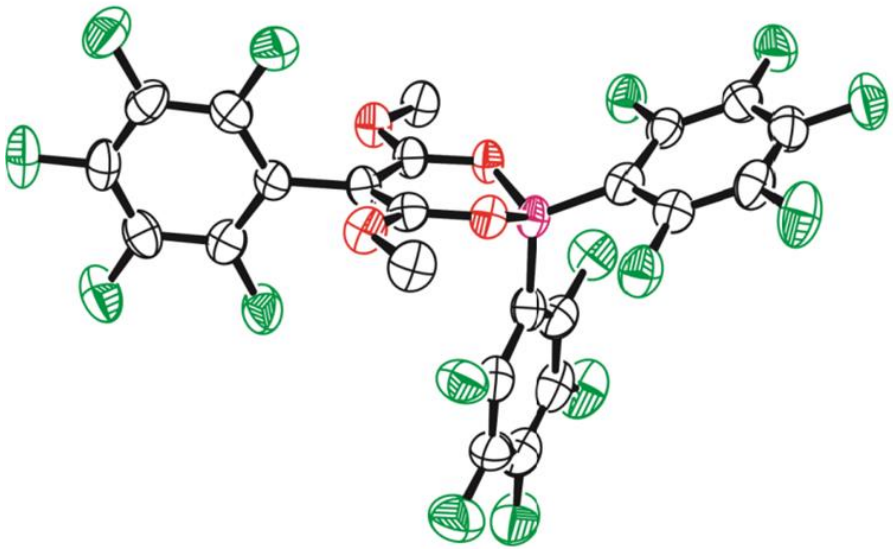

Figure 5.10: Solid-state structure of product **19a**. Thermal ellipsoids are drawn at 50% probability. H-atoms were omitted for clarity.

*5.3.3 Synthesis and NMR analysis boron dienolate products **19b–19e**.*

The difficulties encountered during isolation and characterisation of boron dienolate **19a** lead to utilising iodonium ylides as alternative carbene precursors.

With a library of iodonium ylides and triarylboranes [B(3,4,5-$F_3C_6H_2)_3$, B(2,4,6-$F_3C_6H_2)_3$ and B(2,6-$F_2C_6H_3)_3$] ready, an investigation into this rare 1,3-carboboration could begin in earnest. Initially, symmetrical bis-ester stabilised ylide **18a** and B(3,4,5-$F_3C_6H_2)_3$ were combined using the same reaction conditions as in Section 5.3.1. The crude residue was washed repeatedly with pentane during the workup to remove the liquid iodophenyl by-product. Gratifyingly, repeated trituration with a spatula transformed the crude residue from a pale-yellow paste to a white free-flowing solid. Finally, as there were still traces of the iodophenyl by-product visible in the ^{1}H NMR spectrum, the solid powder was subjected to a crystallisation (layering, CH_2Cl_2/pentane) under inert conditions resulting in pure **19b** furnished at a yield of 45% (Figure 5.11).

A quick solvent screen revealed that by using either chloroform or toluene, yields could be significantly increased to 56% and 74%, respectively. All subsequent reactions were carried out using toluene as the solvent.

Following the reaction protocols established above, boron dienolates **19c**, **19d** and **19e** were furnished in yields of 50%, 67% and 53%, respectively (Figure 5.11). Once the moisture stability of the boron dienolates was established, the isolation of **19c–19e** was carried under ambient conditions in a -20 ˚C freezer.

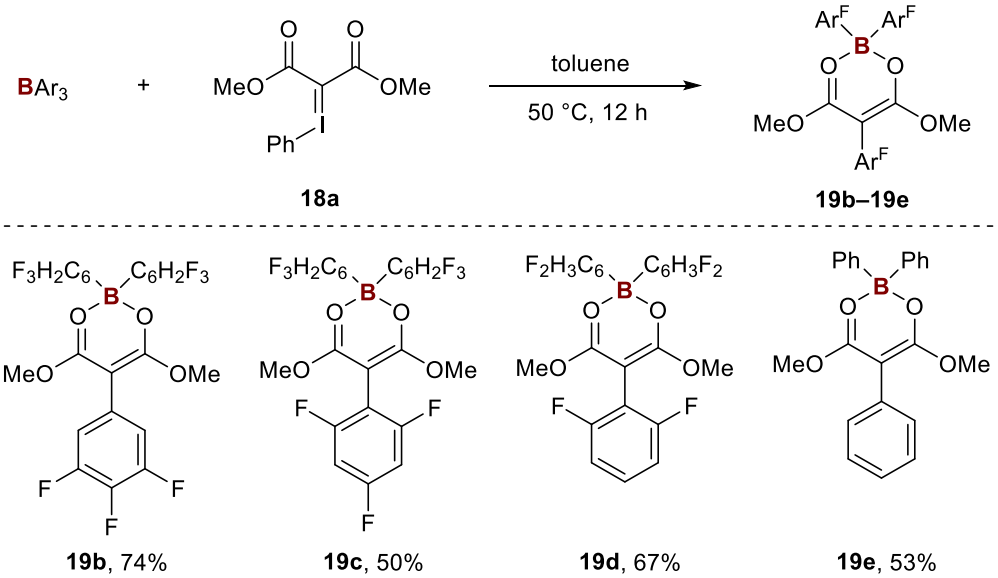

Figure 5.11: Reaction of **18a** with electrophilic triarylboranes.

A cursory glance at the yields obtained indicates a causal link to Lewis's acidity can be made. By using the Gutmann-Beckett Lewis acidity values (*cf.* Chapter 2), boranes can be ranked in order of increasing acidity (Table 2.1). It becomes evident that the increase in product yields can be seemingly traced back to an increase in borane Lewis acidity.

From an analytical perspective, the $^{11}B\{^{1}H\}$ NMR spectrum showed a single broad resonance for all products, with values between δ = 9.2 and 6.6 ppm, characteristic of tetracoordinate boron centres.

Using **19b** as an example, the ^{1}H NMR spectrum was consistent with the release of the iodophenyl group as the aromatic signals were no longer present. Instead, they had been replaced by two multiplet signals at δ = 6.94–6.90 and 6.79–6.76 ppm with an integration ratio of 2:1. These two signals were in the triarylborane proton region and were consistent with two inequivalent ring environments. The singlet matching the two methyl groups had moved slightly upfield to δ = 4.08 ppm.

The ^{19}F NMR spectrum reinforced the observations seen in the ^{1}H NMR spectrum. There were two sets of signals, one at δ = -135.04 (meta, 2F) and -161.32 (para, 1F) and another at δ = -135.70 (meta, 4F) and -162.82 ppm (para, 2F). Thus, two different $C_6H_2F_3$ ring environments were apparent for the fluorine atoms. The NMR spectra of **19b** are presented below.

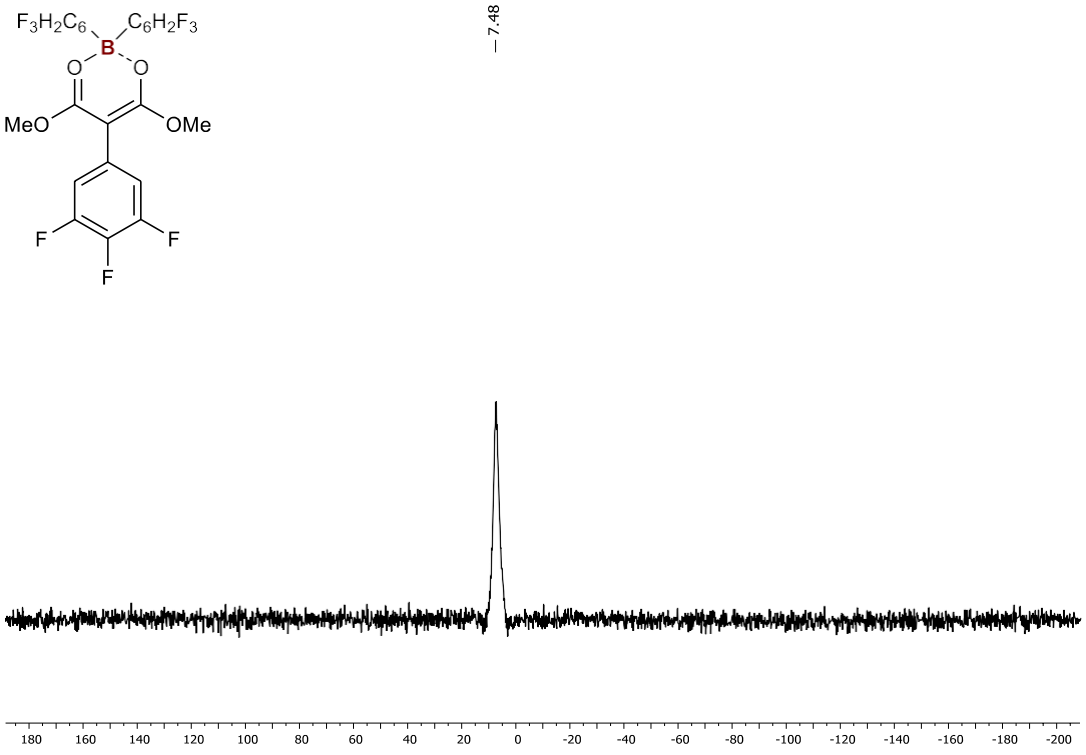

Figure 5.12: $^{11}B\{^{1}H\}$ NMR (128 MHz, $CDCl_3$, 298 K) spectrum of **19b**.

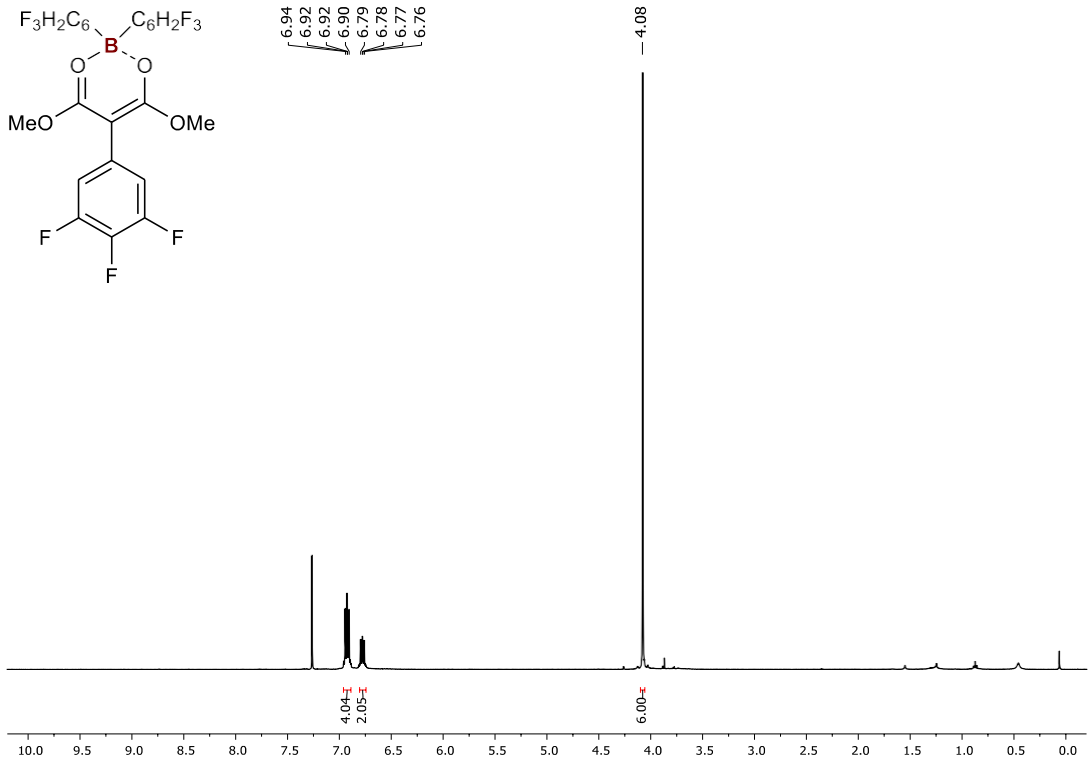

Figure 5.13: ^{1}H NMR (400 MHz, $CDCl_3$, 298 K) spectrum of **19b**.

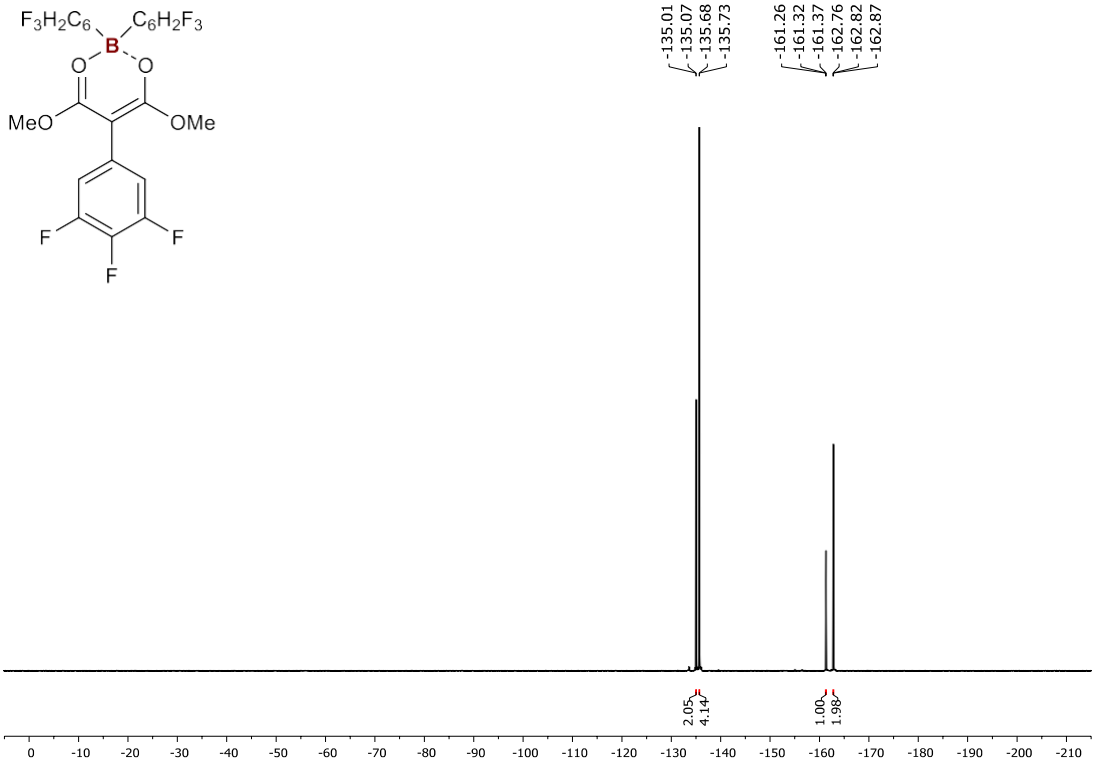

Figure 5.14: ^{19}F NMR (376 MHz, $CDCl_3$, 298 K) spectrum of **19b**.

HRMS was carried out on all boron dienolates, yielding the expected masses within acceptable error margins (5 ppm) (see Section 7.5.2).

*5.3.4 Solid-state structural analysis of boron dienolate **19b***

In conjunction with multinuclear NMR spectroscopy and HRMS analysis, the solid-state structure of **19b** was also ascertained. The crystallisation was performed by Dr Darren Ould using the layering method (CH_2Cl_2/pentane) under inert conditions to afford single crystals as colourless needles.

Upon structure solution and refinement (implemented by Dr Darren Ould), **19b** was found to crystallise in the *P*-1 space group with one molecule constituting the asymmetric cell, increasing to two for the unit cell. The boron centre is tetracoordinate and attached to the two oxygen atoms as in **19a**. In addition, the bond metrics and geometry were largely comparable to those of boron dienolate **19a** (see table 5.2), with a negligible increase in bond shortening because of the increased Lewis acidity of $B(3,4,5\text{-}F_3C_6H_2)_3$. The B–O [1.522(2) Å and 1.526(4) Å], C–O [1.287(3) Å and 1.288(3) Å], and C–C [1.388(4) Å and 1.394(4) Å] bond lengths are intermediate between double and single bond lengths.[12] This is a clear sign of resonance character within the core C_2O_2B ring. In addition, the C_2O_2B ring deviates from planarity with a root mean square deviation value of 0.104.

Table 5.2: Space group and selected bond metrics of boron dienolate **19b**.

	19b
Space group	*P*-1
Selected bond	
B–O	1.522(2) Å
	1.526(4) Å
C–O	1.287(3) Å
	1.288(3) Å
C–C	1.388(4) Å
	1.394(4) Å
Selected Angle	

O–B–O	107.6(4) °

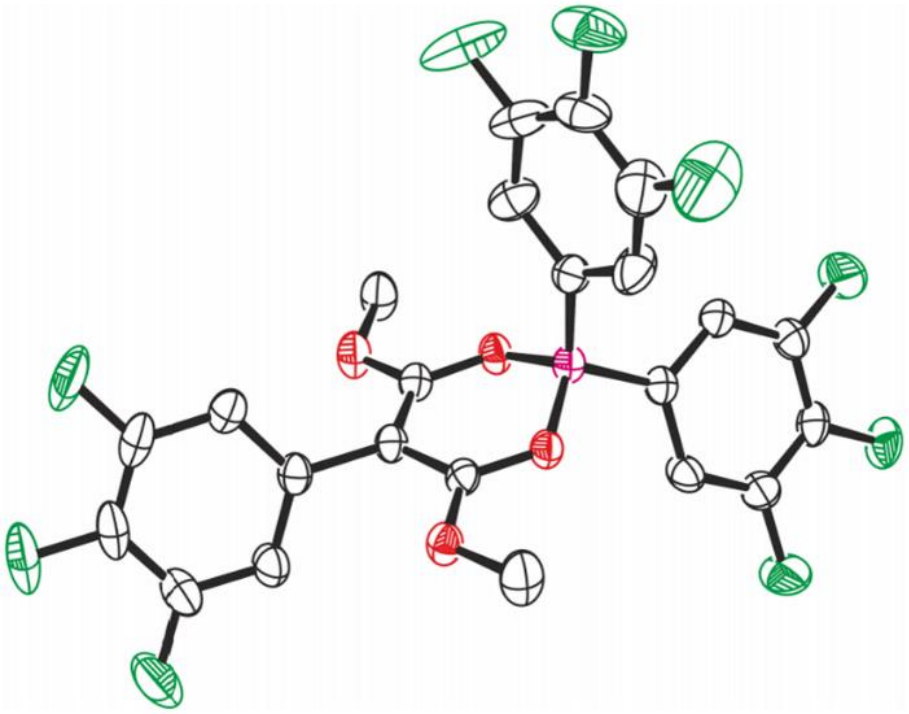

Figure 5.15: Solid-state structure of boron dienolate **19b**. Thermal ellipsoids are drawn at 50% probability. H-atoms were omitted for clarity.

*5.3.5 Synthesis and NMR analysis of **20a–20b***

The previous section focused on altering the triarylborane component of the 1,3-carboboration to observe the effect, if any, of Lewis acidity on yields, reaction rates and other factors. This section aims to expand the applicability of this transformation to less stable iodonium ylides **18b** and **18c** (Figure 5.16). $B(3,4,5\text{-}F_3C_6H_2)_3$ was selected for this set of reactions as it previously provided the highest yielding product (**19b** at 74%). Upon following the reaction protocol previously employed for **19b**–**19e**, boron dienolates **20a** and **20b** were furnished in good yields (61% and 70%, respectively).

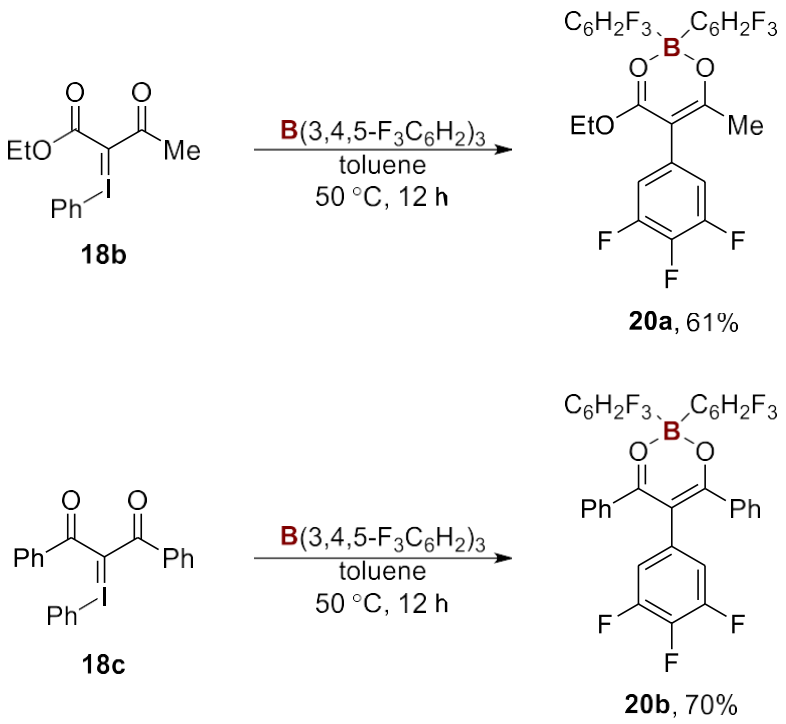

Figure 5.16: Reaction of iodonium ylides **18b** and **18c** with $B(3,4,5\text{-}F_3C_6H_2)_3$.

Spectroscopically the $^{11}B\{^1H\}$ NMR spectra displayed broad singlets at δ = 7.7 ppm for **20a** and δ = 7.3 ppm for **20b**. This is, once more, evidence of a four-coordinate boron centre whose Lewis acidity has been tempered by complexation.

When looking at the ^1H NMR spectroscopic data of **20a**, it was consistent with iodophenyl release with no aromatic signals present. In addition, the carboboration exerted minimal influence on the alkyl region, as the resonances located therein mainly remained unchanged and were located at δ = 4.57, 2.14 and 1.39 ppm. Finally, two fluorophenyl ring environments were visible, this time appearing as triplets at δ = 6.94 (4H) and 6.75 (2H) ppm.

The ^{19}F NMR spectrum of **20a** also supported aryl transfer to the dienolate moiety with two sets of signals at slightly more downfield positions than starting triarylborane. Thus, the signals for the two fluorophenyl rings still attached to the borane were at positions δ = -136.14 and -163.47 ppm, whereas the fluorophenyl embedded on the dienolate had signals at δ = -133.59 and -160.06 ppm. For reference, the $^{11}B\{^1H\}$, ^1H and ^{19}F NMR spectra of **20a** are presented below.

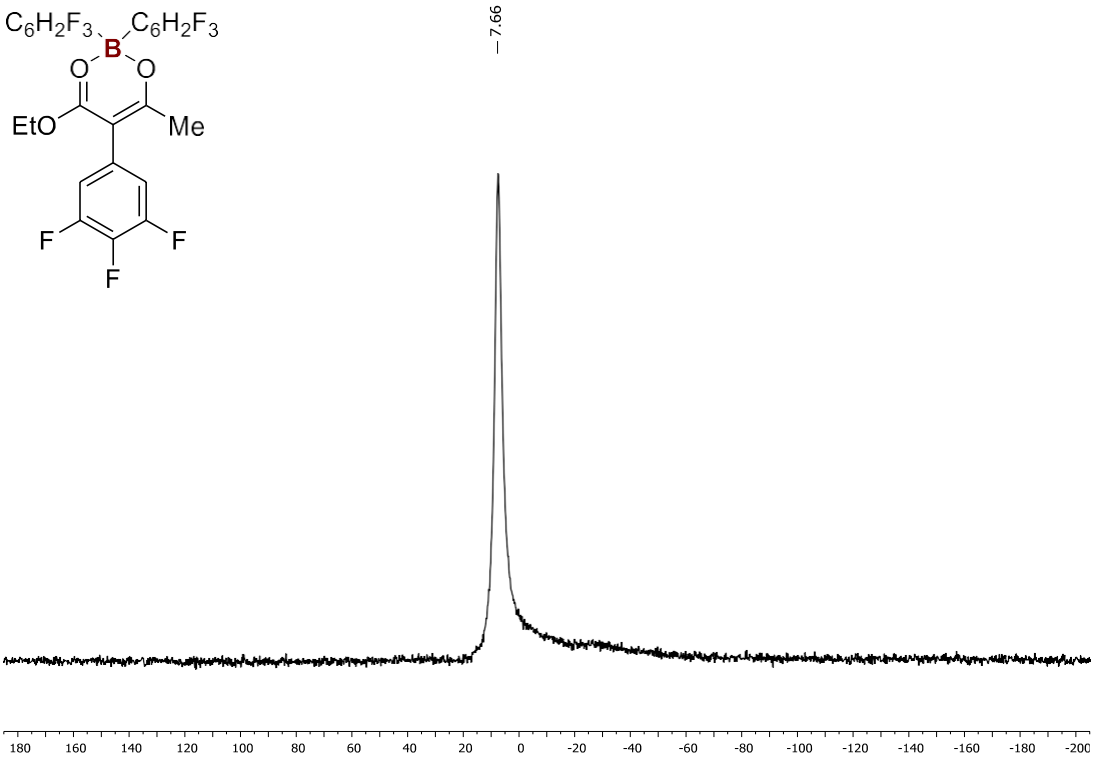

Figure 5.17: $^{11}B\{^{1}H\}$ NMR (128 MHz, $CDCl_3$, 298 K) spectrum of **20a**.

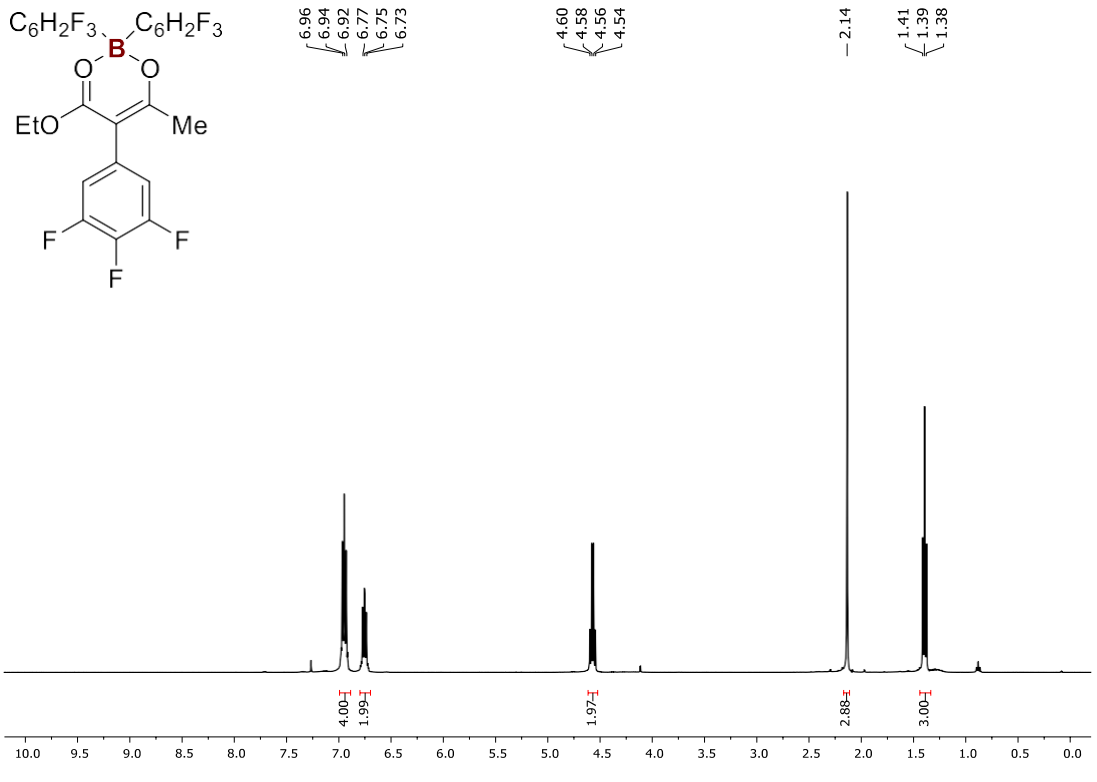

Figure 5.18: ^{1}H NMR (400 MHz, $CDCl_3$, 298 K) spectrum of **20a**.

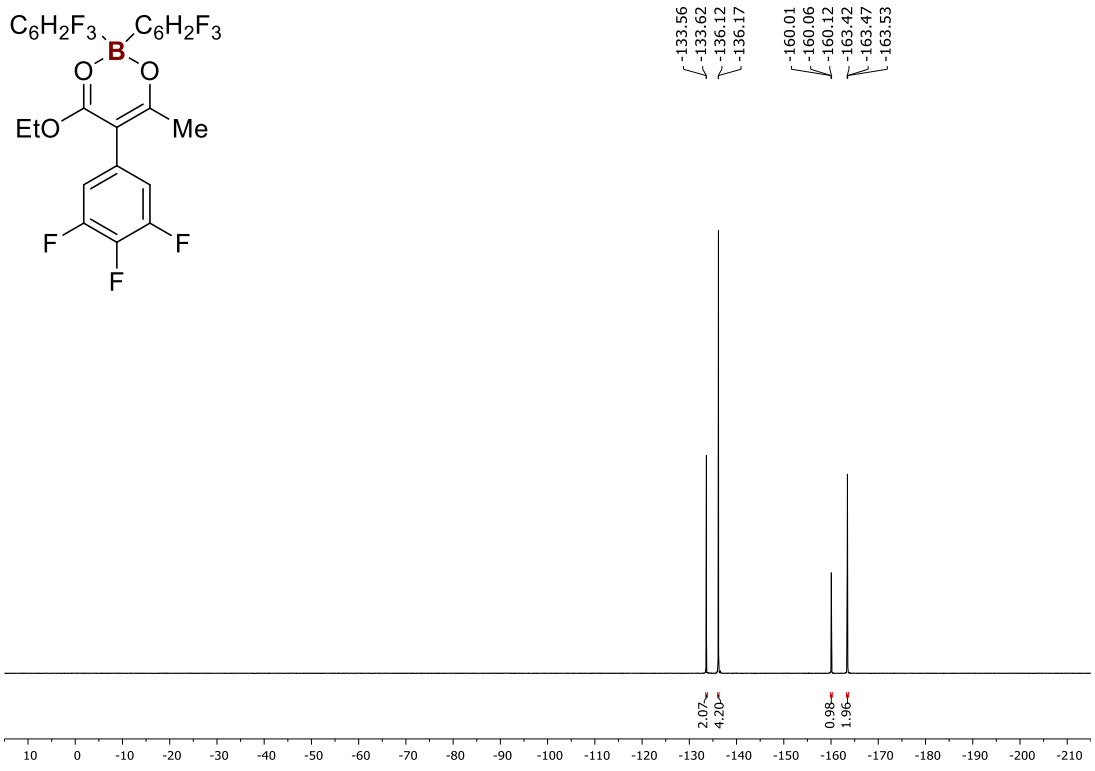

Figure 5.19: ^{19}F NMR (376 MHz, $CDCl_3$, 298 K) spectrum of **20a**.

*5.3.6 Solid-state structural analysis of **20a**–**20b**.*

Single crystal X-ray diffraction assisted in unambiguously identifying the structure and geometry of both products. Compound **20a** crystallised in the monoclinic $P2_1/c$ space group with one molecule in the asymmetric unit and four molecules in the unit cell. On the other hand, **20b** had the same space group as **19b** (*P*1), with one molecule in the asymmetric unit cell, rising to four in the unit cell. Albeit both crystals had similar metrics to **19b**, it was evident from the bond parameters that a decrease in resonance character had occurred. Accordingly, the tetracoordinate boron centre of **20a** had B–O lengths of 1.488(3) Å and 1.540(3) Å. The C–C bonds [1.366(4) Å and 1.419(4) Å] and C–O bonds [1.278(3) Å and 1.316(3) Å] were also slightly elongated in comparison to **19b**.

A similar pattern emerged for **20b** with an elongation of the B–O bonds [1.508(2) Å and 1.518(3) Å], C–C [1.402(3) Å and 1.405(3) Å] and C–O bonds [1.300(2) Å and 1.293(2) Å] serving as a strong indication of reduced resonance character.

As a consequence of this decrease in rigidity, the root mean square deviation values (rmsd) of **20a** and **20b** were 0.126 and 0.136, respectively, thus denoting a greater degree of conformational freedom than **19b**.

Table 5.4: Space groups and selected bond metrics of products **20a–20b**.

	20a	**20b**
Space group		
	$P2_1/c$	$P1$
Selected bond		
B–O	1.488(3) Å	1.508(2) Å
	1.540(3) Å	1.518(3) Å
C–C	1.366(4) Å	1.402(3) Å
	1.419(4) Å	1.405(3) Å
C–O	1.278(3) Å	1.300(2) Å
	1.316(3) Å	1.293(2) Å
Selected Angle		
O–B–O	108.4(3) °	107.3(4) °

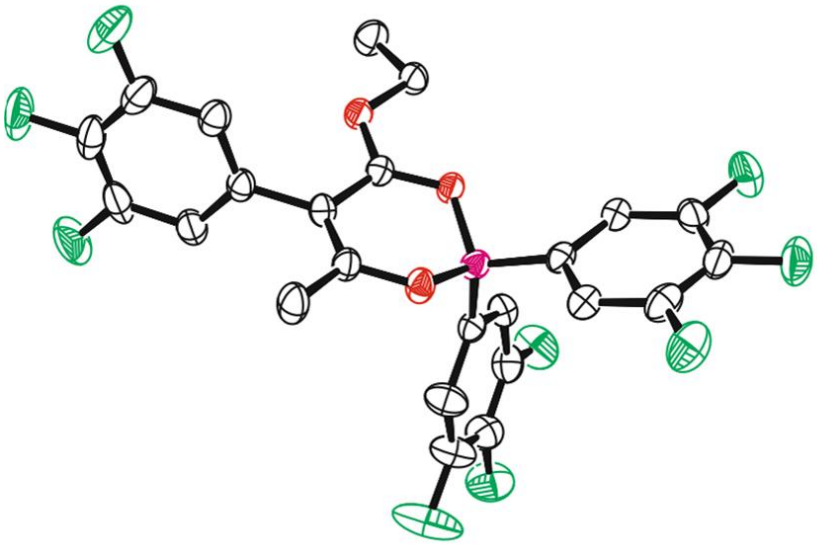

Figure 5.20: Solid-state structure of boron dienolates **20a**. Thermal ellipsoids are drawn at 50% probability. H-atoms were omitted for clarity.

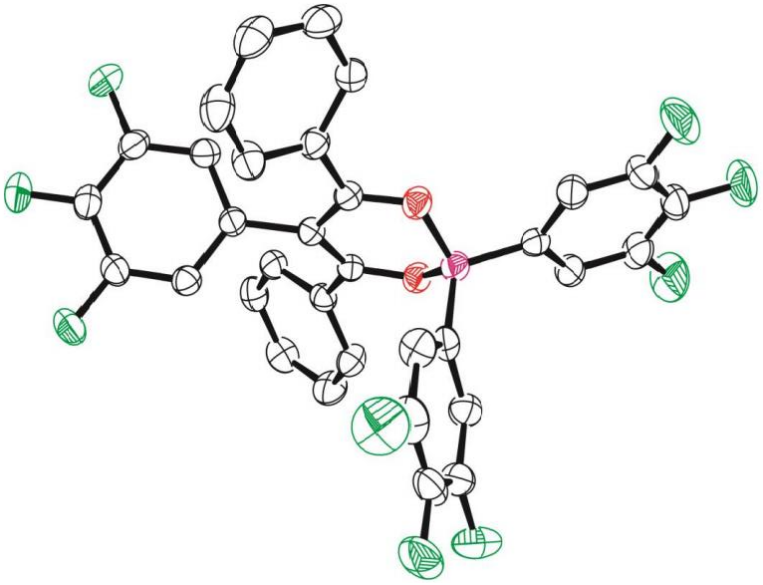

Figure 5.21: Solid-state structure of boron dienolate **20b**. Thermal ellipsoids are drawn at 50% probability. H-atoms were omitted for clarity.

5.3.7 Computational analysis of dienolate formation

Having attained a catalogue of boron dienolates whose analytic and crystallographic properties have been fully explored, the focus shifted to the mechanistic aspects of this reaction. DFT calculations were performed by Professor Jeremy Rawson from the University of Windsor using the Jaguar v 9.8. software.[14] The calculations focused on the formation of boron dienolate **19c** using the crystal structure of $B(2,6\text{-}F_2C_6H_3)_3$. This structure was taken from the Cambridge Structural Database [CSD code: GIMBEL].[15] Unfortunately, the structure of $2,6\text{-}F_2C_6H_3I{=}C(CO_2Me)_2$ was unavailable in the CSD database. Instead, it was produced from the crystal structure of related analogue, $2\text{-}MeOC_6H_4I{=}C(CO_2Me)_2$ [CSD code: NAXBOF][16], with the MeO and H functionalities at the 2' and 6' positions substituted with F (Figure 5.22).

When the M06-2X functional and cc-PVTZ-PP basis set were used, they could not converge the heavier I atom to a sufficient degree. This observation is in agreement with previous studies.[17] Henceforth, the LACVP+ basis set was implemented as it employs an effective core potential for iodine and explicitly includes the outer core orbitals. A 6-31G+ basis was utilised for lighter atoms.

Energy optimisations were carried out for the starting materials and the geometries of the two al conformations of the 1:1 adducts (Figure 5.22). No imaginary frequencies were present, and the structures were minima on the potential energy surface.

As previously described, it became evident that adduct formation was an energetically favoured process (ΔE = 115 kJ/mol).[18] Furthermore, out of the two conformations possible, the “exo” conformer was determined as more energetically favoured than the endo conformer by *circa* 11 kJ/mol (Figure 5.22).

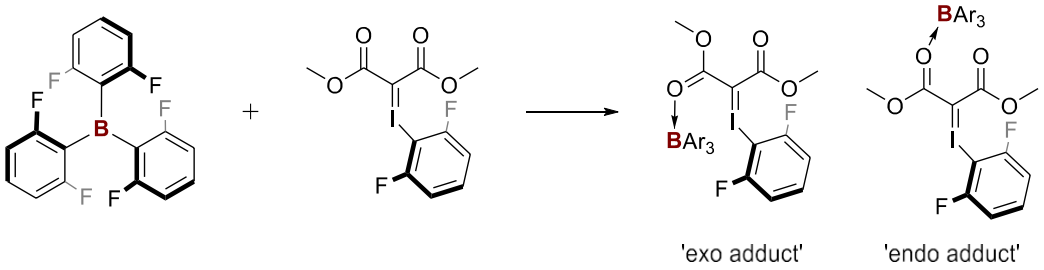

Figure 5.22: The two potential conformations after adduct formation.

Subsequently, aryl group migration was investigated from the borane to the ylidic carbon by steadily decreasing the CAr···C=I distance. At each step, a geometry optimisation was performed. Calculations revealed that aryl migration resulting from the preferred ‘exo’ adduct passed through a lower activation pathway (95 kJ/mol). This transition state has a four-coordinate species with low C–I bond weakening.

Overall, aryl group migration was energetically favourable (ΔE = -260 kJ/mol). Concomitantly, the elimination of the aryl iodide (Ar–I) occurs. Finally, ring closure leads to the six-membered cyclic product as the most stable species in the potential energy surface seen below. Overall, the reaction has a ΔE of -471 kJ/mol.

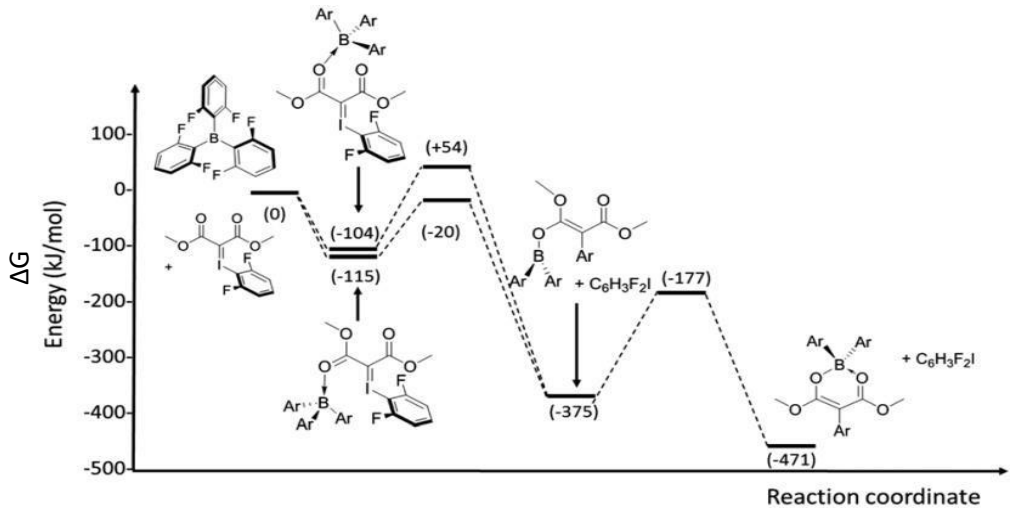

Figure 5.23: Reaction profile of triarylborane $B(2,6\text{-}F_2C_6H_3)_3$ and iodonium ylide $C_6H_3F_2I{=}C(COOMe)_2$.

Chapter 5.4 Further reactivity

5.4.1 Attempted hydrolysis of boron dienolates.

The susceptibility of tetracoordinate boron species to hydrolysis is widely recognised and exploited to glean industrially relevant species such as in the production of hydrogen from boron hydrides (Figure 5.24).[19] The driving force behind this observation is the strong B–O bond with 523 kJ/mol required to cleave it.[20]

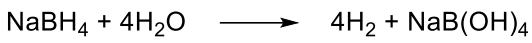

Figure 5.24: Hydrogen release from sodium borohydride.

This principle has also been widely applied towards triarylborane mediated transformations of diazos and analogues during the workup step (see Introduction). Thus, it was envisioned that a similar process would occur herein, yielding dienolate compounds with an aryl functionality embedded into the framework (Figure 5.25).

However, the boron dienolates proved remarkably stable and resistant to hydrolysis in acidic, basic and aqueous media. Numerous attempts were carried out using established workup methodologies such as (i) $NaOH/H_2O_2$; (ii) Ag_2O/BnBr in MeCN; (iii) $N_2H_4.H_2O$/AcOH in EtOH (to yield the corresponding pyrazole); (iv) Na_2CO_3 in EtOH, H_2O then HCl. The majority of reactions were performed using **19b** as the boron dienolate with $NaOH/H_2O_2$ hydrolysis of **19c** and **19d** also attempted.

Upon realising the remarkable stability of these boron dienolates, storage and crystallisation of them were performed under ambient conditions outside the glovebox, thus streamlining their generation.

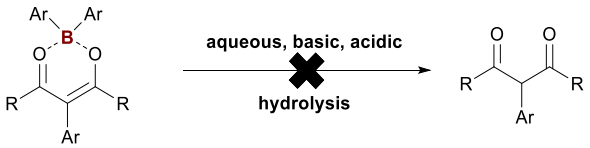

Figure 5.25: Attempted hydrolysis of boron dienolates.

*5.4.2 Synthesis and NMR analysis of **21**.*

As compounds **19a–19e** and **20a–20b** could not be hydrolysed despite using a variety of aqueous, acidic and basic media, it was hypothesised that the intramolecular O–B–O chelate was too stable. Disrupting the ylide's ability to form such a strong connection might allow for boron cleavage to occur. To this end,

structurally rigid dimedone iodonium ylide **18d** was chosen as a substrate. With **18d**, only one B–O linkage is feasible, conceivably enabling hydrolysis.

Unfortunately, the reaction of **18d** with $B(3,4,5\text{-}F_3C_6H_2)_3$, $B(2,4,6\text{-}F_3C_6H_2)_3$ and $B(2,6\text{-}F_2C_6H_3)_3$ resulted in complex mixtures from which no single product could be identified. This result was contrary to expectations as acyclic iodonium ylides **18a–18c** had proven highly amenable to this transformation. Nonetheless, when using $B(C_6F_5)_3$, adduct **21** was furnished following recrystallisation in 48% yield (Figure 5.26).

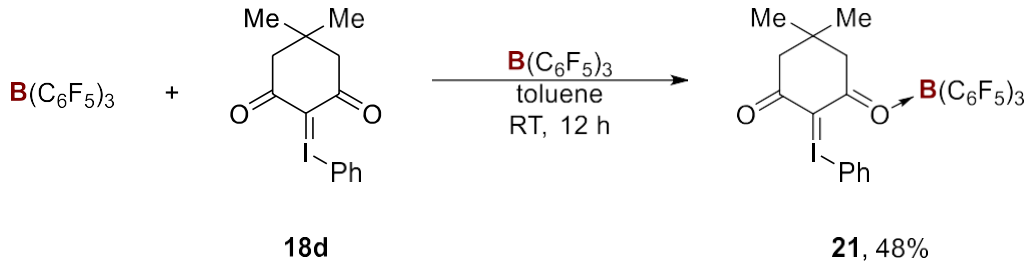

18d **21**, 48%

Figure 5.26: Reaction of **18d** with $B(C_6F_5)_3$.

The formation of a tetracoordinate species was confirmed via $^{11}B\{^1H\}$ NMR spectroscopy, wherein a singlet emerged at δ = -1.86 ppm. The ^1H NMR spectrum revealed that the aromatic signals of the iodophenyl group were still present at δ = 7.84–7.81, 7.61–
7.58 and 7.40–7.37 ppm. The dimedone signals were now located at δ = 2.35 and 2.25 ppm, with the six methyl signals having converged into a singlet at δ = 0.81 ppm. The ^{19}F NMR spectrum supported adduct formation with the expected three singlets at the downfield positions of δ = -133.78, -157.75 and -163.93 ppm with an integration ratio of 2:1:2. The NMR spectra of this adduct are included below.

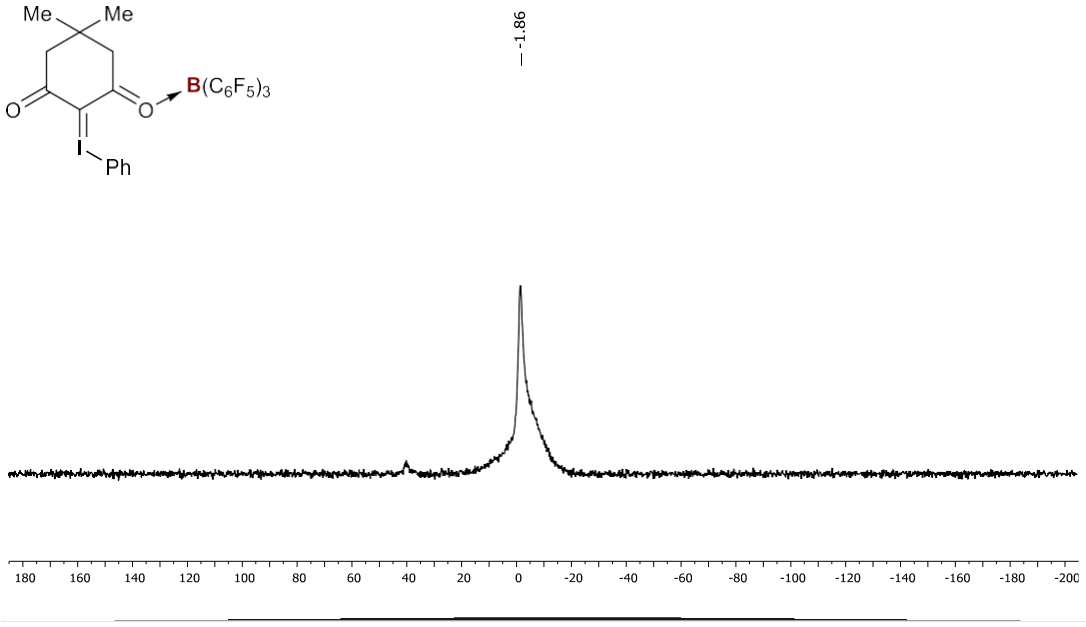

Figure 5.27: $^{11}B\{^{1}H\}$ NMR (160 MHz, $CDCl_3$, 298 K) spectrum of **21**.

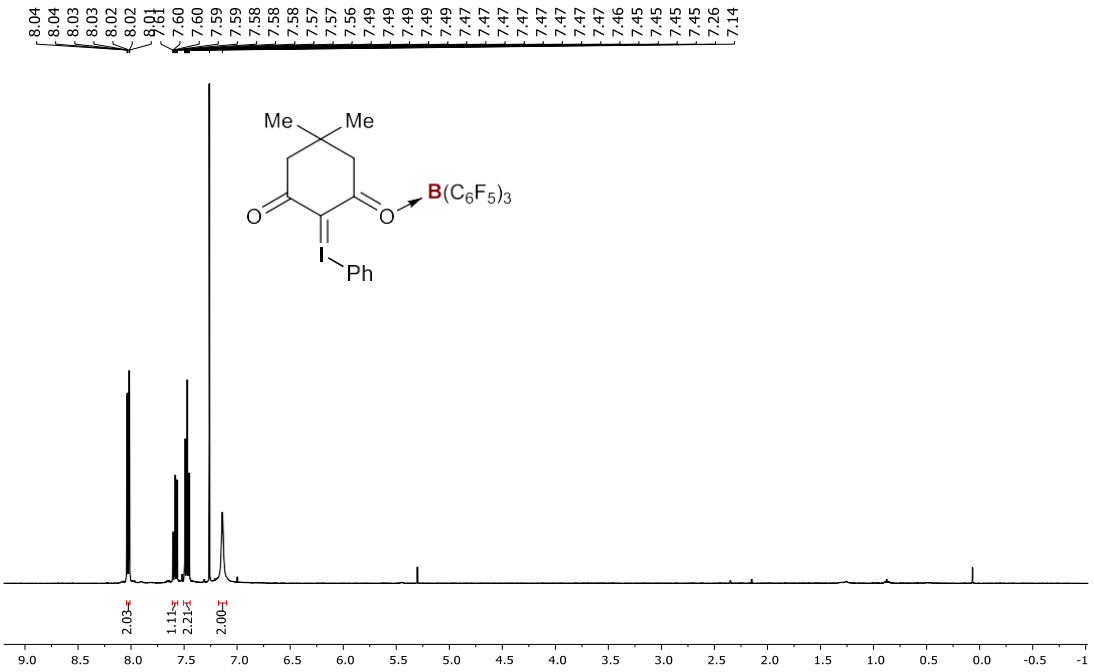

Figure 5.28: ^{1}H NMR (500 MHz, $CDCl_3$, 298 K) spectrum of **21**.

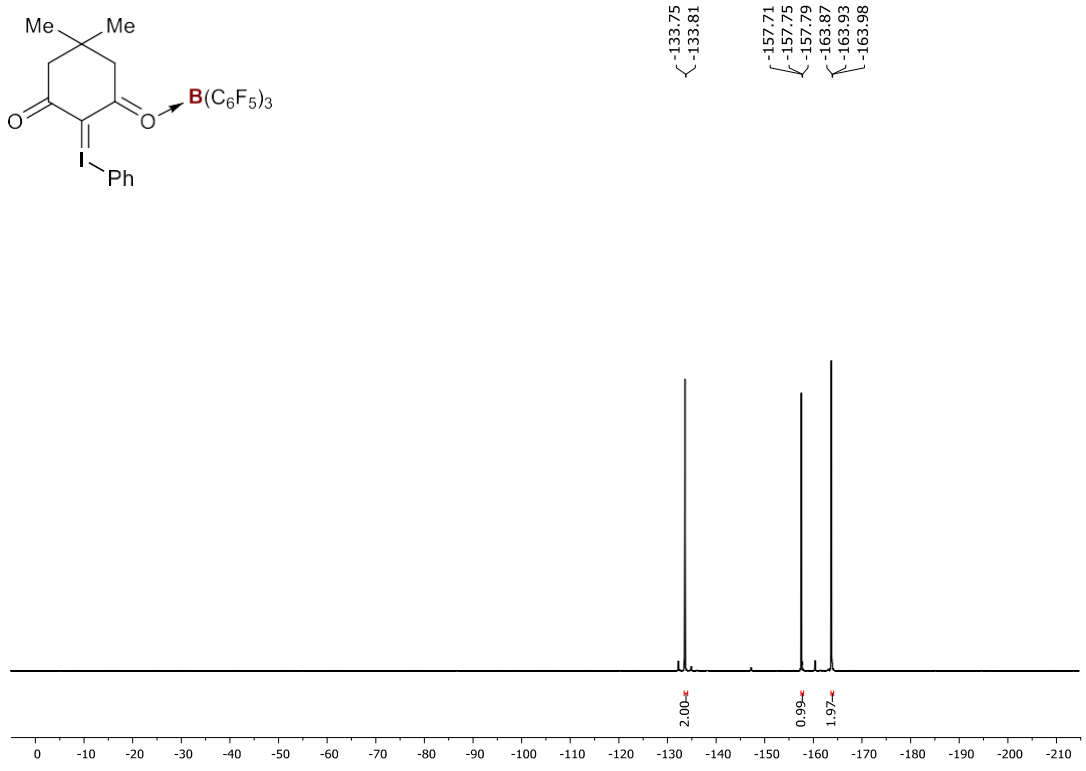

Figure 5.29: ^{19}F NMR (471 MHz, $CDCl_3$, 298 K) spectrum of **21**.

Finally, the observed HRMS mass using the ASAP method of 851.9910 corresponded closely to the theoretical mass of 851.9928.

Adduct **21** could not be induced to perform the carboboration reaction as it was very resilient against elevated temperatures (up to 100 °C). Decomposition to a complex mixture occurred above this temperature range.

From a cursory glance, this observation indicates that a single B–O linkage is unable to activate the boron and affect the transfer in this system. Secondary factors, however, must also be considered. Short intramolecular C–I···O contacts are postulated to make cyclic iodonium ylides more stable than their acyclic counterparts. These can also be observed in the solid-state structure of **20** (see Section 5.4.3). However, this weak coordination should not be able to withstand elevated temperatures. These two factors likely work synergistically to prevent aryl transfer.

*5.4.3 Solid-state structural analysis of **21***

To gain further insights into the metric parameters of **21**, single crystals were obtained by placing a CH_2Cl_2 saturated solution under cold, inert conditions and layering pentane on top of it. Within 3–4 days, single crystals of suitable quality were obtained and analysed by single crystal X-ray diffraction.

Adduct **21** crystallised in the $P2_1/n$ space group with one molecule in the asymmetric unit and four in the unit cell. Structurally, the expected tetracoordinate boron centre was attached to one of the C=O groups. The iodophenyl functionality was still occupying the same space in the molecule. The bond metrics observed were unremarkable and corresponded to literature reported values.[12]

The packing arrangement of **21** reveals the expected two short intramolecular C–I···O contacts in the solid-state at 2.916 Å and 3.105 Å, longer than similar compounds in the absence of the $B(C_6F_5)_3$ adduct[21], a sign of weakening of these bonds.

Table 5.5: Space group and selected bond metrics of adduct **21**.

	21
Space group	$P2_1/n$
Selected bond	
B–O	1.514(6) Å
C–I	2.087(5) Å

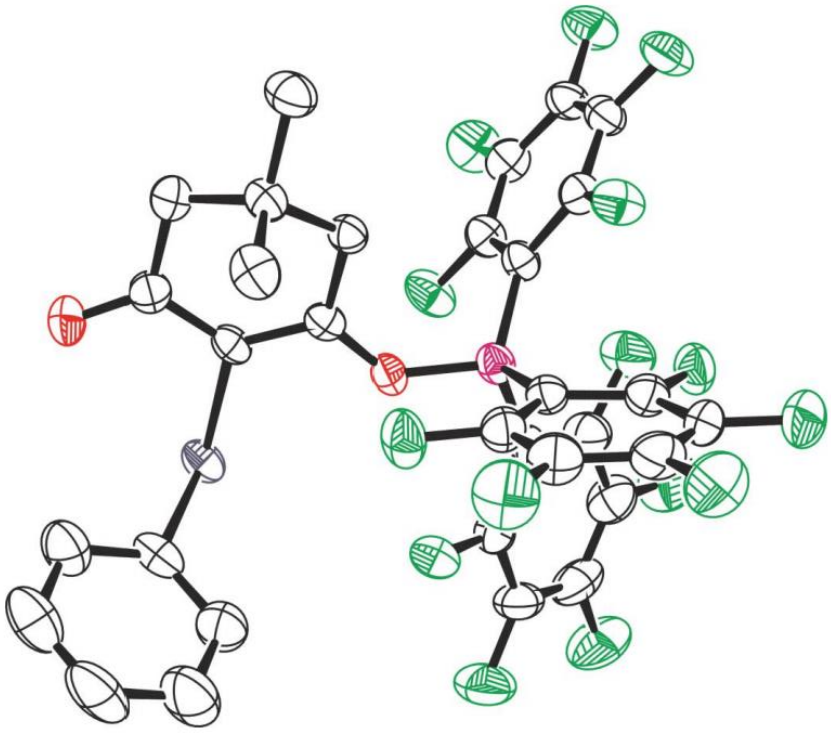

Figure 5.30: Solid-state structure of adduct **21**. Thermal ellipsoids are drawn at 50% probability. H-atoms were omitted for clarity.

Chapter 5.5 Conclusions

In summary, an extensive study into an unprecedented triarylborane 1,3-carboboration resulting in boron dienolate products has been conducted. When utilising diazo **17** or symmetric iodonium ylide **18a**, crystals of **19a** were furnished. Through X-ray analysis, the first glimpse into this novel reactivity was obtained.

Expanding the scope to other triarylboranes resulted in **19b–19e**. A causal relationship between an increase in Lewis acidity and an increase in product yields was apparent.

Unsymmetrical ylide variants also readily underwent this reaction, furnishing products **20a** and **20b** in good yields of 61% and 70%, respectively. All products generated up to this point proved stable at ambient conditions and resistant to hydrolysis under a range of acidic, basic and aqueous conditions. Conformationally restricted cyclic ylide **18d** was utilised as a substrate to explore this stability further. Contrary to expectations, carbene formation because of iodophenyl release did not occur. Instead, adduct **21** was formed with the iodophenyl functionality still attached and a dative bond between the triarylborane and one of the oxygen atoms of the dimedone. Attempts to induce a 1,3-carboboration using this adduct proved unsuccessful with complex spectral data. This evidence suggests that a single B–O linkage is insufficient to affect the carboboration in this instance. However, secondary factors, such as strong C–I···O short contacts should not be discounted. Complete characterisation (NMR, HRMS and single crystal X-ray diffraction) of this species was achieved. The generation of these aryl-substituted products in a metal-free fashion provides a facile route to boron dienolates.

DFT computational studies afforded mechanistic insights into the net 1,3-carboboration of simplified 2-$MeOC_6H_4I{=}C(CO_2Me)_2$, and $B(2,6\text{-}F_2C_6H_3)_3$ were attained. These revealed that the reaction initially proceeds through adduct formation, with the exo variant being the most energetically favourable. This adduct promptly undergoes an aryl migration with a concomitant aryl iodide release. The final stage is simply a cyclisation resulting in the observed boron dienolates

Crystallography once more proved invaluable in this Chapter, with the acyclic crystal structures of **19a**, **19b**, **20a–20b** being analysed. These revealed an envelope type geometry around the tetracoordinate boron centre with fold angles located around the O–O vector.

In general, an increase in the Lewis acidity of the triarylborane resulted in a more conformationally rigid boron dienolate, a result of greater resonance character imposing a higher degree of planarity. The unsymmetrical boron dienolates **20a–20b** had a slightly reduced resonance character compared to **19b**.

Finally, the crystal structure of adduct **21** was also analysed. Its bond metrics largely conformed to literature values. Of note was the characteristic intermolecular O…I contact which confers a quantifiable degree of stability to this adduct.

A summary of the results obtained is given in Figure 5.30 and Table 5.6 below.

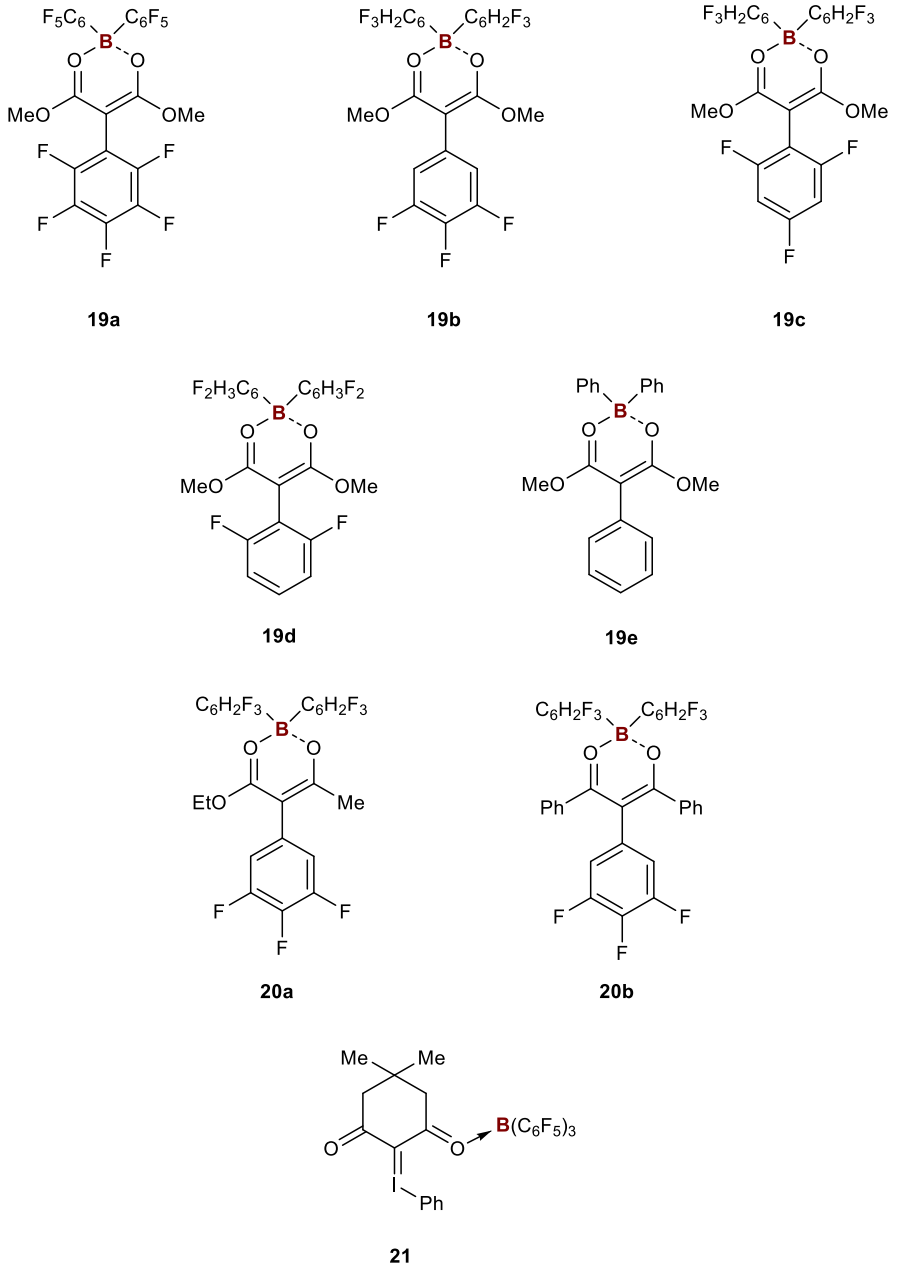

Figure 5.31: Summary of novel compounds synthesised in Chapter **5**.

Table 5.6: Summary of key characteristics of compounds **19a**, **19b**, **20a**, **20b** and **21**.

	19a	**19b**
$^{11}B\{^1H\}$ NMR chemical shift	N/A	7.5 ppm
Space group	$P2_1/n$	P-1
Selected bonds		
B–O	1.523(3) Å	1.522(2) Å
	1.525(3) Å	1.526(4) Å
C–O	1.287(3) Å	1.287(3) Å
	1.288(3) Å	1.288(3) Å
C–C	1.389(3) Å	1.388(4) Å
	1.396(3) Å	1.394(4) Å
Selected Angle		
O–B–O	107.5(4) °	107.6(4) °
	20a	**20b**
$^{11}B\{^1H\}$ NMR chemical shift	7.7 ppm	7.3 ppm
Space group	$P2_1/c$	P1
Selected bonds		
B–O	1.488(3) Å	1.508(2) Å
	1.540(3) Å	1.518(3) Å
C–C	1.366(4) Å	1.402(3) Å
	1.419(4) Å	1.405(3) Å
C–O	1.278(3) Å	1.300(2) Å
	1.316(3) Å	1.293(2) Å
Selected Angle		
O–B–O	108.4(3) °	107.3(4) °

	21
$^{11}B\{^{1}H\}$ NMR chemical shift	-1.9 ppm
Space group	$P2_1/n$
Selected bonds	
B–O	1.514(6) Å
C–I	2.087(5) Å

Chapter 5.6 References

1 T. Gazis, J. Carden, M. Alharbi and R. Melen, *Triarylboranes in the Activation of Azo Containing Compounds*, EIBC, 2021.

2 M. Santi, D. Ould, J. Wenz, Y. Soltani, R. Melen and T. Wirth, *Angew. Chem. Int. Ed.*, 2019, **58**, 7861.

3 J. Tullis, P. Helquist, A. Courtney and S. Martin, *Organic Synth.*, 1997, **74**, 229.

4 E. Ciganek, *J. Org. Chem.*, 1965, ***30***, 4366.

5 M. Yusubov, A. Yoshimura and V. Zhdankin, *Arkivoc*, 2016, **2016**, 342.

6 A. Dasgupta, C. Thiehoff, P. Newman, T. Wirth and R. Melen*, Org. Biomol. Chem.*, 2021,**19**, 4852.

7 T. Hokamp, L. Mollari, L. Wilkins, R. Melen and T. Wirth, *Angew. Chem., Int. Ed.*, 2018, **57**, 8306; T. Nagata, H. Matsubara, K. Kiyokawa and S. Minakata, *Organic Lett.*, 2017, **19**, 4672.

8 M. Ochiai, N. Tada, T. Okada, A. Sota and K. Miyamoto, *J. Am. Chem. Soc.*, 2008, **130**, 2118.

9 S. Goudreau, D. Marcoux and A. Charette, *J. Org. Chem.*, 2009, **74**, 470.

10 H. Huang, Y. Yang, X. Zhang, W. Zeng and Y. Liang, *Tetrahedron Lett.*, 2013, **54**, 6049.

11 J. Cardinale and J. Ermert, Tetrahedron Lett., 2013, **54**, 2067.

12 F. Allen, D. Watson, L. Brammer, A. Orpen and R. Taylor, *Int. Tables Crystallogr.*, 2006, **9.5(C)**, 790.

13 A. Nagai, K. Kokado, Y. Nagata, M. Arita and Y. Chujo, *J. Org. Chem.*, 2008, **73**, 8605.

14 Jaguar, v9.8, Schrodinger, Inc., New York, NY, 2017; A. Bochevarov, E. Harder, T. Hughes, J. Greenwood, D. Braden, D. Philipp, D. Rinaldo, M. Halls, J. Zhang, R. Friesner, Int. *J. Quantum Chem.*, 2013, **113**, 2110.

15 L. Greb, C. Daniliuc, K. Bergander and J. Paradies, *Angew. Chem. Int. Ed.*, 2013, **52**, 5876.

16 C. Zhu, A. Yoshimura, L. Ji, Y. Wei, V. Nemykin and V. Zhdankin, *Org. Lett.*, 2012, **14**, 3170.

17 A. Varadwaj, P. Varadwaj, H. Marques and K. Yamashita, *PCCP*, 2018, **20**, 15316; A. Bauza, D. Quinonero, P. Deya and A. Frontera, *J. Phys. Chem. A*, 2013, **117**, 2651.

18 A Bähr, L. Wilkins, K. Ollegott, B. Kariuki and R. Melen, *Molecules*, 2015, **20(3)**, 4530.

19 C. Wang, Q. Wang, F. Fu and D. Astruc, *Acc. Chem. Res.*, 2020, **53**, 2483.

20 S. Betharia, *Encyclopedia of Toxicology*, 2014, 536.

21 N. Alcock, A. Bozopoulos, E. Hatzigrigoriou and A. Varvoglis, *Acta Crystallogr. Sect. C: Cryst. Struct. Commun.*, 1990, **46**, 1300.

Conclusions

Like Hercules capturing Kerberos and leading it out of Hades, BAr_3 are able to imprison carbene precursors and lead them down new reaction pathways.

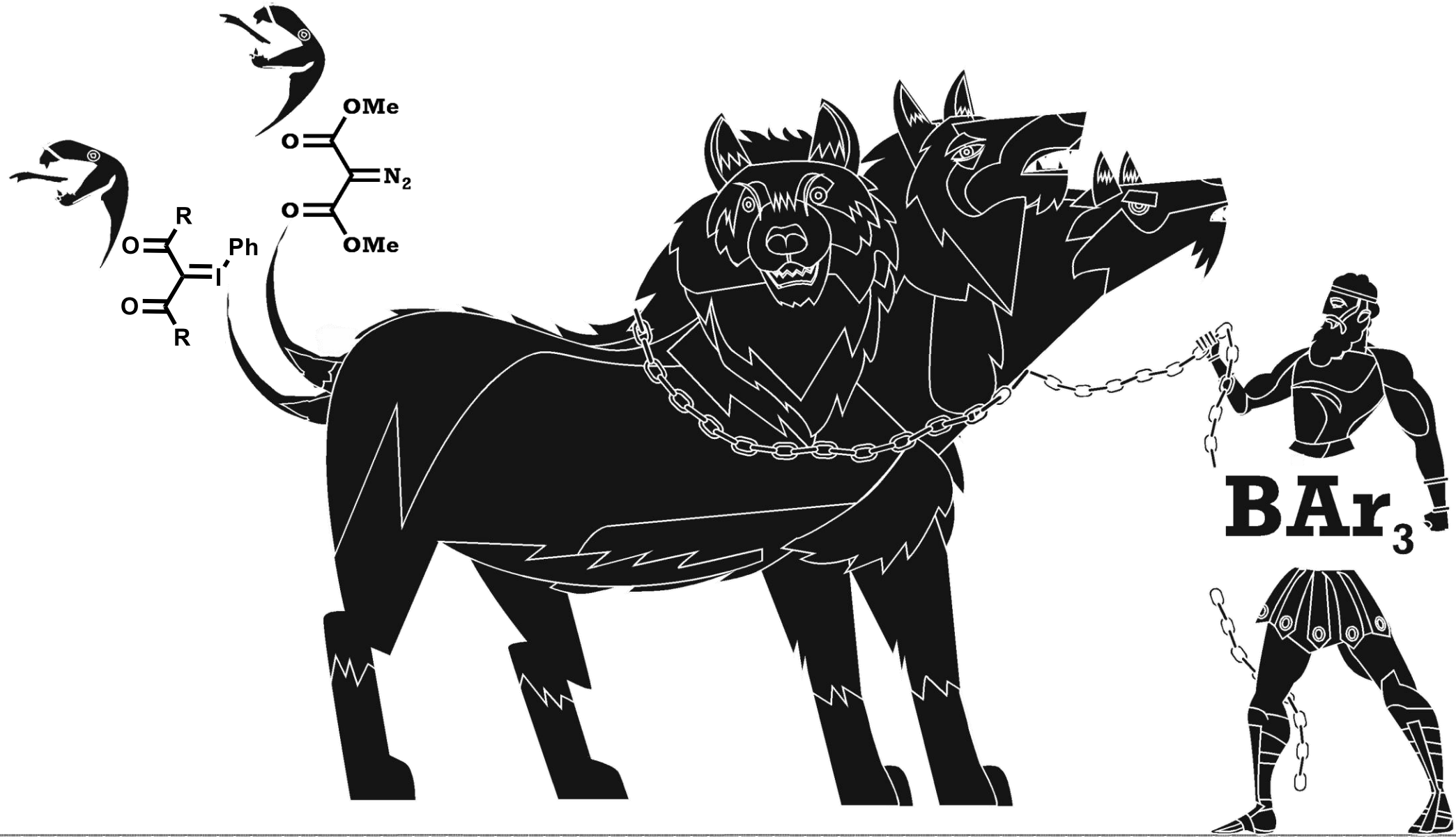

Chapter 6: Experimental

Chapter 6.1: General experimental

Except for starting materials and unless otherwise stated, all reactions and manipulations were carried out under a dry, O_2-free nitrogen atmosphere using a standard Schlenk line with a rotary oil pump. A nitrogen atmosphere-filled glove box (MBraun) was used to manipulate solids, including the storage of starting materials, product recovery and sample preparation for analysis. Except for THF, Et_2O, ethanol and deuterated solvents, all solvents were dried using an MB SPS-800 solvent purification system and stored under a nitrogen atmosphere. THF and diethyl ether were distilled over molten potassium and sodium benzophenone, respectively. They were stored over 3 Å molecular sieves under a nitrogen atmosphere. Deuterated solvents were dried over calcium hydride, degassed, distilled and/or dried over molecular sieves before use. Chemicals were purchased from commercial suppliers and used as received. ^{1}H, $^{13}C\{^{1}H\}$, $^{11}B\{^{1}H\}$, ^{19}F and ^{31}P NMR spectra were recorded on a Bruker Avance II 400 or Bruker Avance 500 spectrometers. Chemical shifts are expressed as parts per million (ppm, δ) downfield of tetramethylsilane (TMS) and are referenced to $CDCl_3$ (7.26/77.16 ppm) or C_6D_6 (7.16/128.1 ppm) as internal standards. Multinuclear NMR spectra were referenced to $CFCl_3$ (^{19}F), $BF_3{\cdot}Et_2O/CDCl_3$ ($^{11}B\{^{1}H\}$). $^{13}C\{^{1}H\}$ and $^{11}B\{^{1}H\}$ NMR spectra were measured as ^{1}H decoupled. The description of signals includes s = singlet, d = doublet, t = triplet, q = quartet, m = multiplet and br. = broad. All coupling constants are absolute values and are expressed in Hertz (Hz). Yields are given as isolated yields. Mass spectra were measured by the School of Chemistry in Cardiff University on a Waters LCT Premier/XE or a Waters GCT Premier spectrometer.

Chapter 6.2 Experimental for triarylboranes

Synthesis of $B(C_6F_5)_3$

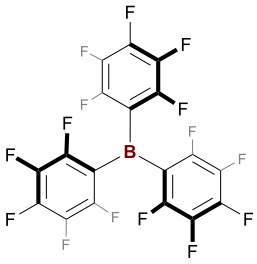

Synthesised according to a literature procedure.[1] Magnesium turnings (1.1 g, 45 mmol, 1.0 equiv.) were suspended in Et_2O (100 mL). C_6F_5Br (5.6 mL, 45 mmol, 3.0 equiv.) was added dropwise over 30 minutes under vigorous stirring, without allowing the mixture to reach reflux. The mixture was allowed to stir for 30 minutes at room temperature and was then transferred *via* filter cannula to a stirred solution of $BF_3{\cdot}OEt_2$ (1.9 mL, 15 mmol, 1.0 equiv.) in toluene (150 mL). The Et_2O solvent was removed *in vacuo,* leaving the mixture as a toluene solution. The reaction was then heated to 100 °C for one hour then left to cool to ambient temperature. The remaining solvent was removed under reduced pressure whilst gently heating in an oil bath until a light brown cake remained. A two-fold sublimation (110 °C, 1 $\times 10^{-3}$ mbar) was performed on the crude to yield pure $B(C_6F_5)_3$ as a white microcrystalline solid (6.7 g, 13.2 mmol, 88%). The spectroscopic data agree with literature established values.[1] **^{19}F NMR** (471 MHz, $CDCl_3$, 298 K) δ/ppm: -127.87 (s, 6F), -142.68 (s, 3F), -159.99 (s, 6F); **^{11}B{^{1}H} NMR** (128 MHz, $CDCl_3$, 298 K) δ/ppm: 58.6 (br., s).

Synthesis of $B(3,4,5\text{-}F_3C_6H_2)_3$

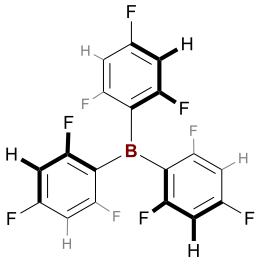

A solution of 5-bromo-1,2,3-trifluorobenzene (1.2 mL, 9.8 mmol) in Et_2O (50 mL) was cooled to -78 °C under nitrogen and ^{n}BuLi (6.7 mL, 1.47 M, 9.8 mmol) in n-hexane was added dropwise. The solution turned yellow and was stirred for an additional two hours until it turned into a white suspension. $BF_3{\cdot}OEt_2$ (0.4 mL, 3.3 mmol) was added dropwise, and the mixture was allowed to stir overnight at room temperature. The solvent was removed *in vacuo*, and the solid residue was sublimed thrice. The desired product was isolated as a white microcrystalline solid (0.219 g, 0.64 mmol, 23% yield). The spectroscopic data agree with literature established values.[2] **^{1}H NMR** (400 MHz, $CDCl_3$, 298 K) δ/ppm: 7.20–7.13 (m, 6H); **^{19}F NMR** (376 MHz, $CDCl_3$, 298 K) δ/ppm: -133.18 (d,^{3}J = 25 Hz, 6F), -152.38 (t, ^{3}J = 25 Hz, 3F); **^{11}B{^{1}H} NMR** (128 MHz, $CDCl_3$, 298 K) δ/ppm: 65.9 (br., s).

Synthesis of $B(2,4,6\text{-}F_3C_6H_2)_3$

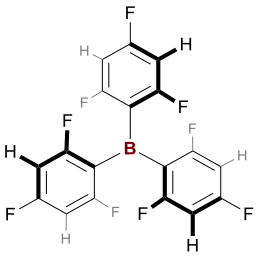

Synthesised according to a literature procedure.[2] 1-bromo-2,4,6-trifluorobenzene (3.5 mL, 30 mmol, 3 equiv.) was dissolved in freshly distilled THF (100 mL) and cooled to -20 ˚C. ^{i}PrMgCl (2.0 M in THF (15 mL, 30 mmol, 3 equiv.) was added portion-wise. The reaction was allowed to warm up for an hour until the temperature reached 0 ˚C. Upon cooling to -50 ˚C, $BF_3{\cdot}Et_2O$ (1.23 mL, 10 mmol, 1 equiv.) was added. The reaction was left for one hour at -50 °C, at which point it was allowed to warm up to room temperature. Removal of all volatiles, followed by a two-fold sublimation (120 °C, 1 × 10^{-3} mbar) of the crude product generated $B(2,4,6\text{-}F_3C_6H_2)_3$ as a white solid (3.35 g, 8.3 mmol, 83%). The spectroscopic data agree with literature established values.[2] **^{1}H NMR** (500 MHz, $CDCl_3$, 298 K) δ/ppm: 6.64 (dd, $^{3}J_{FH}$ = 8 Hz, 14 Hz, 6H); **^{19}F NMR** (471 MHz, $CDCl_3$, 298 K) δ/ppm: -95.74 (d, $^{3}J_{FH}$ = 9 Hz, 6F), -100.30 (t, $^{3}J_{FH}$ = 14 Hz, 9F); **^{11}B{^{1}H} NMR** (128 MHz, $CDCl_3$, 298 K) δ/ppm: 59.6 (br., s).

Synthesis of $B(2,6\text{-}F_2C_6H_3)_3$

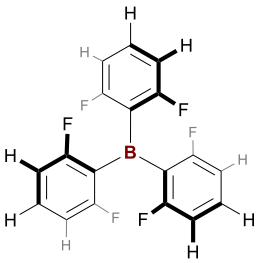

Synthesised according to a literature procedure.[2] 1-bromo-2,6-difluorobenzene (3.4 mL, 30 mmol, 3.0 equiv.) was dissolved in freshly distilled THF (100 mL) and cooled to -20 ˚C. ^{i}PrMgCl (2.0 M in THF), (6.00 mL, 40 mmol, 4.0 equiv.) was added dropwise. The reaction was allowed to warm up to 0 ˚C. Upon cooling to -50 ˚C, $BF_3{\cdot}Et_2O$ (1.2 mL, 10 mmol, 1.0 equiv.) was added dropwise. The reaction was held at -50 ˚C for 60 minutes, then warmed to room temperature. Removal of all volatiles, followed by a two-fold sublimation (120 ˚C, 1 × 10^{-3} mbar) of the crude product generated $B(2,6\text{-}F_3C_6H_2)_3$ as a white microcrystalline solid (2.3 g, 6.6 mmol, 66%). The spectroscopic data agree with literature established values.[2] **^{1}H NMR** (400 MHz, $CDCl_3$, 298 K) δ/ppm: 7.42–7.35 (m, 3H), 6.86–6.82 (m, 6H) **^{19}F NMR** (376 MHz, $CDCl_3$, 298 K) δ/ppm: -100.46 (s, 6F); **^{11}B{^{1}H} NMR** (128 MHz, $CDCl_3$, 298 K) δ/ppm: 63.2 (br., s).

Chapter 6.3: Experimental for activation of hydrazides and hydrazones with Lewis acidic boranes

*6.3.1 Synthesis of precursor **1** and hydrazones (**2a–2c**)*

*Synthesis of 1,4-phenylenebis(phenylmethanone) (**1**)*

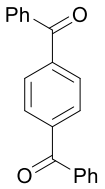

Synthesised according to a literature known procedure.[3] Terrephthaloyl chloride (4.00 g, 19.7 mmol, 1 equiv.) dissolved in dry benzene (25 mL) was added slowly to a stirred solution of $AlCl_3$ (3.15 g., 23.6 mmol, 1.2 equiv.) in dry benzene (20 mL), and the reaction mixture was brought to reflux for two hours. The reaction mixture was extracted using CH_2Cl_2, washed with $NaHCO_3$ and brine, dried over magnesium sulfate and concentrated using vacuum. The title compound was isolated as a white powder (2.26 g, 12.4 mmol, 63%). The spectral data shows good agreement with the literature reported values.[3] **^{1}H NMR** (500 MHz, $CDCl_3$, 298 K) δ/ppm: 7.89 (s, 4H), 7.85–7.84 (m, 4H), 7.65–7.62 (m, 2H), 7.53–7.50 (m, 4H).

General Procedure **A**[4]:

The relevant ketone was added to a stirred solution of excess hydrazine monohydrate in ethanol (20 mL). Next, acetic acid (0.2 mL) was added dropwise to the same reaction mixture. The reaction mixture was heated at reflux for twelve hours. Finally, the resultant solid was filtered and washed with water followed by pentane to afford the desired product.

*Synthesis of (diphenylmethylene)hydrazone (**2a**)*

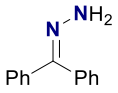

2a was synthesised according to General Procedure **A** using benzophenone (5 g, 27.4 mmol, 1 equiv.) and hydrazine monohydrate (4.8 mL, 156.0 mmol, 4 equiv.). The title compound was isolated as a white crystalline solid (4.46 g, 22.7 mmol, 83%). The spectral data shows good agreement with the literature reported values.[5] **^{1}H NMR** (500 MHz, $CDCl_3$, 298 K) δ/ppm: 7.33–7.30 (m, 2H), 7.26–7.23 (m, 3H), 7.09–7.04 (m, 5H), 5.21 (s, 2H); **^{13}C{^{1}H} NMR** (126 MHz, $CDCl_3$, 298 K) δ/ppm: 149.3, 138.5, 133.1, 129.5, 129.0, 128.9, 128.26, 128.23, 126.5; **HRMS** (ES+) m/z calculated for $[C_{13}H_{13}N_2]^+$ $[M+H]^+$: 197.1073, found: 197.1080.

*Synthesis of 1,4-bis-hydrazoneylidene(phIenyl)methyl)benzene (**2b**)*

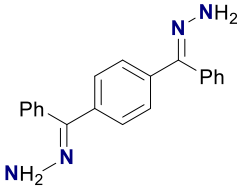

Synthesised according to General Procedure **A** utilising 1,3-phenylene-bis(phenylmethanone) (1.2 g, 4.2 mmol, 1 equiv.) and hydrazine monohydrate (1 mL, 20.9 mmol, 5 equiv.) The title compound (**2b**) was isolated as a pale-yellow powder (1.15 g, 3.6 mmol, 87%). **^{1}H NMR** (500 MHz, DMSO-d^{6}, 298 K) δ/ppm: 7.56–7.53 (m, 4H), 7.47–7.44 (m, 2H), 7.23–7.19 (m, 8H), 6.23 (s, 4H); **^{13}C{^{1}H} NMR** (126 MHz, DMSO-d^{6}, 298 K) δ/ppm: 144.7, 138.1, 133.5, 129.9, 129.1, 129.0, 125.6; **HRMS** (ES+) m/z calculated for $[C_{20}H_{19}N_4]^+$ $[M+H]^+$: 315.1604, found: 315.1614.

*Synthesis of (9H-fluoren-9-ylidene)hydrazone (**2c**)*

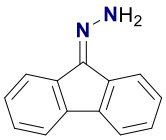

2c was synthesised according to General Procedure **A** using 9H-fluoren-9-one (2.5 g, 13.8 mmol, 1 equiv.) and hydrazine monohydrate (4 mL, 82.4 mmol, 5 equiv.) The title compound was isolated as yellow crystals (2.44 g, 12.5 mmol, 91%). The spectral data shows good agreement with the literature reported values.[3] **^{1}H NMR** (500 MHz, $CDCl_3$, 298 K) δ/ppm: 7.80 (d, $^{3}J_{HH}$ = 10 Hz, 1H), 7.67–7.63 (m, 2H), 7.56–7.54 (m, 1H), 7.33 (t, $^{3}J_{HH}$ = 10 Hz, 1H), 7.26–7.15 (m, 3H), 6.30 (s, 2H); **^{13}C{^{1}H} NMR** (126 MHz, $CDCl_3$, 298 K) δ/ppm: 145.6, 141.4, 138.6, 137.8, 130.3, 129.8, 128.6, 128.0, 127.8, 125.6, 120.8, 120.6, 119.6; **HRMS** (ES+) m/z calculated for $[C_{13}H_{11}N_2]^+$ $[M+H]^+$: 195.0917, found: 195.0918.

*6.3.2 Synthesis of hydrazone adducts **3a–3c**.*

General Procedure **B:**

In a Schlenk tube equipped with a magnetic stirring bar, the hydrazone (1 equiv.) was dissolved in toluene, and the borane (1 equiv.) was added portion-wise to the same reaction tube. The resultant solution was allowed to stir for 10 hours at room temperature. Subsequently, all volatiles were removed *in vacuo*. Finally, the desired product was obtained by recrystallisation.

*Synthesis of compound **3a***

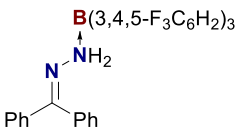

Synthesised according to General Procedure **B** using B(2,4,6-$F_3C_6H_2)_3$ (200 mg, 0.5 mmol, 1 equiv.) and (diphenylmethylene)hydrazone (**2a**) (100 mg, 0.5 mmol, 1 equiv.) in toluene (10 mL). Recrystallisation from a CH_2Cl_2/pentane mixture afforded desired compound (**3a**) as white crystals (187 mg, 0.3 mmol, 61%). **^{1}H NMR** (500 MHz, $CDCl_3$, 298 K) δ/ppm: 7.58–7.42 (m, 6H), 7.35–7.28 (m, 4H), 6.93 (d, $^{3}J_{HH}$ = 10 Hz, 2H), 6.48–6.45 (t, $^{3}J_{HH}$ = 10 Hz, 6H); **^{13}C{^{1}H} NMR** (126 MHz, $CDCl_3$, 298 K)

δ/ppm: 172.8, 165.1, 162.1, 135.3, 132.1, 131.3, 129.9, 129.2, 128.6, 128.0, 99.5, carbon atom attached to boron could not be observed; **^{19}F NMR** (471 MHz, $CDCl_3$, 298 K) δ/ppm: -112.79 (s, 2F), -99.92 (s, 4F); **^{11}B{^{1}H} NMR** (160 MHz, 298 K, $CDCl_3$) δ/ppm: -6.1 (br., s); **HRMS** (ES+) m/z calculated for $[C_{13}H_{13}N_2]^+$ $[M\text{-}B(C_6F_3H_2)_3]^+$: 197.1073 found: 197.1091; **EA** expected for $C_{31}H_{18}BF_9N_2$: C 62.03, H 3.02, N 4.67: obtained C 60.91, H 2.28, N 4.59.

*Synthesis of compound **3b***

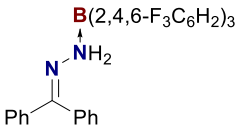

Synthesised according to General Procedure **B** using $B(3,4,5\text{-}F_3C_6H_2)_3$ (200 mg, 0.5 mmol, 1 equiv.) and (diphenylmethylene)hydrazone (**2a**) (100 mg, 0.5 mmol, 1 equiv.) in toluene (10 mL). The desired compound (**3b**) was yielded as white crystals (195 mg, 0.3 mmol, 65%) following recrystallisation from a CH_2Cl_2/pentane. **^{1}H NMR** (500 MHz, $CDCl_3$, 298 K) δ/ppm: 7.69–7.67 (m, 1H), 7.61–7.58 (m, 2H), 7.54–7.51 (m, 1H), 7.46–7.38 (m, 4H), 6.78–6.75 (m, 4H), 6.62–6.59 (m, 6H); **^{13}C{^{1}H} NMR** (126 MHz, $CDCl_3$, 298 K) δ/ppm: 151.0, 138.6, 134.4, 132.7, 131.7, 130.4, 129.6, 129.0, 129.0, 127.7, 117.2, carbon atoms attached to boron and nitrogens could not be observed; **^{19}F NMR** (471 MHz, $CDCl_3$, 296 K) δ/ppm: -135.66 (dd, ^{3}J = 19 Hz, $^{3}J_{FH}$= 9.0 Hz, 6F), -163.24 (m, 3F); **^{11}B{^{1}H} NMR** (160 MHz, 298 K, $CDCl_3$) δ/ppm: -2.6 (br., s); **EA** expected for $C_{31}H_{18}BF_9N_2$: C 62.03, H 3.02, N 4.67: obtained C 61.92, H 2.95, N 4.63.

*Synthesis of compound **3c***

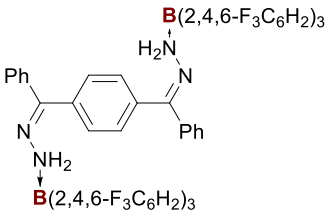

Synthesised according to General Procedure **B** using $B(2,4,6\text{-}F_3C_6H_2)_3$ (80 mg, 0.2 mmol, 2 equiv.) and **2b** (20 mg, 0.1 mmol, 1 equiv.) in toluene (5 mL). Recrystallisation from a CH_2Cl_2/pentane mixture gave the desired compound (**3c**) as white crystals (36 mg, 0.2 mmol, 56%). **^{1}H NMR** (500 MHz, $CDCl_3$, 298 K) δ/ppm: 7.59–7.51 (m, 10H), 7.27–7.26 (m, 4H), 6.86 (d, $^{3}J_{HH}$ = 5 Hz, 4H), 6.46–6.42 (m, 12H); **^{13}C{^{1}H} NMR** (126 MHz, $CDCl_3$, 298 K) δ/ppm: 171.7, 165.5, 162.1, 138.3, 131.6, 130.1, 129.1, 127.9, 127.9, 127.7, 99.6; **^{19}F NMR** (471 MHz, $CDCl_3$, 298 K) δ/ppm: -99.90 (s, 12F), -112.54 (s, 6F); **^{11}B{^{1}H} NMR** (160 MHz, $CDCl_3$, 298 K) δ/ppm: -6.2 (br., s).

*6.3.3 Synthesis of product set **4–5** and **6**.*

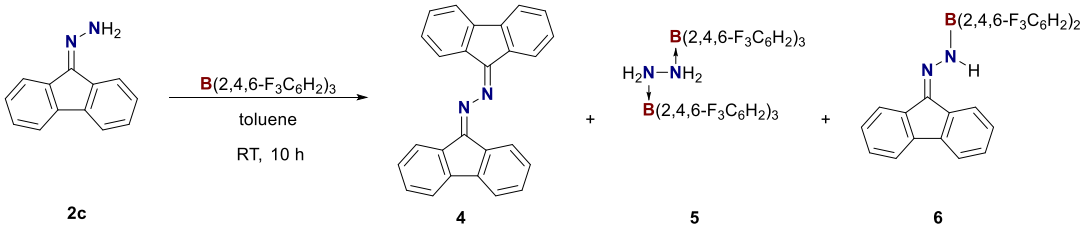

2c 4 5 6

Synthesised according to General Procedure **B** using $B(2,4,6\text{-}F_3C_6H_2)_3$ (40 mg, 0.1 mmol, 1 equiv.) and (9H-fluoren-9-ylidene)hydrazone (**2c**) (20 mg, 0.1 mmol, 1 equiv.) in toluene (5 mL) at room temperature. Recrystallisation of the reaction mixture from a CH_2Cl_2/pentane mixture gives an inseparable mixture of **4**, **5** and **6** (32 mg, 0.1 mmol, 72%).

Characterisation of **4**[6]**:**

Synthesised according to General Procedure **B** using $B(2,4,6\text{-}F_3C_6H_2)_3$ (80 mg, 0.2 mmol, 2 equiv.) and hydrazine monohydrate ($N_2H_4 \cdot H_2O$) (5 mg, 0.1 mmol, 1 equiv.) in CH_2Cl_2 (5 mL) with 4 Å pre-activated molecular sieves. Recrystallisation of the reaction mixture resulted in **5** at 45% yield. **^{1}H NMR** (500 MHz, $CDCl_3$, 298 K) δ/ppm: 8.15–8.05 (m, 4H), 7.67–7.65 (m, 4H), 7.49–7.39 (m, 6H), 7.24–7.23 (m, 2H); **^{13}C{^{1}H} NMR** (126 MHz, $CDCl_3$, 298 K) δ/ppm: 154.7, 142.1, 141.1, 136.4, 131.3, 131.2, 130.8, 129.7, 128.2, 128.1, 122.8, 120.0, 119.9; **HRMS** (ES+) m/z calculated for $[C_{26}H_{18}N_2]^+$ $[M+H]^+$: 357.1396, found: 357.1392. 8

Independent synthesis and characterisation of **5**

^{1}H NMR (500 MHz, $CDCl_3$, 298 K) δ/ppm: 6.85 (s, 4H), 6.43 (t, 12H); **^{13}C{^{1}H} NMR** (126 MHz, $CDCl_3$, 298 K) δ/ppm: 130, 128.9, 99.4, carbon atom attached to boron could not be observed; **^{19}F NMR** (471 MHz, $CDCl_3$, 298 K) δ/ppm: -99.91 (s, 4F). -112.42 (s, 2F); **^{11}B{^{1}H} NMR** (160 MHz, $CDCl_3$, 298 K) δ/ppm: -5.7 (br., s).

Characterisation of **6**

^{1}H NMR (500 MHz, $CDCl_3$, 298 K) δ/ppm: 8.07 (s, 1H), 7.67–7.64 (m, 4H), 7.55–7.50 (m, 2H), 7.44–7.31 (m, 2H), 7.25–7.21 (m, 2H); **^{13}C{^{1}H} NMR** (126 MHz, $CDCl_3$, 298 K) δ/ppm: 166.7, 164.3, 144.1, 140.4, 135.3, 133.6, 132.6, 129.0, 128.9, 128.5, 126.0, 123.7, 121.4, 119.9, 99.5, carbon atom attached to boron and nitrogen could not be observed; **^{19}F NMR** (471 MHz, $CDCl_3$, 298 K) δ/ppm: -99.90 (s, 4F). -112.54

(s, 2F); **^{11}B{^{1}H} NMR** (160 MHz, $CDCl_3$, 298 K) δ/ppm: -4.2 (br., s). **HRMS** (ES+) m/z calculated for $[C_{25}H_{14}BF_6N_2]^+$ $[M+H]^+$: 467.1149, found: 467.1142.

*6.3.4 Synthesis of adducts **7a**, **7b** and heterocycle **8**.*

*Synthesis of compound **7a***

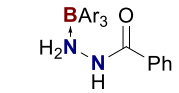

Ar = 2,4,6-$F_3C_6H_2$

Synthesised according to General Procedure **B** using B(2,4,6-$F_3C_6H_2)_3$ (30 mg, 0.2 mmol, 1 equiv.) and benzhydrazide (80 mg, 0.2 mmol, 1 equiv.) in toluene (10 mL). Recrystallisation from a CH_2Cl_2/pentane mixture afforded the desired compound (**7a**) as white crystals (76 mg, 0.1 mmol, 56%). **^{1}H NMR** (500 MHz, $CDCl_3$, 298 K) δ/ppm: 7.74–7.70 (m, 3H), 7.60–7.57 (m, 1H), 7.52–7.51 (m, 2H), 7.46–7.42 (m, 2H), 6.55–6.52 (m, 6H); **^{13}C{^{1}H} NMR** (126 MHz, $CDCl_3$, 298 K) δ/ppm: 166.9, 165.7, 162.7, 133.8, 129.3, 129.2, 127.1, 100.8, carbon attached to boron cannot be observed; **^{19}F NMR** (471 MHz, $CDCl_3$, 298 K) δ/ppm: -105.32 (s, 6F), -110.68 (m, 3F); **^{11}B{^{1}H} NMR** (160 MHz, $CDCl_3$, 298 K) δ/ppm: -6.1 (br., s).

*Synthesis of compound **7b***

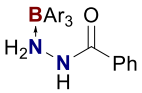

Ar = C_6F_5

Synthesised according to General Procedure **B** using B($C_6F_5)_3$ (50 mg, 0.1 mmol, 1 equiv.) and benzhydrazide (13 mg, 0.1 mmol, 1 equiv.) in toluene (8 mL) to afford the desired compound (**7b**) as white crystals (45 mg, 0.1 mmol, 71%). **^{1}H NMR** (400 MHz, $CDCl_3$, 298 K) δ/ppm: 7.97 (br., s, 2H), 7.68–7.64 (m, 2H), 7.55–7.47 (m, 4H); **^{13}C{^{1}H} NMR** (126 MHz, $CDCl_3$, 298 K) δ/ppm: 166.9, 149.1, 146.7, 138.6, 134.4, 129.4, 128.0, 127.0; carbon attached to boron cannot be observed; **^{19}F NMR** (376 MHz, $CDCl_3$, 298 K) δ/ppm: -135.60 (dd, ^{3}J = 20.1, 6.6 Hz, 6F), -153.98 (t, ^{3}J = 20.3 Hz, 3 F), -161.64 (m, 6F).; **^{11}B{^{1}H} NMR** (128 MHz, 298 K, $CDCl_3$): δ/ppm: -6.2 (br., s).

*Synthesis of compound **8***

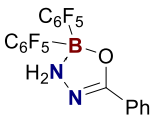

Synthesised according to General Procedure **B** using B($C_6F_5)_3$ (108 mg, 0.2 mmol, 1 equiv.) and benzhydrazide (30 mg, 0.2 mmol, 1 equiv.) in toluene (5 mL).The desired compound (**8**) was yielded as pink crystal (97 mg, 0.2 mmol, 82%) following recrystallisation from a CH_2Cl_2/pentane. **^{1}H NMR** (400 MHz, $CDCl_3$, 298 K) δ/ppm: 8.04–8.01 (m, 2H), 7.61–7.56 (m, 1H), 7.49–7.45 (m, 2H), 7.14 (br., s, 2H); **^{13}C{^{1}H} NMR** (100 MHz, $CDCl_3$, 298 K) δ/ppm: 173.1, 147.5, 141.0, 137.3, 133.0, 128.6, 128.5, 125.9, carbon attached to boron cannot be observed; **^{19}F NMR** (376 MHz, $CDCl_3$, 298 K) δ/ppm: -135.6 (dd, ^{3}J = 19 Hz, 4F), -153.98 (t, ^{3}J = 18 Hz, 2F), -161.64 (m, 4F); **^{11}B{^{1}H} NMR** (128 MHz, $CDCl_3$, 298 K)

δ/ppm: -4.3 (br., s); **HRMS** (ES+) m/z calculated for $[C_{19}H_8BF_{10}N_2O]^+$ $[M+H]^+$: 480.0606, found: 480.0609.

Chapter 6.4: Experimental for reactivity of diaziridines with triarylboranes and Frustrated Lewis Pairs.

*6.4.1 Synthesis of precursor **9** and diaziridines **10a–10b**.*

*Synthesis of 2,2,2-trifluoro-1-phenylethan-1-one O-tosyl oxime (**9**)*

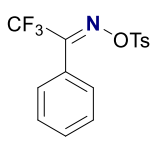

Synthesised according to an adapted literature procedure.[7] To begin with, 2,2,2-trifluoro-1-phenylethanone (2.4 mL, 17.4 mmol, 1 equiv.) was dissolved in pyridine (60 mL), then hydroxylamine hydrochloride (1.45 g, 20.9 mmol, 1.2 equiv.) was added. The mixture was stirred at 70 °C for one hour. Subsequently, it was subjected to rotary evaporation to remove the pyridine. The resultant residue was dissolved in ethyl acetate and washed with 1M HCl. The organic layer was separated, washed with water and brine, dried over $MgSO_4$ and evaporated. The crude product was used in the next step without any further purification.

The residue was dissolved in acetone (60 mL) at 0 °C. Triethylamine (7.3 mL, 52.1 mmol, 3 equiv.) and p-toluenesulfonyl chloride (3.98 g, 20.9 mmol, 1.2 equiv.) were added. The reaction mixture was stirred at room temperature for one hour. After evaporation, the residue was dissolved in CH_2Cl_2 and washed with water. The organic layer was separated, dried over Na_2SO_4 and subjected to rotary evaporation. The resulting residue was washed with diethyl ether/hexane. All volatiles were removed *in vacuo* leading to the isolation of the title compound (**9**) as an off-white solid (3.84g, 11.7 mmol, 67%). The spectral data shows good agreement with the literature reported values.[8] **^{1}H NMR** (400 MHz, $CDCl_3$, 298 K) δ/ppm: 7.91–7.88 (m, 2H), 7.53–7.37 (m, 7H), 2.47 (d, J = 7.5 Hz, 3H); **^{19}F NMR** (376 MHz, $CDCl_3$, 298 K) δ/ppm: -61.49 (s, 1F), -66.78 (s, 2F).

*Synthesis of 3-phenyl-3-(trifluoromethyl)diaziridine (**10a**)*

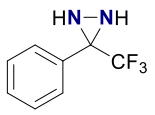

10a was synthesised according to a literature known procedure.[8] 2,2,2-trifluoro-1-phenylethan-1-one O-tosyl oxime (500 mg, 1.5 mmol) was dissolved in diethyl ether (20 mL) and cooled to -78 °C. Approximately 5 mL of liquid ammonia was added, and the mixture was stirred in a sealed vessel for sixteen hours at room temperature. **Caution:** The vessel used must be of a suitable pressure rating. Albeit no explosion occurred during this preparation, the use of a blast shield is highly recommended.

The ammonia was then evaporated at room temperature, and the crystallised p-toluenesulfonylamine was removed by filtration and washed with diethyl ether. The resultant solution was extracted twice with water. The organic phase was dried over

$MgSO_4$. Evaporation of the solvent at 0 °C lead to crystallisation of the title compound (**10a**) as a white solid (227 mg, 1.2 mmol, 83%). **Note:** Degradation was observed within 3–4 days regardless of storage conditions (freezer, inert atmosphere, glovebox freezer). The title compound was thus freshly prepared whenever it was required. The spectral data shows good agreement with the literature reported values.[9] **^{1}H NMR** (400 MHz, $CDCl_3$, 298 K) δ/ppm: 7.64–7.61 (m, 2H), 7.47–7.41 (m, 3H), 2.81 (d, J = 8.5 Hz, 1H), 2.25 (d, J = 8.5 Hz, 1H); **^{13}C{^{1}H} NMR** (101 MHz, $CDCl_3$, 298 K) δ/ppm: 131.8, 130.3, 128.9, 128.3, 58.2. **^{19}F NMR** (376 MHz, $CDCl_3$, 298 K) δ/ppm: -75.59 (s, 3F).

*Synthesis of 3,3-pentamethylenediaziridine (**10b**)*

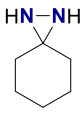

10b was synthesised according to a literature known procedure.[9] Cyclohexanone (15.5 mL, 149.8 mmol, 1.3 equiv.) in 40 mL of aqueous ammonia was cooled to 0 °C. Whilst maintaining the temperature between 0 °C and 10 °C, freshly prepared hydroxylamine-O-sulfonic acid[10] (12.7 g, 112.3 mmol, 1 equiv.) was added in portions of about 0.1 grams over the course of one hour. The mixture was stirred for another hour at 0 °C and left overnight in the freezer at -15 °C. The precipitated crystalline cake was filtered and pressed tight with a glass stopper. The solid was washed with 20 mL portions of ice-cold ether, toluene, and finally ether. The product was boiled briefly with a 20 mL portion of toluene. The solution was decanted from small salt residues and cooled to 0 °C for two hours. The precipitates were filtered with suction and washed with 50 mL of ice-cold petroleum ether. The title compound (**10b**) was isolated as a microcrystalline off-white solid (5.32 g, 47.4 mmol, 42%). To avoid degradation, the product was stored in the glovebox freezer (-30 °C). The spectroscopic data shows good agreement with literature reported values.[10] **^{1}H NMR** (400 MHz, $CDCl_3$, 298 K) δ/ppm: 1.68–1.50 (m, 12H); **^{13}C{^{1}H} NMR** (101 MHz, $CDCl_3$, 298 K) δ/ppm: 57.6, 36.2, 25.1, 25.0.

*6.4.2 Synthesis of adduct **11** and aryl elimination product **12**.*

General Procedure **C**:

To a vial equipped with a magnetic stirring bar, the appropriate diaziridine (1.0 equiv.) was dissolved in approximately 2 mL of toluene. The appropriate borane (1.0 equiv.) was dissolved in approximately 2 mL of toluene in a separate vial. Upon combining the two vials, the resultant solution was allowed to stir for 30 minutes at room

temperature. Subsequently, all volatiles were removed *in vacuo*. The desired product was obtained by successive washes of the crude with pentane.

General Procedure **D**:

To a vial equipped with a magnetic stirring bar, the appropriate diaziridine (1.0 equiv.) was dissolved in approximately 2 mL of toluene. The appropriate borane (1.0 equiv.) was dissolved in approximately 2 mL of toluene in a separate vial. The contents of the two vials were combined. The resultant solution was heated at a suitable temperature for ten hours. Subsequently, all volatiles were removed *in vacuo.* The desired product was isolated by recrystallisation using the layering method (CH_2Cl_2 /pentane).

*Synthesis of compound **11***

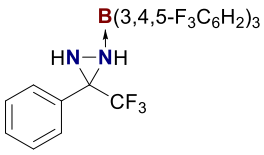

Synthesised according to General Procedure **C** using $B(3,4,5\text{-}F_3C_6H_2)_3$ (160 mg, 0.4 mmol, 1.0 equiv.) and 3-phenyl-3-(trifluoromethyl)diaziridine (**10a**) (75 mg, 0.4 mmol, 1.0 equiv.) to afford a mixture of products as a white solid. Single crystals suitable for X-ray diffraction were obtained by slow evaporation of the solvent (toluene). The multinuclear NMR spectra obtained did not correspond to a single species and could not be accurately assigned.

*Synthesis of compound **12***

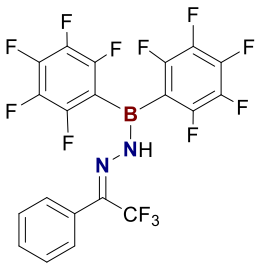

Synthesised according to General Procedure **D** using $B(C_6F_5)_3$ (160 mg, 0.4 mmol, 1.0 equiv.) and 3-phenyl-3-(trifluoromethyl)diaziridine (**10a**) (75 mg, 0.4 mmol, 1.0 equiv.) to afford a mixture of products as a paste. Single crystals suitable for X-ray diffraction were obtained by slow evaporation of the solvent (toluene). The multinuclear NMR spectra obtained did not correspond to a single species and could not be accurately assigned.

*6.4.3 Synthesis of adducts **13a–13d**.*

*Synthesis of compound **13a***

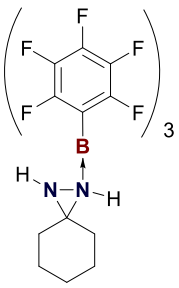

Synthesised according to General Procedure **C** using $B(C_6F_5)_3$ (205 mg, 0.4 mmol, 1.0 equiv.) and 3,3-pentamethylene diaziridine *(**10b**)*. (45 mg, 0.4 mmol, 1.0 equiv.) to afford the desired compound (**13a**) as a white solid (213 mg, 0.3 mmol, 85%). **^{1}H NMR** (400 MHz, $CDCl_3$, 298 K) δ/ppm: 5.30 (s, 1H), 2.90 (d, 1H), 2.34–2.28 (m, 1H); 2.05–1.96 (m, 2H), 1.83–1.75 (m, 2H), 1.67–1.58 (m, 1H), 1.45–1.25 (m, 3H), 1.13–1.01 (m, 1H) **^{13}C{^{1}H} NMR** (101 MHz, $CDCl_3$, 298 K) δ/ppm: 147.8, 140.5, 137.3, 115.2, 70.4, 36.3, 28.6, 24.7; **^{19}F NMR** (376 MHz, $CDCl_3$, 298 K) δ/ppm: -132.80 (d, J = 22.9 Hz, 6F), -155.08 (t, J = 21.05 Hz, 3F), -162.48 (t, J = 22.01 Hz; 6F); **^{11}B{^{1}H} NMR** (128 MHz, 298 K, $CDCl_3$) δ/ppm: -6.4 (br., s). **HRMS** (ES-) m/z calculated for $[C_{24}H_{11}N_2{}^{10}BF_{15}]^-$ $[M-H]^-$: 623.0776 found: 623.0775.

*Synthesis of compound **13b***

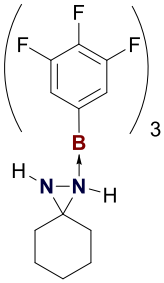

Synthesised according to General Procedure **C** using B(3,4,5-$F_3C_6H_2)_3$ (160 mg, 0.4 mmol, 1.0 equiv.) and 3,3-pentamethylene diaziridine (**10b**) (45 mg, 0.4 mmol, 1.0 equiv.) to afford the desired compound (**13b**) as a white solid (180 mg, 0.4 mmol, 87%). **^{1}H NMR** (400 MHz, $CDCl_3$, 298 K) δ/ppm: 6.54–6.49 (m, 6H), 5.49 (s, 1H), 2.86 (d, 1H, HN), 2.27–1.10 (m, 10H); **^{13}C{^{1}H} NMR** (101 MHz, $CDCl_3$, 298 K) δ/ppm: 165.5, 161.2, 99.9, 68.8, 36.6, 28.4, 24.7, 24.5; **^{19}F NMR** (376 MHz, $CDCl_3$, 298 K) δ/ppm: -139.52 (s, 6F), -153.16 (s, 3F); **^{11}B{^{1}H} NMR** (128 MHz, 298 K, $CDCl_3$) δ/ppm: -6.1 (br., s).

*Synthesis of compound **13c***

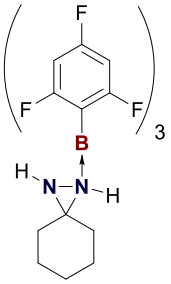

Synthesised according to General Procedure **C** using B(2,4,6-$F_3C_6H_2)_3$ (160 mg, 0.4 mmol, 1.0 equiv.) and 3,3-pentamethylene diaziridine (**10b**) (45 mg, 0.4 mmol, 1.0 equiv.) to afford the desired compound (**13c**) as an off-white solid (183 mg, 0.4 mmol, 90%).**^{1}H NMR** (400 MHz, $CDCl_3$, 298 K) δ/ppm: 6.83–6.79 (m, 6H), 3.88 (s, 1H), 2.76 (s, 1H, NH), 2.19–1.05(m, 10H); **^{13}C{^{1}H} NMR** (101 MHz, $CDCl_3$, 298 K) δ/ppm: 165.3, 162.2, 115.8; 99.8, 68.7, 36.4, 28.2, 24.6, 24.4, 24.3. **^{19}F NMR** (376 MHz, $CDCl_3$, 298 K) δ/ppm: -98.10 (s, 6F), -111.72 (s, 3F); **^{11}B{^{1}H} NMR** (128 MHz, 298 K, $CDCl_3$) δ/ppm: -6.3 (br., s).

*Synthesis of compound **13d***

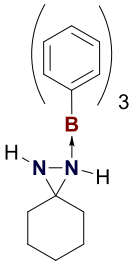

Synthesised according to General Procedure **C** using triphenyl borane (100 mg, 0.4 mmol, 1.0 equiv.) and 3,3-pentamethylene diaziridine (**10b**) (46 mg, 0.4 mmol, 1.0 equiv.) to afford compound **13d** as a white solid (138 mg, 0.4 mmol, 94%). **^{1}H NMR** (400 MHz, $CDCl_3$, 298 K) δ/ppm: 7.28–7.04 (m, 15H), 3.34 (s, 2H), 1.46–1.32 (m, 10H); **^{13}C{^{1}H} NMR** (101 MHz, $CDCl_3$, 298 K) δ/ppm: 134.3, 127.6, 126.1, 67.1, 33.4, 24.6 24.5, carbon attached to boron not visible; **^{11}B{^{1}H} NMR** (128 MHz, 298 K, $CDCl_3$) δ/ppm: 2.3 (br., s).

*6.4.4 Synthesis of rearrangement adducts **14a–14d***

*Synthesis of compound **14a***

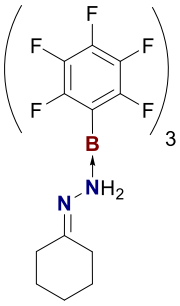

Synthesised according to General Procedure **D** using $B(C_6F_5)_3$ (205 mg, 0.4 mmol, 1.0 equiv.) and 3,3-pentamethylene diaziridine (**10b**). (45 mg, 0.4 mmol, 1.0 equiv.) at 40 °C to afford the desired compound (**14a**) as an off-white solid (146 mg, 0.2 mmol, 58%). **^{1}H NMR** (500 MHz, C_6D_6, 298 K) δ/ppm: 7.15 (s, 2H), 2.23 (s, 4H), 1.63 (br., s, 6H); **^{13}C{^{1}H} NMR** (126 MHz, C_6D_6, 298 K) δ/ppm: 176.7, 147.3, 139.4, 136.5, 34.5, 25.4, 23.5; **^{19}F NMR** (471 MHz, C_6D_6, 298 K) δ/ppm: -133.74 (d, J = 23.2 Hz, 6F), -156.16 (t, J = 20.32 Hz, 3F), -162.83 (m, 6F); **^{11}B{^{1}H} NMR** (160 MHz, 298 K, C_6D_6) δ/ppm: -6.2 (br., s). **HRMS** (ES-) m/z calculated for $[C_{24}H_{11}N_2{}^{10}BF_{15}]^-$ $[M\text{-}H]^-$: 623.0776 found: 623.0778.

*Synthesis of compound **14b***

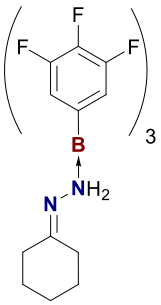

Synthesised according to General Procedure **D** using $B(3,4,5\text{-}F_3C_6H_2)_3$ (160 mg, 0.4 mmol, 1.0 equiv.) and 3,3-pentamethylene diaziridine (**10b**) (45 mg, 0.4 mmol, 1.0 equiv.) at 40 °C to afford the desired compound (**14b**) as a white solid (124 mg, 0.2 mmol, 60%). **^{1}H NMR** (500 MHz, $CDCl_3$, 298 K) δ/ppm: 6.87–6.78 (m, 8H), 2.32–2.16 (m, 4H), 1.67 (s, 2H), 1.60–1.55 (m, 2H), 1.45 (s, 2H); **^{13}C{^{1}H} NMR** (126 MHz, $CDCl_3$, 298 K) δ/ppm: 165.5, 161.2, 99.9, 68.8, 36.6, 28.4, 24.7, 24.6, 24.5; **^{19}F NMR** (471 MHz, $CDCl_3$, 298 K) δ/ppm: -135.43 (s, 6F), -163.53 (s, 3F); **^{11}B{^{1}H} NMR** (160 MHz, 298 K, $CDCl_3$) δ/ppm: -1.5 (br., s).

*Synthesis of compound **14c***

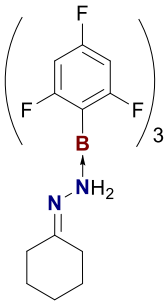

Synthesised according to General Procedure **D** using $B(2,4,6\text{-}F_3C_6H_2)_3$ (162 mg, 0.4 mmol, 1.0 equiv.) and 3,3-pentamethylene diaziridine (**10b**) (45 mg, 0.4 mmol, 1.0 equiv.) at 70 °C to afford the desired compound (**14c**) as a yellow oil (139 mg, 0.3 mmol, 67%). **^{1}H NMR** (500 MHz, $CDCl_3$, 298 K) δ/ppm: 7.33 (s, 2H), 6.52–6.48 (m, 6H), 2.12 (dt, J = 60.4, 6.2 Hz, 4H), 1.60–1.53 (m, 6H); **^{13}C{^{1}H} NMR** (126 MHz, $CDCl_3$, 298 K) δ/ppm: 175.7, 165.7, 162.1, 99.6, 36.1, 26.9, 26.8, 26.1, 25.3; **^{19}F NMR** (471 MHz, $CDCl_3$, 298 K) δ/ppm: -100.01 (s, 6F), -112.75 (s, 3F); **^{11}B{^{1}H} NMR** (160 MHz, 298 K, $CDCl_3$) δ/ppm: -6.3 (br., s).

*Synthesis of compound **14d***

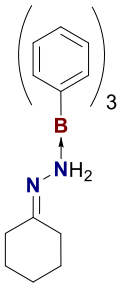

Synthesised according to General Procedure **D** using triphenyl borane (98 mg, 0.4 mmol, 1.0 equiv.) and 3,3-pentamethylene diaziridine (**10b**) (46 mg, 0.4 mmol, 1.0 equiv.) at 70 °C to afford the desired compound (**14d**) as a white solid (117 mg, 0.3 mmol, 82%). **^{1}H NMR** (500 MHz, $CDCl_3$, 298 K) δ/ppm: 7.46–7.43 (m, 7H), 7.36–7.28 (m, 10H), 2.23 (dt, J = 36.6, 6.2 Hz, 4H), 1.59–1.46 (m, 6H); **^{13}C{^{1}H} NMR** (126 MHz, $CDCl_3$, 298 K) δ/ppm: 166.6, 138.1, 128.1, 126.8, 35.7, 29.5 28.5, 26.9, 25.4; **^{11}B{^{1}H} NMR** (160 MHz, 298 K, $CDCl_3$) δ/ppm: 1.0 (br., s). **HRMS** (ASAP+) m/z calculated for $[C_{24}H_{26}N_2{}^{10}B]^+$ $[M+H]^+$: 353.2183 found: 353.2182.

*6.4.5 Synthesis of aryl elimination product **15***

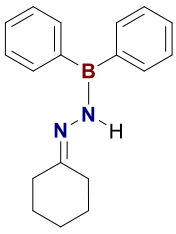

Method A: **15** was synthesised according to General Procedure **D** using triphenyl borane (97 mg, 0.4 mmol, 1.0 equiv.) and 3,3-pentamethylene diaziridine (**10b**) (46 mg, 0.4 mmol, 1.0 equiv.) at 90 °C to afford the desired compound (**15**) as a white solid (65 mg, 0.2 mmol, 61%).

Method B: **15** was synthesised by heating **11b** (100mg, 0.3 mmol) to 90 °C for ten hours to afford the desired compound (**15**) as a white solid (58 mg, 0.2 mmol, 74%).

^{1}H NMR (500 MHz, $CDCl_3$, 298 K) δ/ppm: 7.93–7.91 (m, 1H, NH), 7.54–7.29 (m, 10H), 2.42–2.33 (m, 4H), 1.80–1.53 (m, 6H); **^{13}C{^{1}H} NMR** (126 MHz, $CDCl_3$, 298 K) δ/ppm: 158.4, 136.0, 131.4, 128.0, 35.8, 27.7, 26.5, 26.1, 26.0; **^{11}B{^{1}H} NMR** (160 MHz, 298 K, $CDCl_3$) δ/ppm: 40.1 (br., s). **HRMS** (ASAP+) m/z calculated for $[C_{18}H_{22}N_2{}^{10}B]^+$ $[M+H]^+$: 277.1876 found: 277.1880.

*6.4.6 Synthesis of compound **16**.*

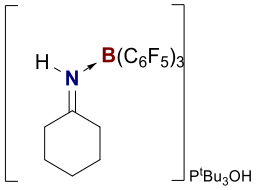

To a microwave vial equipped with a magnetic stirring bar, $B(C_6F_5)_3$ (203 mg, 0.4 mmol, 1.0 equiv.) and tri-tert-butylphosphine (80 mg, 0.4 mmol, 1.0 equiv.) were dissolved in approximately 2 mL of deuterated chloroform. The resultant pale-yellow solution was added to a solution of 3,3-pentamethylene diaziridine (45 mg, 0.4 mmol, 1.0 equiv.) in approximately 0.5 mL of deuterated benzene. An immediate colour change to white was observed. The mixture was stirred for 30 minutes at room temperature. Subsequently, all volatiles were removed *in vacuo.* Crystals suitable for X-ray diffraction were obtained by scratching the crude residue with a spatula inside the glovebox.

Chapter 6.5: Experimental for 1,3-carboboration of carbene precursors.

*6.5.1 Synthesis of diazo malonate **17** and iodonium ylides **18a–18d**.*

*Synthesis of dimethyl 2-diazomalonate (**17**)*

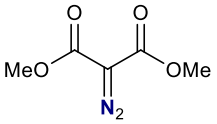

Synthesised according to a literature known procedure.[11] To a suspension of 4-acetamidobenzenesulfonyl azide (1 g, 4.2 mmol 1.0 equiv.) in acetonitrile (25 mL) was added triethylamine (440 mg, 4.4 mmol, 1.05 equiv.). Upon cooling to 0 °C, dimethyl malonate (550 mg, 4.2 mmol, 1.0 equiv.) was added portion-wise over 5 minutes. The cooling bath was removed, and the reaction mixture was stirred at room temperature for 15 hours. The solid 4-acetamidobenzenesulfonamide by-product was removed and washed with a 1:1 mixture of petroleum ether and diethyl ether (20 mL). The filtrates are concentrated, giving a yellow oil. Finally, a distillation affords **17** as a red oil (425 mg, 2.7 mmol, 65%). The product showed good agreement with literature values. **^{1}H NMR** (400 MHz, $CDCl_3$, 298 K) δ/ppm: 3.68 (s, 6H); **^{13}C{^{1}H} NMR** (101 MHz, $CDCl_3$, 298 K) δ/ppm: 53.4, 65.2, 162.1.

General Procedure **E**[12]:

To a suspension of KOH (6.0 equiv.) in acetonitrile (20 mL) was added the appropriate 1,4-dicarbonyl compound (1.0 equiv.) The heterogeneous mixture was stirred vigorously for 5 minutes at 0 °C. To this was added phenyliodonium diacetate (1.1 equiv.) in one portion and stirred at 0 °C for a further two hours. Water was subsequently added to the resultant mixture and stirred for 1 minute. The faint yellow biphasic mixture was filtered, and the solid was washed with water (2 x 5 mL), carefully removing the solvent between each wash entirely. A final wash with ethanol (10 mL) yielded the desired iodonium ylide, which was dried under reduced pressure.

Synthesis of *bis(methoxycarbonyl)(phenyliodinio)methanide (**18a**)*

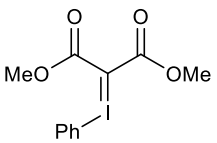

18a was synthesised according to General Procedure **E** using iodobenzene diacetate (1.72 g, 5.3 mmol, 1.0 equiv.), potassium hydroxide (1.8 g, 32.0 mmol, 6.0 equiv.) and dimethyl malonate (0.6 mL, 5.3 mmol, 1.0 equiv.). The title compound was isolated as an off-white solid (1.15 g, 3.4 mmol, 65%). The spectral data shows good agreement with the literature reported values.[13] **^{1}H NMR** (400 MHz, $CDCl_3$, 298 K) δ/ppm: 7.75–7.72 (m, 2H), 7.55–7.51 (m, 1H), 7.43–7.38 (m, 2H), 3.74 (s, 6H); **^{13}C{^{1}H} NMR** (101 MHz, $CDCl_3$, 298 K) δ/ppm: 166.5, 131.7, 131.5, 130.4, 114.5, 52.5, ylide carbon could not be

observed. The product was partially degraded during preparation of the NMR sample.
[13]

Synthesis of *ethyl 3-oxo-2-(phenyliodaneylidene)butanoate (**18b**)*

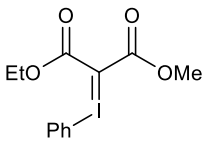

18b was synthesised according to General Procedure **E** using iodobenzene diacetate (2.56 g, 7.9 mmol, 1.0 equiv.), potassium hydroxide (2.66 g, 47.3 mmol, 6.0 equiv.) and dimethyl malonate (1.0 mL, 7.9 mmol, 1.0 equiv.). The title compound was isolated as an off white solid (423 mg, 1.3 mmol, 16%). **^{1}H NMR** (400 MHz, $CDCl_3$, 298 K) δ/ppm: 7.78–7.77 (m, 2H), 7.54–7.51 (m, 1H), 7.40–7.37 (m, 2H), 4.13 (q, J = 7.1 Hz, 2H,), 2.59 (s, 3H), 1.22 (t, J = 7.1 Hz, 3H); **^{13}C{^{1}H} NMR** (126 MHz, $CDCl_3$, 298 K) δ/ppm: 187.2, 165.2, 133.2, 131.6, 131.4, 112.8, 60.6, 26.0, 14.8. The product partially degraded during the preparation of the NMR sample.

Synthesis of *1,3-diphenyl-2-(phenyliodaneylidene)propane-1,3-dione (**18c**)*[13]

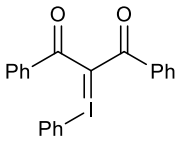

A solution of potassium hydroxide (6.90 g, 123.1 mmol, 20.0 equiv.) in methanol (10 mL) was added to dibenzoyl methane (1.38 g, 6.0 mmol, 1.0 equiv.) in methanol (10 mL) at -5 °C. Subsequently, a solution of iodobenzene diacetate (2.00 g, 6 mmol, 1.0 equiv.) in methanol (20 mL) was added portion-wise while the temperature was not allowed to exceed 0 °C. The stirring was continued for 30 minutes at 0 °C. The resultant mixture was poured onto ice water (50 mL), and the product was extracted with CH_2Cl_2 (3×20 mL) and dried with magnesium sulfate. The solvent was removed *in vacuo,* and the solid residue was recrystallised from cold ethanol to give **18c** as a yellow powder (538 mg, 1.3 mmol, 21%). **^{1}H NMR** (400 MHz, $CDCl_3$, 298 K) δ/ppm: 8.03–8.00 (m, 2H), 7.57–7.52 (m, 1H), 7.43–7.38 (m, 2H), 7.24–7.22 (m, 4H), 7.05–7.01 (m, 2H), 6.93–6.91 (m, 4H); **^{13}C{^{1}H} NMR** (126 MHz, $CDCl_3$, 298 K) δ/ppm: 186.4, 139.1, 137.6, 134.5, 131.6, 130.4, 129.8, 129.2, 127.5, 112.1. **HRMS** (ASAP+) m/z calculated for $[C_{15}H_1O_2]$ $[M\text{-}C_6H_5I]^+$: 223.0754 found: 223.0756.

*Synthesis of 5,5-dimethyl-2-(phenyliodaneylidene)cyclohexane-1,3-dione (**18d**)*[14]

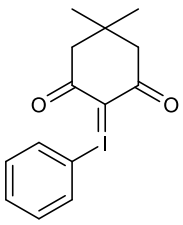

To iodobenzene diacetate (1 g, 3.1 mmol, 1.0 equiv.) in CH_2Cl_2 (15 mL) at 10–15 °C was added in one portion KOH (1.73 g, 30.9 mmol, 10.0 equiv.) and dimedone (581 mg, 4.1 mmol, 1.3 equiv.). The reaction mixture was allowed to stir for 50 minutes until complete conversion was confirmed by TLC analysis (8% MeOH in CH_2Cl_2). The crude was diluted with CH_2Cl_2 (15 mL), filtered through cotton and glass wool,

washed with CH_2Cl_2 (20 mL) and dried over Na_2SO_4. The drying agent was filtered off, and the solvent was removed under reduced pressure at room temperature. Precipitation at -20 °C for one hour using CH_2Cl_2 (15 mL) and hexane (40 mL) afforded the iodonium ylide, which was further washed with hexane before being dried in high vacuum. The title compound (**18d**) was isolated as a white fibrous solid (564 mg, 1.7 mmol, 53%). The spectral data shows good agreement with the literature reported values. [15] **^{1}H NMR** (500 MHz, $CDCl_3$, 298 K) δ/ppm: 7.82 (d, J = 6.9 Hz, 2H), 7.53–7.50 (m, 1H), 7.37–7.34 (m, 2H), 2.50 (s, 4H), 1.05 (s, 6H); **^{13}C{^{1}H} NMR** (126 MHz, $CDCl_3$, 298 K) δ/ppm: 188.5, 134.0, 131.7, 131.5, 111.9, 94.6, 50.8, 32.1, 28.2.

*6.5.2 Synthesis of boron dienolates **19a–19e** and **20a–20b**.*

General Procedure **F**:

To a Schlenk tube equipped with a magnetic stirring bar, either dimethyl diazomalonate **17** or the appropriate iodonium ylide **18** (1.0 equiv.) was dissolved in toluene, and the appropriate borane (1.0 equiv.) was added portion-wise. The resultant solution was allowed to stir for twelve hours at 50 °C. Subsequently, all volatiles were removed *in vacuo*. The desired product was obtained by successive washes of the crude with pentane.

*Synthesis of compound **19a***

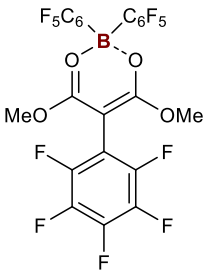

19a was synthesised according to General Procedure **F** using (250 mg, 0.5 mmol, 1.0 equiv.) and dimethyl 2-(phenyliodaneylidene)malonate (**17**) (163 mg, 0.5 mmol, 1.0 equiv.) in toluene (15 mL). to afford a mixture of products as a white solid. Crystals were obtained from a CH_2Cl_2/pentane mixture at room temperature. The multinuclear NMR spectra obtained did not correspond to a single species and could not be accurately assigned.

*Synthesis of compound **19b***

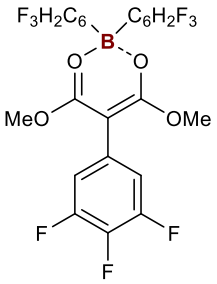

Synthesised according to General Procedure **F** using B(3,4,5-$F_3C_6H_2)_3$ (123 mg, 0.3 mmol, 1.0 equiv.) and dimethyl diazomalonate (**18a**) (102 mg, 0.3 mmol, 1.0 equiv.) in toluene (15 mL). to afford the desired compound (**19b**) as a white solid (120 mg, 0.2 mmol, 74%). **^{1}H NMR** (400 MHz, $CDCl_3$, 298 K) δ/ppm: 6.94–6.90 (m, 4H), 6.79–6.76 (m, 2H), 4.08 (s, 6H); **^{13}C{^{1}H} NMR** (101 MHz, $CDCl_3$, 298 K) δ/ppm: 172.8, 152.5, 150.0, 139.1, 129.2, 128.4, 115.6, 114.2, 82.3, 55.9, carbon atom attached to boron could not be observed; **^{19}F NMR** (376 MHz, $CDCl_3$, 298 K) δ/ppm: -135.04 (d, J = 20.7 Hz, 2F), -35.70 (d, J = 20.1 Hz, 4F), -161.32 (t, J = 20.8 Hz, 1F), -162.82 (t, J = 20.1 Hz, 2F); **^{11}B{^{1}H} NMR** (128 MHz, 298 K, $CDCl_3$) δ/ppm: 7.5 (br., s); **HRMS** (ASAP+) m/z calculated for $[C_{17}H_{10}O_4{}^{10}BF_6]^+$ $[M–C_6F_5]^+$: 403.0571 found: 403.0567.

*Synthesis of compound **19c***

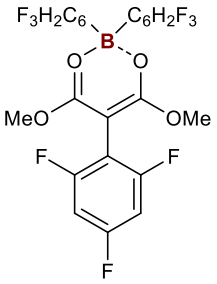

Synthesised according to General Procedure **F** using B(2,4,6-$F_3C_6H_2)_3$ (95 mg, 0.2 mmol, 1.0 equiv.) and dimethyl 2-(phenyliodaneylidene)malonate (**18a**) (79 mg, 0.2 mmol, 1.0 equiv.) in toluene (15 mL). to afford the desired compound (**19c**) as a white solid (62 mg, 0.1 mmol, 50%). **^{1}H NMR** (500 MHz, $CDCl_3$, 298 K) δ/ppm: 6.68–6.65 (m, 2H), 6.55–6.51 (m, 4H), 3.99 (s, 6H); **^{13}C{^{1}H} NMR** (126 MHz, $CDCl_3$, 298 K) δ/ppm: 173.2, 166.0, 164.1, 162.6, 161.2, 103.5, 99.9, 99.5, 70.1, 56.0, carbon atom attached to boron could not be observed; **^{19}F NMR** (470 MHz, $CDCl_3$, 298 K) δ/ppm: -103.27 (d, J = 7.5 Hz, 4F, -106.77 (d, J = 6.7 Hz, 2F), -107.88 (t, J = 6.7 Hz), -110.98 (m, 2F); **^{11}B{^{1}H} NMR** (160 MHz, 298 K, $CDCl_3$) δ/ppm: 6.6 (br., s); **HRMS** (ASAP+) m/z calculated for $[C_{23}H_{11}O_4{}^{10}BF_9]$+ $[M-H]^+$: 533.0618 found: 533.0607.

*Synthesis of compound **19d***

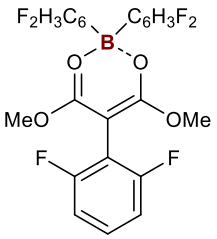

Synthesised according to General Procedure **F** using B(2,6-$F_2C_6H_3)_3$ (250 mg, 0.7 mmol, 1.0 equiv.) and dimethyl 2-(phenyliodaneylidene)malonate (**18a**) (238.6 mg, 0.7 mmol, 1.0 equiv.) in toluene (10 mL) to afford the desired compound (**19d**) as a white solid (230 mg, 0.5 mmol, 67%). **^{1}H NMR** (400 MHz, $CDCl_3$, 298 K) δ/ppm: 7.30–7.24 (m, 1H), 7.23–7.15 (m, 2H), 6.90–6.86 (m, 2H), 6.79–6.75 (m, 4H), 4.01 (s, 6H); **^{13}C{^{1}H} NMR** (101 MHz, $CDCl_3$, 298 K) δ/ppm: 173.2, 165.9, 161.4, 129.9, 129.3, 111.3, 110.8, 107.3, 70.7, 55.9, carbon atom attached to

boron could not be observed; **^{19}F NMR** (376 MHz, $CDCl_3$, 298 K) δ/ppm: -105.85 (s, 2F), -109.69 (s, 4F); **^{11}B{^{1}H} NMR** (128 MHz, 298 K, $CDCl_3$) δ/ppm: 6.9 (br., s); **HRMS** (ASAP+) m/z calculated for $[C_{23}H_{14}O_4{}^{10}BF_6]^+$ $[M\text{-}H]^+$: 481.1046 found: 481.1057.

*Synthesis of compound **19e***

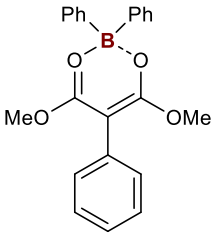

Synthesised according to General Procedure **F** using BPh_3 (250 mg, 1 mmol, 1.0 equiv.) and dimethyl 2-(phenyliodaneylidene)malonate (**18a**) (345 mg, 1 mmol, 1.0 equiv.) in toluene (10 mL) to afford the desired compound (**19e**) as an off-white solid (132 mg, 0.4 mmol, 43%). **^{1}H NMR** (400 MHz, $CDCl_3$, 298 K) δ/ppm: 7.54–7.52 (m, 4H), 7.37–7.24 (m, 9H), 7.17–7.14 (m, 2H), 4.02 (s, 6H); **^{13}C{^{1}H} NMR** (101 MHz, $CDCl_3$, 298 K) δ/ppm: 173.1 134.7, 131.4, 131.1, 128.0, 127.4, 127.1, 126.8, 83.5, 54.9, carbon atom attached to boron could not be observed; **^{11}B{^{1}H} NMR** (128 MHz, 298 K, $CDCl_3$) δ/ppm: 9.2 (br., s); **HRMS** (ASAP+) m/z calculated for $[C_{23}H_{20}O_4{}^{10}B]^+$ $[M\text{-}H]^+$: 371.1457 found: 371.1455.

*Synthesis of compound **20a***

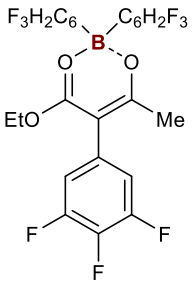

Synthesised according to General Procedure **F** using B(3,4,5-$F_3C_6H_2)_3$ (100 mg, 0.3 mmol, 1.0 equiv.) and methyl 3-oxo-2-(phenyliodaneylidene)butanoate (**18b**) (83 mg, 0.3 mmol, 1.0 equiv.) in toluene (10 mL). to afford the desired compound (**20a**) as a white powder (78 mg, 0.3 mmol, 61%). Crystals were obtained from a CH_2Cl_2/pentane mixture at -30 °C. **^{1}H NMR** (400 MHz, $CDCl_3$, 298 K) δ/ppm: 6.96–6.92 (m, 4H), 6.77–6.73 (m, 2H), 4.57 (q, J = 7.2 Hz, 2H), 2.14 (s, 3H), 1.39 (t, 7.2 Hz, 3H); **^{13}C{^{1}H} NMR** (101 MHz, $CDCl_3$, 298 K) δ/ppm: 185.4, 172.5, 152.3, 149.8, 140.5, 138.0, 127.3, 115.5, 114.0, 100.6, 66.5, 22.7, 14.1, carbon atom attached to boron could not be observed; **^{19}F NMR** (376 MHz, $CDCl_3$, 298 K) δ/ppm: -133.59 (d, J = 22.5 Hz, 2F), -136.14 (d, J = 20.1 Hz, 4F), -160.06 (t, J = 20.6Hz, 1F), -163.47 (t, J = 22.4 Hz, 2F); **^{11}B{^{1}H} NMR** (128 MHz, 298 K, $CDCl_3$) δ/ppm: 7.7 (br., s); **HRMS** (ASAP+) m/z calculated for $[C_{24}H_{14}{}^{10}BF_9O_3]^+$ $[M\text{-}H]^+$: 532.0887 found: 532.0881.

*Synthesis of compound **20b***

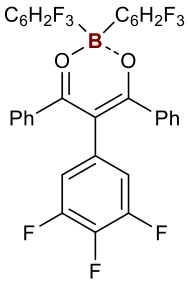

Synthesised according to General Procedure **F** using B(3,4,5-$F_3C_6H_2)_3$ (95 mg, 0.2 mmol, 1.0 equiv.) and 1,3-diphenyl-2-(phenyliodaneylidene)propane-1,3-dione (**18c**) (100 mg, 0.2 mmol, 1.0 equiv.) in toluene (5 mL). to afford the desired compound (**20b**) as a yellow powder (103 mg, 0.2 mmol, 70%). Crystals were obtained from slow evaporation of the solvent. **^{1}H NMR** (400 MHz, $CDCl_3$, 298 K) δ/ppm: 7.58–7.50 (m, 2H), 7.40–7.32 (m, 8H), 7.06–7.02 (m, 4H), 6.53 (m, 2H); **^{13}C{^{1}H} NMR** (101 MHz, $CDCl_3$, 298 K) δ/ppm: 186.3, 151.3, 140.7, 138.2, 133.7, 133.6, 130.5, 129.5, 129.2, 128.8, 116.8, 114.2, 113.4, carbon atom attached to boron could not be observed; **^{19}F NMR** (376 MHz, $CDCl_3$, 298 K) δ/ppm: -132.06 (d, J = 20.5 Hz, 2F), -135.99 (d, J = 20.2 Hz, 4F), -158.96 (t, J = 20.7 Hz, 1F), -163.34 (t, J = 20.1 Hz, 2F); **^{11}B{^{1}H} NMR** (128 MHz, 298 K, $CDCl_3$) δ/ppm: 7.3 (br., s); **HRMS** (ASAP+) m/z calculated for $[C_{33}H_{15}{}^{10}BF_9O_2]^+$ $[M-H]^+$: 626.1214 found: 626.1185.

6.5.3** Synthesis of compound **21

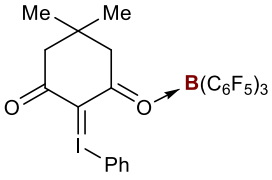

Synthesised according to General Procedure **F** using $B(C_6F_5)_3$ (200 mg, 0.4 mmol, 1.0 equiv.) and (**18d**) (163 mg, 0.4 mmol, 1.0 equiv.) in toluene (15 mL). to afford the desired compound (**21**) as a faint brown solid (156 mg, 0.2 mmol, 48%). **^{1}H NMR** (500 MHz, $CDCl_3$, 298 K) δ/ppm: 7.84–7.81 (m, 2H), 7.61–7.58 (m, 1H), 7.40–7.37 (m, 2H), 2.35 (s, 2H), 2.25 (s, 2H), 0.81 (s, 6H); **^{13}C{^{1}H} NMR** (126 MHz, $CDCl_3$, 298 K) δ/ppm: 189.5, 187.7, 147.7, 139.9, 137.1, 135.7, 133.2, 132.6, 110.6, 99.7, 50.3, 45.0, 33.2, 27.6. **^{19}F NMR** (471 MHz, $CDCl_3$, 298 K) δ/ppm: -133.78 (d, J = 29.3 Hz), -157.75 (t, J = 20.4 Hz), -163.93 (t, J = 26.9 Hz); **^{11}B{^{1}H} NMR** (160 MHz, 298 K, $CDCl_3$) δ/ppm: -1.9 (br., s); **HRMS** (ASAP+) m/z calculated for $[C_{32}H_{14}O_2I^{127}B^{10}F_{15}]^-$ $[M-H]^-$: 851.9928 found: 851.9910.

Chapter 6.6 X-ray crystallographic data

6.6.1 General X-ray experimental

Crystallographic studies on **3a–3c**, **4**, **5**, **6**, **7b**, **8**, **11**, **12**, **13a**, **14a**, **16**, **19a–19b**, **20a–20b** and **21** were undertaken of a single crystal mounted in paratone and studied on an Agilent SuperNova Dual Atlas three-circle diffractometer using Mo- or Cu-Kα radiation and a CCD detector. Measurements were carried out at temperatures ranging between 150(2) K and 293(2) K. Temperatures were maintained using an Oxford cryostream unless otherwise stated. Data were collected, integrated and corrected for absorption using a numerical absorption correction based on Gaussian integration over a multifaceted crystal model within CrysAlisPro.[15] The structures were solved by direct methods and refined against F2 within SHELXL-2013.[16] OLEX2 was used for analysis.[17]

The following corrections were performed under the guidance of Professor Jeremy Rawson (Windsor University, Canada):

A disordered CH_2Cl_2 solvent molecule was noted in the data of **3c**. The Cl atom was refined anisotropically. However, as the central C atom was on a symmetry element, the same principle could not be applied. Although possible to use the Part -n command to turn off the local symmetry for this atom, this would add an unnecessary layer of complexity to the data. In the end, the disordered molecule was refined over two sites via a pivot about one of the Cl atoms. The C atom was treated as isotropic, thus giving an acceptable overall refinement factor (R1) of approximately 5% for **3c**.

19a co-crystallised with a heavily disordered CH_2Cl_2 solvent molecule positioned at a symmetry element (1, 1.5, 0). SQUEEZE[18] was applied, resulting in notably better R1 and wR2. The SQUEEZE function reported 43 e- per solvent-accessible void per unit cell in agreement with that computed for a unique CH_2Cl_2 molecule (42 e-).
20a was plagued by twinning resulting. To counteract this, **20a** was refined from an HKLF5 file, and the twin law -1 0 0 0 -1 0 0 0 1 as stipulated in TwinRotMat (within Platon[20]) was implemented. Thus, the R1 value was brought to acceptable levels (6%).

Compound **21** possessed a significantly disordered lattice solvent. A $CHCl_3$ molecule was located on a general position but with significant rotational disordered about the C–H bond. Another was centred about a special position (1, 1, ½) and again appeared disordered over multiple sites, exacerbated by the symmetry position. Using a value of 1.5 $CHCl_3$ molecules per lattice solvent per asymmetric unit leads to

348 electrons per unit cell which is in reasonable agreement with the estimate based on SQUEEZE[19] within PLATON[19] (396 electrons). Subsequent refinement proceeded smoothly.

The structures of **3a**, **3b**, **3c**, **4**, **5**, **6**, **7b**, **8**, **19a**, **19b**, **20a**, **20b** and **21** are deposited with the Cambridge Structural Database (CCDC deposition numbers: 1897205, 1897206, 1897207, 1897208, 1897209, 1897210, 1897211, 1903201, 1935886, 1935888, 1935890, 1936166, 1963748). These data can be obtained free of charge from the CCDC via www.ccdc.cam.ac.uk/data_request/cif.

6.6.2 X-ray refinement data

Table 6.1: Crystal data and structure refinement for compound **3a–c**.

Compound	**3a**	**3b**	**3c**
Empirical Formula	$C_{31}H_{18}BF_9N_2$	$C_{31}H_{18}BF_9N_2$	$C_{56}H_{30}B_2F_{18}N_4$ $2(CH_2Cl_2)$
Crystal System	Monoclinic	Triclinic	Triclinic
Space Group	*P*21/n	*P*-1	*P*-1
a	9.5166(4) Å	9.7975(7) Å	9.4053(6) Å
b	21.8157(8) Å	10.9639(11) Å	11.2224(7) Å
c	13.1104(5) Å	13.8619(15) Å	13.6936(8) Å
α	90°	106.193(9)°	103.791(5)°
β	99.132(4)°	102.430(7)°	98.886(5)°
γ	90°	105.643(7)°	90.099(5)°
V	2687.37(18) $Å^3$	1307.3(2) $Å^3$	1385.73(16) $Å^3$
Z	4	2	1
T	150(2) K	150(2) K	150(2) K
D_C	1.484 g/cm^3	1.525 g/cm^3	1.549 g/cm^3
Crystal size	0.21 × 0.18 × 0.11 mm	0.20 × 0.16 × 0.11 mm	0.12 × 0.04 × 0.03 mm
Total data	14715	10154	10704
Unique data	6315	6080	6091
R_{int}	0.022	0.031	0.041
$R1[F^2>2\,\sigma(F^2)]$	0.042	0.056	0.065
wR2 (all data)	0.105	0.149	0.169
GoF	1.06	1.08	1.030
ρmin/ρmax	-0.22/0.28 $eÅ^{-3}$	-0.30/0.25 $eÅ^{-3}$	-0.39/0.66 $eÅ^{-3}$
CCDC code	1897205	1897206	1897207

Table 6.2: Crystal data and structure refinement for compounds **4**, **5** and **6**.

Compound	**4**	**5**	**6**
Empirical Formula	$C_{36}H_{16}B_2F_{18}N_2$	$C_{25}H_{13}BF_6N_2$	$C_{25}H_{14}BF_9N_2O$
Crystal System	Monoclinic	Monoclinic	Monoclinic
Space Group	I2/*a*	*P*21/*c*	C2/*c*
a	15.7866(8) Å	14.8884(9) Å	25.9971(10) Å
b	9.6410(4) Å	10.6742(5) Å	15.1972(6) Å
c	22.4406(11) Å	14.1291(7) Å	13.0295(4) Å
α	90°	90°	90°
β	108.694(6)°	115.392(7)°	94.668(3)°
γ	90°	90°	90°
V	3235.2(3) $Å^3$	2028.5(2) $Å^3$	5130.7(3) $Å^3$
Z	4	4	8
T	150(2) K	170(2) K	200(2) K
D_C	1.725 g/cm^3	1.526 g/cm^3	1.399 g/cm^3
Crystal size	0.82 × 0.28 × 0.09 mm	0.57 × 0.27 × 0.12 mm	0.50 × 0.37 × 0.16 mm
Total data	8430	10152	10904
Unique data	3884	4614	5055
Rint	0.020	0.020	0.017
$R1[F^2>2\sigma(F^2)]$	0.037	0.041	0.124
wR2 (all data)	0.095	0.113	0.405
GoF	1.02	1.04	1.82
ρmin/ρmax	-0.21/0.35 $eÅ^{-3}$	-0.23/0.30 $eÅ^{-3}$	-0.38/4.7 $eÅ^{-3}$
CCDC code	1897208	1897209	1897210

Table 6.3: Crystal data and structure refinement for compounds **7b** and **8**.

Compound	**7b**	**8**
Empirical Formula	$C_{25}H_8BF_{15}N_2O$	$C_{19}H_7BF_{10}N_2O$
Crystal System	Monoclinic	Triclinic
Space Group	$P2_1/c$	P-1
a	10.8497(5) Å	11.8326(5) Å
b	16.1722(8) Å	12.0001(7) Å
c	13.6947(6) Å	13.9711(6) Å
α	90	73.338(4)
β	104.795(5)°	89.047(3)°
γ	90°	75.159(4)°
V	2323.27(19) $Å^3$	1833.64(16) $Å^3$
Z	3	4
T	200 K	150(2) K
D_C	1.853 g/cm^3	1.739 g/cm^3
Crystal size	0.30 × 0.27 × 0.16 mm	0.45 × 0.33 × 0.22 mm
Total data	1853	15395
Unique data	12738	8650
Rint	5617	0.031
$R1[F^2>2\ \sigma(F^2)]$	0.040	0.052
wR2 (all data)	0.113	0.147
GoF	1.03	1.04
ρmin/ρmax	-0.29/0.28 $eÅ^{-3}$	-0.38/0.35 $eÅ^{-3}$
CCDC code	1903201	1897211

Table 6.4: Crystal data and structure refinement for compounds **11**, **12**, **13a**.

Compound	**11**	**12**	**13a**
Empirical Formula	$C_{27}H_{13}BF_{12}N_2$	$C_{20}H_6BF_{13}N_2$	$C_{24}H_{12}BF_{15}N_2$
Crystal System	Orthorhombic	Monoclinic	Monoclinic
Space Group	*Fdd*2	*P*21/*c*	$P2_1/n$
a	46.1905(8) Å	15.3987(8) Å	10.6045(6) Å
b	19.9096(4) Å	8.0553(3) Å	19.1546(11) Å
c	10.4845(2) Å	16.3052(8) Å	11.9980(7) Å
α	90°	90°	90°
β	90°	105.907(5)°	108.586(6)°
γ	90°	90°	90°
V	9641.9(3) $Å^3$	1945.06(17) $Å^3$	2310.0(2) $Å^3$
Z	42	4	4
T	200(2) K	200(2) K	200(2) K
D_C	1.635 g/cm^3	1.817 g/cm^3	1.795 g/cm^3
Crystal size	0.27 × 0.17 × 0.16 mm	0.58 × 0.30 × 0.23 mm	0.26 × 0.20 × 0.15 mm
Total data	4906	3556	12146
Unique data	1373	1373	5541
Rint	0.046	0.012	0.023
$R1[F^2>2\,\sigma(F^2)]$	0.039	0.024	0.042
wR2 (all data)	0.108	0.063	0.101
GoF	1.02	1.05	1.03
ρmin/ρmax	-0.35/0.15 e$Å^{-3}$	-0.18/0.12 e$Å^{-3}$	-0.22/0.26 e$Å^{-3}$

Table 6.5: Crystal data and structure refinement for compounds **14a** and **16**.

Compound	**14a**	**16**
Empirical Formula	$C_{24}H_{12}BF_{15}N_2$	$(C_{12}H_{28}NO)\cdot C_{24}H_{11}BF_{15}N)\cdot(C_6H_6)$
Crystal System	Monoclinic	Triclinic
Space Group	$P2_1/c$	P-1
a	14.8472(11) Å	11.2457(4) Å
b	8.9332(6) Å	12.7330(5) Å
c	18.0445(16) Å	17.4126(6) Å
α	90	104.556(3)
β	99.570(8)°	96.468(3)°
γ	90°	114.051(4)°
V	2360.0(3) $Å^3$	2137.56(15) $Å^3$
Z	4	4
T	200(2) K	209 K
D_C	1.757 g/cm^3	1.405 g/cm^3
Crystal size	0.23 × 0.16 × 0.11 mm	0.33 × 0.17 × 0.10 mm
Total data	14431	20446
Unique data	5800	8882
R_{int}	0.032	0.026
$R1[F^2>2\,\sigma(F^2)]$	0.082	0.045
wR2 (all data)	0.250	0.125
GoF	1.04	1.03
ρmin/ρmax	-0.44/0.96 $eÅ^{-3}$	-0.39/0.38 $eÅ^{-3}$

Table 6.6: Crystal data and structure refinement for compound **19a** and **19b**.

Compound	**19a**	**19b**
Empirical Formula	$C_{23}H_6BF_{15}O_4$	$C_{23}H_{12}BF_9O_4$•0.5(CH_2Cl_2)
Crystal System	Monoclinic	Triclinic
Space Group	*$P2_1/n$*	*P-1*
a	13.3140(16) Å	7.8542(4) Å
b	10.1081(14) Å	10.5570(10) Å
c	18.044(3) Å	15.6690(9) Å
α	90°	71.330(5)°
β	111.202(16)°	75.721(5)°
γ	90°	84.401(4)°
V	2263.9(6) $Å^3$	1193.50(12) $Å^3$
Z	4	2
T	293(2) K	200.0(2) K
D_C	1.884 g/cm^3	1.604 g/cm^3
Crystal size	0.35 × 0.26 × 0.17 mm	0.77 × 0.55 × 0.30 mm
Total data	12879	8874
Unique data	5342	4677
R_{int}	0.080	0.019
$R_1[F^2>2\ \sigma(F^2)]$	0.070	0.064
wR2 (all data)	0.180	0.185
GoF	1.00	1.05
ρ_{min}/ρ_{max}	-0.34/0.28 $eÅ^{-3}$	-0.96/1.02 $eÅ^{-3}$
CCDC code	1935890	1935888

Table 6.7: Crystal data and structure refinement for compound **20a**, **20b** and **21**.

Compound	**20a**	**20b**	**21**
Empirical Formula	$C_{24}H_{14}BF_9O_3$	$C_{33}H_{16}BF_9O_2$	$C_{32}H_{15}BF_{15}IO_2$ 1.5 $CHCl_3$
Crystal System	Monoclinic	Triclinic	Monoclinic
Space Group	*$P2_1/c$*	*P-1*	*$P2_1/n$*
a	9.0378(8) Å	9.7170(4) Å	16.1557(4) Å
b	17.4814(12) Å	10.2493(5) Å	37.6672(11) Å
c	14.4485(10) Å	15.4586(9) Å	16.7091(4) Å
α	90°	85.283(4)°	90°
β	96.721(7)°	75.672(4)°	104.564(3)°
γ	90°	66.7463(4)°	90°
V	2267.1(3) $Å^3$	1367.33(13) $Å^3$	9841.5(5) $Å^3$
Z	4	2	12
T	150(2) K	200.0(2) K	293 K
D_C	1.559 g/cm^3	1.521 g/cm^3	1.729 g/cm^3
Crystal size	1.0 x 0.47 x 0.20 mm	0.44 x 0.28 x 0.19 mm	0.33 × 0.13 × 0.10 mm
Total data	5375	6362	22003
Unique data	5375	4319	15239
R_{int}	0.0285	0.021	0.050
$R_1[F^2>2\ \sigma(F^2)]$	0.061	0.047	0.053
wR2 (all data)	0.161	0.158	0.139
GoF	1.03	0.95	1.04
ρ_{min}/ρ_{max}	-0.26/0.32 e$Å^{-3}$	-0.21/0.28 e$Å^{-3}$	-1.31/2.53 e$Å^{-3}$
CCDC code	1936166	1935886	1963748

Chapter 6.7 References

1 S. Lancaster, *ChemSpider SyntheticPage*s, 2003.

2 Y. Soltani, L. Wilkins and R. Melen, *Angew. Chem. Int. Ed.*, 2017, **56**, 11995.

3 R. Murray and A. Trozzolo, *J. Org. Chem.*, 1961, **26**, 3109.

4 M. Bartucci, P. Wierzbicki, C. Gwengo, S. Shajan, S. Hussain and J. Ciszek, *Tetrahedron Lett.*, 2010, **51**, 6839.

5 C. Tang, Q. Liang, A. Jupp, T. Johnstone, R. Neu, D. Song, S. Grimme and D. Stephan, *Angew. Chem., Int. Ed*., 2017, **56**, 16588,

6 J. Lasri, N. Eltayeb, A. Ismail, *J. Mol. Struct.*, 2016, **1121**, 35.

7 L. Wang, Y. Murai, T. Yoshida, A. Ishida, K. Masuda, Y. Sakihama, Y. Hashidoko, Y. Hatanaka and M. Hashimoto, *Org. Lett.*, 2015, **17**, 616.

8 S. Brunner, S. Serin and F. Richards, *J. Biol. Chem.*, 1980, **255(8)**, 3313.

9 E. Schmitz, R. Ohme, E. Corey and R. Glass, *Org. Synth.*, 1965, **45**, 83.

10 W. Rathke, A. Millard, A. Brossi and J. Minamikawa, *Org. Synth.*,1978, **58**, 32.

11 J. Tullis, P. Helquist, A. Courtney and S. Martin, *Org. Synth.*, 1997, **74**, 229.

12 S. R. Goudreau, D. Marcoux and A. Charette, *J. Org. Chem.*, 2009, **74**, 470.

13 H. Huang, Y. Yang, X. Zhang, W. Zeng and Y. Liang, *Tetrahedron Lett.*, 2013, **54**, 6049.

14 J. Cardinale and J. Ermert, *Tetrahedron Lett.*, 2013, **54**, 2067.

15 CrysAlisPro, Agilent Technologies, Version 1.171.37.33 (release 27-03-2014 CrysAlis171.NET).

16 SHELXL-2013, G. Sheldrick, University of Göttingen, Germany (2013).

17 O. Dolomanov, L. Bourhis, R. Gildea, J. Howard and H. Puschmann, *J. Appl. Cryst.*, 2009, **42**, 339.

18 SQUEEZE: A. Spek, *Acta Cryst.*, 2015, **C71**, 9.

19 PLATON: A. Spek, *Acta Cryst.*, 2009, **D65**, 148.

Chapter 7. Conclusions and future work

The initial aim of this thesis was to react a range of azo containing compounds to expand the frontiers of triarylborane mediated nitrogen activation. During this thesis, the scope was expanded to include the activation of iodine-containing carbene precursors. This thesis has realised these goals by exploring in detail the reactivity of hydrazines, hydrazides, diaziridines, diazos and iodonium ylides, thus providing valuable insights into the reactivity of triarylboranes with various classes of compounds.

In chapter 3, the stoichiometric reactions of hydrazines and hydrazines with triarylboranes took centre stage. The investigations resulted in the generation of a multitude of products ranging from adducts to heterocyclic and chain compounds. These products were characterised by multinuclear NMR spectroscopy and single-crystal X-ray diffraction. In addition, mechanistic understandings into the reactivity of select examples were also obtained.

Chapter 4 built on the foundations established above by introducing diaziridines, a class of highly strained azo compounds, to triarylboranes. In this instance, by adjusting the temperature and the triarylborane Lewis acidity, it was possible to induce adduct formation, rearrangement to a hydrazine adduct and finally, aryl elimination in a sequential fashion. Attempts were made to expand the scope to Frustrated Lewis Pairs, but these proved unsuccessful as hydrolysis obscured the reactivity. Multinuclear NMR spectroscopy and single-crystal X-ray diffraction were used once more to analyse the products obtained.

Finally, Chapter 5 initially probed the reaction of **17** with the archetypal triarylborane, $B(C_6F_5)_3$. Crystallographic evidence revealed a rare 1,3-carboboration reaction had occurred, leading to boron dienolate **19a**. As this product could not be obtained in an analytically pure fashion, alternative carbene precursors **18a–18d** were utilised. Heating these acyclic hypervalent iodines in the presence of triarylboranes yielded products **19b–19e** and **20a–20b**. They were stable under a range of aqueous, acidic and basic conditions. Cyclic hypervalent iodine **18d** could not be induced to undergo this 1,3-carboboration instead, forming adduct **21** with $B(C_6F_5)_3$.

As mentioned earlier, this thesis serves as an in-depth preliminary investigation into triarylborane reactivity with a range of diazo analogues and hypervalent iodine compounds. Several steps can be undertaken to advance our understanding of this underexplored area further.

Chapter 3: Additional studies into the independent synthesis and reactivity of **5** in hydrogen release should be undertaken. Experiments should also be undertaken to synthesise structural analogues of **5** with triarylboranes other than $B(2,4,6\text{-}F_3C_6H_2)_3$.

Chapter 4: The FLP reaction which led to hydrolysed product **16** should be repeated to uncover the underlying reactivity. It would be interesting to introduce diazirines (structural analogues of diazos) to triarylboranes and FLPs. As this nitrogen species is photoactive, light exposure could lead to markedly divergent reactivity than previously observed.

Chapter 5: This chapter exclusively focused on synthesising and analysing the boron dienolates. Preliminary investigations highlighted the potential photophysical properties of these species. This potential application could be further explored to design new fluorophores.

I sincerely hope this thesis has piqued the readers' interest in triarylborane activation and encouraged them to explore this fascinating field further.

Appendix

List of publications

T. Gazis, J. Carden, M. Alharbi and R. L. Melen, *Triarylboranes in the Activation of Azo Containing Compounds*, EIBC, 2021.

T. Gazis, A. Dasgupta, M. Hill, J. Rawson, T. Wirth and R. Melen, *Dalton Trans.*, 2019, **48**, 12391.

T. Gazis, D. Willcox and R. Melen, *Lewis Acidic Boranes in Frustrated Lewis Pair Chemistry*, Springer, 2020, 209.

T. Gazis, B. Mohajeri Thaker, D. Willcox, D. Ould, J. Wenz, J. Rawson, M. Hill, T. Wirth and R. Melen, *Chem. Comm.*, 2020, **56**, 3345.

Y. Soltani, A. Dasgupta, T. Gazis, D. Ould, E. Richards, B. Slater, K. Stefkova, V. Vladimirov, L. Wilkins, D. Willcox and R. Melen, *Cell Rep. Phys. Sci.*, 2020, **1**, 100016.

A HERCULEAN EFFORT

Triarylboranes in Azo Activation (and Beyond!)

Theodore A. Gazis and Rebecca L. Melen
School of Chemistry, Cardiff University, Cardiff, CF10 3AT, UK

BAr_3 RISE TO THE CHALLENGE

Introduction

I have sought to expand the classes of nitrogen containing compounds BAr_3 can activate. I began by exploring the reactivity of hydrazones (propellants/ pharmaceuticals) and diaziridines (fluorophores).

Activation

As with noble metals, adducts (activation) readily occurs (**1** and **2**). The low temperatures (25 °C) and short reaction times (30 min.) required demonstrate BAr_3 are viable alternatives to their metal counterparts.

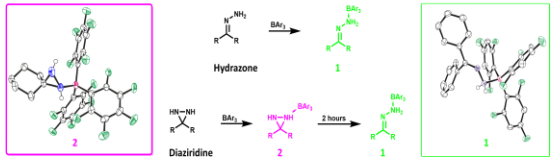

Hydrazone

Diaziridine

Gazis T. A., Rebecca L. Melen, et. al, *EJIC*, 2021, manuscript accepted

Fluorenone

Out of the numerous compounds generated to compare the reactivity of BAr_3 to metals, two stand out. The first is a chromophore used in optoelectronic devices (**3**). The second constitutes a potent hydrogen storage material (**4**). Before my work, their formation relied on harsh reaction conditions with carcinogens. My research made them readily accessible.

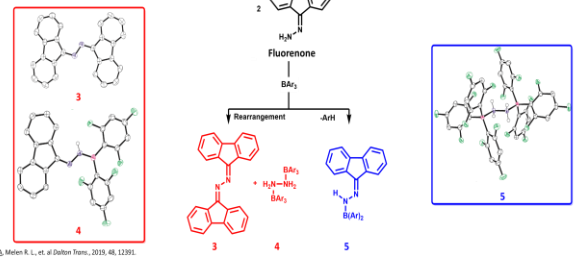

Fluorenone

Rearrangement

-ArH

Gazis T.A, Melen R. L., et. al *Dalton Trans.*, 2019, 48, 12391.

Conclusions

Like Hercules bending the great Cretan Bull to his will, BAr_3 are able to tame and control highly volatile nitrogen compounds.

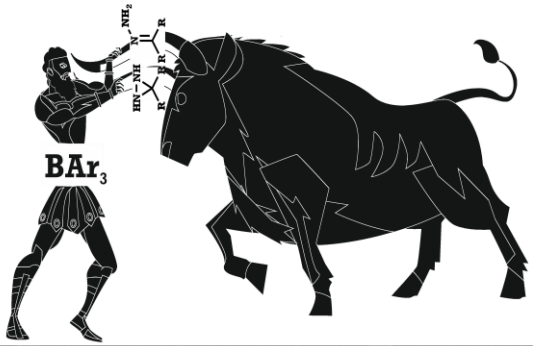

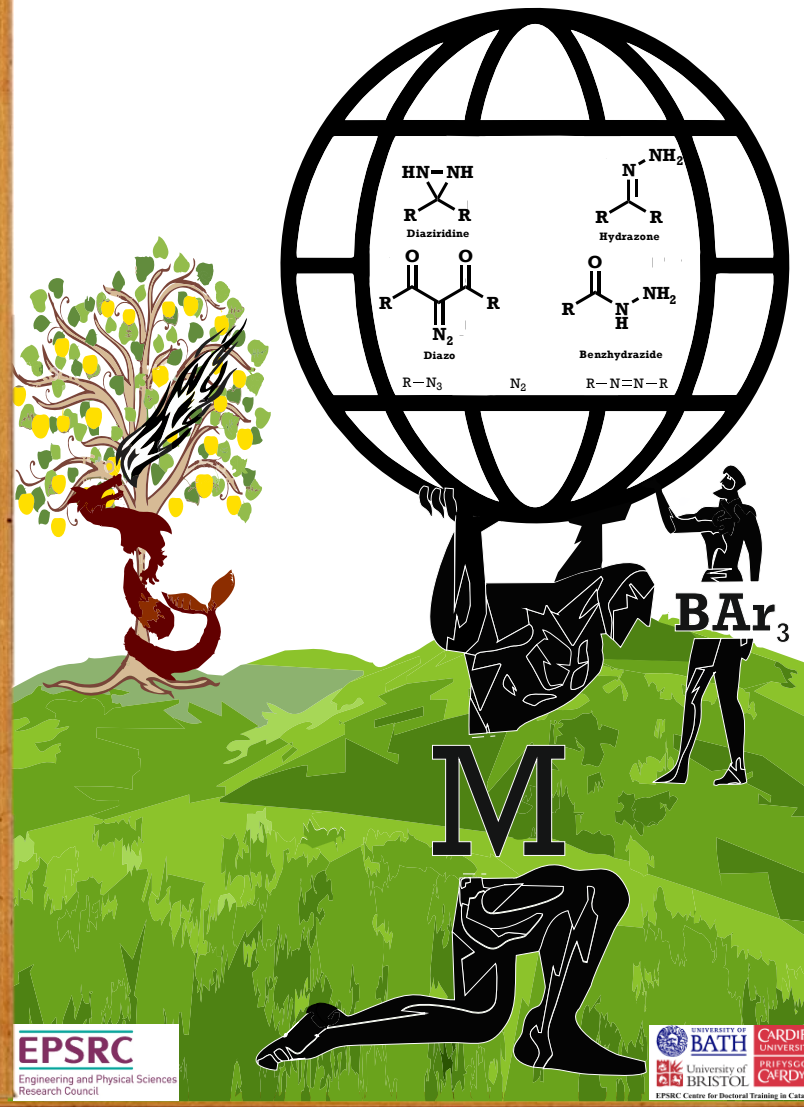

BAr_3 BREAK NEW GROUND

Introduction

Thanks to distinct structural features of BAr_3 they can transcend mere mimicry of metal systems and exhibit unique reactivity. Heating of benzhydrazides (antimicrobial agents) and diazos (carbene precursors) resulted in two reaction pathways being discovered.

Heterocycle formation

The reaction of benzhydrazide with $B(Ar)_3$ gave **6** (71%). *In situ* heating to 110 °C lead to loss of ArH and generated heterocycle **7** (81%). This heterocycle offered unique insights into the bonding and behaviour of nitrogen compounds with BAr_3.

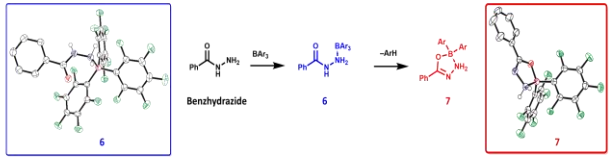

Benzhydrazide

Gazis T.A, Melen R. L., et. al *Dalton Trans.*, 2019, 48, 12391.

1,3 Carboboration

Diazo compounds represent highly volatile compounds known for their propensity to release N_2. When heated in the presence of BAr_3 one of the Ar groups was transferred 3 positions away to give **8**. The same reactivity was observed when using iodonium ylides.
This transformation was previously considered thermodynamically impossible. The examples I have discovered are the only literature known ones to date.

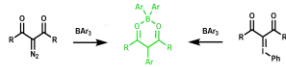

Diazo

Iodonium Ylide

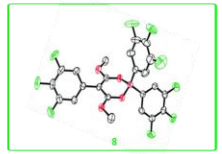

Gazis T.A., Melen,* R.L., *Chem. Commun.*, 2020, **56**, 3345.

Conclusions

Like Hercules capturing Kerberos and leading it out of Hades, BAr_3 are able to imprison nitrogen compounds and lead them down new reaction pathways.